

Effect of Tool Edge Preparation and Hardness of Workpiece  
on Machinability of AISI 1045 Steel

By

MOHAMED SHNFIR

MANUSCRIPT-BASED THESIS PRESENTED TO ÉCOLE DE  
TECHNOLOGIE SUPÉRIEURE IN PARTIAL FULFILLMENT  
FOR THE DEGREE OF DOCTOR OF PHILOSOPHY  
Ph.D.

MONTREAL, MAY 11<sup>th</sup>, 2020

ÉCOLE DE TECHNOLOGIE SUPÉRIEURE  
UNIVERSITÉ DU QUÉBEC

© Copyright 2020 reserved by Mohamed Shnfir

© Copyright reserved

Reproduction, saving or sharing of the content of this document, in whole or in part, is prohibited. A reader who wishes to print this document or save it on any medium must first obtain the author's permission.

**BOARD OF EXAMINERS THESIS PH.D.**

THIS THESIS HAS BEEN EVALUATED

BY THE FOLLOWING BOARD OF EXAMINERS

Mr. Victor Songmene, Thesis Supervisor

Department of Mechanical Engineering at École de Technologie Supérieure

Mr. Lotfi Guizani, President of the Board of Examiners

Department of Construction Engineering at École de Technologie Supérieure

Mr. Vincent Demers, Member of the jury

Department of Mechanical Engineering at École de Technologie Supérieure

Mr. Marek Balazinski, External Evaluator

Department of Mechanical Engineering at École Polytechnique Montreal

Mr. Fawzy-Hosny Samuel, External Evaluator

Department of Applied Sciences (DSA) University of Québec in Chicoutimi (UQAC)

THIS THESIS WAS PRESENTED AND DEFENDED

IN THE PRESENCE OF A BOARD OF EXAMINERS AND PUBLIC

MONTREAL, APRIL 23<sup>th</sup>, 2020

AT ÉCOLE DE TECHNOLOGIE SUPÉRIEURE



## **ACKNOWLEDGMENT**

First, I would like to deepest gratitude to my supervisor Prof, Victor Songmene for his suggestions, guidance, and tireless support to the development of this thesis.

I would also like to thank the members of my jury members, Prof. Lotfi Guizani, Prof. Vincent Demers, Prof. Fawzy Hosny Samuel, and Prof. Marek Balazinski for evaluating this thesis.

My thanks also to Dr. Wole Olufayo, Dr. Walid Jomaa, Dr. Jules Kouam and all technicians at the machine workshop for their help and support during the experimental tests.

Special thanks to my friend Dr. Abdurrazag Khaled and Eng. Gheith Elkiizza for their encouragement and support throughout my study's stay in Canada.

Finally, I would like to express my profound gratitude to my mother, my father, my wife and my kids for their unlimited supports and encouragement, without them, I could not have pursued this endeavour.



# Effet de la préparation des arêtes de l'outil et de la dureté de la pièce sur l'usinabilité de l'acier AISI 1045

Mohamed Shnfir

## RÉSUMÉ

L'usinage intermittent à l'aide d'outils en céramique comme le fraisage dur est une tâche difficile en raison du choc mécanique important que subissent les plaquettes pendant l'usinage et de la fragilité des plaquettes en céramique. L'objectif principal de cette thèse est d'étudier les effets de la dureté du matériau de la pièce, de la préparation des arêtes des outils de coupe (arrondie, chanfreinée), de la nuance des plaquettes (céramique à base de nitrure de silicium (SiAlON), céramique Whisker avec une matrice de  $Al_2O_3 + SiC$ ) sur l'usinabilité de l'acier AISI 1045 trempé. Les pièces en acier AISI 1045 ont été traitées pour avoir les duretés 17 HRC, 38 HRC et 48 HRC avant les essais d'usinage. En plus des conditions d'usinage mentionnées ci-dessus, les effets des paramètres d'usinage (avance et vitesse), du type de fraisage (conventionnel et en montée) ont également été étudiés. Les indicateurs de performance d'usinage testés comprennent la force de coupe résultante, la puissance de coupe, la rugosité de surface des pièces et l'usure des outils. L'analyse a été réalisée à l'aide d'un plan orthogonal de Taguchi  $L_{32} (2^1 4^4)$  et évaluée à l'aide d'outils statistiques tels que l'analyse de la variance (ANOVA), les effets principaux et les interactions.

Les résultats de la réduction des forces de coupe résultantes ont été obtenus avec des plaquettes de bord affûtées de qualité céramique SiAlON. De plus, une diminution des efforts de coupe résultants a été associée à l'utilisation de faibles vitesses d'avance pendant l'usinage des matériaux les plus durs. La vitesse d'avance, la vitesse de coupe et la dureté de la pièce ont également été identifiées comme les principaux facteurs influençant la puissance de coupe. Une usure accrue en dépouille des plaquettes a été observée à une faible vitesse de coupe et à des vitesses d'avance élevées, tandis que le micro-écaillage de l'outil résultait principalement de la charge cyclique.

Les effets de la vitesse de coupe, de l'avance et de la dureté de la matière de la pièce sur la concentration du nombre de particules (particules fines et ultrafines) pendant le fraisage ont également été étudiés expérimentalement. Un plan expérimental fractionné à trois niveaux ( $L_{27}$ ) a été utilisé. Les résultats montrent que la dureté de la pièce était le principal facteur affectant la génération de particules métalliques fines et ultrafines pour les deux outils de coupe utilisés. D'autres effets significatifs tels que l'interaction entre les paramètres de fraisage ont été également étudiés. Dans l'ensemble, il est démontré que l'utilisation d'un outil de coupe avec une arête arrondie réduit l'émission de particules métalliques.

Cette thèse peut aider à déterminer les conditions dans lesquelles l'acier AISI 1045 doit être usiné afin d'améliorer les performances de l'outil et la qualité de surface de la pièce usinée tout en minimisant l'émission de particules métalliques fines et ultrafines.

*Mots-clés: usinabilité, fraisage, acier AISI 1045, outil de coupe en céramique.*



## **Effect of Tool Edge Preparation and Hardness of Workpiece on Machinability of AISI 1045 Steel**

Mohamed SHNFIR

### **ABSTRACT**

Intermittent machining using ceramic tools such as hard milling is a challenging task due to the severe mechanical shock that the inserts undergo during machining and the brittleness of ceramic inserts. The main aim of this thesis is to investigate the effects of the workpiece material's hardness, cutting tool edge preparation (Honed, T-land), inserts grade (Silicon Nitride (SiAlON) based ceramic, Whisker ceramic with a matrix of  $Al_2O_3 + SiCW$ ) on the machinability of AISI 1045 hardened steel. AISI 1045 steel workpieces were hardened to 17 HRC, 38 HRC and 48 HRC prior to the machining experiments.

In addition to the above mentioned machining conditions, the effects of the machining parameters (feed and speed), milling type (conventional and climb) were also investigated. The indicators tests include resultant cutting force, power consumption, surface roughness and tool wear. The analysis was performed using Taguchi orthogonal array design  $L_{32} (2^1 4^4)$  and evaluated using statistical tools such as analysis of variance (ANOVA), main effects and interactions. The results of lower resultant cutting forces were obtained with honed edge inserts of SiAlON ceramic grade. In addition, a decrease in resultant cutting forces was associated with the use of low feed rates during machining of hardest material. The feed rate, cutting speed and workpiece hardness were also identified as the greatest influencing factors on the cutting power. Increased flank wear was observed at a low cutting speed and high feed rates, while micro-chipping of the tool mostly ensued from the cyclic loading.

The effects of cutting speed, feed rate and workpiece material hardness on the particles number concentration (fine and ultrafine particles) during the milling were also experimentally investigated. The three levels fractional experimental design ( $L_{27}$ ) was used. The results show that the hardness of the workpiece material was the main factor affecting the generation of fine and ultrafine metallic particles for both cutting tools used. Other significant effects such as the interaction between the milling parameters are also investigated. Overall, it is shown that the use of a cutting tool with a honed edge reduces the metallic particles emission. This thesis can help determine the conditions in which AISI 1045 steel should be machined in order to enhance tool performance and improve the surface quality of the machined part while minimizing the emission of fine and ultrafine metallic particles.

**Keywords:** *machinability, hard milling, AISI 1045 steel, ceramic cutting tool.*





3.4.3	Analysis of Tool Wear .....	67
3.5	Confirmation Tests.....	71
3.6	Conclusions.....	76
CHAPTER 4	MULTI-OBJECTIVE OPTIMIZATION IN FACE MILLING OF AISI 1045 STEEL USING TAGUCHI-BASED GREY RELATIONAL AND DESIRABILITY FUNCTION ANALYSIS .....	79
4.1	Introduction.....	80
4.2	Experimental Procedure.....	83
4.2.1	Workpiece Material, Equipment and Cutting Tools .....	83
4.2.2	Experimental Measurements.....	84
4.2.3	Experimental Design with Taguchi .....	86
4.2.4	Multi-objective optimization approach - Grey Relational Analysis (GRA) .....	89
4.2.5	Desirability Function Analysis (DFA).....	92
4.3	Results and Discussion .....	93
4.3.1	Measurement of Response Factors .....	93
4.3.2	Comparison for Roughing Parameters.....	96
4.3.3	GRA Analysis for Roughing Operation.....	96
4.3.4	DFA Analysis for Roughing Operation .....	99
4.4	Confirmation Test for Roughing.....	102
4.5	Finishing Optimization Parameters.....	103
4.5.1	GRA Analysis for Finishing Operation .....	103
4.5.2	DFA Analysis for Finishing Operation.....	106
4.6	Confirmation Test for Finishing Conditions.....	109
4.7	Comparison of Optimization Techniques on Roughing and Finishing Results.....	110
4.8	Conclusions.....	113
CHAPTER 5	ON FINE PARTICLES EMISSION DURING FACE MILLING OF HARDENED AISI 1045 STEEL.....	115
5.1	Introduction.....	115
5.2	Experimental procedure .....	118
5.2.1	Workpiece Material .....	118
5.2.2	Machining Tests.....	119
5.2.3	Experimental Design.....	121
5.3	Results and Discussion .....	122
5.4	Conclusions.....	134
CHAPTER 6	ULTRAFINE PARTICLES EMISSION DURING HIGH-SPEED MILLING OF HARDENED AISI 1045 STEEL.....	137
6.1	Introduction.....	137
6.2	Experimental Procedure.....	139
6.2.1	Design of Experiment .....	139
6.2.2	Workpiece Material .....	140
6.2.3	Machining Tests.....	140
6.3	Experimental Results and Discussions .....	142

6.4	Conclusions.....	151
	CONCLUSIONS .....	153
	MAIN CONTRIBUTIONS.....	155
	RECOMMENDATIONS.....	157
APPENDIX I	EXPERIENCE PLANS FOR ORTHOGONAL ARRAY L <sub>32</sub> (2 <sup>1</sup> 4 <sup>4</sup> ) OF TAGUCHI DESIGN .....	159
APPENDIX II	EXPERIENCE PLANS FOR ORTHOGONAL ARRAY L <sub>27</sub> (3 <sup>3</sup> ) STUDY OF METALLIC PARTICLES EMISSION DURING MILLING PROCESS .....	163
	LIST OF REFERENCES.....	171



## LIST OF TABLES

		Page
Table 1-1	Type of cutting edges and their common application (Kandráč et al., 2013).....	17
Table 2-1	Cutting conditions and their levels for L <sub>32</sub> .....	35
Table 2-2	Cutting conditions and their levels for L <sub>27</sub> .....	36
Table 2-3	Chemical composition of workpiece material (% weight). ....	36
Table 2-4	Heat treatment process for AISI 1045 steel. ....	37
Table 2-5	Specification of the ceramic insert (Kennametal, 2013).....	41
Table 2-6	Specification (a) cutting tool holder and (b) cutting edge in mm (Kennametal, 2013).....	43
Table 3-1	Matrix of Experiments. ....	54
Table 3-2	Orthogonal array L <sub>32</sub> (2 <sup>1</sup> 4 <sup>4</sup> ) of Taguchi design. ....	55
Table 3-3	The chemical composition of workpiece material (% weight). ....	59
Table 3-4	Specification of the cutting tool.....	61
Table 3-5	Workpiece and cutting tool material properties (Collin & Rowcliffe, 2000; de Faoite, Browne, & Stanton, 2013; De Godoy & Diniz, 2011; Iqbal, Mativenga, & Sheikh, 2007; Jun, Jianxin, Jianhua, & Xing, 1997). ....	61
Table 3-6	ANOVA for resultant force. ....	62
Table 3-7	Means response for resultant force. ....	64
Table 3-8	ANOVA for power. ....	65
Table 3-9	Means response for power. ....	66
Table 3-10	ANOVA for tool wear. ....	69
Table 3-11	Means response for tool wear. ....	70
Table 3-12	Initial and recommended parameters combination. ....	75

Table 4-1	Current research using multi-objective optimization in the machining of steel. ....	82
Table 4-2	Heat treatment process for AISI 1045 steel. ....	84
Table 4-3	Chemical composition of workpiece material (% weight). ....	84
Table 4-4	Characteristic of used ceramic inserts.....	84
Table 4-5	Cutting parameters and their levels.....	87
Table 4-6	Taguchi L <sub>32</sub> experimental design plan. ....	88
Table 4-7	Grey relational normalized values, coefficient and grey relational grade values. ....	97
Table 4-8	ANOVA for Grey Relational Grade in roughing conditions. ....	98
Table 4-9	Main effects on mean Grey Relational Grade in roughing conditions. ....	99
Table 4-10	ANOVA for Desirability Function Analysis in roughing conditions. ....	101
Table 4-11	Response table for Desirability Function Analysis in roughing conditions. ....	102
Table 4-12	Confirmation test GRA grade optimization parameters in roughing conditions. ....	102
Table 4-13	Confirmation test DFA optimization parameters in roughing conditions. ....	103
Table 4-14	Grey relational normalized values, coefficients and grey relational grades. ....	104
Table 4-15	ANOVA for Grey Relational Grade in finishing conditions. ....	105
Table 4-16	Main effects on mean Grey Relational Grade for finishing conditions. ....	105
Table 4-17	ANOVA for Desirability Function Analysis in finishing conditions. ....	107
Table 4-18	Response table for Desirability Function Analysis in finishing conditions.....	108
Table 4-19	Confirmation tests for GRA grade optimization parameters in finishing conditions.....	109
Table 4-20	Confirmation tests for DFA optimization parameters in finishing conditions.....	110

Table 5-1	Chemical composition AISI 1045 steel workpiece material (% weight).....	118
Table 5-2	Cutting parameters and their levels.....	119
Table 5-3	Taguchi L <sub>27</sub> orthogonal design of experiment. ....	122
Table 5-4	Analysis of Variance for FP (Honed tool) .....	123
Table 5-5	Analysis of Variance for FP (T-land tool) .....	127
Table 6-1	Chemical composition of material AISI 1045 steel (% weight). ....	140
Table 6-2	Cutting parameters and their levels.....	140
Table 6-3	Analysis of Variance for UFP (Honed tool). ....	144
Table 6-4	Analysis of Variance for UFP (T-land tool). ....	145



## LIST OF FIGURES

		Page
Figure 0-1	Input-output aspects of the cutting edge preparation process according to Rodriguez (Rodríguez, 2009).....	2
Figure 1-1	Types of milling operations: (a) Up (conventional) and (b) Down (climb). .....	8
Figure 1-2	Hot hardness of tool materials (Toenshoff & Denkena, 2013). .....	9
Figure 1-3	Main effects of the cutting edge preparation(Bassett et al., 2012). .....	13
Figure 1-4	Types of cutting tool edges preparation design (Carl-Frederik Wyen, Knapp, & Wegener, 2012) .....	15
Figure 1-5	Cutting edge characterization of rounded edge (Denkena et al., 2005).....	16
Figure 1-6	Types of chamfer edges preparation design (Denkena & Biermann, 2014).....	16
Figure 1-7	Microstructure of the microalloyed steels under conditions of (a) as-received, (b) furnace-cooled, (c) air-cooled, and (d) water cooled (Demir, 2008). .....	21
Figure 1-8	Microstructures of the 6820 steel (Verdeja et al., 2009).....	22
Figure 1-9	Microstructure of H13 tool steel (a) as received, (b) water quenched, (c) quenched and single tempered for 1 h, (d) quenched and single tempered for 2 h, (e) quenched and double tempered for 1 h and (f) quenched and double tempered for 2 h (Demir et al., 2018).....	24
Figure 1-10	The main locations and types of wear on cutting tool (Groover, 2010). ..	26
Figure 1-11	Cutting force on milling process (B. Li, Zhang, Yan, & Jiang, 2018).....	27
Figure 1-12	Mechanisms of chip formation (Toenshoff & Denkena, 2013).....	30
Figure 1-13	Dust production zones in milling process (Abdelhakim Djebara, 2012)..	33
Figure 2-1	Tempering characteristics for AISI 1045 steel (Dossett & Boyer, 2006)....	37
Figure 2-2	Heat treatment process for AISI 1045 steel .....	38
Figure 2-3	Olympus LEXT OLS4100 laser scanning digital microscope.....	39

Figure 2-4	Microstructures of AISI 1045 steel as received material ferrite (bright) and pearlite (dark): (a) magnification 200x and (b) magnification 500x.....	39
Figure 2-5	Microstructures of AISI 1045 steel after heat treatment.....	40
Figure 2-6	Workpiece preparation and slag thickness (Drawing not to scale).....	41
Figure 2-7	CNC milling machine (MAZAK NEXUS 410A).....	42
Figure 2-8	(a) Shell mill, (b) ceramic insert, (c) and (d) microgeometry of the honed and chamfered (T-land) cutting edge, respectively. ....	42
Figure 2-9	Face milling setup with the cutting tool and force dynamometer.....	43
Figure 2-10	Digital microscope KEYENCE VHX-500 FE.....	44
Figure 2-11	Scanning ElectronMicroscope (SEM) HITACHI TM3000.....	44
Figure 2-12	Surface roughness tester Mitutoyo SJ-400. ....	45
Figure 2-13	Surface roughness of Honed tool for cutting speed 350 m/min and feed rate 0.1 mm/th with two different material hardness (17 and 48 HRC).....	46
Figure 2-14	Surface roughness of T-land tool for cutting speed 350 m/min and feed rate 0.1 mm/th with two different material hardness (17 and 48 HRC).....	47
Figure 2-15	Aerosol Particle Sizer (APS), Scanning Mobility Particle Sizer (SMPS) and Condensation Particle Counter (CPC).....	48
Figure 3-1	Illustration of milling force components in the cutting zone.....	56
Figure 3-2	(a) Milling forces' signals in the X and Y directions, and (b) resultant force signal for machining test 8. ....	57
Figure 3-3	(a) Face milling setup with the cutting tool and force dynamometer, and micro-geometry of the (b) honed and (c) chamfered (T-land) cutting edge and (d) cutting edge forms with parametric edge dimensions (adapted from (Abdulkadir et al., 2018)).....	60
Figure 3-4	Main effects plot for resultant force.....	64
Figure 3-5	Main effects plot for power.....	67

Figure 3-6	Sample wear observed on honed and chamfered tool edge preparation at increased hardness (53 HRC). ....	68
Figure 3-7	SEM image of the microstructural morphology of used ceramic inserts...	68
Figure 3-8	Main effects plot for tool wear.....	70
Figure 3-9	Comparison of the predicted cutting forces as a function of workpiece hardness and milling modes. ....	72
Figure 3-10	Comparison of the predicted power requirements as a function of workpiece hardness and milling modes. ....	73
Figure 3-11	Comparison of the predicted tool wear as a function of workpiece hardness and milling modes.....	74
Figure 3-12	Performance chart between initial process parameters and improved experimental values for each response factors.....	76
Figure 4-1	Experimental setup for face milling and surface roughness tester. ....	85
Figure 4-2	Definition of the Arithmetic average height (Ra), and Maximum height of the profile (R <sub>t</sub> ) parameters. ....	86
Figure 4-3	Flowchart of the multi-objective optimization approach (adapted from (Jomaa, Levesque, Bocher, Divialle, & Gakwaya, 2017)).....	89
Figure 4-4	Grey relational analysis procedures.....	90
Figure 4-5	Example of SEM of tool wear in face milling experiments. (a) Experiment: Honed – (300m/min, 0.17mm/th, 53HRC) (b) Experiment: Chamfered – (200m/min, 0.17mm/th, 53HRC).....	94
Figure 4-6	Sample force time acquisition (experiment 12).....	95
Figure 4-7	Main effects plot for GRA. ....	99
Figure 4-8	Desirability response optimization plot for roughing operation. ....	100
Figure 4-9	Main effects plot for DFA.....	101
Figure 4-10	Main effects plot of GRA for finishing operation .....	106
Figure 4-11	Desirability response optimization plot for finishing operation .....	107
Figure 4-12	Main effects plot for DFA of finishing operation. ....	108

Figure 4-13	Comparison of optimal parameters between GRA and DFA for roughing operation. ....	111
Figure 4-14	Comparison of optimal parameters between GRA and DFA for finishing operation. ....	112
Figure 5-1	Microstructures of AISI 1045 steel: (a) before heat treatment consists of ferrite and pearlite structures, (b) after heat treatment consists of martensitic structures in retained austenite. ....	119
Figure 5-2	Cutting tools used: (a) tool holder, (b) ceramic insert, (c) specification cutting edge for honed and chamfered (T-land) in mm. ....	120
Figure 5-3	Metallic particles sampling instruments: APS (Aerosol Particles Sizer), SMPS (Scanning Mobility Particles Sizer) and CPC (Condensation Particles Counter) .....	121
Figure 5-4	Means response for Fine Particles (Honed tool).....	124
Figure 5-5	Main effects plot for Fine Particles (Honed t.....	125
Figure 5-6	Interaction plots for particles number concentration (Honed tool).....	126
Figure 5-7	Means response for Fine Particles when using a T-land tool. ....	128
Figure 5-8	Main effects plot for Fine Particles when using a T-land tool.....	128
Figure 5-9	Interaction plots for particles number concentration when using T-land tool.....	129
Figure 5-10	Particles number concentration as function of aerodynamic diameter for different workpiece hardness and feed rates: (a) Feed rate $f = 0.15$ mm/th; (b) Feed rate $f = 0.20$ mm/th.....	131
Figure 5-11	Particles number concentration for T-land tool as function of aerodynamic diameter for different workpiece hardness and feed rates: (a) Feed rate $f = 0.15$ mm/th; (b) Feed rate $f = 0.20$ mm/th. ....	132
Figure 5-12	SEM image of chip showing the effect of tool on the morphology of the free surface of the chip (workpiece hardness = 38 HRC) under the same cutting parameters settings. ....	133
Figure 6-1	Specification cutting edge (a) honed, (b) T-land (chamfered) in mm. ....	141
Figure 6-2	APS (Aerosol Particles Sizer), SMPS (Scanning Mobility Particles Sizer) and CPC (Condensation Particles Counter).....	141

Figure 6-3	Main effects plot for UFP (Honed tool).....	142
Figure 6-4	Interaction plots for number concentration ultrafine particles (Honed tool).....	143
Figure 6-5	Main effects plot for UFP (T-land tool).....	146
Figure 6-6	Interaction plots for particles number concentration ultrafine (T-land tool).....	147
Figure 6-7	Particles number concentration of ultrafine particles as a function of diameter with vsrious hardness of workpiece mterials used honed tool. ....	149
Figure 6-8	Particles number concentration of ultrafine particles as a function of diameter with vsrious hardness of workpiece mterials.....	150
Figure 6-9	Average of total particles number concentration UFP during honed and T-land tools.....	151



## LIST OF ABBREVIATIONS

ANOVA	Analysis of Variance
APS	Aerodynamic Particles Sizer
BUE	Built-Up Edge
CBN	Cubic Boron Nitride
CNC	Computer Numerical Control
CPC	Condensation Particles Counter
CVD	Chemical Vapor Deposition
DFA	Desirability Function Analysis
DOE	Design of Experiments
EPA	Environment Protection Agency
HSS	High-Speed Steel
FP	Fine Particles
GRA	Grey Relational Analysis
MQL	Minimum Quantity of Lubrication
MR	Machinability Rating
MRR	Material Removal Rate
PCBN	Polycrystalline Cubic Boron Nitride
PCD	Polycrystalline Diamond
PVD	Physical Vapor Deposition
RSM	Response Surface Methodology
SEM	Scanning Electron Microscopy
SMPS	Scanning Mobility Particles Sizer
UFP	Ultrafine Particles



## LIST OF SYMBOLS AND UNITS OF MEASUREMENTS

$A_c$	Uncut chip cross-section	[mm <sup>2</sup> ]
$C_t$	Specific heat of the cutting tool material	[N/mm <sup>2</sup> °C]
$C_w$	Specific heat of the workpiece material	[N/mm <sup>2</sup> °C]
$f_n$	Feed rate	[mm/tooth]
$F_c$	Cutting force	[N]
$F_x, F_y, F_z$	Cutting force components in x, y and z directions	[N]
$F_t$	Tangential force	[N]
$K_t$	Thermal conductivity of the cutting tool material	[W/m.°C]
$K_w$	Thermal conductivity of the workpiece material	[W/m.°C]
$P$	Power	[Kw]
$R_a$	Arithmetic average height	[μm]
$R_p$	Maximum height of peaks	[μm]
$R_q$	Root-mean-square roughness	[μm]
$R_t$	Maximum height of the profile	[μm]
$R_v$	Maximum depth of valleys	[μm]
$t_1$	Uncut chip	[mm]
$V_c$	Cutting speed	[m/min]
$\theta$	Cutting tool rotation angle	[deg.]
$\rho_t$	Density of the cutting tool material	[kg/m <sup>3</sup> ]
$\rho_w$	Density of the workpiece material	[kg/m <sup>3</sup> ]



## INTRODUCTION

Traditionally, machinability is a general term used to rate the ease (or difficulty) of metal removal. Today, the main goal of machining is to produce parts with high quality in a shorter cycle time and lower manufacturing costs, with environmentally friendly machining processes (green machining).

Machining of hardened steels and super alloys has become common in many industries for its advantages over grinding processes, it reduces production costs, reduces cycle time (Bouacha, Yallese, Mabrouki, & Rigal, 2010; Tamizharasan, Selvaraj, & Haq, 2006), avoids using coolant, improves material properties, decreases power and increases productivity (Davoudinejad & Noordin, 2014).

Recent improvements in machines, cutting tool materials (such as strength at higher temperatures, good resistance to wear, chemical stability inactivity, and improved toughness) and cutting tool geometry and edge preparation have led to an increase in the use of high-speed machining as the preferred industrial method for hardened steel and other alloy materials (Akhyar & Sayuti, 2015; Ashley, 1995; Dudzinski et al., 2004; Janmanee, Wonthaisong, & Araganont, 2014; Janmanee, Wonthaisong, Saodaen, & Ithisoponakul, 2014; B. Li, Zhang, Yan, & Jiang, 2018; B. Li, Zhang, Yan, & Zhang, 2018; Z. Liu, Ai, Zhang, Wang, & Wan, 2002; Vipindas, Anand, & Mathew, 2018; Z. Y. Zhao, Xiao, Zhu, & Liu, 2010).

The main objective of cutting-edge preparation is to produce a specific shape in the counter of a cutting edge tool (example honed, T-land, or combination of both). Furthermore, it improves the resistance of the cutting edge (resistance to chipping, notch-wear and fracture) and prepares the tool for the coating process (Kandráč, Maňková, & Vrabel, 2013).

Two types of cutting edge (sharp edge and prepared edge), as indicated in Figure 0-1, are usually manufactured. From Figure 0-1-a, the sharp cutting edge (before the edge preparation process) displays typical edge defects (burrs, micro fractures and irregularities). These defects on the surface cause chipping of the edge and impact the performance of the machining processes, resulting in a low cutting tool life and negative impact on the machined

part quality. By performing edge preparation, these problems can be solved by elimination of defects, generation of new edge geometry, modification of micro-topography of the edge (notch-less) and micro-structuring between the face and flank tool as shown in Figure 0-1-b.

During the cutting process, improvements in tool life and workpiece quality can be obtained by using a cutting tool with appropriate edge preparation. Cutting edge preparation creates new edge geometry and adjusts the micro topography of the edge. Moreover, it modifies the texture and roughness of the tool surface closest to the edge, therefore avoiding edge defects, improving the strength and performance of the tool, and enhancing the quality of the workpiece.

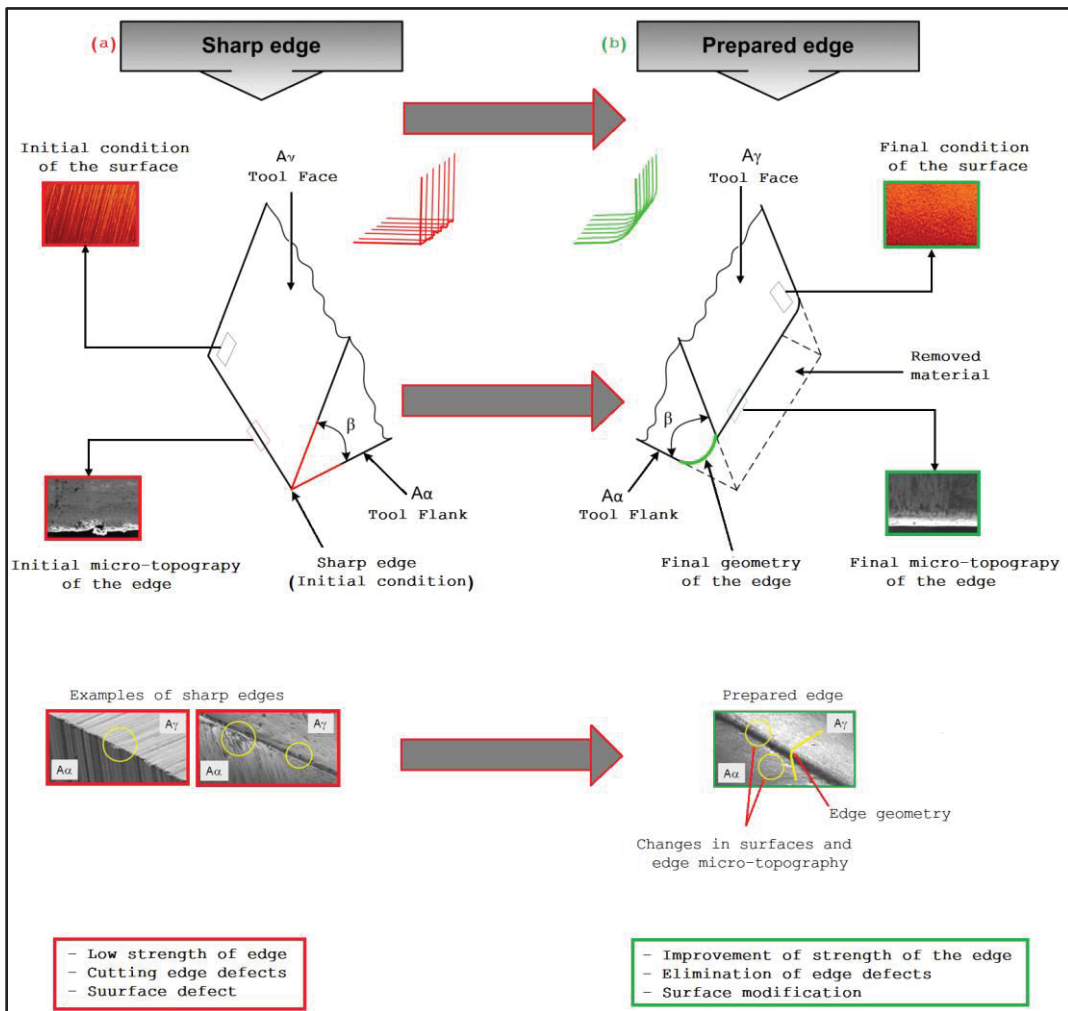


Figure 0-1 Input-output aspects of the cutting edge preparation process according to Rodríguez (Rodríguez, 2009)

Due to the development of new cutting tools (material, geometry), the machining of hardened steels has been widely investigated and is successfully replacing costly grinding operations (Lalwani, Mehta, & Jain, 2008). To reduce the wear and failure of the cutting tool and withstand the cutting pressure during the machining of hardened materials, cutting tool manufacturers have generated different new cutting edge micro-geometries (Denkena & Biermann, 2014). The edge preparations are used on advanced cutting tools made of polycrystalline cubic boron nitride (PCBN), cubic boron nitride (CBN) and ceramic. Elbestawi *et al.* (Elbestawi, Chen, Becze, & El-Wardany, 1997) have investigated the milling of AISI H13 steel (55 HRC) using PCBN ball-nose end mills with various edge preparations. This study shows that sharp edge preparations outperform honed and chamfered edges contrary to the tool manufacturer's specifications. Wojciechowski S. (Szymon Wojciechowski, 2015; S. Wojciechowski, Wiackiewicz, & Krolczyk, 2018) found that when milling with a flexible ball end nose tool, the obtained surface roughness is very sensitive to the selection of the cutting speed, while in the case of milling with a rigid tool, the surface roughness depends less on the cutting speed.

The influence of the cutting preparation on the machinability of hardened AISI H11 steel (40 – 50 HRC) was investigated by Benlahmidi *et al.* (Benlahmidi *et al.*, 2017). The authors observed that surface roughness decreases with increases of the cutting speed and hardness of the workpiece material, and increases with a decrease in feed rate, whereas the influence of the depth of cut was considered negligible. Aurich *et al.* (Aurich, Zimmermann, & Leitz, 2011) applied uncoated cemented carbide tools with edge radii ranging from 9 to 47  $\mu\text{m}$  to the face milling study of cast iron. They found that longer tool times and better machined surface roughness were obtained by rounded edges in comparison with a commercial product. Moreover, the performance of the prepared tools improved with the dimension of the generated hone radius.

Khettabi *et al.* (Khettabi, Songmene, & Masounave, 2007; Khettabi, Songmene, & Masounave, 2010; Khettabi, Songmene, Zaghbani, & Masounave, 2010) have identified in their research that cutting tool geometry (lead angle and rake angle) and the cutting speed have important effects on the generated metallic particles emission. Furthermore, Cheng *et al.* (Cheng, Liu, Wang, Wu, & Liu, 2014) found that dust concentration decreases with a

decrease of the insert rake angle and an increase of the cutting speed. Balout *et al.* (Balout, Songmene, & Masounave, 2007) and Songmene *et al.* (V Songmene, Balout, & Masounave, 2008a, 2008b) found that brittle materials generate dust emission less than ductile materials during dry drilling.

In this doctoral research study, we investigate experimentally, the cutting tool (inserts grade, edge preparation) and workpiece material interactions during the dry machining of hardened materials (AISI 1045 steels) used in industry. The studied cutting tools are honed and T-land with two type grades (KY2100, KY4300). The AISI 1045 steel was machined as received and after having been heat treated from 38 to 53 HRC. It is medium carbon steel characterized by good machinability and high tensile strength and it is using in several structural components (gears, crankshaft, etc.) for automotive industries. This material is selected in an attempt to provide a comprehensive study between the metallic particle emissions, the tool performance and productivity on manufacturers.

The orthogonal array design of experiments (DOE) named  $L_{32} (2^1 4^4)$  and  $L_{27} (3^3)$  are used to study the machinability indicators during hard milling of the AISI 1045 steel. Minitab 17 statistical software is used to design the experiments and to perform the analysis. The milling tool with ceramic inserts (material grade, edge preparation) inserts is employed. In these experimental tests, the three-component dynamometer, Mitutoyo SURFTEST SJ-410, an Aerosol Particles Sizer (APS), a Scanning Mobility Particles Sizer (SMPS) and a digital microscope are used to measure the cutting forces, surface roughness, dust emission, and tool wear, respectively.

The study is also performed to determine the optimal heat treatment conditions for balanced mechanical properties, cutting tool edge preparation, and machinability. Consequently, the results are useful for the heat treatment conditions at which the workpiece should be machined, and for the appropriate cutting tool profile. The best tool edge preparation and machining conditions for improved tool life, product quality as well as minimized dust emission are also presented.

## **Research Objectives**

The present study experimentally investigates the influences of the hardness of material and tool edge preparation during the machining of AISI 1045 steel. Hence, the main objectives of the present study are:

- 1- Study the effects of face milling of hardened AISI 1045 steel (38, 43,48, and 53 HRC) and tool cutting (edge preparation and grade materials) on machinability. The input machining factors to be studied include milling type, cutting speed, feed rate, material hardness, and tool cutting.
- 2- Investigate the cutting force and surface roughness during the machining of AISI 1045 hardened steel at optimal conditions. This investigation to be conducted using two multi-objective response methods (Taguchi-based grey relational and desirability function analysis).
- 3- Investigate the metal particles emission by studying the influence of workpiece material hardness and tool edge preparation on dust emission when machining AISI 1045 steel. The protection of workers and the environment in the workshop has become another machining performance variable to consider. Thus, reducing dust emission is essential during the machining process.

## **Thesis Outline**

The thesis contents are presented in six chapters in addition to the introduction, which includes thesis statement and objectives. The thesis is written by manuscript style.

Chapter 1 is dedicated to the literature review on machining of hard material, on the tool cutting (material, geometry and edge preparation), and on machinability.

Chapter 2 describes the experimental procedure (devices and equipment, workpiece materials and cutting tools) used to accomplish the declared objectives.

Chapter 3 is devoted to the applications of the Taguchi method (ANOVA) for the selection of optimum setting levels of cutting parameters for face milling of hardened steel AISI 1045 with ceramic inserts (various grades and different edges preparations).

Chapter 4 presents a comparison of two methods, Taguchi-based grey relational, and desirability function analysis to identify the most efficient method. Confirmation tests are also conducted to validate the result of the tests.

Chapters 5 and 6 focus, respectively, on fine and ultrafine metallic particles emission. An Aerodynamic Particles Sizer (APS) and a Scanning Mobility Particles Sizer (SMPS) are used to measure fine and ultrafine particles emissions, respectively. The factors investigated are cutting speed, feed rate, and material hardness by using two types of edge preparation.

The conclusions, main contributions, and recommendations are presented in additional sections at the end of the thesis.

## **CHAPTER 1**

### **LITERATURE REVIEW**

In manufacturing industries, it is fundamental to produce high quality products at low costs. This can be obtained by selecting the machining parameters that achieve high accuracy and low machining time. Recently, a great interest has arisen in cutting edge preparation. This interest has grown from multiple aspects, including the requirements of quality of finished products, decrease costs, flexibility, decrease production times, high productivity, and capacity to process new in materials.

#### **1.1 Machining of Hardened Steel**

##### **1.1.1 Hard Milling Machining**

Hard milling machining is a new technology that defined as the cutting process for a hardened workpiece material that has hardness state (45–65 HRC) and that directly uses cutter tools with special cutting materials and cutting edges. The hard-materials group includes hardened steels, high-speed steels, tool steels, Inconel, and cobalt alloys. These materials are used in the automotive, bearing, and machining molds and dies, as well as, for other components that are used in advanced industries (J Paulo Davim, 2014). Dry hard milling is competing with grinding and electrical discharge machining to produce good surfaces finish, especially in the manufacture of precision mechanical components such as dies and molds (Klocke, Brinksmeier, & Weinert, 2005; Toenshoff & Denkena, 2013; Zeilmann, Ost, & Fontanive, 2018). Furthermore, it is a lower cost, faster, more flexible, and environmentally friendly. Therefore, it more sustainable than grinding processes in many cases (Jovane et al., 2008; W. Li, Guo, & Guo, 2013).

Recently, the technologies have been developed new cutting tool materials and rigid machine, thus the hard-milling machining has become possible. Mixed ceramic, Cubic Boron Nitride (CBN), and Polycrystalline Cubic Boron Nitride (PCBN) tools generally used to machine the hard materials (Ajaja et al., 2019; Aslantas, Uzun, & Cicek, 2012; Benlahmidi et al., 2017; Hosseini, Hussein, & Kishawy, 2015).

### 1.1.2 Mode of Milling

The milling operations can be divided into up (conventional) and down (climb) milling operations as shown in Figure 1-1. In up milling, the motion of cutter rotation against the feed direction, while in down milling, the motion of cutter rotation is in the same direction as the feed motion. The uncut chip thickness differs continuously in milling. In up milling, the uncut chip thickness starts from zero and it increases with cutter rotation, while in down milling the uncut chip thickness starts from the largest thickness and it decreases to reach zero. The down milling has some advantages over the up milling:

- It requires simple and cheap fixtures because the cutting force in down milling is directed downward and tending to hold the workpiece on the machine table.
- The cutting force and power consumption in down milling are less compared to up milling.
- The chip length in down milling is less than in up milling. This means that the cutting tool is engaged in the workpiece for less time per volume of material cut, thus improving tool life.
- The surface finish produced in down milling is better than up milling.

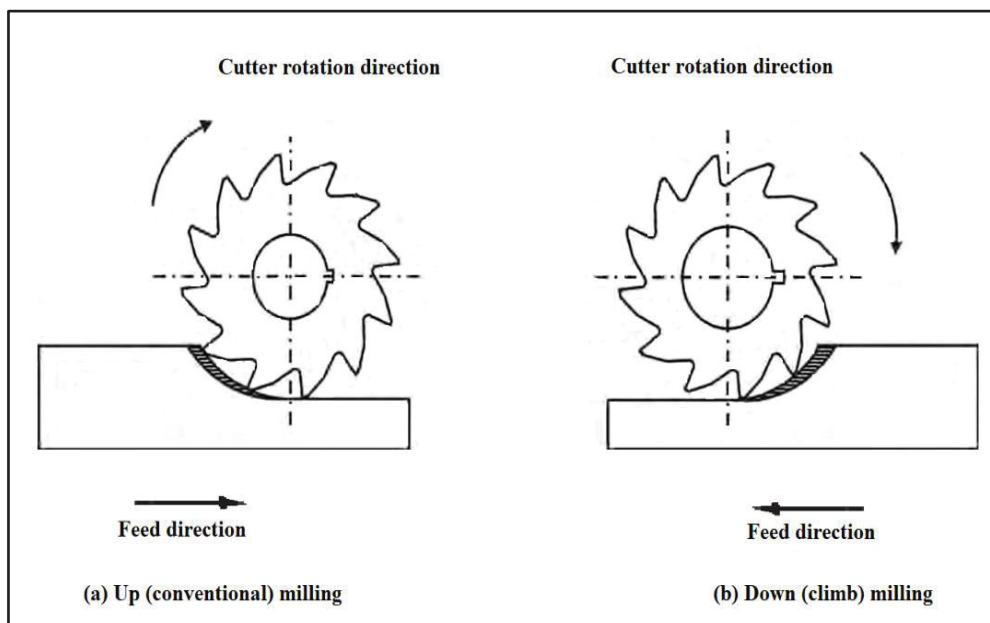


Figure 1-1 Types of milling operations: (a) Up (conventional) and (b) Down (climb).

## 1.2 Cutting Tool Materials

The cutting tool material is one of the important elements of the machining systems. Cutting tools are required to operate under high loads at elevated temperatures, often well in excess of 1000 °C. The material and geometry of the tool must be precisely chosen according to the workpiece material to be machined, the kinematics and stability of the machine tool to be employed, the amount of the material to be removed, and the required accuracy and finishing. Figure 1-2 illustrates hardness as a function of temperature for several tool materials.

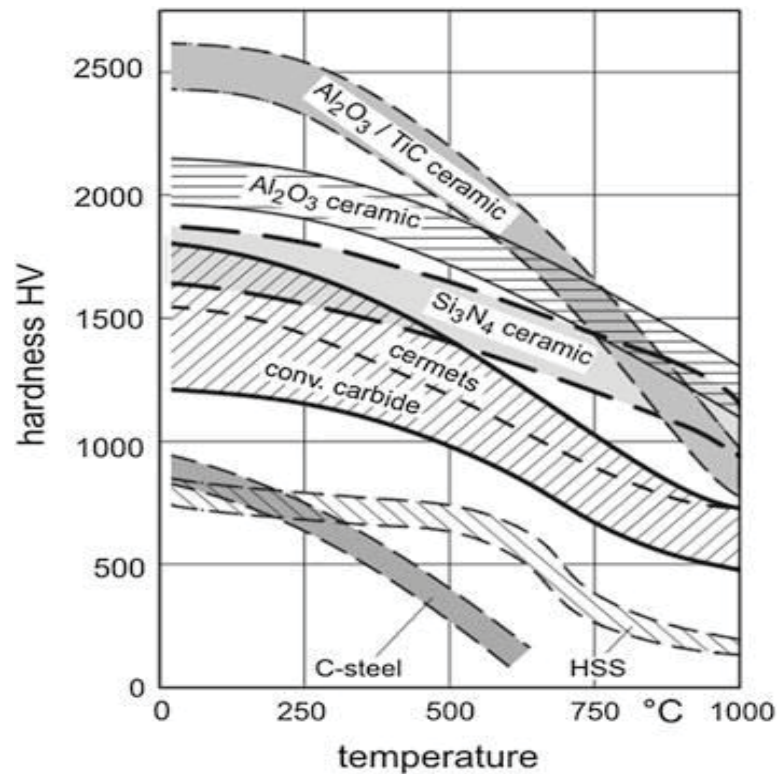


Figure 1-2 Hot hardness of tool materials (Toenshoff & Denkena, 2013).

Tool steel, before 1870 all lathe tools were forged from tool steel (carbon steel) consisting of about 1% carbon, 0.2% manganese, and the remainder iron. Carbon steel obtains its hardness and wear resistance by hardening process, which outputs a martensitic structure. These tools had a low hardness at elevated temperature (limited hot-hardness) and could only be used to

machine steel at relatively low speeds (up to about 0.08 m/s) as shown in Figure 1-2. Tool steel for higher loads additionally contains approximately the composition 2% carbon, 1.6% manganese, 5.5% tungsten, and 0.4% chromium. As a result, it could be used to speeds of about 0.13 (m/s). They are commonly applied for hand tools such as files and hand-reamers and for woodworking tools (Toenshoff & Denkena, 2013).

High Speed Steel (HSS) developed by Taylor and White (1901) are used to cut material at higher speeds (0.32 m/s) with more stability. The composition of this HSS was approximately 1.9% carbon, 0.3% manganese, 8% tungsten, and 3.8% chromium. Later, there were two additional significant developments in HSS. The first development, T group (tungsten) contains tungsten, chromium, vanadium, cobalt and carbon as principal alloying elements, while M group contains molybdenum, tungsten, chromium, vanadium, cobalt, and carbon. The maximum working temperature of HSS is around 500 °C. The mean hardness of HSS is 70 HRC. HSS tools are tough and suitable for interrupted cutting. HSS are used to manufacture tools of complex shape such as drills, reamers, taps, end mill and gear cutters. Tools could be coated to improve wear resistance. HSS can be used at cutting speeds between 10 m/min to 60 m/min (Smith, 2008).

Cemented Tungsten carbide tools were first developed in Germany in 1927 and produced by the Widia Corporation. These tools consisted of finely ground tungsten carbide particles sintered together with cobalt binder. Gradually during the 1930s, tools of the greater shock resistance were produced, but carbide tools were used mainly to turn cast iron and nonferrous metals due to greater tendency for steel to cause tool-face cratering. In about 1938, it was found that the tendency for carbide tools to crater when cutting steel could be reduced by adding titanium and tantalum carbides. During World War II the use carbide tools expanded rapidly.

Titanium and tantalum carbides are more stable than tungsten carbide and have a greater resistance to decomposition in the presence of  $\gamma$ -iron (FCC). Titanium carbides having a greater resistance to decomposition, have a dramatic effect on crater resistance of carbide tools when steel is machined at a high cutting speed (high tool-face temperature). The addition titanium carbide decreases the strength and abrasive wear resistance of tungsten

carbide tool. Tantalum carbide also provides crater resistance with less loss of impact strength than titanium carbide since it gives rise to less grain growth during sintering but costs more than an equivalent amount of titanium carbide. The net result of all of this is that there are two types of sintered tungsten carbide- one for machining gray cast iron, nonferrous metals, and abrasive non-metals such as fiber glass and graphite (ISO K-type) and one for machining ferrous metals (ISO P-type) (Shaw, 2005).

Ceramic tools are more refractory and harder than carbide tools, withstanding more than 1500 °C with good chemical stability. It recommends being used cut of hardened material (600 – 650 HV) at high cutting speed in dry cutting conditions. Ceramic tools are two basic types of ceramics: aluminum oxide based ( $\text{Al}_2\text{O}_3$ ) and silicon-nitride based ( $\text{Si}_3\text{N}_4$ ). The pure oxide-based ceramic has relatively low strength, toughness values, as well as low thermal conductivity. The additions of small amounts of zirconium oxide titanium, magnesium, chromium oxide to composition significantly improved toughness the pure ceramic. It is excellent for machining grey cast iron in dry and wet conditions at cutting speeds over 450 (m/min). The silicon-nitride ceramic has high toughness and high resistance thermal shock compared to pure oxide-based ceramic.

The ceramics reinforced by a non-homogeneous matrix of silicon carbide (SiC) whiskers ( $\text{Al}_2\text{O}_3 + \text{SiCw}$ ) are used mainly on the milling operation. The fine-grained silicon carbide crystal called a whisker. Whiskers are grained like hairs. The whiskers form 20–40 % of the total ceramic, improving highly tool toughness, hot hardness, wear resistance and making them suitable for milling operations. Whisker-reinforced ceramics are successfully applied to hard ferrous materials and difficult-to-machine super alloys.

Polycrystalline Diamond (CD) Industrial or synthetic diamonds date back to 1950s and are fabricated by heating graphite to around 300°C under very high pressure. Little or no binder is used. The crystals have a random orientation and this adds considerable toughness to the sintered polycrystalline diamond tools (SPD) compared with single crystal diamonds (SCD). Tool inserts are typically made by depositing a layer of SPD about (0.5) mm thick on the surface of a cemented carbide base. Very small inserts have also been made of 100% SPD (Groover, 2010). Polycrystalline diamond cutting tools are not utilised for machining ferrous

work pieces, this is because when machining under the high temperatures and sustained pressures that occur during cutting, the diamond has a tendency to revert back to graphite, after only a few seconds in-cut (Smith, 2008).

Cubic Boron Nitride (CBN) is one of the hardest materials available, and for machining operations, it can be considered as an ultra-hard cutting tool. It was first manufactured in the late 1950s. In many ways, CBN and natural diamond are very similar materials, as they both share the same atomic cubic crystallographic structure. Both materials exhibit high thermal conductivity, although they have greatly different properties. For example, diamond is prone to graphitization and it will easily oxidize in air, reacting to ferrous workpieces at high temperatures. However, CBN is stable at higher temperatures and can readily machine ferrous workpieces, such as tool steels, hard white irons, grey cast irons, and hard alloys. Normally, CBN tools should be used on workpiece materials with hardness greater than 48 HRC because the cutting edge will result in excessive tool wear (Smith, 2008). CBN inserts will provide extremely good wear resistance for a hard, sharp cutting edge. By using CBN inserts, an excellent machined surface finish with hard steel can be obtained. CBN has longer tool life than cemented carbide and ceramics, but it is high cost. Dry machining is always recommended to avoid thermal cracking (Coromant, 1994). Both CBN and PCD cutting tools can successfully machine: super-alloys (with low iron content), grey cast iron and non-ferrous metals, but show distinct differences when other workpiece materials are to be productively machined.

### **1.3 Cutting Edge Preparation**

The modern machining processes require good quality of the finished product, reduced production time, lower costs, ability to cutting new materials, flexibility and environmental. Therefore, the development of the new characteristics in cutting tools (material, coating, edge preparation) is helped to reach all these requirements. The edge geometry of cutting tools characterizes the actual shape of cutting-edge, which is the intersection between the flank and rake faces of the cutting tool. The main effects of cutting-edge preparation on cemented carbide inserts are summarized as a pre- and post-coating process as shown in Figure 1-3. The purpose of per-coating treatments is to achieve a consistent geometry to cutting-edge preparation (honed or chamfer). Accordingly, this preparation can be used to decrease the

chipping after grinding and burrs after sintering operations. Post-coating treatments purpose to reshape the cutting edge after coating and remove potential coating droplets (Bassett, Köhler, & Denkena, 2012).

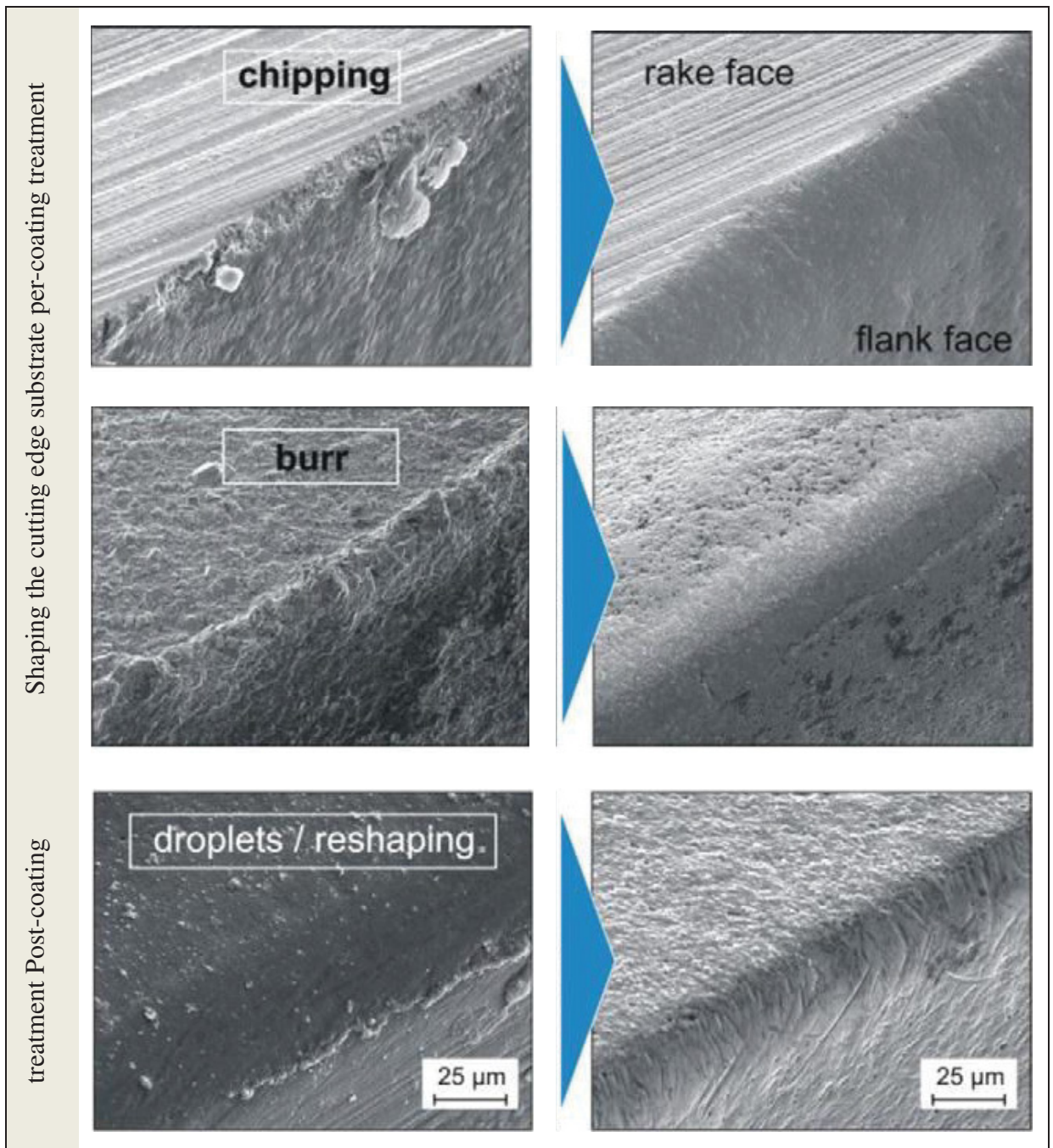


Figure 1-3 Main effects of the cutting edge preparation (Bassett et al., 2012).

Due to the influences of the tool edge preparation on the cutting tools machining performance, the researchers have become more interested in it and they published many researches (K-D Bouzakis et al., 2003; Denkena & Breidenstein, 2011; Toenshoff & Denkena, 2013; Zeilmann et al., 2018). The optimal cutting-edge shape concerning the cutting process is related to the machining parameters, the specifications of cutting tool and workpiece material (Bassett et al., 2012; Fulemova & Janda, 2014; B. Li, Zhang, Yan, & Jiang, 2018; C-F Wyen & Wegener, 2010).

#### 1.4 Classification of Cutting Edge Preparation Geometry

There are different types of edge preparation design supply by tool designers and manufacturers of tools. The major types of edge preparation design (sharp, rounded, and chamfered) are used in commercial cutting tools as shown in Figure 1-4 and 1-5. The sharp edge can be defined by the intersection between the rake face and the flank face.

It can be defined theoretically by the intersection of the rake face and the flank face of the cutting edge of tools. The sharp shape has an irregular and chipped profile with no specific parameters for the description. It is impossible to produce the ideal of cutting-edge shape. It is not suitable for many machining purposes due to its low instability against mechanical loads compared to the chamfered and rounded edges.

The rounded edge, the ideal round is uniform curvature of the rounded profile between rake face and flank face on tool edge. Furthermore, if the rounded edge has a different curvature, it has other types of geometries, namely, trumpet shape and waterfall shape as shown in Figure 1-4 (b). Denkena *et al.* (Denkena, Reichstein, Brodehl, & de León García, 2005) developed a characterization method to describe the asymmetrically rounded profile cutting edge. In this method, five parameters are obtained to describe the rounded profile of cutting edge as shown in Figure 1-5. The cutting-edge segment on the flank face ( $S_\alpha$ ) and the rake face ( $S_\gamma$ ) are the measure distance between the separation point of the cutting edge rounding and the tangent intersection between flank and rake faces, respectively. By on these values, the form-factor K (Kappa), which indicates the asymmetry of the curvature and the average cutting rounding ( $\bar{S}$ ) can be calculated. A ratio of K equal to 1 identify ideal round edge

(asymmetrical),  $k < 1$  identifies waterfall shape (slope towards the flank face) and  $K > 1$  identify trumpet shape (slope towards the rake) face as shown in Figure 1-4 (b). In addition, profile flattening ( $\Delta r$ ) and apex angle ( $\varphi$ ) are applied to characterize the tools' bluntness by measuring the shortest distance and the shift between the ideal sharp tooltip and the actual shape of rounding. By means of those parameters, the cutting-edge profile becomes imaginable.

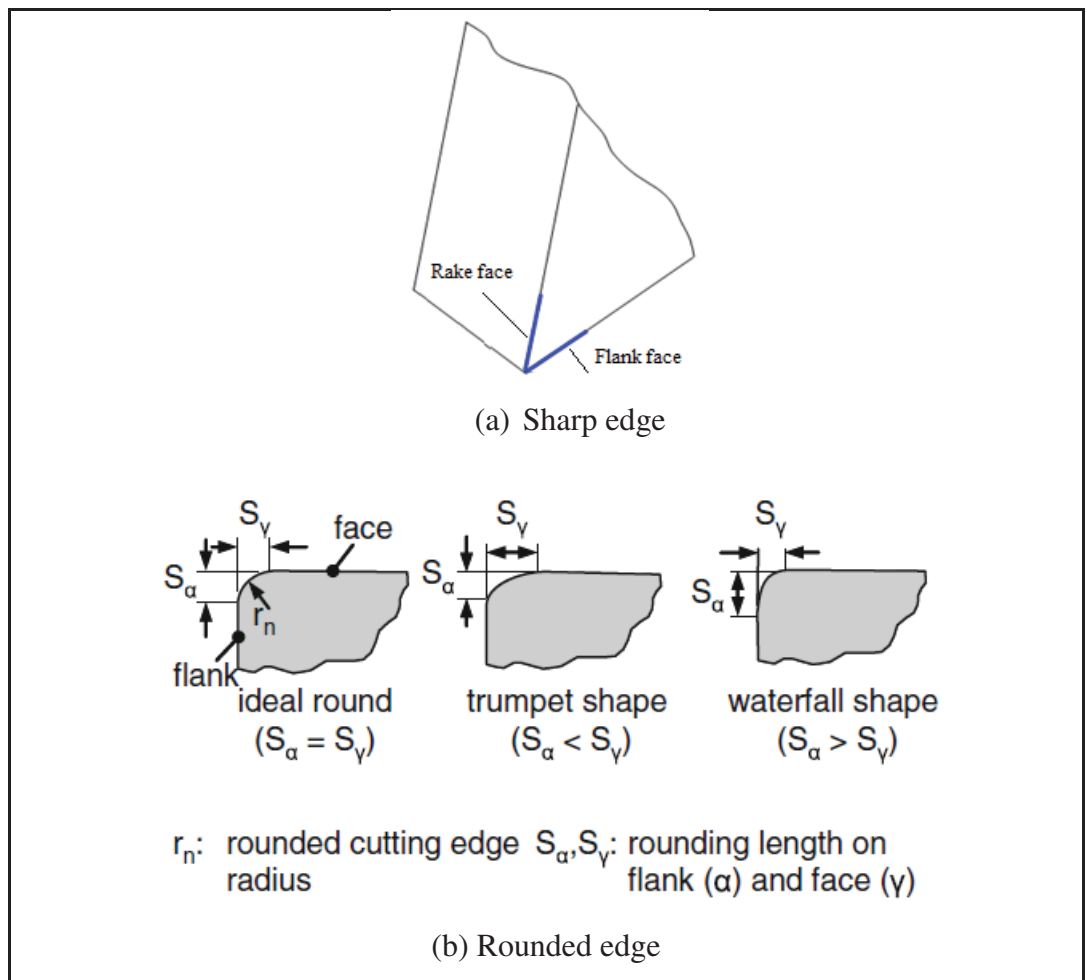


Figure 1-4 Types of cutting tool edges preparation design (Carl-Frederik Wyen, Knapp, & Wegener, 2012).

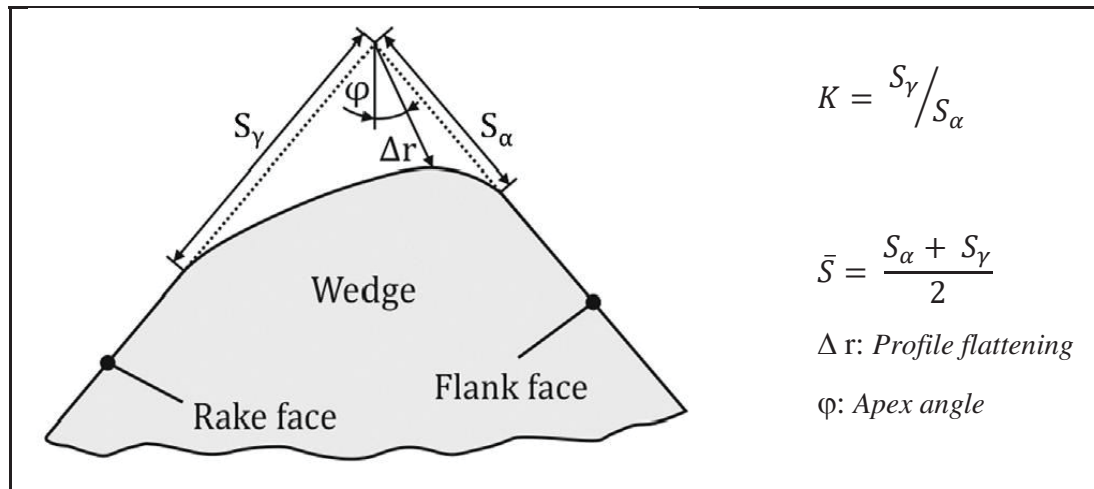


Figure 1-5 Cutting edge characterization of rounded edge (Denkena et al., 2005).

As shown in Figure 1-6, the chamfered can be defined by the plane surface that connects the flank face and the rake face. The chamfer is determined by the chamfer length ( $l_\beta$ ) and the chamfer angle ( $\gamma_\beta$ ). Moreover, the chamfer edges can be classified into single chamfer or double chamfer designed preparations.

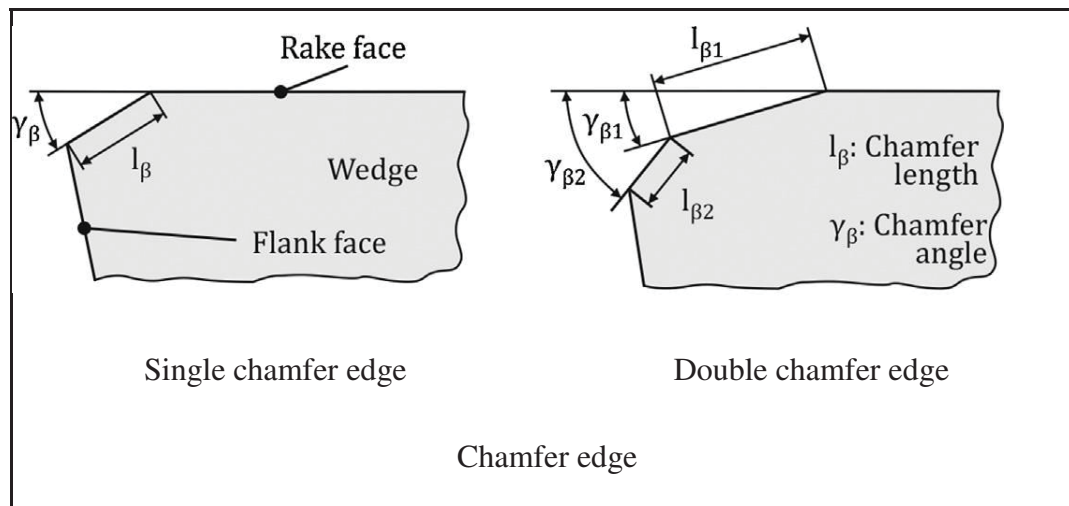


Figure 1-6 Types of chamfer edges preparation design (Denkena & Biermann, 2014).

Honed edge can reduce the initiation of notch wear, and it is usually used in finish and semi finish cutting. Chamfer edge is used in heavy rough cutting and interrupted cutting to increase the strength of cutting edge (Fang & Wu, 2005; Kandrác et al., 2013; Yen, Jain, &

Altan, 2004), and it also added the advantage of providing very stable built-up edge and good surface finish (Shaw, 2005). The most commercial cutting tool inserts are used honed edge radius between 5 and 150  $\mu\text{m}$ , while chamfered edge angle between  $20^\circ$  and  $40^\circ$ , and the chamfer width 0.1-2.0  $\mu\text{m}$ . Honed edges are often used on the diamond, Polycrystalline Diamond (PCD), and cemented carbide tools. Chamfered edges are often used on Cubic Boron Nitride (CBN), Polycrystalline Cubic Boron Nitride (PCBN), and ceramic tools (Fang & Wu, 2005). Table 1-1 shows the types of edge preparations with different cutting tool materials for different applications.

The goals of the cutting tool edge preparation are to strengthen the cutting edge, increase cutting tool, eliminate defects of the cutting edge, improve the quality of the part (surface finish and accuracy), and prepare a surface for deposition of coatings (Konstantinos-Dionysios Bouzakis et al., 2012; Denkena, Koehler, & Rehe, 2012; Denkena, Lucas, & Bassett, 2011; Toenshoff & Denkena, 2013).

Table 1-1 Type of cutting edges and their common application (Kandrač et al., 2013)

Cutting edge preparation	Common application	Commonly used
Round edge	Finished cutting	Diamond
	Semi-finish cutting	Polycrystalline diamond (PCD)
	Precision machining	High speed steel (HSS)
	Micromachining	Cemented carbide tools
Chamfered edge	Hard turning	Cubic boron nitride (CBN)
	Heavy rough cutting	Polycrystalline cubic boron nitride (PCBN)
	Interrupted cutting	Ceramic tools

During the last decade, the research works on the cutting edge preparation field have increased due to their importance in the development of manufacturing processes, and at the same time studying their effects on cutting forces, tool wear, life of tool, chip formation, distribution of temperature, and surface integrity.

The effect of cutting tool edge preparation modifies the chip formation, the cutting force, the surface finishing (Boy, Yaşar, & Çiftçi, 2016; Fang & Wu, 2005; B. Li, Zhang, Yan, & Jiang, 2018; B. Li, Zhang, Yan, & Zhang, 2018; X. F. Zhao, He, Liu, & Zheng, 2016), and the temperature (Bassett et al., 2012; Denkena, Köhler, & Mengesha, 2012; Yen et al., 2004). These parameters can also have an impact on the tool life (Denkena et al., 2011; Kim, Lee, & Sin, 1999; Meyer, Köhler, & Denkena, 2012; Panda, Sahoo, Rout, Kumar, & Das, 2018; Mohamed Shalaby & Veldhuis, 2018; C. Ventura, Köhler, & Denkena, 2015), and on the generation of metallic particles emission. The temperature during the machining process can make changes in the mechanical properties of the material, and it can modify the chip formation mode and the metallic particles emission. Many researchers (Benlahmidi et al., 2017; Chinchankar & Choudhury, 2016; Hua et al., 2005; R. Kumar, Sahoo, Mishra, & Das, 2018; Thiele & Melkote, 1999; C. E. Ventura et al., 2017) have studied influence of the cutting tool edge geometry in surface finish and cutting forces of hardened steels.

Khettabi *et al.*, (Khettabi et al., 2007) studied the influence of tool geometry, workpiece materials and cutting conditions on metallic particles emissions. Cheng *et al.*, (Cheng et al., 2014) studied the dust distribution characteristics using inserts with various groove profiles during the dry milling process. The positive tool rake angle reduces cutting forces, temperature, and power consumption; conversely, the negative tool rake angle (Fang, 2005). In addition, Arumugam *et al.*, (Arumugam, Malshe, & Batzer, 2006; Arumugam, Malshe, Batzer, & Bhat, 2003) found the polished Chemical Vapor Deposition (CVD) tools produce little metallic particles emissions than unpolished CVD and Physical Vapor Deposition (PCD) tools. Cutting tool material and geometry have significantly influenced on the machinability. For this reason, a carefully chosen relying on the type of workpiece material and the machining operation; in addition, lower costs of the tools.

## **1.5 Concept of Machinability**

The concept of machinability is the ability to machine workpiece material, meaning (how easy or difficult) with a cutting tool. The term machinability is used to describe the ease with which workpiece material is cut under selection cutting parameters. Machinability can be defined as an interaction phenomenon between the cutting tool and workpiece materials

under special cutting parameters, which used milling and turning processes. Improving machinability necessitate increasing castings quality, changing the cutting tool geometry and material, the cutting fluid or the condition of the fixtures, etc. The machinability is estimated by indicators such as tool life, tool wear, chip formation, surface integrity, metal removal rate, cutting force/power. (Coromant, 1994; J Paulo Davim, 2010, 2014; Mills & Mills, 1983; Ozcatalbas & Ercan, 2003; Trent & Wright, 2000).

Machinability testing usually involves a comparison of workpiece materials relative to that of base material. The measurement of performance in machinability testing includes tool life, tool wear, cutting force, power in the operation, cutting temperature and material removal rate under standard test conditions. Machinability Rating (MR) is an index number used to express the relative performance. The standard material used is given a machinability rate of 1.00 in which B1112 steel is often used as the base material in machinability comparisons. The materials have a rating of more than 1.00, are easier to machine, whereas the materials have a rating of less than 1.00 are difficult to machine (Groover, 2010).

### **1.5.1 Workpiece Material Condition (annealing, quenching and tempered)**

Annealing is heating of material above its upper critical temperature followed by cooling it to room temperature at a very slow cooling rate. Annealing is used to decrease the strength and hardness of the material, and it increases the ductility to improve the machinability. Furthermore, it modifies the microstructure of the material (desirable mechanical properties).

Quenching is heating of steel above the austenitizing temperature, followed by rapid cooling to produce amounts of martensitic in the microstructure of material; thus, getting a high degree of hardness. The hardness of the metal affects the amount of tool wear. Low values of hardness are usually favourable for machinability exempted from these very ductile materials where problems appear from the formation of the built-up edges in the form of poor surface texture, burr formation, and short tool life. Increasing the hardness by cold drawing has a positive effect on machinability.

### 1.5.2 Microstructural Influences on Machinability

Microstructure plays an important role in the machinability of a material (Hamed Hoseiny et al., 2013). Material structures affect machinability in which some structures can be abrasive properties and the strength of materials is altered with the type of structure. The amount and form of the carbides influence the material property. Chandrasekaran *et al.* (Chandrasekaran & M'Saoubi, 2006) presented a study for the machinability of P20-type steel and AISI H13 hot work tool steels in the hardened condition. The study proves that the influence of the microstructure (precipitates and carbide distribution) on machinability can be stronger than that of machinability enhancing additives.

Carbon is the most important alloying element in carbon steel, and depending on its content, different structures are obtained. There are three types of structures: ferrite, cementite, and pearlite, in addition to austenite that more directly influence machinability. Ferrite is ductile and soft, whereas cementite is hard and abrasive. Pearlite is a mix between ferrite and cementite in the form of lamellas of ferrite and cementite, and it raises an intermediate position in hardness. The hardness of lamellar pearlite additionally depends on the lamellas size. The fine lamellar pearlite type gives higher hardness than coarse. The amount of ferrite, pearlite, and cementite in steel structure depends fundamentally on the carbon content. Even small amounts of cementite have considerable influence on tool life and therefore machinability. In addition, ferrite steels in common have better machinability than martensitic steels (Coromant, 1994).

Demir (Demir, 2008) studies the effect of microalloyed steel pre-heat treatment on microstructure and machinability. The study indicated that the variation in machining properties of medium carbon microalloyed steel could be explained in terms of microstructure obtained through heat treatments. Figure 1-7 shows the evaluation of the microstructure for the microalloyed steel under various cooling conditions. Optical micrographs mentioned that the microstructure contains ferrite and pearlite structure, and the mean linear intercept grain sizes of as-received, air-cooled and furnace-cooled specimens were, respectively, 8, 7 and 9  $\mu\text{m}$ . From the figure, an increase is clearly seen in the cooling rate after heat treatment at 900°C for one hour, leading to finer grain sizes.

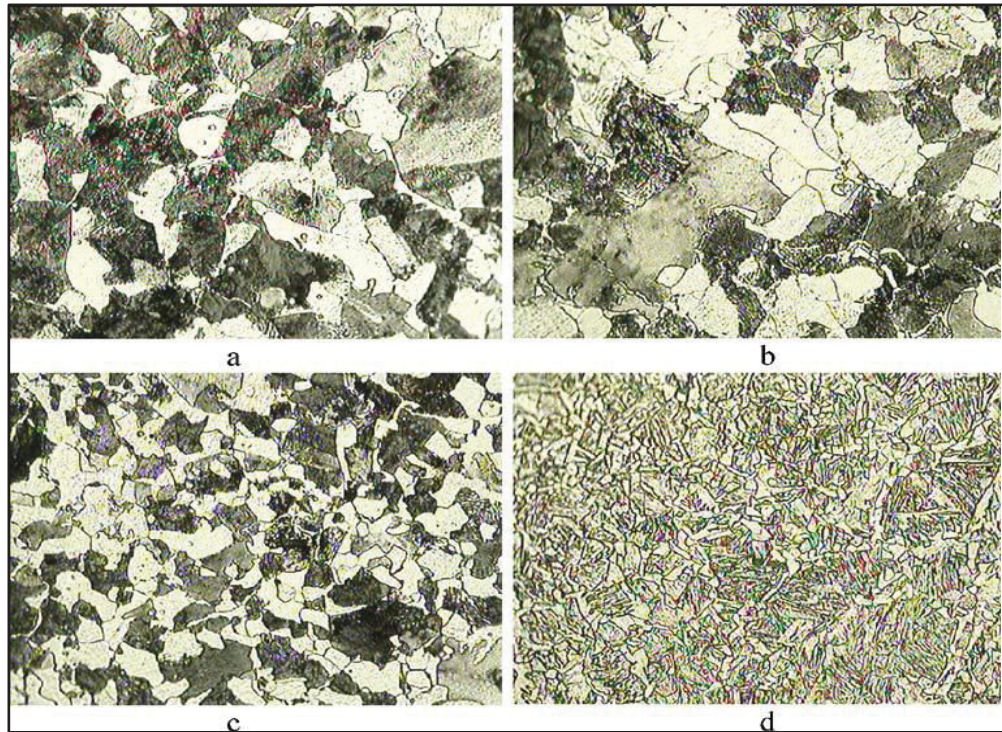


Figure 1-7 Microstructure of the microalloyed steels under conditions of (a) as-received, (b) furnace-cooled, (c) air-cooled, and (d) water cooled (Demir, 2008).

The studies by Verdeja *et al.* on the machinability of 8620 low carbon alloyed steel have shown the machinability improvement through heat treatment by  $\sim 16\%$  over the typical as-received cold drawn state. Figure 1-8 shows microstructures of the 6820 steel with different heat treatment (Verdeja, Verdeja, & González, 2009).

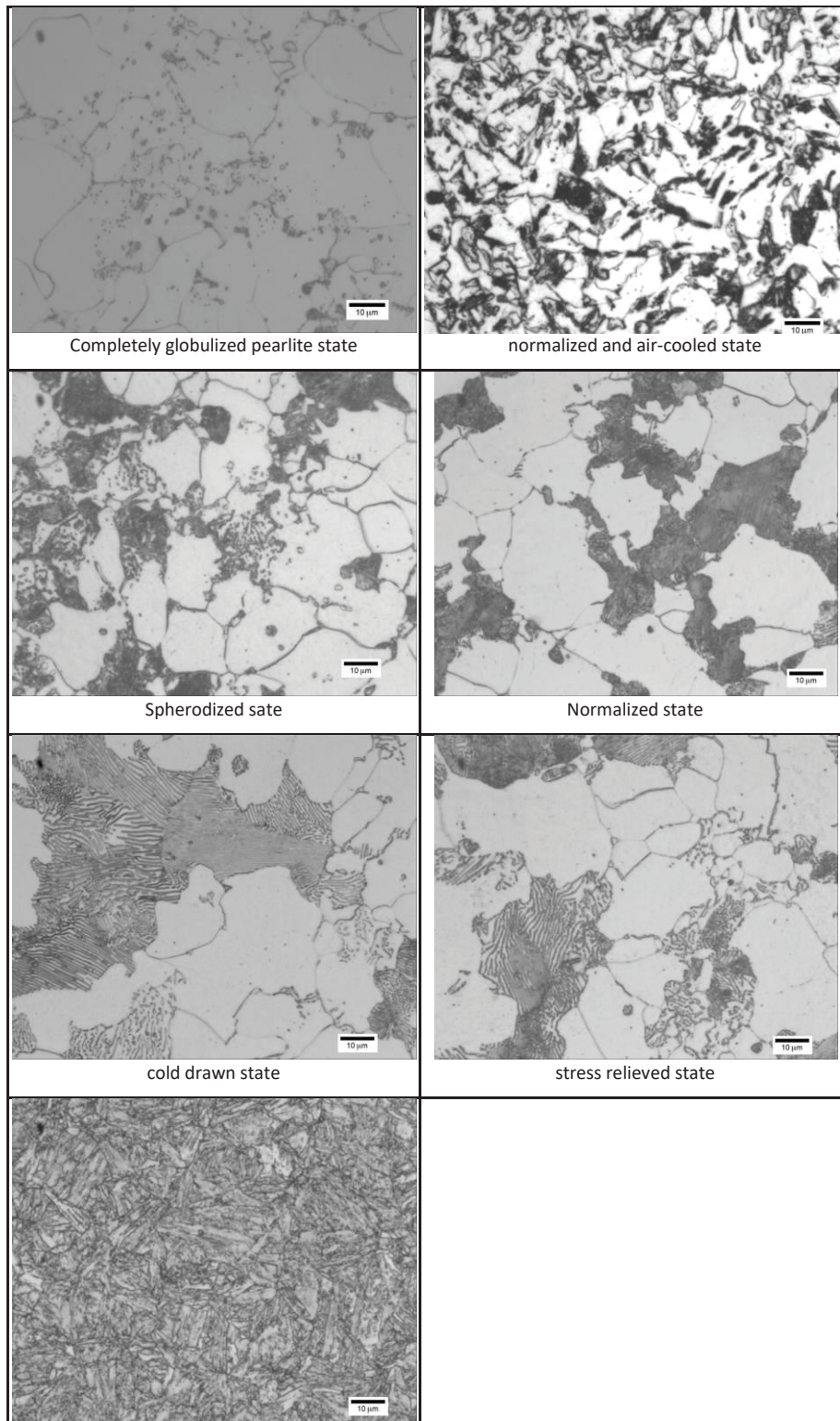


Figure 1-8 Microstructures of the 6820 steel (Verdeja et al., 2009).

Tan *et al.* (Tan, Ovali, Mavi, Kaplan, & Okay, 2015) have investigated the influence of repeated tempering on the machinability and microstructure of an AISI 52100 steel. The experimental results show that repeated tempering temperature and number of the passes significantly affect the microstructure and machinability of AISI 52100 steel. The hardness reduces with an increasing number of tempering and tempering temperature. The decreasing cutting force is found by increasing cutting speed and decreasing feed rate. By repeated tempering heat treatment, the machinability of AISI 52100 can be optimized.

More recent studies by Demir *et al.* (Demir, Gündüz, & Erden, 2018) investigated the influence of heat treatment on the microstructure and machinability of AISI H13 tool steel at various cutting speeds. In Figure 1-9, the microstructure of H13 tool steel with various heat treatments is illustrated. The microstructure of the steel in the as-received condition has a ferrite with the alloy carbides (Figure 1-9 (a)). The microstructure after quenching in water consists of martensite with fewer amounts of alloy carbides (Figure 1-9 (b)). Figures 1-9 (c, d), the samples show the microstructures of quenched and single tempered for 1 h and 2 h, respectively. Figure 1-9 (c) presents a tempered martensite structure composed of homogeneous distribution of alloy carbides in the ferrite phase. While in Figure 1-9 (d) the sample shows tempered martensite structure with some carbide particles, Figures 1-9 (e, f) show quenched samples and double tempered for 1 and 2 h, respectively. These changes in microstructure structures affect the mechanical properties and machinability of AISI H13 tool steel. The experimental results show that heat treatment conditions and the cutting speed affect the surface roughness of samples. Nevertheless, cutting forces are not affected by steel microstructure and cutting speed except to those of water-quenched samples.

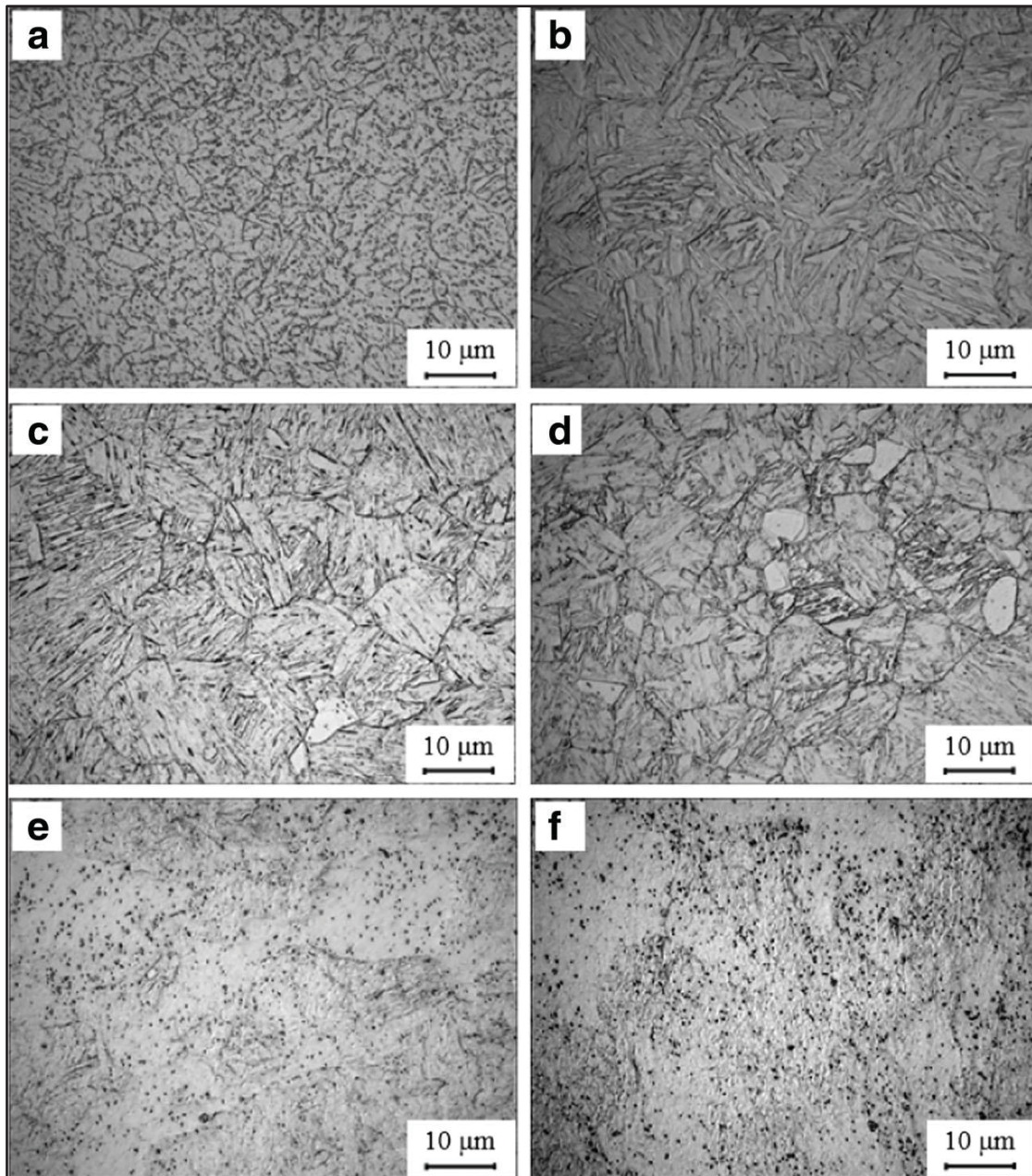


Figure 1-9 Microstructure of H13 tool steel (a) as received, (b) water quenched, (c) quenched and single tempered for 1 h, (d) quenched and single tempered for 2 h, (e) quenched and double tempered for 1 h and (f) quenched and double tempered for 2 h (Demir et al., 2018).

The machinability is significantly influenced by microstructures of material; however, the machinability depends on types of structure. Ferrite is ductile behaviour than cementite while pearlite is mixed between them. The spheroidized pearlite structure provides a better

machinability than lamellar pearlite structure because a lamellar pearlite is harder than a spheroidized pearlite (Okushima, Iwata, & Kurimoto, 1964). Lamellar pearlite size has more influence than hardness on machinability (Björkeborn, Klement, & Oskarson, 2010). Furthermore, the machinability on mold steel decreases with an increase in the martensite packet size (H Hoseiny et al., 2012). The grain size has a critical effect on the mechanical properties of workpiece material. Hence, the material with coarse grain size has good machinability than fine grain size. According to Vojcak (Vojcak, 1992), the increasing on the grain size (20 to 56  $\mu\text{m}$ ) reduced the tool wear by 10–50% depending on the structure.

The machinability can be improved by controlling on the microstructure of the material by optimizing heat treatment and achieving balancing between mechanical properties with machinability. In addition, improving product quality and reducing machining costs can be obtained with optimum heat treatment conditions. When developing a new microstructure of metals, the effect on machinability should always be given high priority in the industry.

## **1.6 Machinability Indicators**

### **1.6.1 Tool Wear Mechanisms**

All cutting tools wear during machining are working until they come to the end of their tool-life. The tool life was simply when the tool could not cut anymore. Today the usual significant parameters are surface texture, accuracy, tool-wear pattern, chip formation, and predicted reliable tool-life. The selection of the right cutting tool, in particular, the choices of tool-material and cutting geometry is crucial for achieving maximum productivity during machining. Tool wear is the product of a combination of load factors on the cutting edge, and it is the result of interaction between tool, workpiece material, and machining condition. The basic wear mechanisms dominate metal cutting such as abrasion wear, diffusion wear, oxidation wear, fatigue wear, and adhesion wear.

Most of these tool-wear mechanisms are accelerated at higher cutting speeds and temperatures. Diffusion and chemical reactions are especially sensitive to elevated temperature. During operation, wear occurs at two principal locations on a cutting tool: the top rake face (crater wear) and the flank (wear-land wear) illustrated in Figure 1-10.

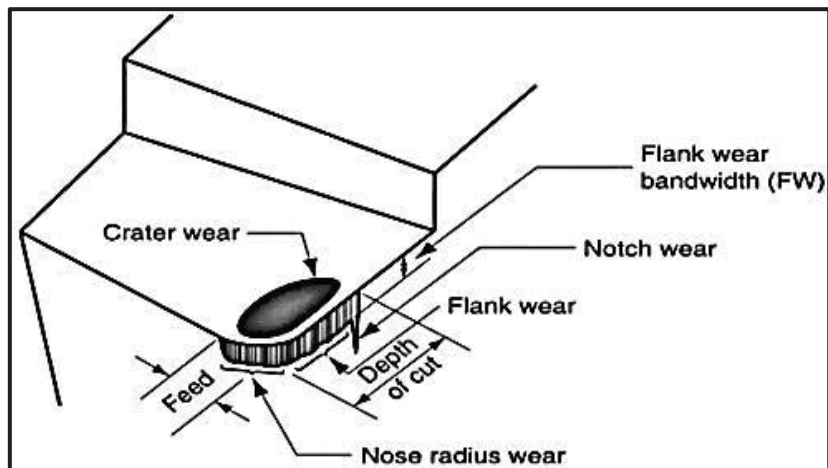


Figure 1-10 The main locations and types of wear on cutting tool (Groover, 2010).

### 1.6.2 Cutting Forces

Metal cutting needs a lot of power to separate the chip from the workpiece. There is a relationship between the power needed for the cutting process and the cutting forces involved. Cutting forces can be calculated theoretically and measured with a dynamometer. The workpiece material is placed on a dynamometer which mounted on the machined table. During the milling operation, the three cutting force components ( $F_x$ ,  $F_y$ , and  $F_z$ ) can be measured by the dynamometer relative to the machine table. For most workpiece material, increasing cutting speed leads to lower cutting force. The higher temperature in the flow-zone and reduced contact area contribute towards this effect. The decrease in forces varies with the type and condition of the material.

The movement of the insert is the combination of rotation and translation. Therefore, the cutting force ( $F_c$ ) and feed force ( $F_t$ ) for each cutting tool rotation angle ( $\theta$ ) can be calculated by using forces in the  $x$ - ( $F_x$ ) and  $y$ - ( $F_y$ ) directions, as shown in Figure 1-11. The uncut chip thickness or depth of cut ( $t_f$ ) varies with the tool rotation angle ( $\theta$ ) according to the relation. Cutting force ( $F_c$ ) and feed force ( $F_t$ ) can be obtained using the equations (1-1 and 1-2), respectively. (B. Li, Zhang, Yan, & Jiang, 2018; H.-T. Young, Mathew, & Oxley, 1994).

$$F_c = f_x \sin\theta + f_y \cos\theta, \quad (1-1)$$

$$F_t = f_x \sin\theta - f_y \cos\theta, \quad (1-2)$$

$$t_1 = f \sin \theta, \quad (1-3)$$

where  $f$  is the feed in mm/tooth.

The cutting force is proportional to undeformed chip thickness; thus, during a milling process, the largest cutting force appears when the cutting inserts just entering the workpiece and the rotation angle is very small which can be regarded as zero. If the cutting force is reduced, the required power of the cutting tool will be reduced as well. The power at the cutting tool can be obtained from equation (Sarhan, Sayuti, & Hamdi, 2012) as following:

$$P = \frac{F_c V_c}{1000}, \quad (1-4)$$

where  $P$  is the power in (KW),  $F_c$  is the cutting force in (N), and  $V_c$  is the cutting speed in (m/min).

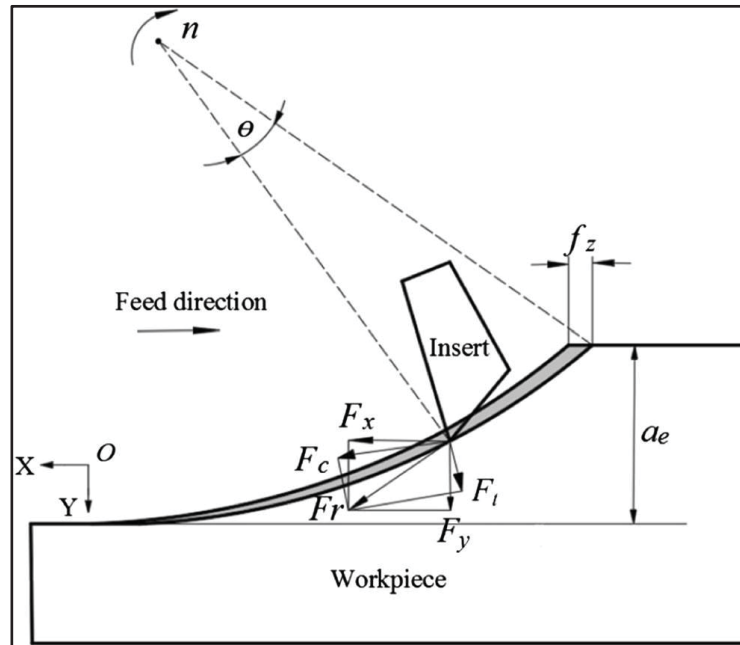


Figure 1-11 Cutting force on milling process  
(B. Li, Zhang, Yan, & Jiang, 2018).

### 1.6.3 Surface Roughness

Surface roughness plays an important role as it affects the fatigue strength, wear rate, coefficient of friction, and corrosion resistance of the machined components. In the machining process, the surface finish is influenced by several factors of the most important cutting tool (tool material, geometry edge preparation of tool), cutting parameters (cutting speed, feed rate, depth of cut), workpiece material characteristics, and cutting fluid (Singh & Rao, 2007).

Kumar *et al.* (A. S. Kumar, Durai, & Sornakumar, 2003) investigated machinability of EN 24 steel (40 and 45 HRC) using alumina based ceramic cutting tools. Two types of ceramic (Ti[C,N] mixed alumina ceramic and zirconia alumina ceramic) tools were used. They found that Ti[C,N] mixed alumina ceramic tool produces the surface finish better than zirconia alumina ceramic. Ghani *et al.* (Ghani, Choudhury, & Hassan, 2004) found that good surface finish can be obtained when end milling of AISI H13 hardened steel using at high cutting speed, low feed and low depth of cut when using the Taguchi method.

Benga and Abrao (Benga & Abrao, 2003) experimentally investigated the influences of cutting speed and feed rate on surface roughness when cutting during machining of 100Cr6 bearing steel (62–64 HRC) using ceramic and CBN tools. They found that feed rate was the highest significance factor on surface finish while cutting speed has less significance on the surface finish for both cutting tools.

Vivancos *et al.* (Vivancos, Luis, Costa, & Ortiz, 2004; Vivancos, Luis, Ortiz, & González, 2005) studied the effects of cutting parameters (cutting speed, feed rate, axial and radial depth of cut) on surface roughness and presented a mathematical model of surface roughness in high-speed milling of hardened steel using the technique of Design of Experiments (DOE).

Yang *et al.* (Yang, Chuang, & Lin, 2009) applied the Taguchi method to optimize dry machining parameters in end milling operation when machining high-purity graphite. The experimental results indicated that the feed rate was the most important factor to achieve a good surface finish and to improve the groove difference based on the first-order model.

Pu *et al.* (Pu & Singh, 2013) presented an experimental study to investigate tool wear mechanism and surface integrity in high-speed milling of hardened AISI A2 tool steel using coated tungsten carbide and PCBN tools. PCBN tools produce a better surface finish and less work hardening.

#### **1.6.4 Chip Formation**

The form of chip produced in machining is an important practical problem concern since it has important implications relative to personal safety, possible damage to equipment and product, handling and disposal of swarf after machining and cutting forces, temperatures, and tool-life. In cutting processes, the cutting penetrates into the workpiece edge material, which is thus plastically deformed and slides off along the rake face of the cutting edge. This is called chip formation. Figure 1-12 illustrates four types of chips, continuous chip, discontinuous chip, continuous chip with a built-up edge, and serrated chip.

Long continuous chips are formed when most ductile materials, such as wrought iron, mild steel, copper and aluminum, are machined at high cutting speeds and relatively small feeds and depth. Continuous chips formation in ductile materials is associated with reduced cutting forces (Boothroyd & Knight, 2006), and a good surface finish. A sharp cutting edge on the tool and low tool–chip friction encourages the formation of continuous chips as shown in Figure (1-12 a).

Discontinuous chips are formed into separate segments (discontinuous chip) when brittle materials, such as cast irons or cast brass, are machined at low cutting speeds. This tends to impart an irregular texture to the machined surface. Large depth, high feed, and high tool–chip friction of cut promote the formation of this chip type as shown in Figure (1-12 b).

Serrated chips are the discontinuous formation of a chip with still more or less connected elements that it possesses a saw-tooth appearance as shown in Figure (1-12 c). It occurs with negative rake angles, lower cutting speeds and a higher chip thickness (Toenshoff & Denkena, 2013). This type of chip is associated with certain difficult to machine metals such as titanium alloys, nickel-base superalloys, and austenitic stainless steels.

Continuous chip with Built-Up Edge (BUE) is formed when machining ductile materials at low-to-medium cutting speeds. The friction between tool and chip tends to cause portions of the work material to adhere to the rake face of the tool near the cutting edge as shown in Figure (1-12 d) (Boothroyd & Knight, 2006). The formation of a BUE is cyclical; it forms and grows then becomes unstable and then it breaks off. Much of the detached BUE is carried away with the chip, sometimes taking portions of the tool rake face with it, which reduces the life of the cutting tool. Portions of the detached BUE that are not carried off with the chip become imbedded in the newly created work surface, causing the surface to become rough (Groover, 2010). The size of the BUE tends to reduce as cutting speed increases when machining ductile materials.

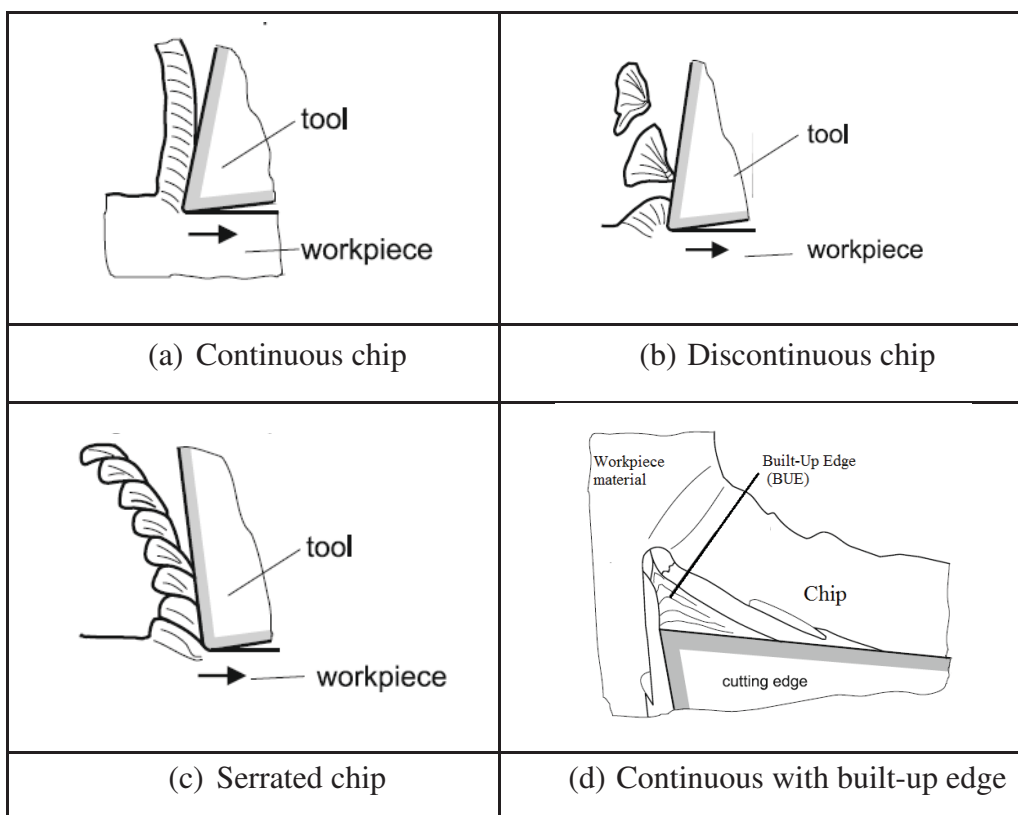


Figure 1-12 Mechanisms of chip formation (Toenshoff & Denkena, 2013).

## 1.7 Metallic Particle Emission and Measurement

### 1.7.1 Metallic Particle Emission

The protection of operators and the environment has become an additional machining process performance indicator, which must be taken into consideration. Aerosols and metallic particles (dust emission) generated during machining processes (milling, turning, grinding, and drilling) are harmful to both operators health and to the environment, and can deteriorate machine-tool parts (Cheng et al., 2014; Khettabi, Songmene, & Masounave, 2010; V Songmene et al., 2008a; Tönshoff, Karpuschewski, & Glatzel, 1997).

In general, exposure to metallic particles can generate health problems ranging from respiratory diseases to asthma and several types of cancer as fine particles (particles with aerodynamic diameters between 2.5  $\mu\text{m}$  and 10  $\mu\text{m}$ ) can go as far as into the alveoli and into the deepest parts of the lung (P. E. Holt, 1988; O. Witschger ; F. Fabrie`s, 2005). Some recent findings show that such particles, also known as nanoparticles, can be as harmful as fine particles (FP) when absorbed by body cells (Zhang, Kusaka, & Donaldson, 2000). Oberdörster *et al.* (Oberdörster, Oberdörster, & Oberdörster, 2005) prove that some inert particles could become biologically active if their dimensions are reduced to the nanometer scale. Ultrafine Particles (UFP) can migrate along the olfactory nerve (Kreyling et al., 2002) and penetrate the central neural system, eventually reaching the brain (Katz, Burkhalter, & Dreyer, 1984). Elder *et al.* (Elder et al., 2004) confirmed that some such particles could be found in the liver, kidney, and other organs. On the other hand, large particles do not represent a danger for human health, as they are easily expelled from the human body during coughing and sneezing.

The United States Environment Protection Agency (EPA) has promulgated new air quality standards concerning the fine particles  $\text{PM}_{2.5}$  (McClellan & Miller, 1997) that are implemented in 2005. At the same time, the cases of ultrafine particles started to raise scientific and researcher interests. The size of particles 0.1  $\mu\text{m}$  and under are considered as high risk factors for worker's health because they have high specific toxicity (Victor Songmene, Khettabi, & Kouam, 2012).

The work of Malshe *et al* (Malshe et al., 1998) indicates that most of the dust generated during machining consist of very fine particles (diameter smaller than  $1\mu\text{m}$ ). Their numeric concentration is around 10 to 35 times greater than that of the biggest particles around  $5\mu\text{m}$  in diameter, and they depend on the type of cutting tool used. Aitken *et al* (R. Aitken, Creely, & Tran, 2004) estimate that in England, around one million workers would be exposed to UFP via processes such as welding, working or processing of metallic materials.

### 1.7.2 Mechanisms of Particle Emission Production

The cutting process is used to produce the final product from metallic materials. Despite the several advantages of cutting machines, it is considered risky for workers and for the surrounding environment. In fact, all cutting processes produce aerosols in a liquid or solid form in different sizes that are harmful to both worker health and the environment. Solid aerosols are generated from part materials during dry and wet machining, while liquid aerosols are produced when cutting fluids are used (R. J. Aitken, Chaudhry, Boxall, & Hull, 2006; Zhong Chen, Atmadi, Stephenson, Liang, & Patri, 2000; Z Chen, Liang, & Yamaguchi, 2002; Zhong Chen, Wong, Li, Liang, & Stephenson, 2001; Dhar, Islam, Islam, & Mithu, 2006; Sutherland, Kulur, King, & Von Turkovich, 2000; Yue, Sun, Gunter, Michalek, & Sutherland, 2004). Sutherland *et al.* (Sutherland et al., 2000) found that the cutting process in wet condition produces more dust emission than the dry condition. In addition, the particles size is  $1\text{-}4\mu\text{m}$  generated during the dry cutting process, while the particles size is smaller than  $1\mu\text{m}$  in the wet cutting condition at high cutting speed.

The generation of dust particles during the cutting process is caused by different phenomena (Balout et al., 2007; V Songmene et al., 2008a). A schematic of the process (Figure 1-13) illustrates different sources of particles emission. The amount of dust is generated at the shearing zone ( $Z_1$ ). The deformation of the chip with friction during its formation produces an extra quantity of dust ( $Z_2$ ). Tool-chip friction zone, when the chip sliding on the rake face of the tool, undergoing a second deformation and friction, which leads to the production of a certain amount of dust ( $Z_3$ ). Tool-workpiece material friction zone, the cutting tool rubbing on the new cut surface of the workpiece produces more dust ( $Z_4$ ).

Khettabi *et al.* (Khettabi et al., 2007; Khettabi, Songmene, & Masounave, 2010; Khettabi, Songmene, Zaghbani, et al., 2010) found that cutting speed and cutting tool geometry (lead angle and rake angle) have a significant effect on the generated dust emission depending on the type of material. The authors further found that during experimentation the lead angle of  $90^\circ$  with a null or negative rake angle at high cutting speed generates less dust emission. Furthermore, Cheng *et al.* (Cheng et al., 2014) found that dust concentration is decreased with the insert rake angle decrease at high cutting speed.

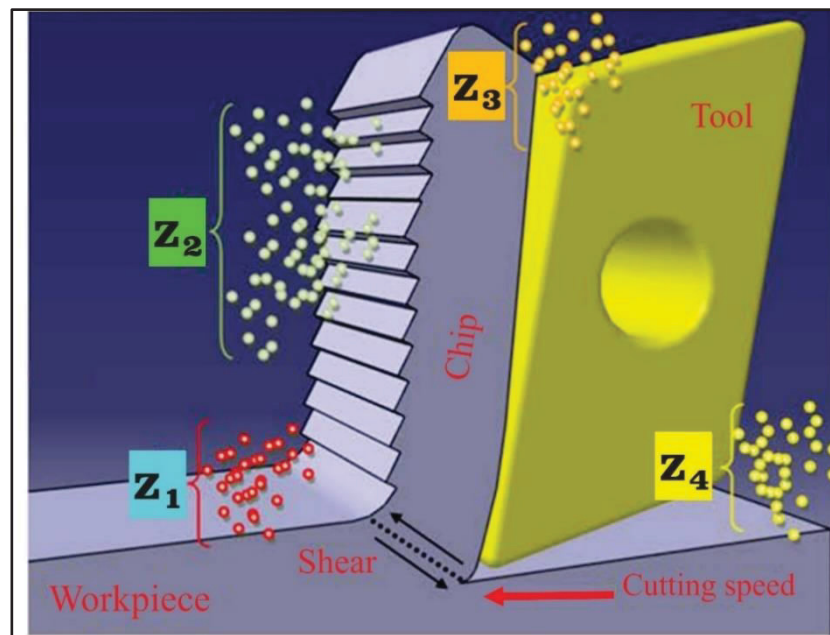


Figure 1-13 Dust production zones in milling process (Abdelhakim Djebara, 2012).

Kamguem *et al.* (Kamguem, Djebara, & Songmene, 2013) found that TiCN-coated tool generated low metallic particles emission compared to multi-layers (TiCN +  $Al_2O_3$ ), and reduced dust generation during milling machining of aluminum alloys (6061-T6, 2024-T351 & 7075-T6). Balout *et al.* (Balout et al., 2007) and Songmene *et al.* (V Songmene et al., 2008a, 2008b) found that brittle materials generate dust emission less than ductile materials. In the same manner, Khettabi *et al.* (Khettabi, Songmene, Zaghbani, et al., 2010) and Kouam *et al.* (Kouam, Songmene, Djebara, & Khettabi, 2012) show that the brittle material produces less emission dust than ductile materials.

However, there is not enough information in literature about the effect of tool edge preparation and heat treatment on dust emissions when machining hardened AISI 1045 steel. Therefore, in this research, the behaviour of dust emissions during the face milling of AISI 1045 steel is investigated. In addition, the optimum cutting parameters are selected to minimize dust emissions during face milling cutting.

## **1.8 Conclusion**

The literature review chapter summarizes the main conclusions connected to this research investigation and the main topics that have not received enough consideration and require further investigation.

Several criteria can be used to determine the machinability of metal such as the life of the cutting tool, cutting force, power consumption, surface texture, and metallic particles emission. The machinability of metal is affected both by cutting parameters (cutting speed, feed rate, axial and radial depth of cut) and by the metallurgical conditions of the workpiece itself. In AISI 1045 steel, metallurgical status like microstructure and hardness greatly influences the machinability index, and all these influences should be thoroughly investigated. Determining effect of the edge preparation tool and hardness value of the workpiece on the machinability characteristics of AISI 1045 steel is the major aim of this thesis. The relationship of these factors with the generation of metallic particles emission during dry machining is also investigated.

## CHAPTER 2

### METHODOLOGY AND EXPERIMENTAL PROCEDURE

This chapter is dedicated to methodology and experimental procedures that will be carried out in my research. The orthogonal array design of experiments named  $L_{32}$  ( $2^1 4^4$ ) and  $L_{27}$  ( $3^3$ ) will be used to study machinability hard milling of the AISI 1045 steel. The metallographic analysis is conducted to illustrate the microstructures of material before and after the heat treatment. The face milling with ceramic inserts is employed. In these experimental tests, the three-component dynamometer and the digital microscope are used to measure the cutting forces and the tool wear, respectively.

#### 2.1 Experimental Details

The orthogonal array  $L_{32}$  ( $2^1 4^4$ ) and  $L_{27}$  ( $3^3$ ) are selected to determine the optimal cutting conditions and to analyze the effects on the machinability index. The effect of different cutting conditions (milling type, cutting speed, feed rate and hardness of workpiece material) and ceramic cutting insert (edges preparation and grade of material) on machinability will be investigated with a set of designed multi-parameter orthogonal milling experiments. The axial depth of cut ( $a_p$ ) and radial depth of cut ( $a_e$ ) are constants. The cutting conditions and their levels for  $L_{32}$  and  $L_{27}$  are shown in Table 2-1 and Table 2-2, respectively.

Table 2-1 Cutting conditions and their levels for  $L_{32}$ .

Cutting Parameters	Level 1	Level 2	Level 3	Level 4
Milling type	Up	Down		
Cutting Speed [m/min]	200	300	400	500
Feed rate [mm/tooth]	0.05	0.09	0.13	0.17
Hardness [HRC]	38	43	48	53
Tools	T1 Honed (KY2100)	T2 T-land (KY2100)	T3 Honed (KY4300)	T4 T-land (KY4300)
Axial depth of cut [mm]	2.00			
Radial depth of cut [mm]	25.40			

Table 2-2 Cutting conditions and their levels for L<sub>27</sub>.

Cutting Parameters	Level 1	Level 2	Level 3
Cutting Speed [m/min]	250	350	450
Feed rate [mm/tooth]	0.10	0.15	0.20
Hardness [HRC]	17 (as-received)	38	48
Tools	Honed (KY4300)	T-land (KY4300)	
Axial depth of cut [mm]	1.0		
Radial depth of cut [mm]	25.40		

In the Orthogonal array L<sub>32</sub>, the increment in hardness of workpiece material was by 5 HRC as showed in Table 2-1 and in the Orthogonal array L<sub>27</sub> the increment was 10 HRC as illustrated in Table 2-2.

## 2.2 Workpiece Material

In this study, AISI 1045 steel rectangular blocks are used as the workpiece material. The two sizes of the workpiece material that used in this research are 100 mm × 45 mm × 25 mm, and 250 mm × 100 mm × 25mm, respectively. The chemical composition of AISI 1045 steel is listed in Tables 2-3.

Table 2-3 Chemical composition of workpiece material (% weight).

C	Mn	P	S	Si	Fe
0.459	0.721	0.0086	0.0027	0.259	balance

Four different hardness are used in the experimental tests. All samples of AISI 1045 steel were austenized at temperature of 850 °C for 1.5 hours in a muffle furnace, and followed by quenching process in media of water, and tempering in the range of 260 – 470 °C for 2 hours depending on the targeted hardness value (38, 43, 48, 53 HRC), respectively. These processes are based on Figure 2-1 (Dossett & Boyer, 2006). Details of the thermal treatment process for 1045 steel workpiece are given in Table 2-4 and are illustrated in Figure 2-2.

The metallographic samples were etched in a nital solution (3%) after coarse, medium grinding, and final polishing with 1-micron diamond. The Olympus LEXT OLS4100 laser scanning digital microscope (Figure 2-3) was used to analyze the microstructure of as-received material, and after the tempering process, as shown in Figures 2-4 and 2-5, respectively.

Table 2-4 Heat treatment process for AISI 1045 steel.

Hardness of workpiece material	Temperature (°C)	
	Quench	Temper
38 HRC	850	470
43 HRC		410
48 HRC		345
53 HRC		260

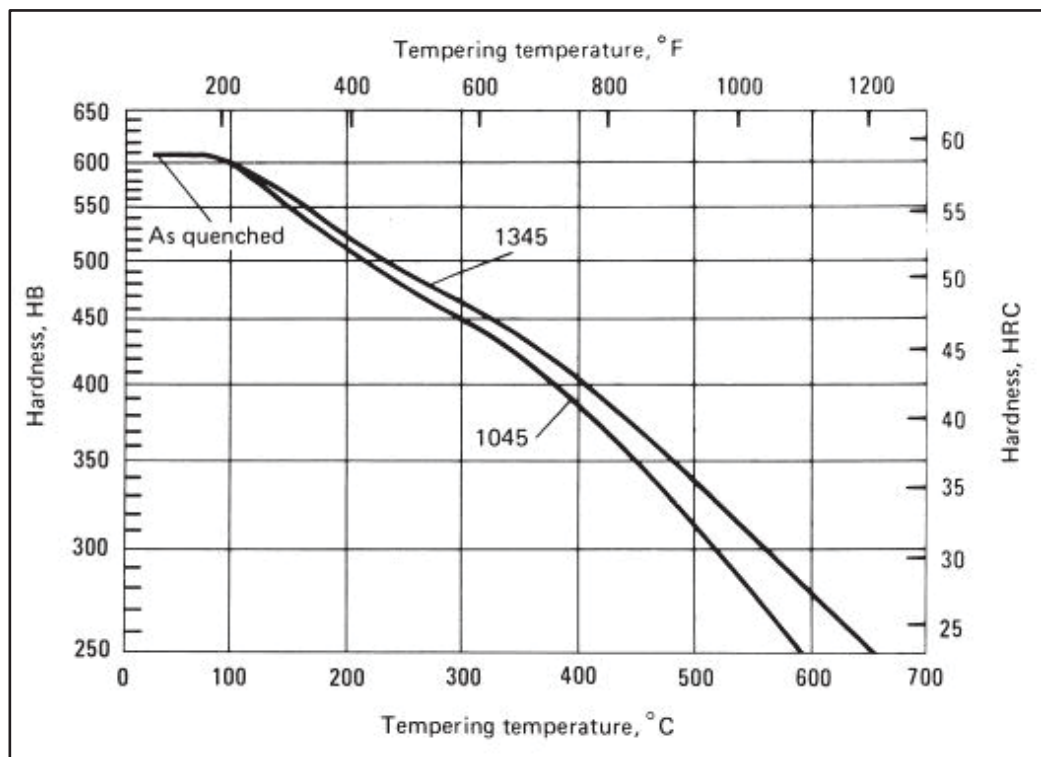


Figure 2-1 Tempering characteristics for AISI 1045 steel (Dossett & Boyer, 2006).

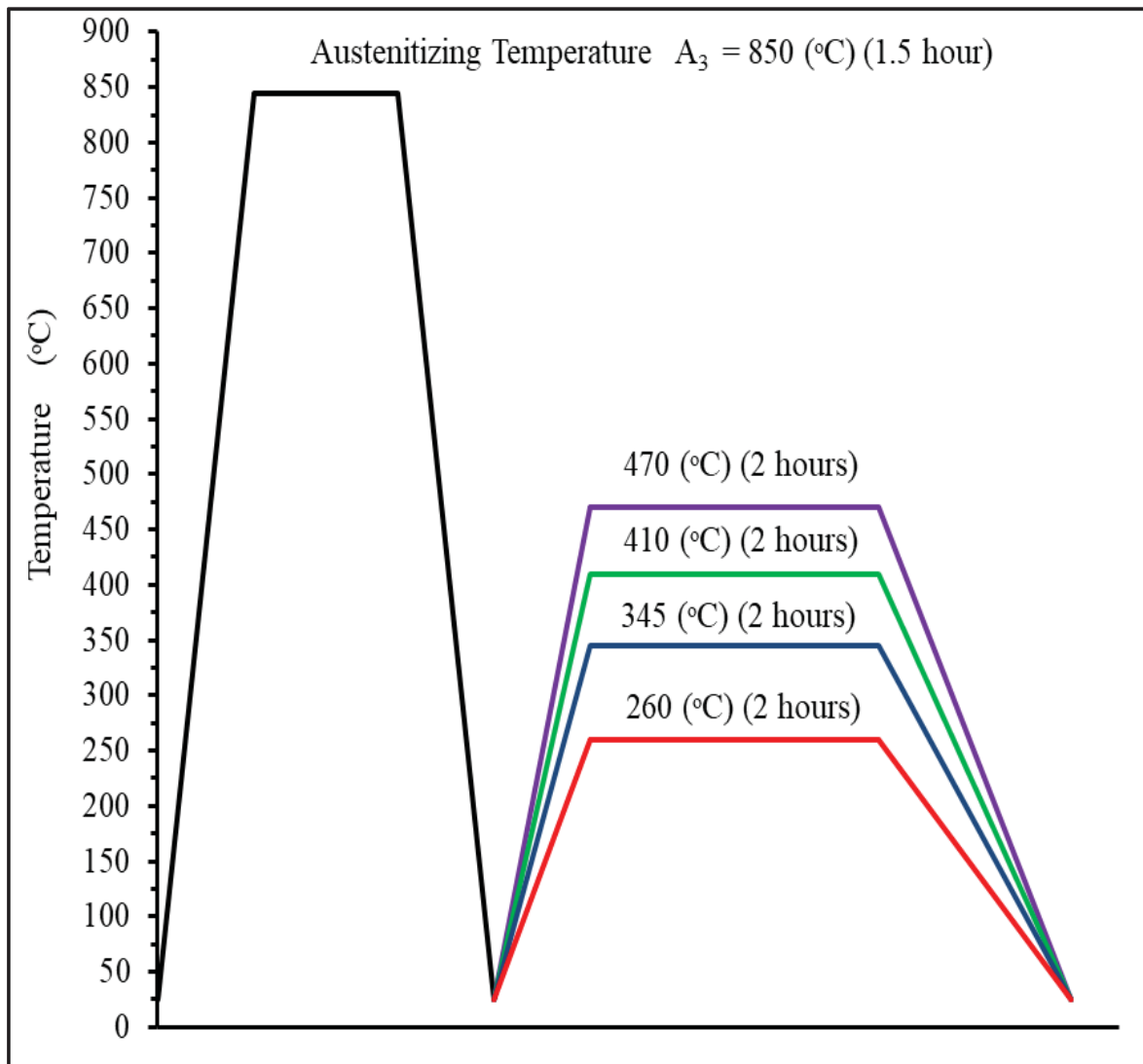


Figure 2-2 Heat treatment process for AISI 1045 steel

The microstructure consists of ferrite and pearlite structures as-receive material and after heat treatment the microstructure consists of martensitic structures in retained austenite. After heat treatment of AISI 1045 steel, cleaning the slag from all sides of workpiece material are machined by milling process with slag thickness of (0.2-0.3 mm) as shown in Figure 2-6.



Figure 2-3 Olympus LEXT OLS4100 laser scanning digital microscope.

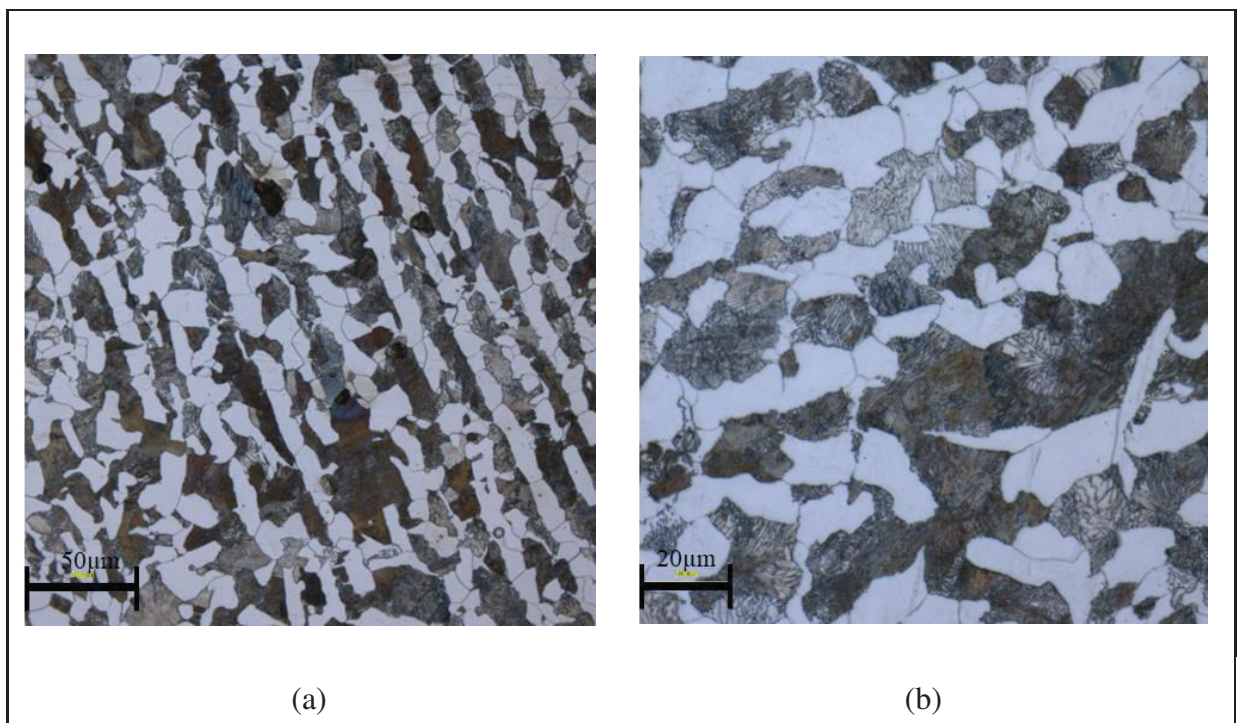


Figure 2-4 Microstructures of AISI 1045 steel as received material ferrite (bright) and pearlite (dark): (a) magnification 200x and (b) magnification 500x.

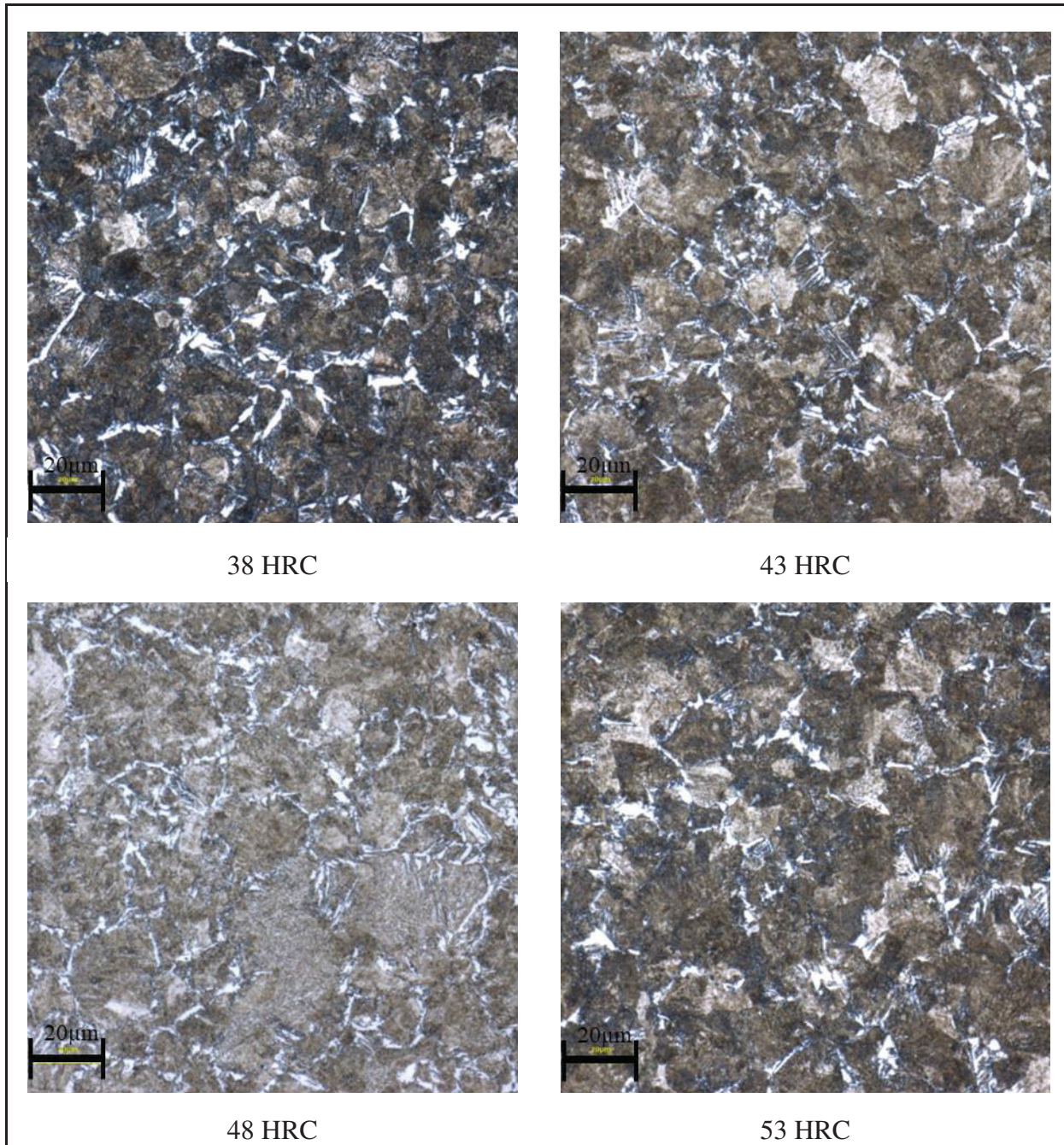


Figure 2-5 Microstructures of AISI 1045 steel after heat treatment.

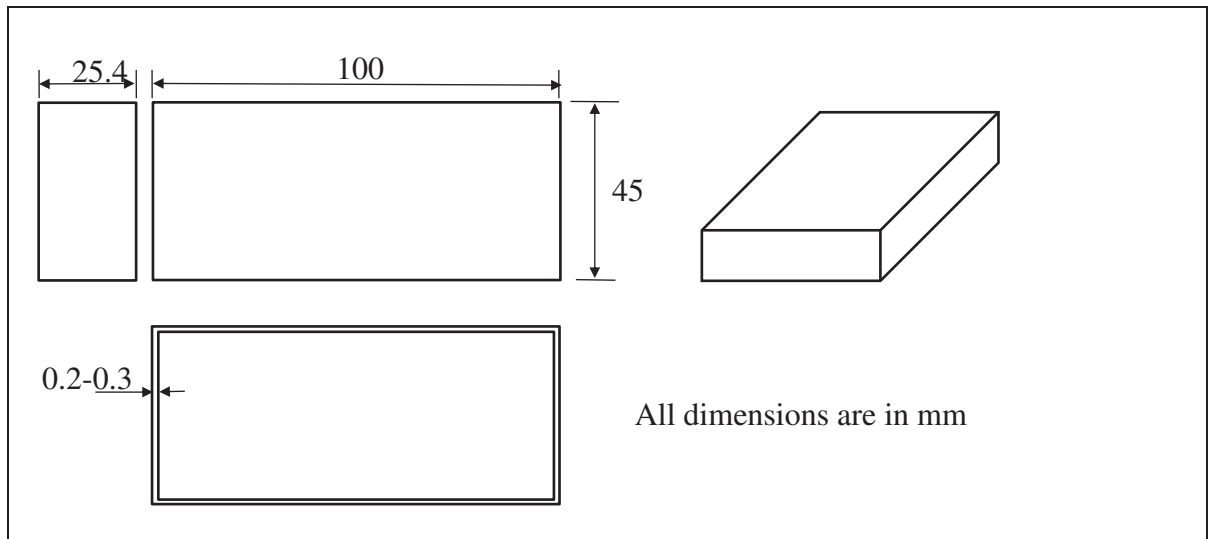


Figure 2-6 Workpiece preparation and slag thickness (Drawing not to scale).

### 2.3 Face Milling Tests

In this study, the experimental tests are carried out on a MAZAK NEXUS 410A vertical CNC milling machine (Max. RPM = 12000 rev/min, power at 5000 rpm = 25HP) under dry machining conditions as shown in Figure 2-7. The cutting tool, round ceramic inserts with two edge preparation (T-land and honed), and two different grades (KY2100, KY4300) are used in the machining tests as indicated in Table 2-5. A shell mills type KDNR250RN40C3 tool holder (from Kennametal) with four inserts is used as shown in Figure 2-8. The cutting tool holder and cutting edge that used in this research are summarized in Table 2-6. New cutting inserts were used after each cutting pass experiment. All cutting conditions were selected based on the tool manufacturer's recommendations for the machining of hardened steel during environmentally friendly machining processes (dry machining).

Table 2-5 Specification of the ceramic insert (Kennametal, 2013).

Tool ID	Edge preparation	Kennametal Grade Name	Grade Description
1	Honed (RNG45E)	KY2100	Silicon Nitride (SiAlON) base ceramic
2	T-land (RNG45T0420)		
3	Honed (RNG45E)	KY4300	Whisker ceramic with a matrix of $Al_2O_3 + SiCW$
4	T-land (RNG45T0420)		



Figure 2-7 CNC milling machine (MAZAK NEXUS 410A).

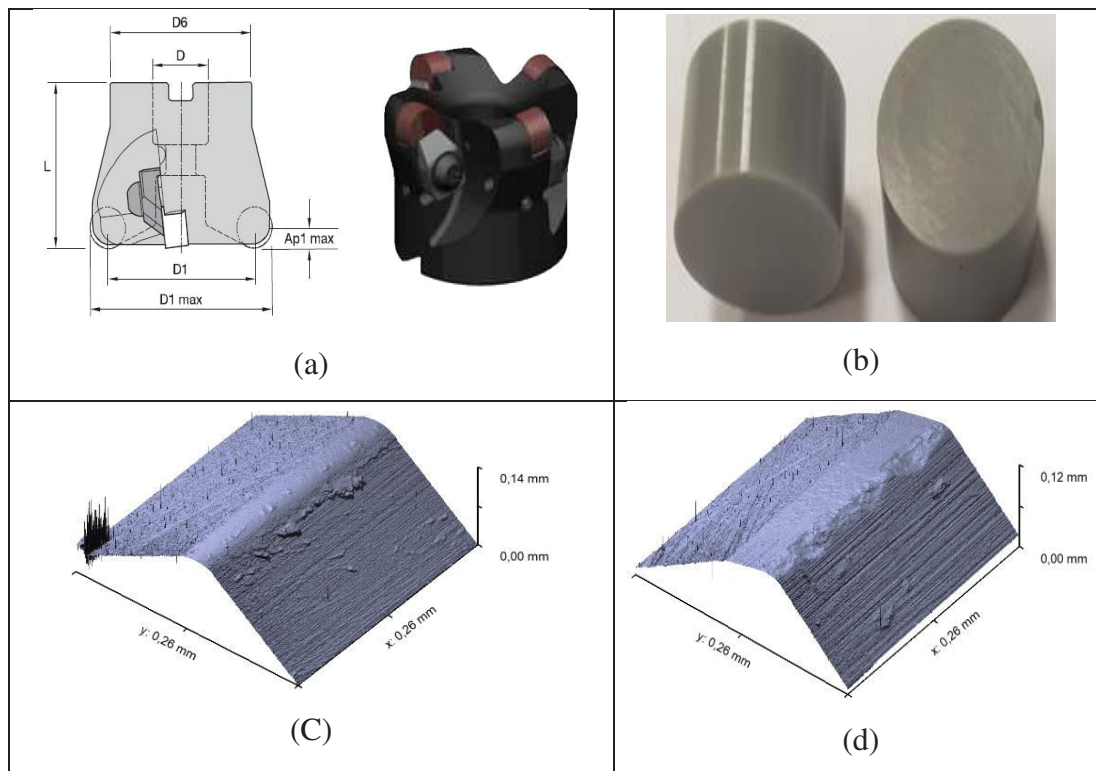
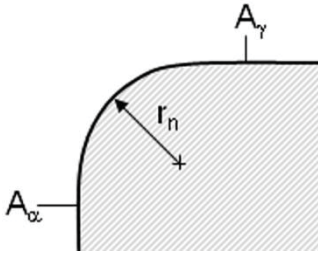
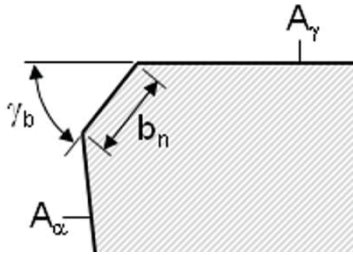


Figure 2-8 (a) Shell mill, (b) ceramic insert, (c) and (d) microgeometry of the honed and chamfered (T-land) cutting edge, respectively.

Table 2-6 Specification (a) cutting tool holder and (b) cutting edge in mm (Kennametal, 2013).

(a)							
Catalog number	D1 <sub>max</sub>	D1	D	D6	L	Ap1 <sub>max</sub>	z
KDNR250RN40C3	63.5	50.8	19.15	49.53	50.8	6.324	4
(b)							
	$r_n$	0.03048 $\pm 0.010$		$A_\alpha$	0°		
	$A_\gamma$	0°					
	$b_n$	0.1016					
	$\gamma_b$	20°					

The three cutting force components ( $F_x$ ,  $F_y$ , and  $F_z$ ) were measured during the machining process using a three-component dynamometer Kistler® dynamometer (Kistler 9255-B) erected in the milling machine (Figure 2-9). The cutting force signals were acquired at a sampling rate of 48 kHz. Following the force acquisition, MATLAB® was used to process the cutting forces signals.

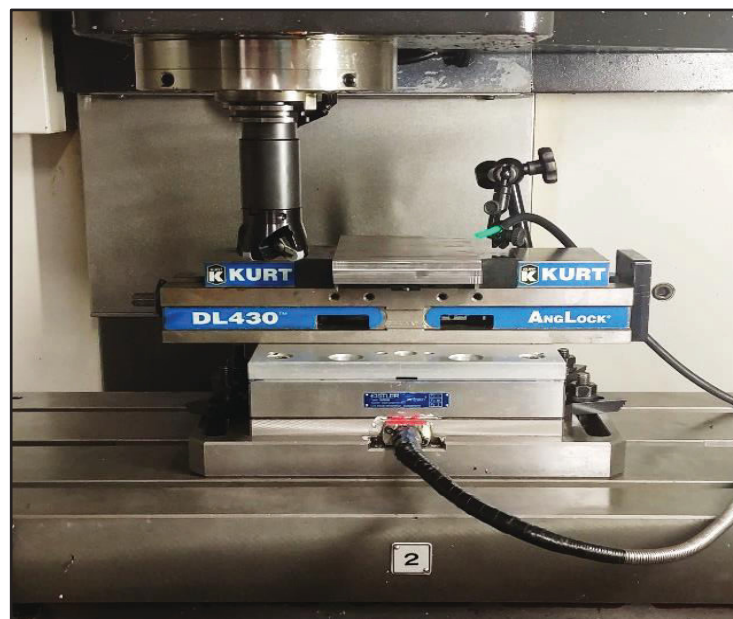


Figure 2-9 Face milling setup with the cutting tool and force dynamometer.

After each cutting machining, tool wear measurement was performed using the KEYENCE VHX-500 FE digital microscope and a scanning electron microscope (SEM) as shown in Figures 2-10 and 2-11, respectively.



Figure 2-10 Digital microscope KEYENCE VHX-500 FE.

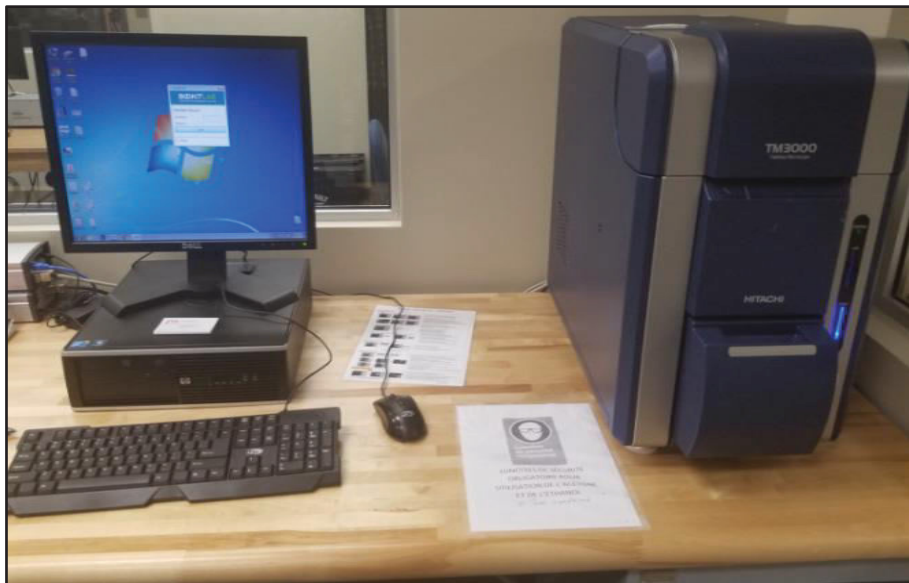


Figure 2-11 Scanning ElectronMicroscope (SEM) HITACHI TM3000.

## 2.4 Surface Roughness

Surface roughness measurements were made using surface roughness tester (Mitutoyo SJ-400) measurement machine following each applicable run as shown in Figure 2-12. The three readings are taken for every test, and then the average is obtained. These Figures 2-13 and 2-14 are some examples showing surface roughness of Honed tool and T-land tool for same cutting speed and feed rate (cutting speed 350 m/min, Feed rate 0.1 mm/th) at two different hardness of material (17 and 48 HRC).

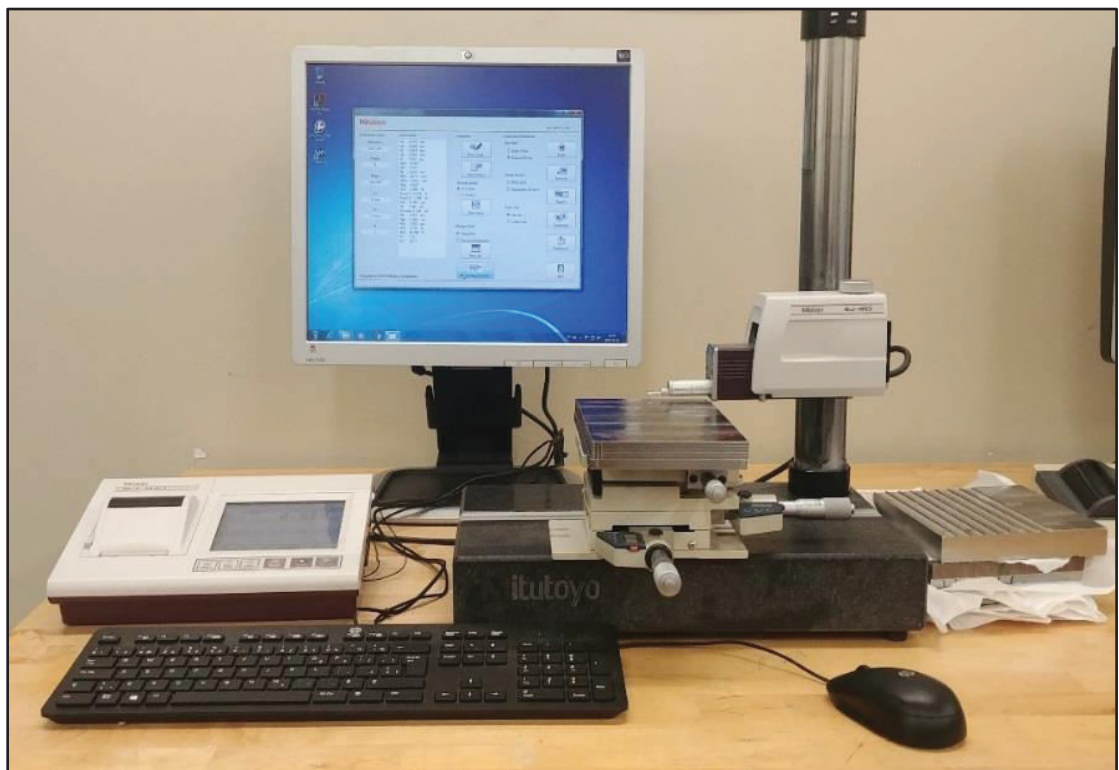


Figure 2-12 Surface roughness tester Mitutoyo SJ-400.

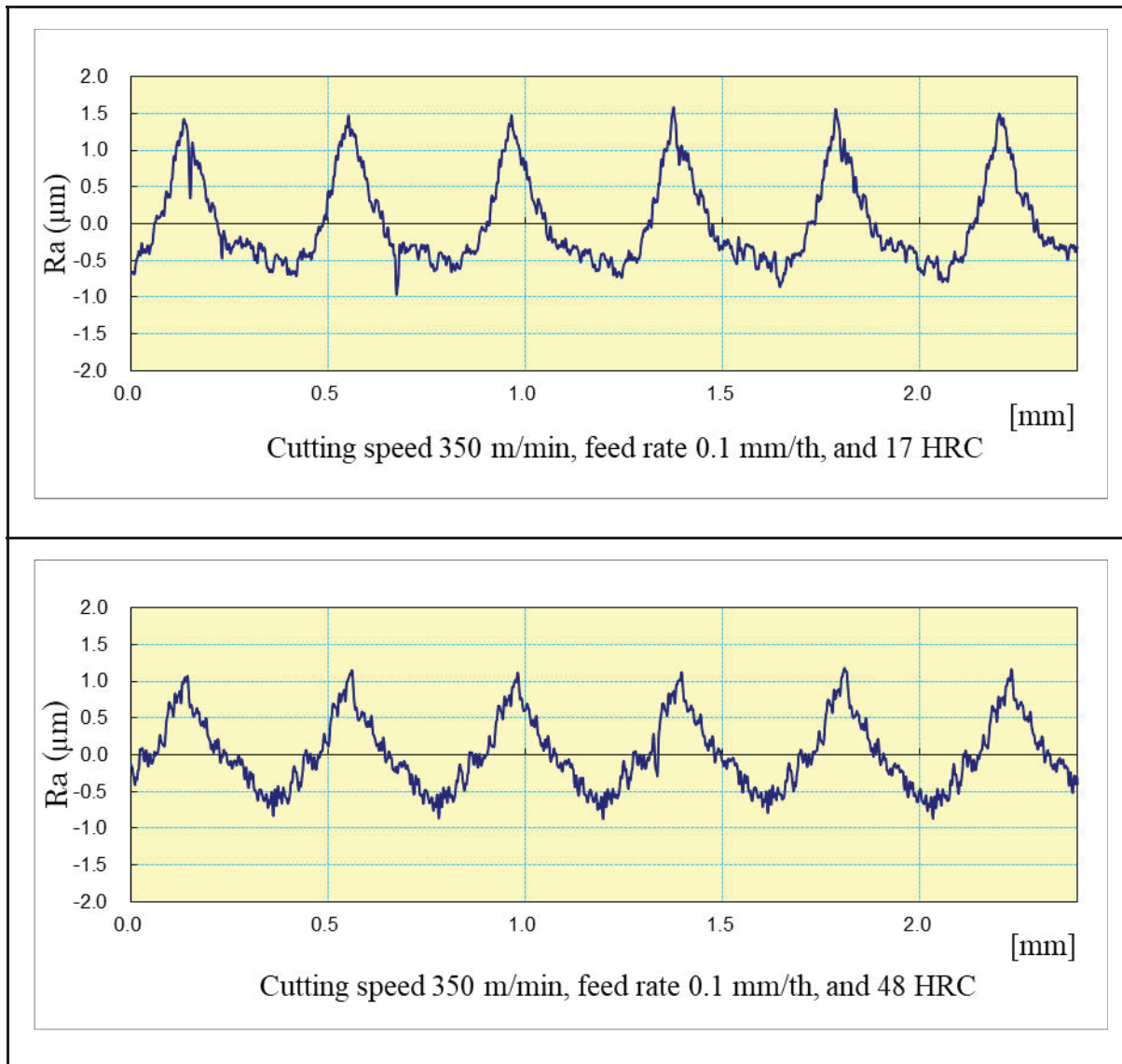


Figure 2-13 Surface roughness of Honed tool for cutting speed 350 m/min and feed rate 0.1 mm/th with two different material hardness (17 and 48 HRC).

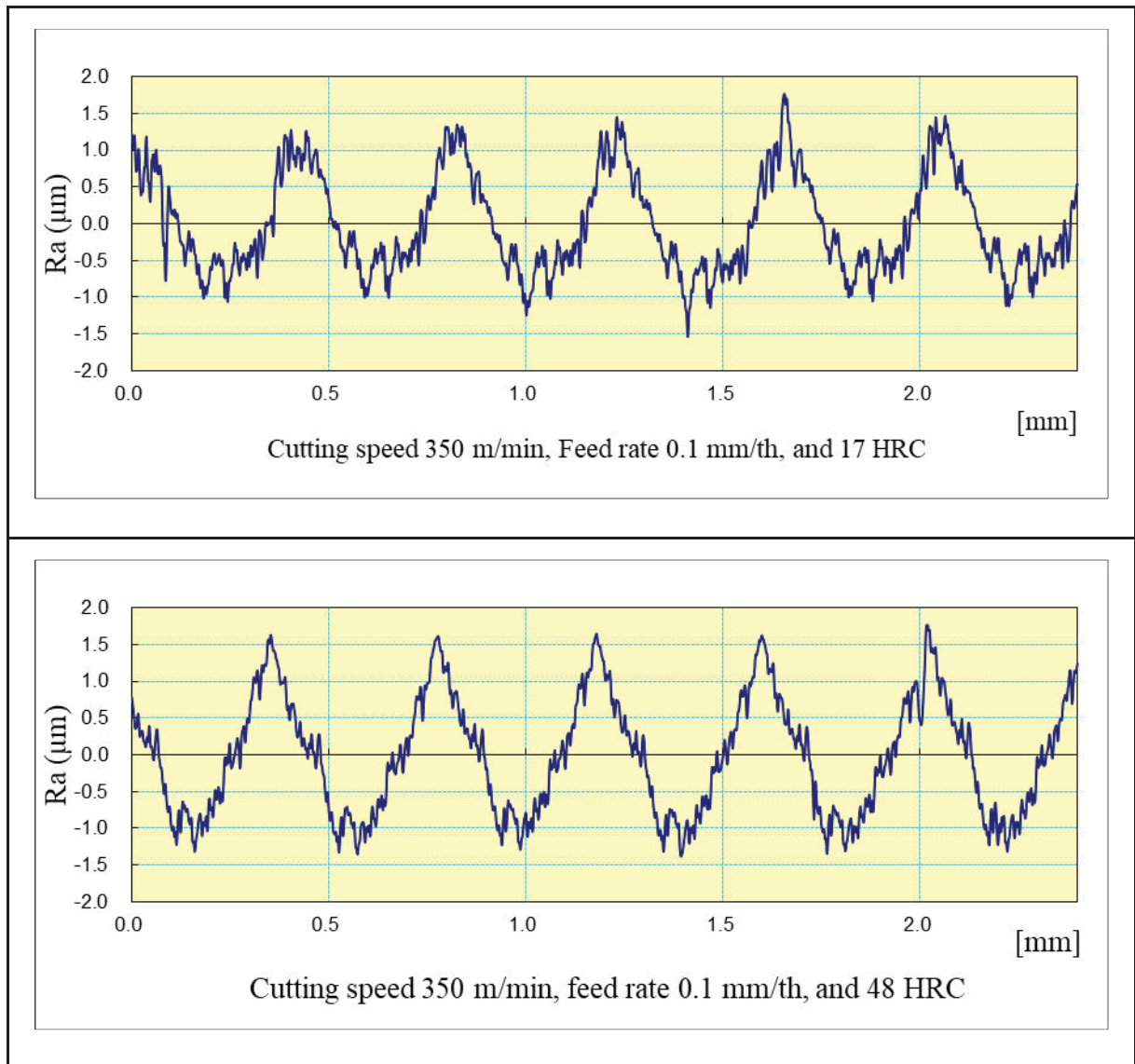


Figure 2-14 Surface roughness of T-land tool for cutting speed 350 m/min and feed rate 0.1 mm/th with two different material hardness (17 and 48 HRC).

## 2.5 Dust Emission

The metallic particles emission from machining operations was collected through the Aerodynamic Particles Sizer (APS) spectrometer (Model 3321, TSI Inc.) and Scanning Mobility Particles Sizer (SMPS) spectrometer (SMPS model #3080, TSI. Inc) as shown in Figure 2-15. The APS gives the total particles concentration, specific area concentration and mass concentration for fine particles (FP) diameter ranging between 0.5 to 20  $\mu\text{m}$ . The SMPS can measure ultrafine particles (UFP) diameters ranging from 10 to 1000 nm.

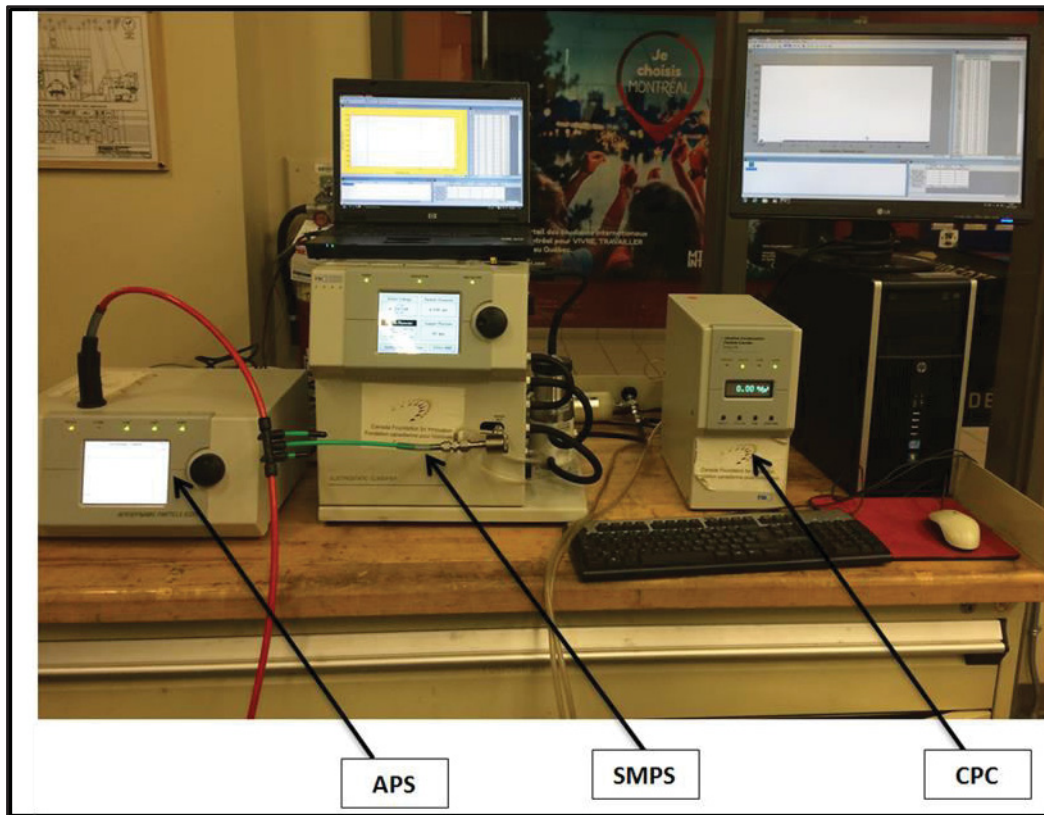


Figure 2-15 Aerosol Particle Sizer (APS), Scanning Mobility Particle Sizer (SMPS) and Condensation Particle Counter (CPC).

## CHAPTER 3

### MACHINABILITY STUDY OF HARDENED 1045 STEEL WHEN MILLING WITH CERAMIC CUTTING INSERTS

M. Shnfir<sup>1</sup>, O.A. Olufayo<sup>1</sup>, W. Jomaa<sup>2</sup>, and V. Songmene<sup>1</sup>

<sup>1</sup>Department of Mechanical Engineering, École de Technologie Supérieure (ÉTS),  
1100 Notre-Dame St. West, Montréal, QC H3C 1K3, Canada;

<sup>2</sup>Cégep Édouard-Montpetit, Centre technologique en aérospatiale (CTA),  
5555 Place de la Savane, Saint-Hubert, Québec, QC J3Y 8Y, Canada

Paper published in Materials, December 2019, 3974; doi:10.3390/ma12233974

#### **Abstract:**

Intermittent machining using ceramic tools such as hard milling is a challenging task due to the severe mechanical shock that the inserts undergo during machining and the brittleness of ceramic inserts. This study investigates the machinability of hardened steel AISI 1045 during face milling using SiAlON and whisker (SiCW) based ceramic inserts. The main focus seeks to identify the effects of cutting parameters, milling configuration, edge preparation and work material hardness on machinability indicators such as resultant cutting force, power consumption and flank tool wear. The effects of these varying cutting conditions on performance characteristics were investigated using a Taguchi orthogonal array design L<sub>32</sub> (2<sup>1</sup> 4<sup>4</sup>) and evaluated using ANOVA. Results indicate lower resultant cutting forces were recorded with honed edge inserts of SiAlON ceramic grade. In addition, a decrease in resultant cutting forces was associated with reduced feed rates and increased hardness. The feed rate and cutting speed were also identified as the greatest influencing factors in the amount of cutting power. The main wear mechanisms responsible for flank wear on the ceramic inserts are micro-scale abrasion and micro-chipping. Increased flank wear was observed at low cutting speed and high feed rates, while micro-chipping mostly ensued from the cyclic loading of the radial tool edge form, which is more susceptible to impact

fragmentation. Thus, the use of tools with chamfered tool-edge preparation greatly improved observed wear values. Additional confirmation tests were also conducted to validate the results of the tests.

**Keywords:** machinability; hard milling; AISI 1045 steel; ceramic tools; hardness; edge preparation.

### 3.1 Introduction

Due to the development of high-performance machine tools and advanced cutting tool materials, hard machining technology was accepted as a reliable technique in the manufacturing of structural components made of hardened materials (hardness exceeding 45 HRC). Many aspects of the hard machining processes such as parts' surface integrity (Guo, Li, & Jawahir, 2009; M'Saoubi, Outeiro, Chandrasekaran, Dillon Jr, & Jawahir, 2008), machinability indexes (Bartarya & Choudhury, 2012; Chinchankar & Choudhury, 2015) and ecological trends (Krolczyk et al., 2019) have been extensively studied. It was demonstrated that these aspects were significantly sensitive to various technological parameters and their interactions (Ajaja et al., 2019). In addition to the standard machine-tool parameters (cutting speed, feed rate and depth of cut), the cutting tool edge preparation and material, the workpiece material hardness and/or microstructure are amongst the critical factors that should be considered in the optimization of the hard machining processes, particularly, during milling operations (intermittent cutting). Cutting tool manufacturers have designed different cutting edge micro-geometries in order to withstand the high cutting pressure and reduce the catastrophic failure of the cutting tool during the machining of difficult-to-cut materials (Denkena & Biermann, 2014). The edge preparations were principally applied to advanced cutting tools made of ceramic, cubic boron nitride (CBN) and polycrystalline cubic boron nitride (PCBN) tools. Compared to hard turning process, milling of hardened steel using advanced cutting tools was less attractive over the last two decades (Bartarya & Choudhury, 2012; Chinchankar & Choudhury, 2015; Guo et al., 2009; M'Saoubi et al., 2008). Elbestawi *et al.* (Elbestawi et al., 1997) investigated the milling of AISI H13 steel (HRC 55) using PCBN ball-nose end mills with various edge preparations. Results showed that the worst performance was noticed for the honed edge in comparison to sharp and

chamfered edge preparations. More recent studies by Wojciechowski S. have investigated the machinability of hardened steels when using ball-nose end mills (Szymon Wojciechowski, 2015; S. Wojciechowski et al., 2018). They found that when milling with a flexible ball end nose tool, the obtained surface roughness is very sensitive to the selection of the cutting speed while in the case of milling with a rigid tool, the surface roughness depends less on the cutting speed used. The authors explained the first phenomena by the loss of rigidity, radial runout and chatter (Szymon Wojciechowski, 2015). This effect of the chatter and run-out are very important when using ceramic inserts that are very sensitive to vibrations and fluctuations on cutting forces.

Wojciechowski S. (Szymon Wojciechowski, 2015) proposed a model for estimating the cutting forces when milling inclined parts with ball end nose tools and showed that the cutting forces coefficients depend on the tool inclination relative to the cutting direction and that small radial run out value (as small as 3  $\mu\text{m}$ ) can cause considerable cutting force variations during finish milling with ball tool. This result shows the importance of balancing the cutter prior to the milling process. Although the proposed model is more accurate, it could be applied directly (without some modifications) to rigid milling with the tool having round inserts.

To lower machining cost by using cheaper cutting tools, researchers investigated hard machining using carbide tools with advanced coating and/or specific edge preparation. Li *et al.* (B. Li, Zhang, Yan, & Jiang, 2018) studied the effect of the edge hone radius in hard milling of AISI H13 steel (50 HRC) using cemented carbide inserts. The authors found that when edge radius increases, cutting forces, plastic deformation and compressive residual stress increase whereas the surface roughness decreases to a certain limiting value. Another study by Li *et al.* (B. Li, Zhang, Yan, & Zhang, 2018), investigating the hard milling of AISI H13 steel explored the effect of edge hone radius on the chip formation mechanisms. The results showed that when the edge hone radius increases, the chip segmentation intensity and frequency increases, leading to high cutting force fluctuations. Denkena *et al.* (Denkena, Koehler, et al., 2012) demonstrated that the wear behavior of a honed cutting edge strongly depends on the micro-geometry of the honed edge during the slot milling of a quenched and tempered 42CrMo4 steel using cemented carbide inserts. The results showed that the tool

wear type shift from a flank wear to a rake face wear depending on a defined micrometrical parameter named the “form factor K”. The authors have also shown that the tool life of sharp cutting edges is limited by chipping wear. This concept was adopted by Fulemova and Janda (Fulemova & Janda, 2014) for studying the cutting forces and cutting tool life when milling ferrite-martensite steel (EN ISO X12CrMoVNbN9-1) using sub-micron sintered carbide tools. The authors pointed out that an edge radius of 15  $\mu\text{m}$  is optimal in terms of tool wear and cutting forces. Conversely, Elbestawi *et al.* (Elbestawi et al., 1997) showed that sharp edge outperforms both honed and chamfered PCBN cutting tool edges during the hard milling of AISI H 13 steel.

Despite their introduction into the machining industry in the early 1970s, the use of ceramic cutting tools for hard milling remains very limited compared to the turning process (X. Cui, Jiao, Zhao, & Guo, 2017). The fundamental idea behind the use of the ceramic tool is to take advantage of their high-temperature resistance, reduced costs and achieve increased material removal rates during machining of hardened alloys (A. S. Kumar, Durai, & Sornakumar, 2006). A recent study by Wang *et al.* (B. Wang & Liu, 2016) investigated the cutting tools performances of four solid ceramic end milling tools as well as Ti (C, N),  $\text{Si}_3\text{N}_4$ , SG4 and LT55 in machining hardened AISI H13 steel (60–62 HRC). Wang investigated that the cutting forces of ceramic end milling tools are smaller than cemented carbide tool, and such ceramic tools of  $\text{Si}_3\text{N}_4$ , Ti (C, N) and LT55 gave the best surface finish and had a longer tool life. Koshy *et al.* (Koshy, Dewes, & Aspinwall, 2002) investigated the performances of two different cutting tools, including an indexable ball nose end mills (with carbide and cermet insert), and a solid carbide ball nose end mills, in face milling of hardened D2 tool steel (58 HRC). Results showed that cutting performance of an indexable cermet insert is lesser than both types of cemented carbide tools. However, several studies demonstrated the encouraging potential of ceramic tools in producing favorable surface integrity (Ajaja et al., 2019; Jomaa, Songmene, & Bocher, 2016) and reasonable tool life (Gaitonde, Karnik, Figueira, & Davim, 2009; C. S. Kumar & Patel, 2017; Özel, Karpat, Figueira, & Davim, 2007; MA Shalaby et al., 2014) at relatively high cutting speed when turning hardened steel. Research studies have shown that ceramic tools are significantly superior to carbide tools (A.

S. Kumar et al., 2003) and in some cases can outperform CBN/PCBN tools (MA Shalaby et al., 2014) in terms of cutting tool life.

In addition to tool materials and edge preparation, the workpiece material hardness effect during hard machining was also the subject of some research studies. However, only a few focused on the hard milling process. In investigating the influence of workpiece material hardness in high-speed milling of hardened AISI H13 steel (45 HRC and 55 HRC), Elbestawi *et al.* (Elbestawi et al., 1997) showed that the higher the workpiece hardness, the lower the wear on high CBN cutting tools. Wang and Zheng (J. J. Wang & Zheng, 2003) studied the ball end milling of hardened AISI H13 steel (20 HRC and 41 HRC) using a TiAlN coated carbide tool. Results showed that the specific chip shearing energy and friction coefficient were greater for the soft/ductile material (20 HRC). On the other hand, several studies focusing on the effect of workpiece material hardness during hard turning were carried out. Poulachon *et al.* (G Poulachon, Moisan, & Jawahir, 2001) reported the existence of a limiting value of hardness at 50 HRC in hard turning 100Cr6 steel using PCBN tools. Below this limit, the cutting forces decrease, and the wear resistance is controlled by the bonding strength of the tool grains. Above the limit of 50 HRC, the cutting forces increase, and abrasion is the main tool wear mechanism. Furthermore, results showed equivalence between cutting speed and workpiece material hardness. These results were in agreement with those obtained by Ng and Aspinwall (Ng & Aspinwall, 2002) for hard turning AISI H13 steel. Results reported by Thiele and Melkote (Thiele & Melkote, 1999) gave evidence of a significant interaction between edge preparation and workpiece material hardness during hard turning AISI 52100 steel. Nevertheless, most of the findings in hard turning were not yet validated in hard milling.

The AISI 1045 steel is also heat-treated steel, which is well used in the manufacturing of several structural components for different industrial applications. Although it is considered as the most studied steels from the machining point of view, the AISI 1045 steel was rarely investigated under hard milling conditions using ceramic tools (Bartarya & Choudhury, 2012; Chinchankar & Choudhury, 2015; X. Cui et al., 2017; Guo et al., 2009; M'Saoubi et al., 2008). In fact, most of the studied AISI 1045 steel have annealed microstructures with hardness not exceeding 234 HB (22 HRC) and milled using carbide tools (Bartarya &

Choudhury, 2012; Brito et al., 2016; Costa, Brito, de Paiva, Leme, & Balestrassi, 2016; Junior, Sales, da Silva, Costa, & Machado, 2017; Muñoz-Escalona, Díaz, & Cassier, 2012; Reddy & Rao, 2006; Richetti, Machado, Da Silva, Ezugwu, & Bonney, 2004; Suresh Kumar Reddy & Venkateswara Rao, 2005). To this end, the present paper aims to explore the performance of ceramic tools in hard milling of AISI 1045 steel. In addition to standard technological parameters such as cutting speed, feed rate and milling configuration, the study also focuses on the specific effects of cutting-edge preparation and workpiece material hardness on machinability indexes, including cutting forces, cutting power and tool wear under dry machining conditions. A future article will focus on ecological aspects, especially on fine and ultrafine particles emission.

### 3.2 Methodology

To study the hard milling of the AISI 1045 steel, a standard orthogonal array design of experiments (DOE) named  $L_{32} (2^1 4^4)$  was employed. This DOE was selected due to its ability to identify the main effects of the factors and their interactions. The factors' levels and the design matrix are given in Tables 3-1 and 3-2, respectively. All the experiments were carried out under dry condition using fixed axial ( $a_p = 2$  mm) and radial ( $a_e = 25.4$  mm) depths of cut.

Table 3-1 Matrix of Experiments.

<i>Cutting Parameters</i>	<i>Level 1</i>	<i>Level 2</i>	<i>Level 3</i>	<i>Level 4</i>
<i>MT: Milling Type</i>	Up	Down	---	---
<i><math>v_c</math>: Cutting Speed (m/min)</i>	200	300	400	500
<i><math>f_n</math>: Feed rate (mm/th)</i>	0.05	0.09	0.13	0.17
<i>H: Hardness (HRC)</i>	38	43	48	53
<i>CT: Cutting Tools</i>	T1	T2	T3	T4

Table 3-2 Orthogonal array L32 ( $2^1 4^4$ ) of Taguchi design.

No.	Milling Type	Cutting Speed (m/min)	Feed Rate (mm/th)	Hardness (HRC)	Tool
1	Up	200	0.05	38	T1
2	Up	200	0.09	43	T2
3	Up	200	0.13	48	T3
4	Up	200	0.17	53	T4
5	Up	300	0.05	38	T2
6	Up	300	0.09	43	T1
7	Up	300	0.13	48	T4
8	Up	300	0.17	53	T3
9	Up	400	0.05	43	T3
10	Up	400	0.09	38	T4
11	Up	400	0.13	53	T1
12	Up	400	0.17	48	T2
13	Up	500	0.05	43	T4
14	Up	500	0.09	38	T3
15	Up	500	0.13	53	T2
16	Up	500	0.17	48	T1
17	Down	200	0.05	53	T1
18	Down	200	0.09	48	T2
19	Down	200	0.13	43	T3
20	Down	200	0.17	38	T4
21	Down	300	0.05	53	T2
22	Down	300	0.09	48	T1
23	Down	300	0.13	43	T4
24	Down	300	0.17	38	T3
25	Down	400	0.05	48	T3
26	Down	400	0.09	53	T4
27	Down	400	0.13	38	T1
28	Down	400	0.17	43	T2
29	Down	500	0.05	48	T4
30	Down	500	0.09	53	T3
31	Down	500	0.13	38	T2
32	Down	500	0.17	43	T1

The proposed DOE allows studying the effects of machining technological parameters on machinability indicators: cutting force, cutting power and tool wear.

### 3.2.1 Resultant cutting force (F)

In the milling process, different cutting force components can be extracted from force signals. Ceramic inserts are significantly sensitive to vibration phenomenon, which in turn depends on the cutting forces in the  $x$ -direction ( $F_x$ ) and  $y$ -direction ( $F_y$ ; Figure 3-1). Hence, the maximum resultant cutting force  $F$  (Figure 3-2b) operating in the  $(x, y)$  plane was adopted in the present study.  $F$  is given by the following formula:

$$F(j, t) = \sqrt{F_x(j, t)^2 + F_y(j, t)^2} \quad (3-1)$$

An illustration of  $x$  and  $y$  forces and their resultant force  $F(t)$  signals are depicted in Figure 3-2 (a and b), respectively. In the present study, the resultant force  $F$  used in the statistical analysis is calculated as follows:

$$F = \frac{\sum_{j=1}^4 F_{max}(j, t)}{4}, \quad (3-2)$$

where,  $F_{max}(j, t)$  is the maximum values of the resultant force recorded for the  $j$ th insert.

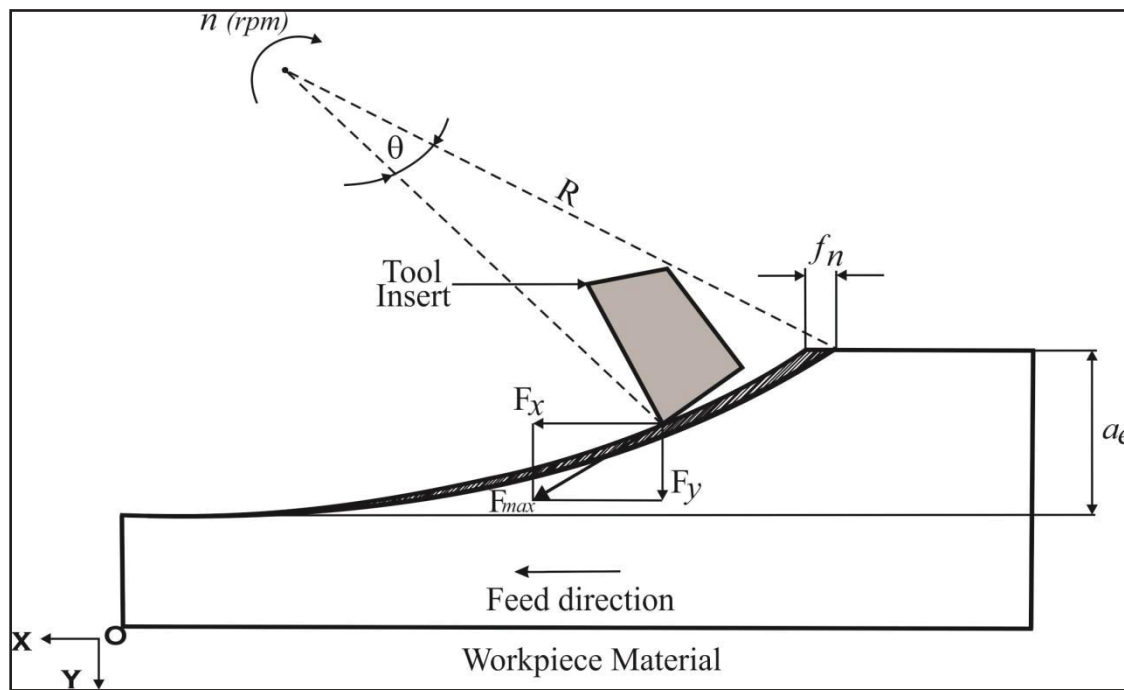


Figure 3-1 Illustration of milling force components in the cutting zone.

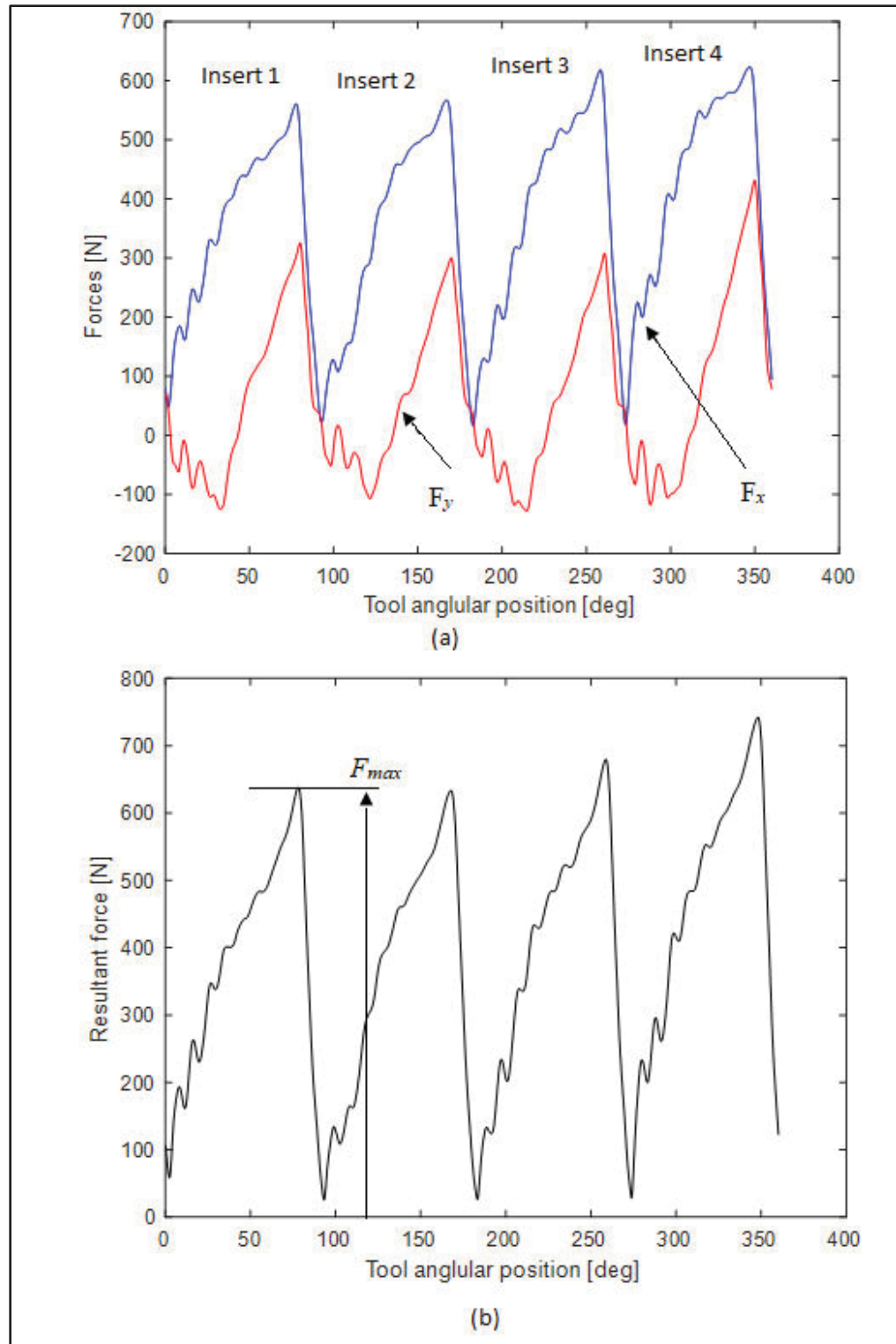


Figure 3-2 (a) Milling forces' signals in the X and Y directions, and (b) resultant force signal for machining test 8.

### 3.2.2 Cutting power ( $P_c$ )

The cutting power ( $P_c$ ) is a relevant indicator of the total power consumption during the machining. It depends on the cutting speed ( $v_c$ ) and the tangential cutting force component ( $F_t$ ). The later should be extracted from the cutting forces measured in the  $x$ ,  $y$  and  $z$  directions (Figure 3-1). The relationship between the global coordinate system linked to the machine tool ( $x, y, z$ ) and the local coordinate system linked to the insert ( $t, r, a$ ) is defined as follows:

$$\begin{pmatrix} F_x(j,\theta) \\ F_y(j,\theta) \\ F_z(j,\theta) \end{pmatrix} = \begin{pmatrix} \cos \theta & \sin \theta & 0 \\ \sin \theta & -\cos \theta & 0 \\ 0 & 0 & 1 \end{pmatrix} \begin{pmatrix} F_t(j,\theta) \\ F_r(j,\theta) \\ F_a(j,\theta) \end{pmatrix} = A \begin{pmatrix} F_t(j,\theta) \\ F_r(j,\theta) \\ F_a(j,\theta) \end{pmatrix}, \quad (3-3)$$

where,  $\theta$  is the tool rotation angle.  $F_t$ ,  $F_r$  and  $F_a$  are the tangential, radial, and axial cutting forces, respectively. They can be calculated by the following equation:

$$\begin{pmatrix} F_t(j,\theta) \\ F_r(j,\theta) \\ F_a(j,\theta) \end{pmatrix} = A^{-1} \begin{pmatrix} F_x(j,\theta) \\ F_y(j,\theta) \\ F_z(j,\theta) \end{pmatrix}, \quad (3-4)$$

then, the cutting power  $P_c$  (kW) can be calculated as follows:

$$P_c = V_c \sum_{j=1}^n F_{t\max}, \quad (3-5)$$

where,  $F_{t\max}(j)$  is the maximum values of the tangential force recorded for the  $j$ th insert.  $n$  denotes the number of inserts operating simultaneously during the machining.

## 3.3 Experimental procedure.

### 3.3.1 Workpiece Material

The workpiece material was a medium carbon steel AISI 1045 widely used in the fabrication of hydraulic shaft, pump shaft, piston rods, cylinders, cams, and crankshafts. The dimensions of the AISI 1045 rectangular block used were 250 mm (length) by 100 mm (width) and 25 mm (thickness). Four varying hardness were employed in the tests. The hardening process consisted of heating the part to an austenitization temperature of 844 °C for 1.5 h and followed by quenching in water and tempering in the range between 260–470 °C for 2 h,

depending on the targeted hardness value (38, 43, 48 and 53 HRC). Table 3-3 lists the percentage weight chemical composition of the AISI 1045 steel.

Table 3-3 The chemical composition of workpiece material (% weight).

<b>C</b>	<b>Mn</b>	<b>P</b>	<b>S</b>	<b>Si</b>	<b>Fe</b>
0.459	0.721	0.0086	0.0027	0.259	balance

### 3.3.2 Face Milling Tests

The experimental trials were carried out on a MAZAK NEXUS 410A vertical CNC milling machine (Yamazaki Mazak Corporation, Oguchi, Japan, Max. RPM = 12,000 rev/min, power at 5000 rpm = 25 HP) under dry machining conditions (Mazak, Oguchi, Japan). Round ceramic inserts with two distinct edge preparations (T-land and honed) and of two different grades (KY2100 and KY4300) were used in the machining tests as indicated in Table 3-4. A shell mills type KDNR250RN40C3 tool holder with four inserts from Kennametal, Latrobe, PA, USA) was also used. The physical and mechanical properties of the workpiece (AISI 1045 steel) and the cutting inserts are depicted in Table 3-5. The assembled tool (cutter plus four inserts) was balanced before the machining process.

Cutting forces measurement was acquired using the Kistler 9255-B three-component dynamometer (Kistler<sup>®</sup>, Winterthur, Switzerland) at a sampling rate of 48 kHz (Figure 3-3). These were later processed used the MATLAB<sup>®</sup> software (version r2017b, MathWorks<sup>®</sup>, Natick, Massachusetts, USA). After machining, tool wear measurement was performed using the KEYENCE VHX-500 FE Digital Microscope (Keyence, Osaka, Japan).

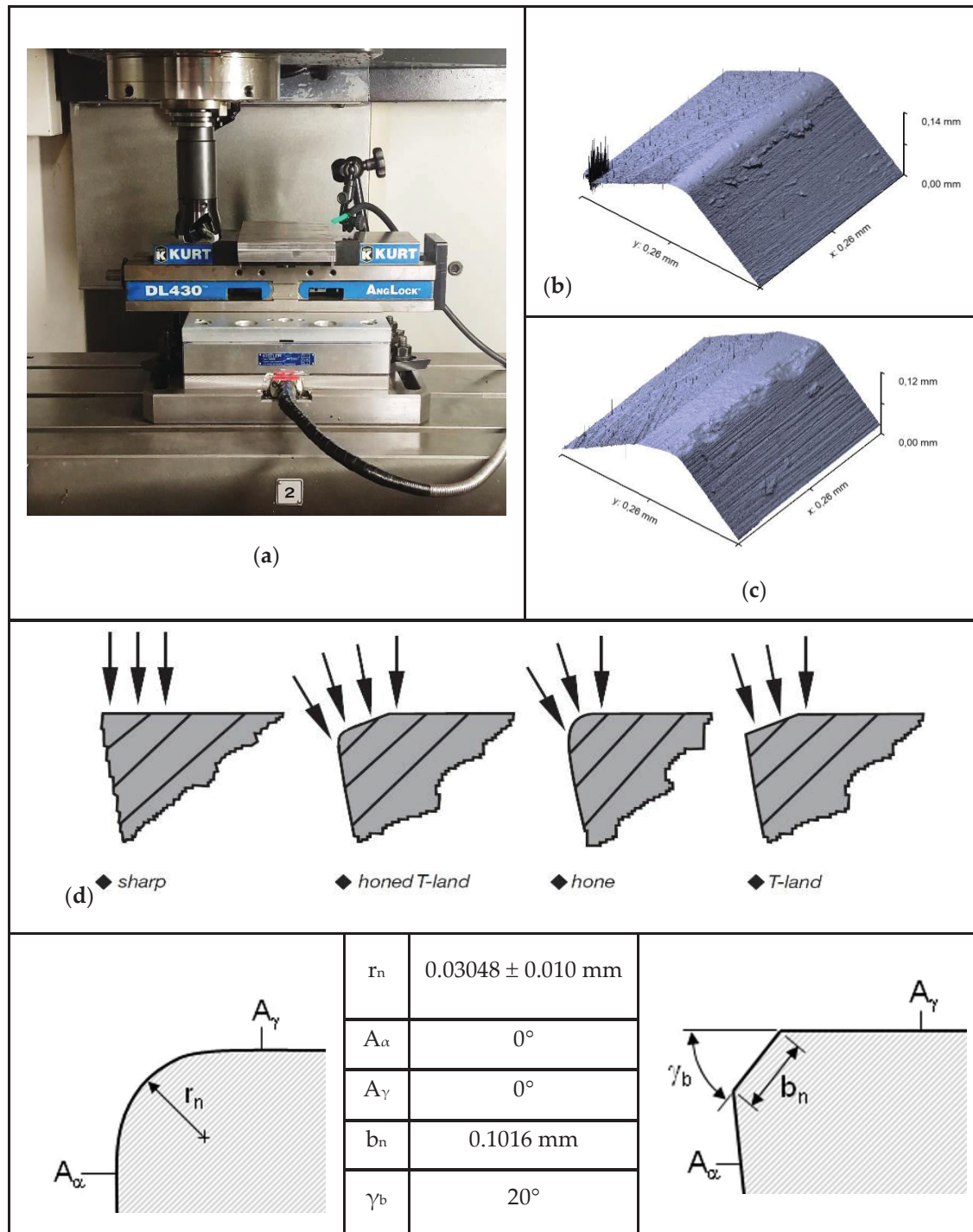


Figure 3-3 (a) Face milling setup with the cutting tool and force dynamometer, and micro-geometry of the (b) honed and (c) chamfered (T-land) cutting edge and (d) cutting edge forms with parametric edge dimensions (adapted from (Abdulkadir et al., 2018)).

Table 3-4. Specification of the cutting tool.

Tool ID	Edge Preparation	Kennametal Grade Name	Grade Description
1	Honed (RNG45E)	KY2100	Silicon Nitride (SiAlON) base Ceramic
2	T-land (RNG45T0420)		
3	Honed (RNG45E)	KY4300	Whisker ceramic with a matrix of $Al_2O_3 + SiCW$
4	T-land (RNG45T0420)		

Table 3-5 Workpiece and cutting tool material properties (Collin &amp; Rowcliffe, 2000; de Faoite, Browne, &amp; Stanton, 2013; De Godoy &amp; Diniz, 2011; Iqbal, Mativenga, &amp; Sheikh, 2007; Jun, Jianxin, Jianhua, &amp; Xing, 1997).

Material	Density $\rho$ (kg/m <sup>3</sup> )	Thermal Conductivity $K$ (W/m <sup>∘</sup> C)	Specific Heat $C$ (J/kg <sup>∘</sup> C)	Fracture Toughness $K_{Ic}$ (MPa <sup>1/2</sup> )	Hardness (HV)
AISI 1045	7844	45	3.7	-	-
Silicon Nitride (SiAlON) base Ceramic	3320	11.5	2.41	6.8	1650
Whisker ceramic with a matrix of $Al_2O_3 + SiCW$	3750	24	3.6	8	2000

### 3.4 Results and Discussions

#### 3.4.1 Analysis of Resultant Force

The aim of the analysis of variance (ANOVA) was to investigate which of the cutting parameters significantly affect the above-mentioned performance characteristics. This is accomplished by separating the total variability of the mean ratios, which is measured by the sum of the squared deviations of all the observations, from their mean to the total mean, into representing it as contributions of each cutting parameters as well as the error.

The total sum of the squared (TSS or SST) deviations comprises of two sources: the sum of the squared deviations due to each cutting parameter (SSd) and its interaction effects and the sum of the squared error (SSE). The percentage contribution by each of the cutting parameter in the total sum of the squared deviations SST can be used to evaluate the importance of a change in that cutting parameter on a specific performance characteristic evaluated. In addition, the F-test named in honor of Sir Ronald Aylmer Fisher is also used to statistically test the equality of means and test the overall significance for a regression model. The probability from the F-statistics allowed us to determine if the model met the null hypothesis. A statistically significant result was found at high F-value and when a probability ( $p$ -value) was less than a pre-specified threshold (significance level), commonly defined as 0.05 (95%).

The analysis of variance (ANOVA) of the resultant force is shown in Table 3-6. It can be seen that the feed rate (F-value = 33.43) was the most significant to the output response of the resultant force, followed by the interaction milling type  $\times$  tool (F-value = 3.55). The hardness, the tool, the milling type and cutting speed had no significant effect on the resultant force. The contribution (%) provided an additional depiction of significance for the interpretation of the results. The results show that the contribution due to the feed rate was 74.58%, whereas the interaction milling type  $\times$  tool contributes 7.91%, the hardness contributed 3.91%, the tool contributed 2.76% and the milling type interaction speed contributed 1.36%.

Table 3-6 ANOVA for resultant force.

SOURCE	DF	SEQ SS	ADJ SS	ADJ MS	F	P	C (%)
MT: Milling Type	1	1325	1325	1325	0.18	0.677	0.135
$v_C$ : Cutting Speed (m/min)	3	4100	4100	1367	0.19	0.903	0.418
<b><math>f_n</math>: Feed Rate (mm/th)</b>	<b>3</b>	<b>730,554</b>	<b>730,554</b>	<b>243,518</b>	<b>33.43</b>	<b>0.00</b>	<b>74.58</b>
H: Hardness (HRC)	3	38,305	38,305	12,768	1.75	0.210	3.91
CT: Cutting Tool	3	26,990	26,990	8997	1.23	0.340	2.76
MT $\times$ $V_C$	3	13,376	13,376	4459	0.61	0.620	1.36
<b>MT <math>\times</math> CT</b>	<b>3</b>	<b>77,516</b>	<b>77,516</b>	<b>25,839</b>	<b>3.55</b>	<b>0.048</b>	<b>7.91</b>
Residual Error	12	87,425	87,425	7285			8.92
Total	31	979,591					100

Bold values show the most significant factors

An analysis of the mean response of the resultant force is shown in Table 3-7. The table shows the optimal levels of the control factors for the resultant force values performed by the Taguchi method. These optimal values are also presented in Figure 3-4. The optimal cutting parameters for minimizing the resultant force could be clearly determined from this figure. The levels and mean ratios for the factors that give the best resultant force were MT (Level 1, mean = 435.7),  $v_c$  (Level 4, mean = 423.7),  $f_n$  (Level 1, mean = 249.4), H (Level 1, mean = 394.5) and CT (Level 1, mean = 393.1). In other words, an optimum resultant force value was obtained during up the milling type at 500 m/min cutting speed, 0.05 mm/tooth feed rate, 38 HRC material hardness and using a honed silicon nitride (SiAlON) base ceramic tool. From Figure 3-4, the use of high cutting speed and low feed rate generated lower cutting forces (Aouici, Bouchelaghem, Yallese, Elbah, & Fnides, 2014; Aouici, Yallese, Belbah, Ameer, & Elbah, 2013; Aouici, Yallese, Fnides, & Mabrouki, 2010; Ghani et al., 2004; Kıvık, Samtaş, & Çiçek, 2012; Lalwani et al., 2008; Pa, Sarhan, Shukor, & Mohamed, 2013; Patel, Mistry, Kapatel, & Joshi, 2015). The decrease in cutting force from higher cutting speed was due to the rise in temperature in the shear plane area, which lowers the shear strength of the material (Aouici et al., 2010). In addition, the increase in the feed rate induced a larger volume of the cut material in the same unit of time, besides establishing a dynamic effect on the cutting forces. It also led to a corresponding increase in the normal contact stress at the tool chip interface and in the tool chip contact area (Aouici et al., 2014; Suresh, Basavarajappa, & Samuel, 2012; Yallese, Chaoui, Zeghib, Boulanouar, & Rigal, 2009). From Figure 3-4, the tool grade material composition further compounded the influence of the honed edge preparation. Conversely, this property bears little or no effect on T-land edge preparation. The maximum resultant force was obtained at about 43 HRC. Further increase in material hardness (48–53 HRC) led to a decrease in the resultant force. This phenomenon has also been previously reported by Matsumoto *et al.* (Y Matsumoto, Barash, & Liu, 1987) and Chao and Trigger (Chao & Trigger, 1951).

Table 3-7 Means response for resultant force.

LEVEL	MT	$v_c$ (m/min)	$f_n$ (mm/th)	H (HRC)	CT
1	<b>435.7</b>	442.2	<b>249.4</b>	<b>394.5</b>	<b>393.1</b>
2	448.6	449.6	392.7	491.1	450.5
3		453.0	457.3	434.0	468.8
4		<b>423.7</b>	669.1	448.9	456.1
Delta	12.9	29.3	419.7	96.7	75.6

Bold values show the optimal levels of control factors

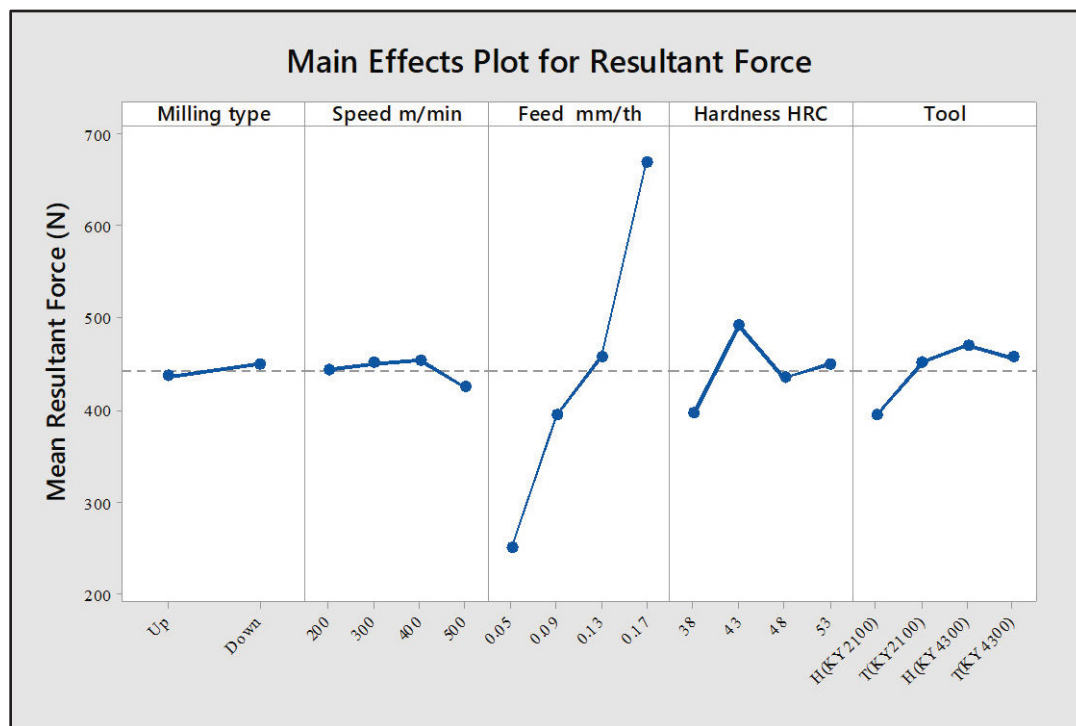


Figure 3-4 Main effects plot for resultant force.

The low delta value for the milling type means response further indicates the low effect milling kinematics bares in resultant force prediction. Experimental test in optimal conditions for other factors and using down milling generated similar/improved results. This is believed to be attributed to the gradual reduction in chip thickness and improved chip flow in this process.

### 3.4.2 Analysis of Power

The analysis of variance (ANOVA) of the cutting power is shown in Table 3-8. From the table, it can be seen that the feed rate (F-value = 7.45) was the most significant terms related to the cutting power, followed by the cutting speed (F-value = 6.96). The table shows that the milling type, hardness and tool were not significant terms to the cutting power. The contributions of milling type, cutting speed, feed rate, hardness, tool, milling type  $\times$  speed and milling type  $\times$  tool on power were found to be 0.204%, 33.78%, 36.13%, 1.72%, 1.74%, 1.18% and 5.82%, respectively. Thus, an equivalent importance of the feed rate (36.13%) and cutting speed (33.78%) were observed to cutting power performance. Similar results were reported by Benlahmidi *et al.* (Benlahmidi et al., 2017) when turning hardened AISI H11 steel (50 HRC) with CBN7020 tools. They reported that the cutting speed, feed rate and depth of cut are the most significant terms on cutting power. This was also confirmed by Davim and Figueira (J. Paulo Davim & Figueira, 2007) during the turning AISI D2 steel using traditional and wiper cutting tools. In milling processes, Fratila *et al.* (Fratila & Caizar, 2011) indicated that the increase in cutting power was associated with a corresponding increase of cutting speeds, feed rates and depth of cuts, when machining AlMg3 with HSS (high-speed steel) tools. This was also observed by Pa Nik *et al.* (Pa et al., 2013) who indicated an increase in cutting power with an increase in cutting conditions (feed rate and depth of cut) in both dry and wet machining conditions.

Table 3-8 ANOVA for power.

SOURCE	DF	SEQ SS	ADJ SS	ADJ MS	F	P	C (%)
MT: Milling Type	1	110,499	110499	110499	0.13	0.728	0.204
<b><math>v_C</math>: Cutting Speed (m/min)</b>	<b>3</b>	<b>18,265,243</b>	<b>18,265,243</b>	<b>6,088,414</b>	<b>6.96</b>	<b>0.006</b>	<b>33.78</b>
<b><math>f_n</math>: Feed Rate (mm/th)</b>	<b>3</b>	<b>19,538,513</b>	<b>19,538,513</b>	<b>6,512,838</b>	<b>7.45</b>	<b>0.004</b>	<b>36.13</b>
H: Hardness (HRC)	3	932,281	932,281	310,760	0.36	0.786	1.72
CT: Tool	3	945,689	945,689	315,230	0.36	0.783	1.74
MT $\times$ $v_C$	3	640,173	640,173	213,391	0.24	0.864	1.18
MT $\times$ CT	3	3,148,771	3,148,771	1,049,590	1.20	0.351	5.82
Residual Error	12	10,495,278	10,495,278	874,606			19.41
Total	31	54,076,445					100

Bold values show the optimal levels of control factors.

The various levels of cutting parameters to minimize cutting power are given in Table 3-9 and their main effect plot is shown in Figure 3-5. The optimal parametric combination for minimized power was at MT (Level 1, mean = 2154),  $v_c$  (Level 1, mean = 1310),  $f_n$  (Level 1, mean = 1310), H (Level 1, mean = 2038) and CT (Level 4, mean = 2032). Thus, an optimum power value was obtained during the up milling type, at 200 m/min cutting speed, 0.05 mm/tooth feed rate, 38 HRC hardness and, using a chamfered tool with a matrix of  $Al_2O_3 + SiC$ .

Table 3-9 Means response for power.

Level	MT	$v_c$ (m/min)	$f_n$ (mm/th)	H (HRC)	CT
1	<b>2154</b>	<b>1275</b>	<b>1310</b>	<b>2038</b>	2268
2	2272	1873	1890	2431	2469
3		2366	2206	2328	2084
4		3338	3447	2056	<b>2032</b>
Delta	118	2062	2137	394	438

Bold values show the optimal levels of control factors

The low delta value between MT mean responses highlights the reduced influence of milling kinematics in power estimation. Further experimental tests at optimal settings and using down milling also resulted in lower power values. The gradual reduction in chip thickness and the improved chip evacuation from the tool cutting zone was believed to be responsible for these results.

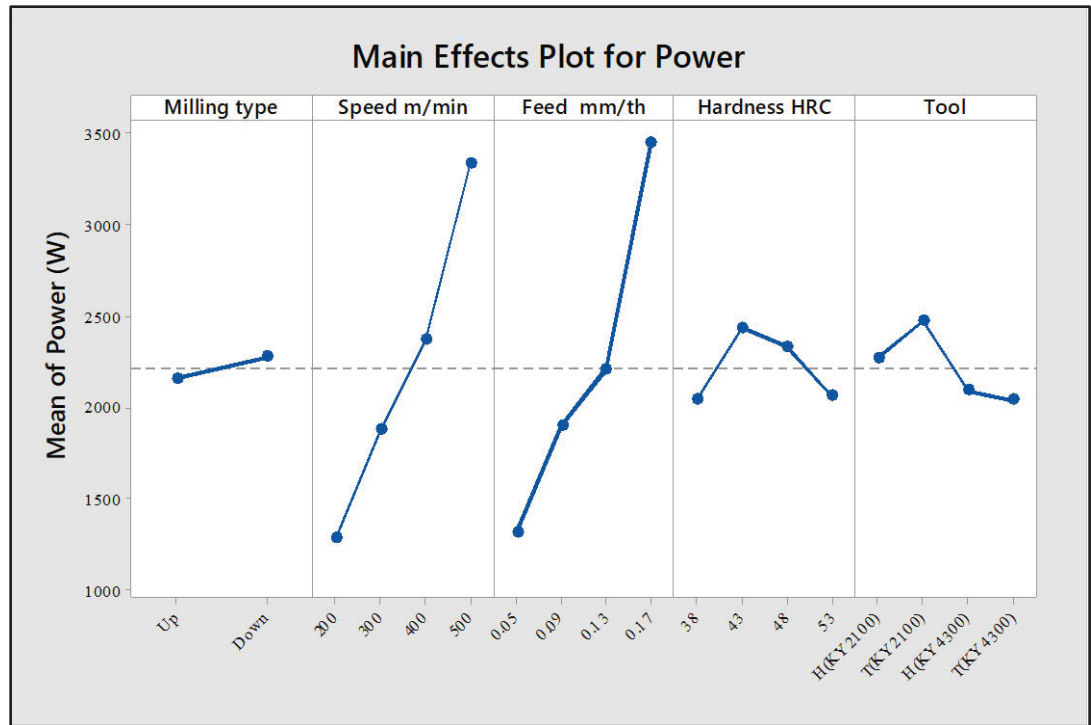


Figure 3-5 Main effects plot for power.

### 3.4.3 Analysis of Tool Wear

Tool wear investigations showed that flank wear and micro-chipping occurred due to abrasion of hard particles and the effect of recurring tool entry into the workpiece (Figure 3-6). No build-up edge (BUE) was observed during the experiments. This can be explained by the fact that the cutting speed used with ceramic is usually high. From the literature, the increase in alumina content improves the dissolution resistance of the material but this is prone to local plastic deformation at high temperatures (Ghali, Sastri, & Elboujdaini, 2007; Ruano & Sherby, 1995). Figure 3-7 shows a preview into the SEM microstructure of a worn part of the KY2100 grade insert with a composition of silicon nitride (SiAlON) and KY4300 with  $Al_2O_3$  matrix reinforced with SiC whiskers. From the figure, the micro-shearing process and dissolution of the tool in KY2100 can be observed. Alternatively, the microstructural texture on a worn area of KY4300 tool grade shows a more compact topography, which is often more influenced by micro-scale abrasion. This is believed to be primarily as a result of the  $Al_2O_3$  composition in the ceramic material, which improves its dissolution resistance during cutting.

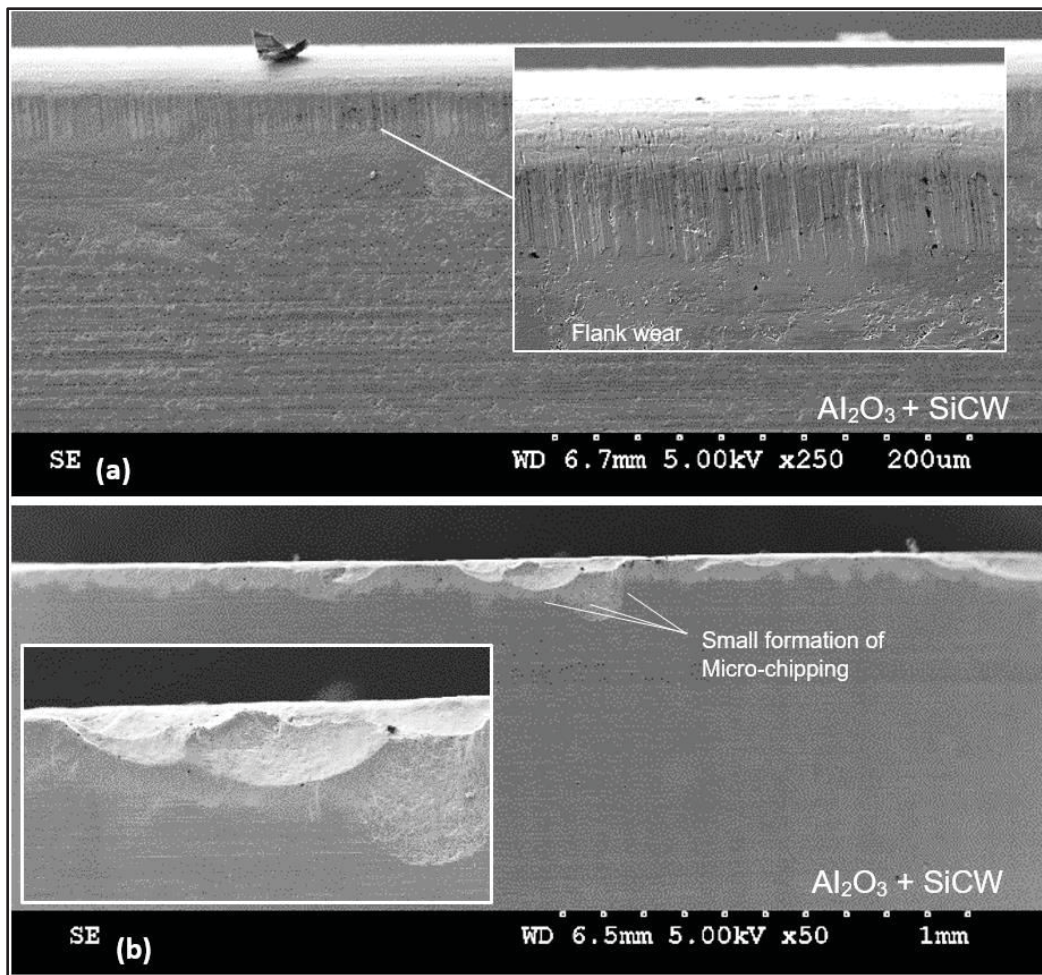


Figure 3-6 Sample wear observed on honed and chamfered tool edge preparation at increased hardness (53 HRC).

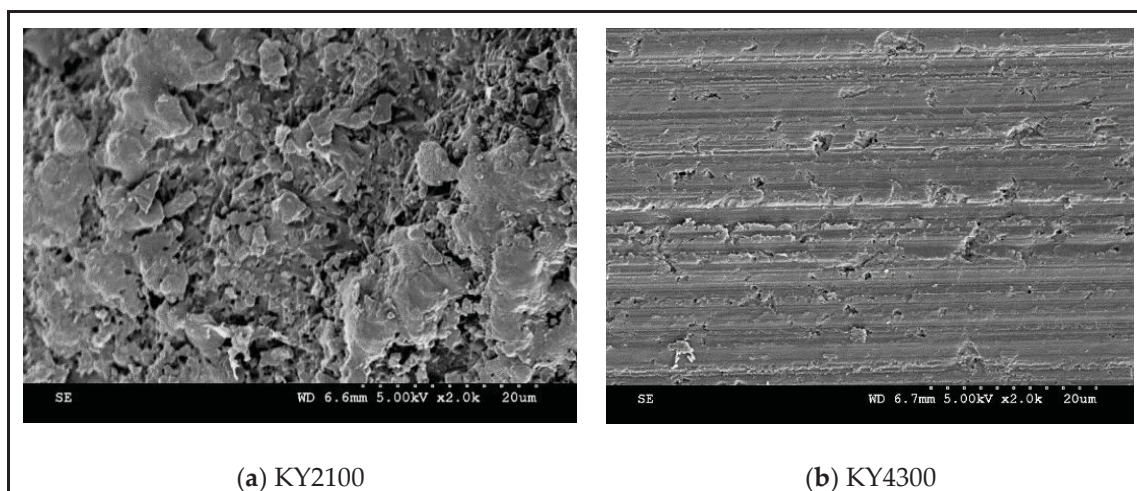


Figure 3-7 SEM image of the microstructural morphology of used ceramic inserts.

The analysis of variance (ANOVA) of the tool wear is shown in Table 3-10. The analysis shows that the milling type (F-value = 6.48), tool (F-value = 6.36) and their interaction (milling type  $\times$  tool, F-value = 4.12) were the significant terms to the tool wear. The hardness, the feed rate, the cutting speed and the other interactions had no significant effect on the tool wear. The most important factors affecting the tool wear were from the cutting tool, the milling type and their interactions with percentage contribution values of 31.54%, 20.42% and 10.71% respectively.

Table 3-10 ANOVA for tool wear.

Source	Df	Seq Ss	Adj Ss	Adj Ms	F	P	C (%)
<b>MT: Milling Type</b>	<b>1</b>	<b>2601.2</b>	<b>2601.2</b>	<b>2601.19</b>	<b>6.48</b>	<b>0.026</b>	<b>10.71</b>
$v_c$ : Cutting Speed (m/min)	3	214.4	214.4	71.48	0.18	0.909	0.88
$f_n$ : Feed Rate (mm/th)	3	1667.9	1667.9	555.96	1.39	0.295	6.86
H: Hardness (HRC)	3	1695.9	1695.9	565.30	1.41	0.288	6.98
<b>CT: ToolL</b>	<b>3</b>	<b>7658.9</b>	<b>7658.9</b>	<b>2552.96</b>	<b>6.36</b>	<b>0.008</b>	<b>31.54</b>
MT $\times v_c$	3	672.9	672.9	224.30	0.56	0.652	2.77
<b>MT<math>\times</math>CT</b>	<b>3</b>	<b>4959.0</b>	<b>4959.0</b>	<b>1653.02</b>	<b>4.12</b>	<b>0.032</b>	<b>20.42</b>
Residual Error	12	4815.1	4815.1	401.26			19.83
Total	31	24,285.3					100

Bold values show the optimal levels of control factors.

An analysis of the mean response for the tool wear, which is made by using the Taguchi method, is shown in Table 3-11 and Figure 3-8, which further highlights the significance of the cutting tool and milling type to wear. These results were in agreement with research carried out by Bouzakis *et al.* (K. D. Bouzakis et al., 2008), which has shown that the kinematics of the milling process (up-milling or down-milling), considerably affects the achievable cutting performance. Hadi *et al.* (Hadi, Ghani, Haron, & Kasim, 2013) also demonstrated an increasing relationship between tool wear and up-milling kinematics. However, owing to the brittle nature of ceramics, there exists a combined effect of milling type and tool edge geometry for the wear generation in ceramics (Table 3-10). Severe chipping wear was often seen on honed tools with low hardness. This extreme wear is believed to be as a result of the sensitivity of the tool edge strength during impact with the

workpiece, as a radial edge formation is more susceptible to impact fragmentation. This condition was reduced in tools with reinforced SiC whiskers.

It is postulated that the high impact force on the lower end of the honed curve on the rake face is responsible for flaking. Optimal tool wear value was obtained with an up milling type at 500 m/min cutting speed, 0.17 mm/tooth feed rate, 48 HRC hardness and using a honed ceramic tool with reinforced SiC whisker.

Table 3-11 Means response for tool wear.

LEVEL	MT	$v_C$ (m/min)	$f_n$ (mm/th)	H (HRC)	CT
1	<b>38.64</b>	46.29	49.87	51.93	73.78
2	56.67	51.84	41.52	57.35	40.41
3		47.58	58.52	<b>39.58</b>	<b>33.52</b>
4		<b>44.93</b>	<b>40.72</b>	41.78	42.92
Delta	18.03	6.91	17.79	17.77	40.26

Bold values show the optimal levels of control factors

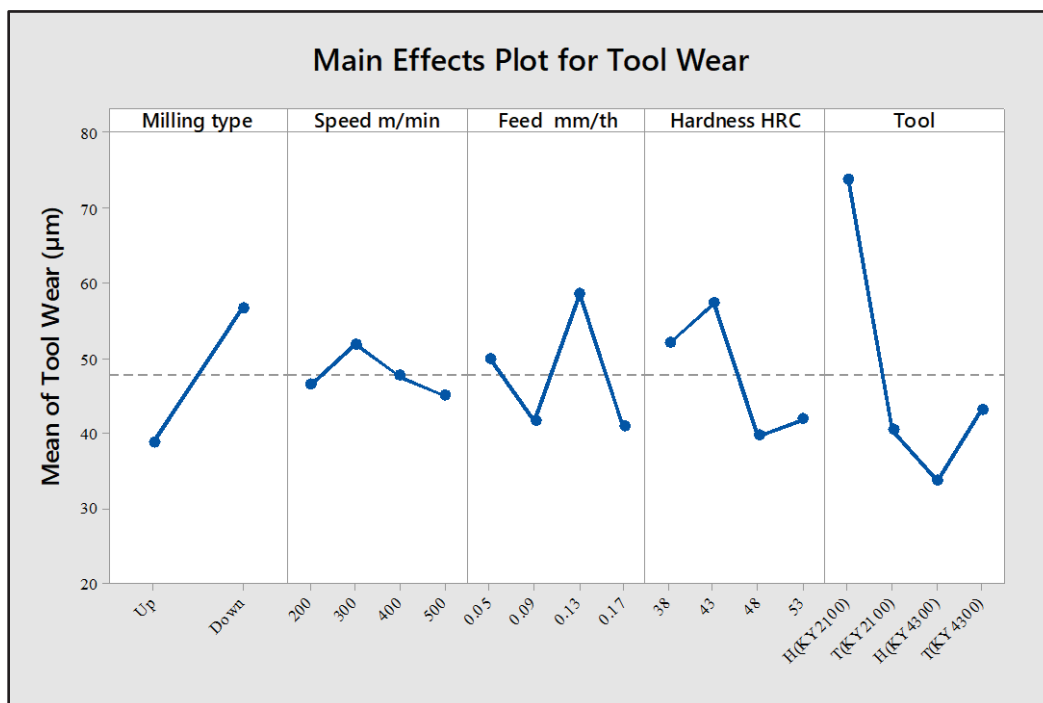


Figure 3-8 Main effects plot for tool wear.

### 3.5 Confirmation Tests

Following the determination of the individual optimal levels for each performance characteristics, a prediction and comparison of the percentage improvement of each was performed (Kivak, 2014). The optimal conditions of each performance characteristics (resultant cutting force (F), power (P) and tool wear (Vb)) are shown in Equations (3-6)–(3-8) below:

$$F_{opt} = \gamma_F + (MT_1 - \gamma_F) + (v_{c4} - \gamma_F) + (f_{n1} - \gamma_F) + (H_1 - \gamma_F) + (CT_1 - \gamma_F), \quad (3-6)$$

$$P_{opt} = \gamma_P + (MT_1 - \gamma_P) + (v_{c1} - \gamma_P) + (f_{n1} - \gamma_P) + (H_1 - \gamma_P) + (CT_4 - \gamma_P), \quad (3-7)$$

$$Vb_{opt} = \gamma_{Vb} + (MT_1 - \gamma_{Vb}) + (v_{c4} - \gamma_{Vb}) + (f_{n4} - \gamma_{Vb}) + (H_3 - \gamma_{Vb}) + (CT_3 - \gamma_{Vb}), \quad (3-8)$$

where, ( $F_{opt}$ ,  $P_{opt}$  and  $Vb_{opt}$ ) represent the optimum level average values of (F, P and Vb) from Tables (3-7, 3-9 and 3-11), respectively. The  $\gamma_F$ ,  $\gamma_P$  and  $\gamma_{Vb}$  state the average of all F, P and Vb values obtained from the experimental study (Tables 3-7, 3-9 and 3-11), which are 442 N, 2213 Watt and 47.66  $\mu\text{m}$ , respectively. From the calculations, it was estimated that  $F_{opt} = 128$  N,  $P_{opt} = -44$  Watt and  $Vb_{opt} = 6.8$   $\mu\text{m}$ . Figures 3-9–3-11 show the comparison of the predicted cutting forces, power and tool wear as a function of workpiece hardness and milling modes.

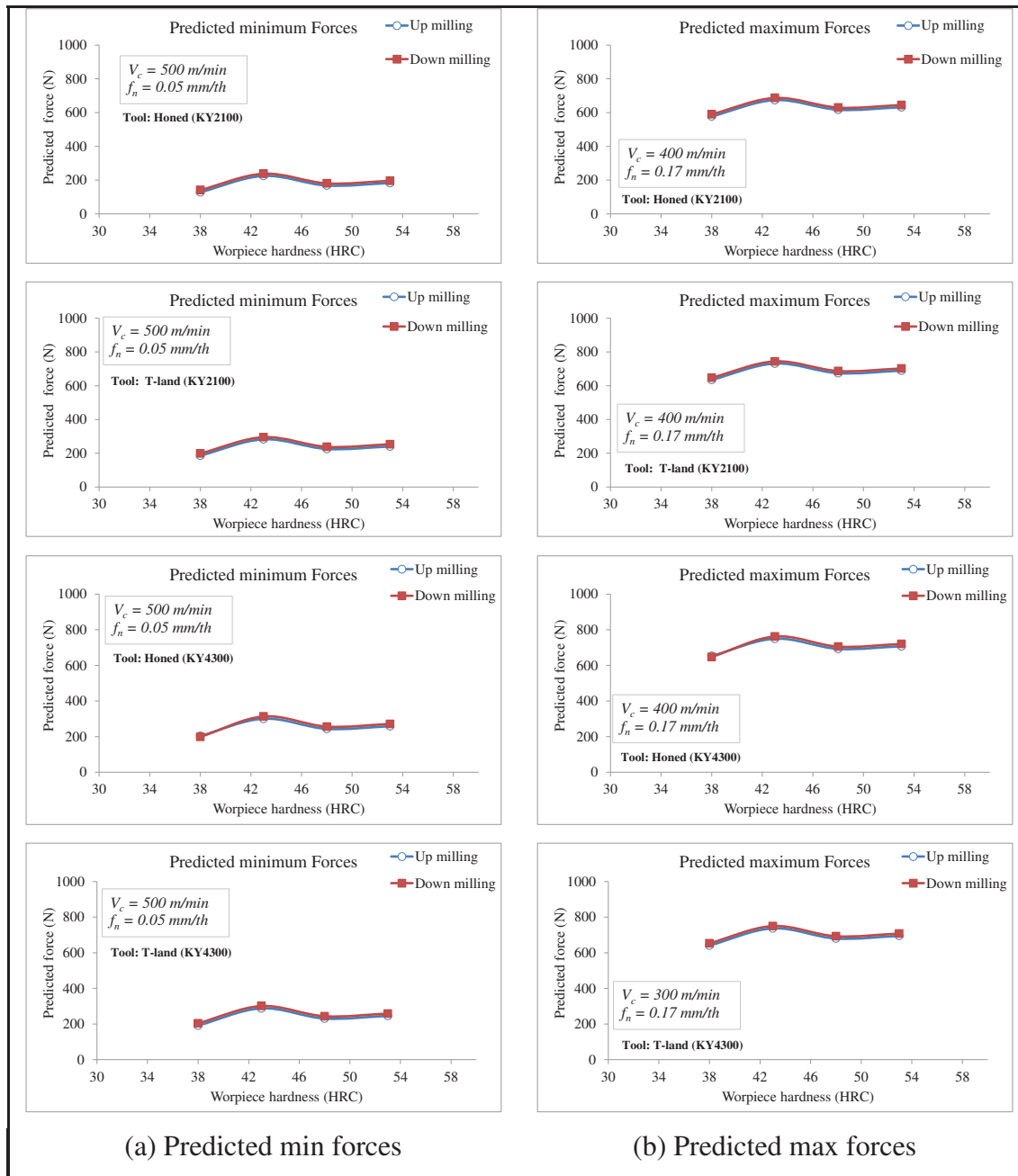


Figure 3-9 Comparison of the predicted cutting forces as a function of workpiece hardness and milling modes.

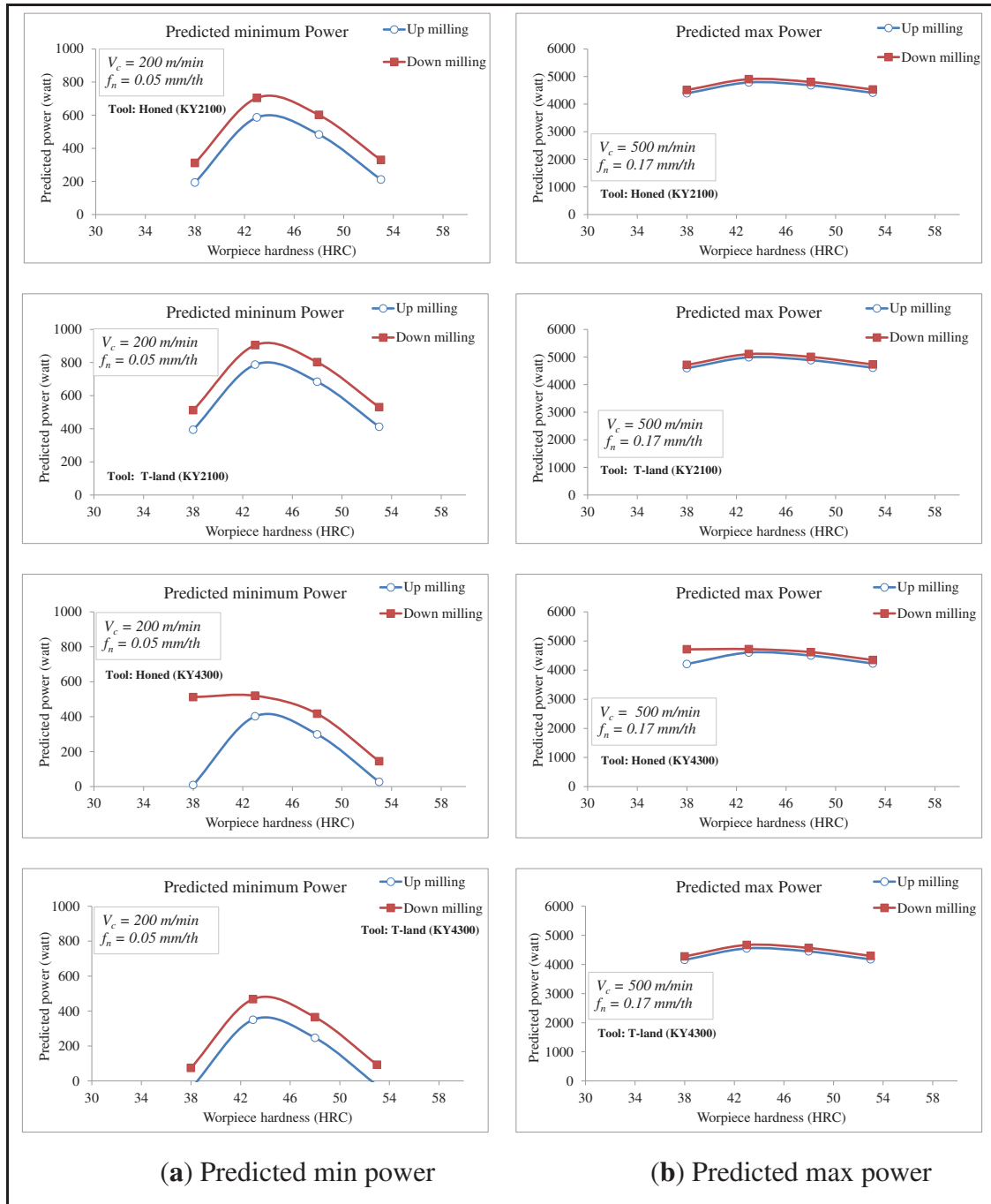


Figure 3-10 Comparison of the predicted power requirements as a function of workpiece hardness and milling modes.

In Figure 3-11, the decrease in predicted wear with the increase in workpiece hardness was believed to be a result of the poor chip breakability during cutting operations.

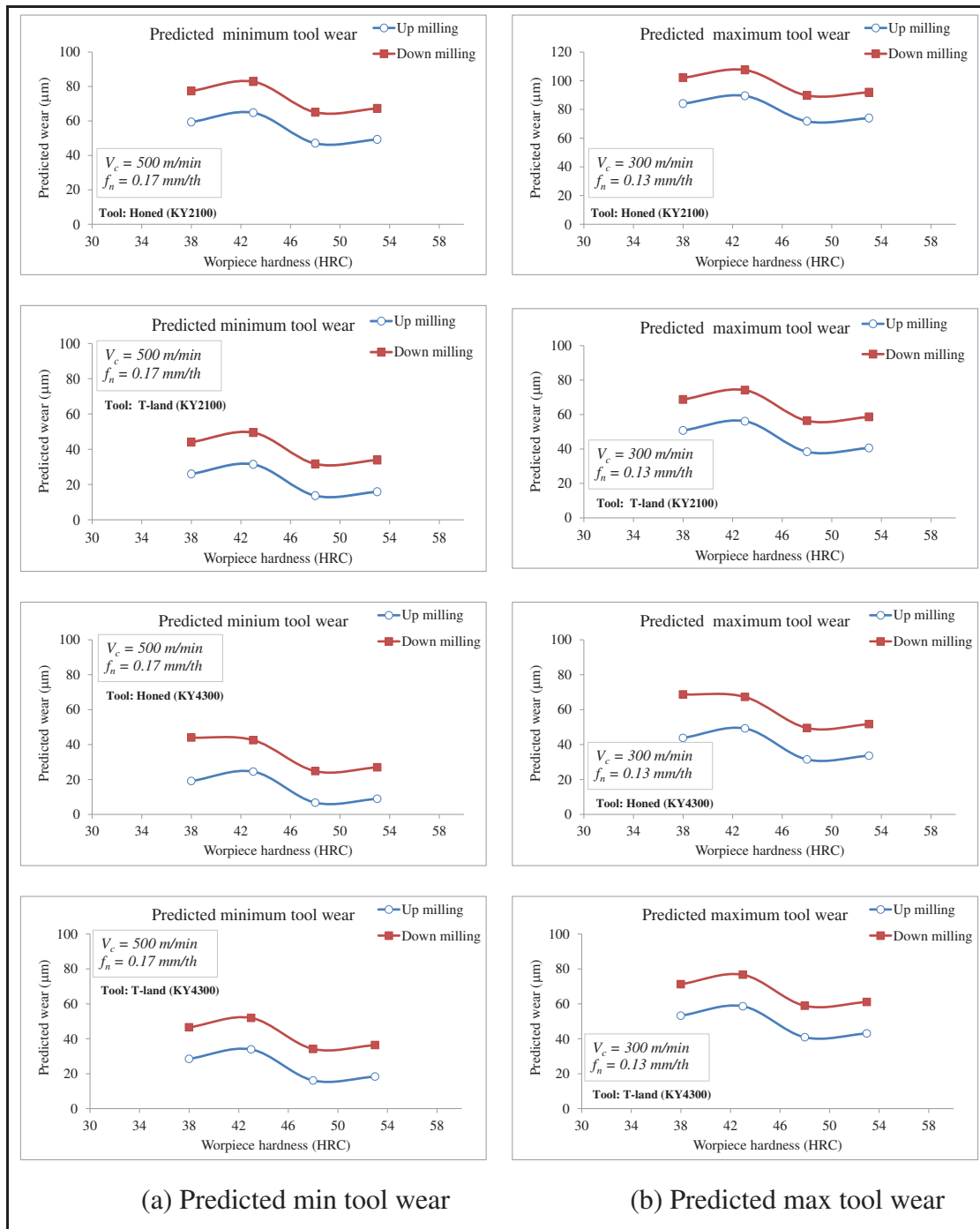


Figure 3-11 Comparison of the predicted tool wear as a function of workpiece hardness and milling modes.

Cutting chips tend to remain longer at the tooltip area in materials with lower hardness and this causes an increase in temperature and workpiece hardening. This further promotes the wear formation observed. On the other hand, good chip evacuation was observed in harder materials with a marginally lower wear occurrence. At low hardness levels (38–43 HRC) the expected effect of hardness on tool wear was observed (higher hardness leading to high wear level). The same tendency is noticed for workpieces with high hardness values (48–53 HRC), which generated short chips. Increasing the hardness from 48 to 53 HRC led to higher cutting tool wear on both honed and chamfered inserts.

A representation of the recommended parametric combination and the initial process combination is shown in Table 3-12.

Table 3-12 Initial and recommended parameters combination.

<b>Performance Characteristics</b>	<b>Initial Process Parameters Levels</b>	<b>Recommended Process Parameters Levels</b>
Resultant force (F)	MT <sub>1</sub> v <sub>c1</sub> f <sub>n4</sub> H <sub>4</sub> CT <sub>4</sub>	MT <sub>2</sub> v <sub>c4</sub> f <sub>n1</sub> H <sub>1</sub> CT <sub>1</sub>
Power (P)	MT <sub>1</sub> v <sub>c1</sub> f <sub>n4</sub> H <sub>4</sub> CT <sub>4</sub>	MT <sub>2</sub> v <sub>c1</sub> f <sub>n1</sub> H <sub>1</sub> CT <sub>4</sub>
Tool wear (Vb)	MT <sub>1</sub> v <sub>c1</sub> f <sub>n4</sub> H <sub>4</sub> CT <sub>4</sub>	MT <sub>1</sub> v <sub>c4</sub> f <sub>n4</sub> H <sub>3</sub> CT <sub>3</sub>

Figure 3-12 indicates an improvement from the initial process parameters when using the newly identified experimental values. An average improvement percentage above 50% is obtained in each of the evaluated responses. However, more ample work is required to establish predictive models for each of these responses. Future research will seek to develop these predictive models and estimate optimal parameters in the milling of AISI 1045 stainless steel using ceramic cutting tools.

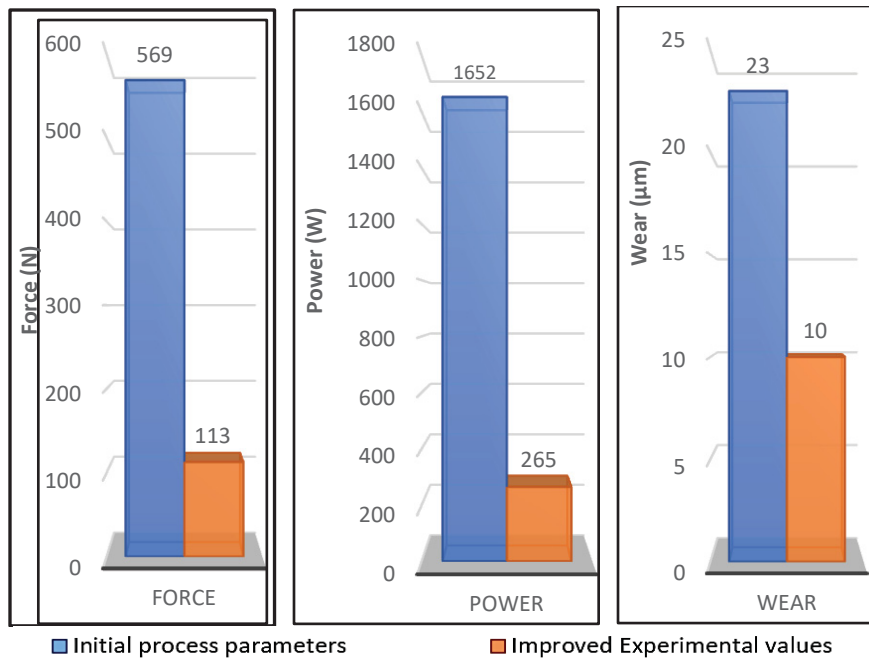


Figure 3-12 Performance chart between initial process parameters and improved experimental values for each response factors.

### 3.6 Conclusions

This study explored the performance of ceramic tools in hard milling of AISI 1045 steel. It focused on parameters such as cutting speed, feed rate and milling configuration, as well as the specific effects of cutting-edge preparation and workpiece material hardness on cutting forces, cutting power and tool wear. For this investigation, a Taguchi experimental design was used. From the results obtained the following conclusions were drawn:

- The feed rate was the most influential parameter related to the resultant force. A decrease in feed yielded significant lower resultant forces during cutting. This parameter had a 74.58% percentage contribution to this response factor.
- Lower power demands were mostly influenced by the feed rate and cutting speed. These were the most important factors affecting the cutting power with comparable percentage contributions of 36.13% and 33.78%, respectively. A reduction in both cutting speed and feed rates significantly lowered cutting power.

- Conversely to other response factors, the choice of the cutting tool and the milling kinematics were much more important in the generation of tool wear. There exist a complex inter-correlation between the choice of cutting tool and the milling kinematics. Despite the increased impact from tool entry during down milling, response factors such as resultant force, and power could be mitigated primarily from cutting parameters (cutting speed and feed rate). Therefore, under these controlled parametric conditions, the tool wear response is mostly due to tool properties (material and edge preparation). The combined influence of the choice of tool material and edge preparation had the greatest percentage contribution to flank wear formed with 31.54%. This is attributed to the sensitivity of the tool edge strength during impact with the workpiece. Honed tools with a radial edge formation were more susceptible to impact fragmentation but this could be mitigated by the strengthened presence of SiC whiskers in the KY4300 tool grade. Consequently, the honed Tool T<sub>3</sub> (RNG45E) KY4300 performed best in experimentation due to the reduced micro-chipping observed from its whisker ceramic reinforced tool edge.
- The material hardness in the range of 38–53 HRC was identified as not been a determinant factor on the machinability index studied in this research. Various contrasting observations of the influence of hardness were identified in the study. However, the adverse effects peaked at a hardness value of 43HRC across responses. Improved results were often identified at hardness extremes in the range studied. This can be explained by the reduction in abrasion wear between the tool and the workpiece at reduced hardness and the fall in micro-chipping wear at elevated hardness.
- The experimental analysis of the process yielded improved performance. The confirmation test results showed an average improved percentage above 50% for each of the response factors i.e., resultant force, cutting power and tool wear.



## CHAPTER 4

### MULTI-OBJECTIVE OPTIMIZATION IN FACE MILLING OF AISI 1045 STEEL USING TAGUCHI-BASED GREY RELATIONAL AND DESIRABILITY FUNCTION ANALYSIS

M. Shnfir<sup>1</sup>, O.A. Olufayo<sup>1</sup>, W. Jomaa<sup>2</sup>, and V. Songmene<sup>1</sup>

<sup>1</sup>Department of Mechanical Engineering, École de Technologie Supérieure (ÉTS),  
1100 Notre-Dame St. West, Montréal, QC H3C 1K3, Canada;

<sup>2</sup>Cégep Édouard-Montpetit, Centre technologique en aérospatiale (CTA),  
5555 Place de la Savane, Saint-Hubert, Québec, QC J3Y 8Y, Canada

Paper submitted for International Journal of Materials Forming and Machining Processes,  
February, 27<sup>th</sup> 2020

#### **Abstract**

Machining conditions optimization is often required to determine optimal conditions leading to low machining cost and cycle time. In this article, an experimental study was carried out to optimize the face milling conditions (roughing and finishing) of AISI 1045 steel with ceramic inserts. The proposed approach establishes the effects of milling type, cutting speed, feed rate, workpiece hardness and cutting tool grades on surface finish, tool wear and cutting forces. The Taguchi L<sub>32</sub> orthogonal array is used for experimental design whereas the Grey Relational Analysis (GRA) and Desirability Function Analysis (DFA) are employed for multi-response optimization of the models and to obtain optimal cutting parameters. The results indicate that the multi-objective optimizations result in significant performance improvements over tool manufacturers' recommended parameters: when DFA analysis is used, there is a 108.5% and 35.7% improvement in roughing and finishing, respectively, compared to GRA analysis, which provides corresponding 20.2% and 3.8% improvements.

**Keywords:** AISI 1045; Ceramic inserts; Face milling; Grey Relational analysis, Desirability function analysis.

## Nomenclature

$a_c$	Radial depth of cut
$a_p$	Depth of cut
CBN	Cubic boron nitride
DFA	Desirability Function Analysis
$f$	Feed rate
$F_x, F_y$ and $F_z$	Cutting forces in the X, Y, and Z directions
GA	Genetic algorithm
GRA	Grey Relational Analysis
H	Hardness
$K_h$	Chip compression ratio
MRR	Metal removal rate
PCA	Principle Component Analysis
PCBN	Polycrystalline cubic boron nitride
PW	Power consumption
$\theta$	Chip-tool interface/cutting temperature
$R_a$	Arithmetic average height $\mu\text{m}$
$R_p$	Maximum height of peaks
$R_q$	Root-mean-square roughness
$R_t$	Maximum height of the profile
$R_v$	Maximum depth of valleys
T	Cutting temperature
tl	Tool life
UC	Undercut
V	Cutting speed
VB	Tool wear
$\beta_{\text{eff}}$	Effective shear angle
$\mu$	Friction coefficient at the tool rake surface and at the chip-tool interface

## 4.1 Introduction

Medium carbon steel AISI 1045 is one of the most widely used types of steel. Due to its high machinability and low cost, its applications are commonly seen in the fabrication of pump shafts, piston rods, cylinders, cams, and crankshafts. Recent advances in cutting machines and tool materials have led to an increase in the use of high-speed machining as the preferred industrial method for hardened steel and other alloy materials (Akhyar & Sayuti, 2015; Ashley, 1995; Janmanee, Wonthaisong, & Araganont, 2014; Janmanee, Wonthaisong, Saodaen, et al., 2014; Z. Liu et al., 2002; Z. Y. Zhao et al., 2010). The goal of using this technique is to manufacture high-quality products within a short time cycle, and at a reduced cost. During the process, high cutting temperatures are generated, which influence the performance of certain cutting tool materials. This being the case, cutting materials with improved resistance to elevated temperatures, such as cubic boron nitride (CBN) and

polycrystalline cubic boron nitride (PCBN), ceramics, cermet, as well as coated and uncoated cemented carbides, are often preferred (Hosseini et al., 2015; More, Jiang, Brown, & Malshe, 2006; Okada, Hosokawa, Tanaka, & Ueda, 2011; Gérard Poulachon, Bandyopadhyay, Jawahir, Pheulpin, & Seguin, 2004; G Poulachon et al., 2001). Ceramic cutting tools are particularly well-suited and widely employed in the high-speed machining of these hardened materials, given their high hardness, good wear resistance, high melting point and chemical stability (Aslan, Camuscu, & Birgoren, 2007; Bian, He, Ding, & Liu, 2017; X. Cui, Zhao, & Tian, 2013; Dewes & Aspinwall, 1997; Horng, Liu, & Chiang, 2008; Z. Liu et al., 2002; Soković et al., 2005; Trent & Wright, 2000). However, they generally have reduced toughness and high fragility, which often generates microchipping of the tool during non-continuous machining, and thus adversely affects the surface quality. For improved toughness, ceramics are commonly reinforced with Ti(C, N), and ZrO<sub>2</sub> additions (Aslan et al., 2007; A. S. Kumar et al., 2003; X. S. Li & Low, 1994; Lo Casto et al., 1996).

To optimize the fabrication of AISI 1045 products, cutting conditions influencing the surface quality in finishing operations, as well as tool wear and cutting forces during roughing tests, must themselves be optimized. Machining parameters, such as cutting speed, feed rate and depth of cut, are often studied because of their direct influence on these conditions. Conventional practice in industry for selecting cutting parameters for machining is often based on the operator's experience, tool manufacturers' directions, and machining data handbooks. This selection method for machining parameters is based on values obtained from experimental studies and fails to consider workpiece configuration, dimensional tolerances and other specific setup conditions employed. Based on these experimental variations, optimal conditions are often not established by these resources, and real-time machining adjustments are performed by the operator based on experience.

In the literature, different methods have been developed for the optimization of cutting conditions (such as the cutting force, surface roughness, tool life, and material removal rate). Taguchi analysis is one of the most widely used techniques in both scientific research and in industry. However, the technique is only used to efficiently optimize machining process parameters for single performance output. For multiple-performance optimization, other methods, such as Grey Relation Analysis (GRA), Genetic algorithm (GA) and Desirability.

Function Analysis (DFA), are often employed. Some recent studies using multi-objective optimization in the machining of steels are shown in Table 4-1.

Table 4-1 Current research using multi-objective optimization in the machining of steel.

Investigators	Major factors	Material	Machining	Responses	Optimization methodology
Manav and Chinchanikar (2018)	V, f, ap	AISI 4340	Hard turning	F, Ra, T, tl	GA
Narayanan, Baskar, and Ganesan (2018)	V, f, ap	OHNS/AISI H13	Hard turning	MRR, Ra	GA
Umamaheswarrao, Raju, Suman, and Sankar (2018)	V, f, ap, Nose radius	AISI 52100	Hard turning	F, Ra, T	Hybrid GRA-PCA
Misal and Sadaiah (2018)	Temperature, time, Concentration	Inconel 601	Photochemical machining	UC, MRR	GRA
Alok and Das (2019)	V, f, ap	AISI 52100	Hard turning	Ff, Fp, Fc, Ra, Vb	DFA
Ramu, Srinivas, and Vekatesh (2018)	V, f, ap	Stainless Steel 316	Turning	MRR, Ra	GRA
Mustafic <i>et al.</i> (2018)	V, f, ap and oil-to-water ratio	X5CrNi18-10 stainless	Turning	Fx, Fy, Fz, Fr, Ra, MRR	GRA
Mia <i>et al.</i> (2018)	V, f, ap	AISI 1060	Turning	Kh, $\mu$ , Beff, Te	GRA
Xavior and Jeyapandiarajan (2018)	Tool geometry, cutting tool material and cutting conditions	AISI D2	Hard Turning	Ra, T $\theta$ , tl, MRR	GRA
Kumari, Kumar, Kumar Yadav, and Vivekananda (2018)	V, f, ap	AISI D2	Turning	MRR, Ra	GRA with Harmony Search
Lobato, Sousa, Silva, and Machado (2014)	V, f, ap	AISI (ABNT) 420	End milling	TL, Fc	DFA, bee firefly, fish algorithm
Bagaber and Yusoff (2017)	V, f, ap	Stainless Steel 316	Turning	PW, Ra, TW	DFA
Ajaja <i>et al.</i> (2019)	Tool materials V, f, ap	300M steel	Hard Turning	Ra, white layer Residual stress	GRA and proportion quality loss reduction (PQLR) methodologies

\*- Speed (V), feed rate (f), depth of cut (ap), Cutting forces (F), Surface Roughness (Ra), Temperature (T), Tool life (tl), Material removal rate (MRR), Power (PW), chip compression ratio (Kh), effective shear angle ( $\beta_{eff}$ ), friction coefficient ( $\mu$ ), interface temperature ( $\theta$ ), undercut (UC) and Principle Component Analysis (PCA).

However, insufficient justification is often given for the choice of approach or for a comparison baseline for optimize techniques. These studies span a wide range of workpiece materials, output responses and selected optimization techniques.

Additionally, a review of research trends as shown in Table 4-1 identifies the optimization of surface roughness and cutting forces as primary responses used for optimization, and these studies are mostly conducted in turning operations. This trend is especially true for AISI 1045 studies, which focus more on turning than other operations. However, a few researchers have also studied the multi-optimization of cutting parameters on steels in milling operations (Lobato et al., 2014). The present study thus seeks to address milling operations in AISI 1045 steels, using two multi-response optimization techniques, to identify optimal cutting parameters for both finishing and roughing conditions. Experimental tests are conducted in face milling using round ceramic tools with varying edge preparations and consider both roughing and finishing conditions. A comparison is also made between the efficacies of both approaches. The robust analysis presented seeks to develop a guideline for multi-objective optimization selection.

## **4.2 Experimental Procedure**

### **4.2.1 Workpiece Material, Equipment and Cutting Tools**

Face milling experiments were performed in dry machining conditions on a NEXUS 410A 3-axis CNC vertical milling machine (Yamazaki Mazak Corporation, Oguchi, Japan). In the face milling tests, AISI 1045 material pieces with varying Rockwell Hardness values of 38, 43, 48, 53 HRC were selected with the following dimensions: 250 mm × 100 mm × and 25 mm. Details of the thermal treatment process for the steel workpiece are given in Table 4-2.

The chemical composition of the workpiece material is given in Table 4-3. Two grades of ceramic inserts were used in the experimental tests. Silicon nitride (SiAlON)-based ceramic and Whisker ceramic with a matrix of  $Al_2O_3 + SiC$  were used with two different edge preparations, namely, a honed cutting edge and chamfer (with negative rake angle). The ceramic inserts were mounted on a Shell mills type KDNR250RN40C3 tool holder with four inserts, as recommended by Kennametal Inc. Straight cutting passes were made along the

length of the workpiece, and the most affected cutting insert on the tool was taken for analysis. The characteristics of the grades of each insert are listed in Table 4-4.

Table 4-2 Heat treatment process for AISI 1045 steel.

Hardness of workpiece material	Temperature (°C)	
	Quench	Temper
38 HRC	850	470
43 HRC		410
48 HRC		345
53 HRC		260

Table 4-3 Chemical composition of workpiece material (% weight).

C	Mn	P	S	Si	Fe
0.459	0.721	0.0086	0.0027	0.259	balance

Table 4-4 Characteristic of used ceramic inserts.

Tool	Edge preparation	Grade Name	Grade Description
1	honed (RNG45E)	KY2100	Silicon Nitride (SiAlON) base Ceramic
2	T-land (RNG45T0420)		
3	honed (RNG45E)	KY4300	Whisker ceramic with a matrix of $Al_2O_3 + SiCW$
4	T-land (RNG45T0420)		

#### 4.2.2 Experimental Measurements

In this study, tool wear, cutting force and surface roughness were measured during the face milling of AISI 1045 steel. Tool wear was measured using a KEYENCE VHX-500 FE digital microscope (Keyence Corporation, Osaka, Japan), while images were captured at magnifications above x50. Only flank wear measurements were considered.

In machining, the cutting force serves as an indicator of cutting process conditions, such as power consumption, wear, productivity and surface roughness. The parameter is widely used in research and industry as a suitable factor to indicate the cutting condition. Therefore, in this study, the three force components ( $F_x$ ,  $F_y$ , and  $F_z$ ) were measured during cutting, with a Kistler dynamometer table erected in the milling machine. The workpiece was mounted on a

vice and set up on the dynamometer (Figure 4-1). Force acquisition was done using a DAQ system and amplified by a gain of 2000, and then processed using LabVIEW® software.  $F_x$ ,  $F_y$ , and  $F_z$  were used for the multi-objective optimization.

The surface finish is often used as the quality index of a product due to its influence on mechanical properties such as frictional coefficients of parts. The surface roughness was measured using a Mitutoyo SURFTEST SJ-410 (Mitutoyo America Corporation, Illinois, United States) over an area of 25 mm × 25 mm. The roughness acquisitions were measured parallel to the feed direction within the area machined at three different points along the length of cut. From these acquisitions, an average value was then determined. Prior to surface roughness measurements, the Mitutoyo profilometer was recalibrated with a standard calibration block.

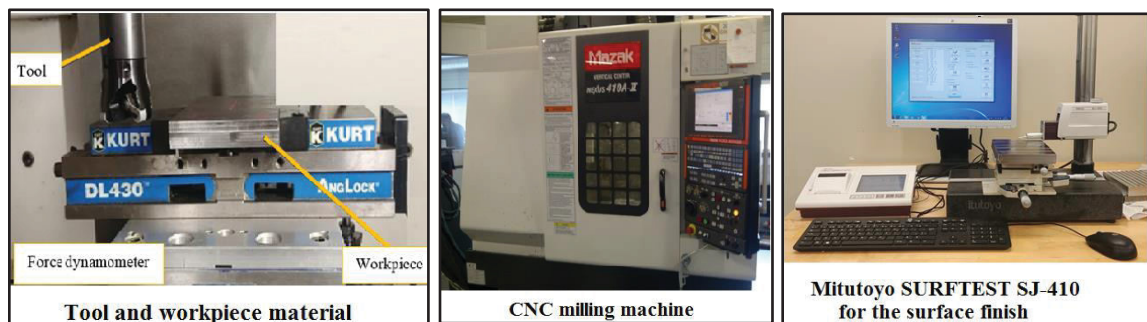


Figure 4-1 Experimental setup for face milling and surface roughness tester.

Several roughness amplitude parameters are often specified to designate the surface finish (Aouici et al., 2016; Fnides, Yallese, Khattabi, Mabrouki, & Girardin, 2017; Gadelmawla, Koura, Maksoud, Elewa, & Soliman, 2002), and the three most common and important of these were considered in this study to quantify the surface quality: the arithmetic average height ( $R_a$ ), the root-mean-square roughness ( $R_q$ ), and the maximum height of the profile ( $R_t$ ) (Bhattacharya, Das, Majumder, & Batish, 2009). These parameters were selected due to their sensitivity to high peaks and deep scratches. Equations 4-1, 4-2 and 4-3 below are used to measure these parameters:

$$R_a = \frac{1}{l} \int_0^l |y(x)| dx = \frac{1}{n} \sum_{i=1}^n |y_i|, \quad (4-1)$$

$$R_q = \sqrt{\frac{1}{l} \int_0^l \{y(x)\}^2 dx} = \sqrt{\frac{1}{n} \sum_{i=1}^n y_i^2}, \quad (4-2)$$

$$R_t = R_p + R_v \quad (4-3)$$

A depiction of the surface profile with its surface roughness measurements parameters is shown in Figure 4-2.

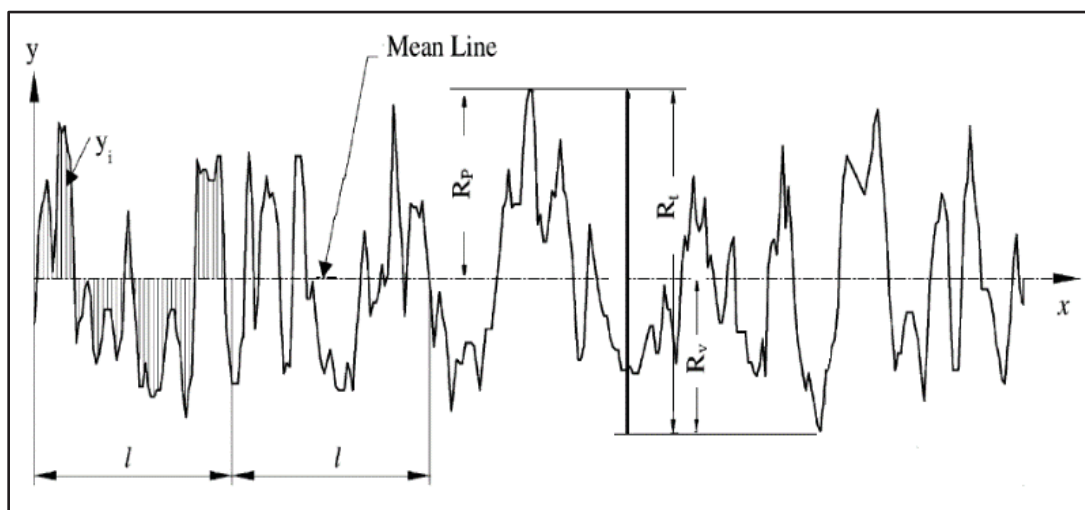


Figure 4-2 Definition of the Arithmetic average height ( $R_a$ ), and Maximum height of the profile ( $R_t$ ) parameters.

$L$  is the relative length of the profile,  $n$  is the number of intersections of the profile at the mean line (intersections),  $R_p$  is maximum height of peaks ( $\mu\text{m}$ ) and  $R_v$  is maximum depth of valleys ( $\mu\text{m}$ ).

### 4.2.3 Experimental Design with Taguchi

The Taguchi method has been commonly used in engineering design of experiments as a powerful investigative tool. By definition, the Taguchi DOE is a powerful optimization tool, which uses orthogonal arrays to examine the quality of factors by employing a reduced amount of experiments. Its main advantage lies in the limited amount of experimental designs it needs in its orthogonal arrays design. It also decreases the effect of uncontrollable factors (also known as noise factors), thus providing a better understanding of machining

variables and their commercial consequences for improved engineering quality in industries (Montgomery, 2017; Phadke, 1989). Recently, many research works have been using the Taguchi method as a statistical tool for process optimization (Bian et al., 2017; Patel et al., 2015; Syahmi Shahrom, Mat Yahya, & Razlan Yusoff, 2013). It has also been applied in the processing of the machining optimization of AISI 1045 steel. Some research has also been performed on the optimization of surface roughness and power consumption during the machining of AISI 1045 (Bhattacharya et al., 2009; Ozcelik & Bayramoglu, 2006; Qasim, Nisar, Shah, Khalid, & Sheikh, 2015).

In the present study, the Taguchi  $L_{32} (2^1 4^4)$  orthogonal array was selected to determine the optimal cutting conditions and to establish the effects of machining parameters. The cutting parameters and conditions, such as milling type (Up, Down), cutting speed, feed rate, hardness and tool, were selected as control factors and surface roughness parameters were selected as output factors. The control factors and their different levels are given in Table 4-5. The characteristics of the ceramic inserts used are given in Table 4-4. The experimental design table is shown in Table 4-6.

Table 4-5 Cutting parameters and their levels.

Cutting Parameters	Unit	Level 1	Level 2	Level 3	Level 4
A: Milling type		Up	Down		
B: Speed	V [m/min]	200	300	400	500
C: Feed	$f_z$ [mm/th]	0.05	0.09	0.13	0.17
D: Hardness	H [HRC]	38	43	48	53
E: Tools	T	T1	T2	T3	T4
Axial depth of cut ( $a_p$ )	[mm]	2			
Radial depth of cut ( $a_e$ )	[mm]	25.4			

Table 4-6 Taguchi L<sub>32</sub> experimental design plan.

No	Milling Type	Speed (m/min)	Feed (mm/th)	Hardness (HRC)	Tool	
1	Up	200	0.05	38	T1	H(KY2100)
2	Up	200	0.09	43	T2	T(KY2100)
3	Up	200	0.13	48	T3	H(KY4300)
4	Up	200	0.17	53	T4	T(KY4300)
5	Up	300	0.05	38	T2	T(KY2100)
6	Up	300	0.09	43	T1	H(KY2100)
7	Up	300	0.13	48	T4	T(KY4300)
8	Up	300	0.17	53	T3	H(KY4300)
9	Up	400	0.05	43	T3	H(KY4300)
10	Up	400	0.09	38	T4	T(KY4300)
11	Up	400	0.13	53	T1	H(KY2100)
12	Up	400	0.17	48	T2	T(KY2100)
13	Up	500	0.05	43	T4	T(KY4300)
14	Up	500	0.09	38	T3	H(KY4300)
15	Up	500	0.13	53	T2	T(KY2100)
16	Up	500	0.17	48	T1	H(KY2100)
17	Down	200	0.05	53	T1	H(KY2100)
18	Down	200	0.09	48	T2	T(KY2100)
19	Down	200	0.13	43	T3	H(KY4300)
20	Down	200	0.17	38	T4	T(KY4300)
21	Down	300	0.05	53	T2	T(KY2100)
22	Down	300	0.09	48	T1	H(KY2100)
23	Down	300	0.13	43	T4	T(KY4300)
24	Down	300	0.17	38	T3	H(KY4300)
25	Down	400	0.05	48	T3	H(KY4300)
26	Down	400	0.09	53	T4	T(KY4300)
27	Down	400	0.13	38	T1	H(KY2100)
28	Down	400	0.17	43	T2	T(KY2100)
29	Down	500	0.05	48	T4	T(KY4300)
30	Down	500	0.09	53	T3	H(KY4300)
31	Down	500	0.13	38	T2	T(KY2100)
32	Down	500	0.17	43	T1	H(KY2100)

#### 4.2.4 Multi-objective optimization approach - Grey Relational Analysis (GRA)

Grey relational analysis is one of the more modest and reliable techniques for machining prediction. It is used to address multi-objective optimization problems. The approach was selected in the present study to determine the optimal combination of milling parameters needed to improve surface roughness in finishing operations and forces in roughing operations. A grey system is indicative of a system with poor and limited relevant information (Wulandhari, Wibowo, & Desa, 2014). A flowchart of its operational process is shown in Figure 4-3.

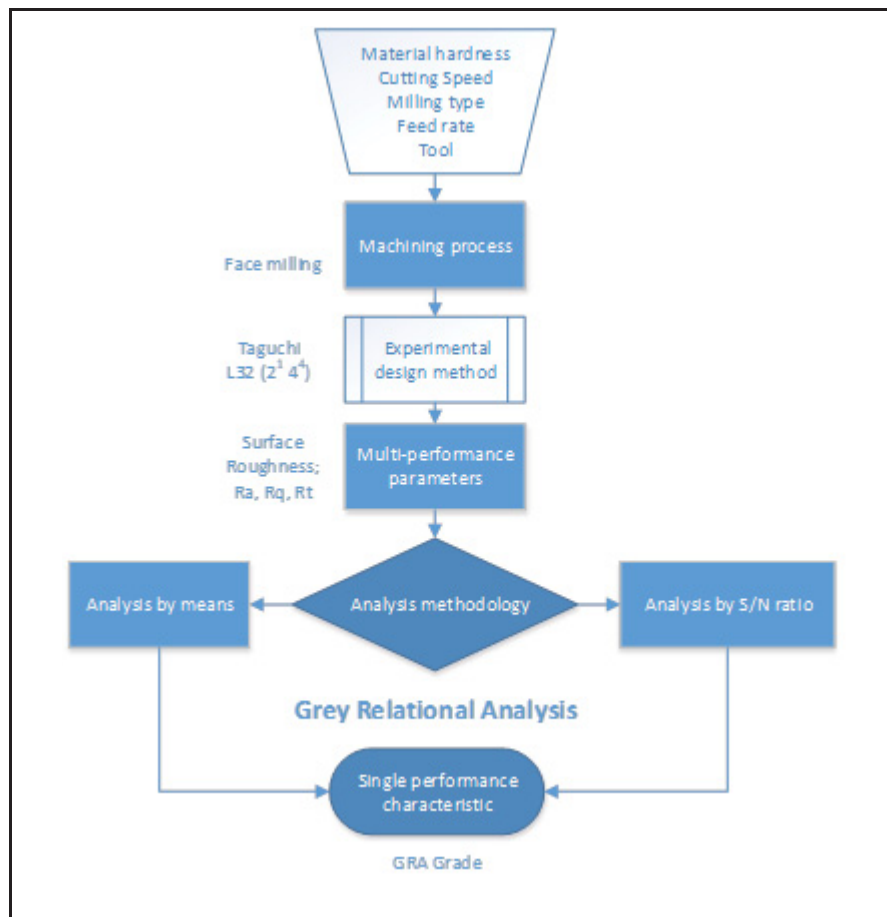


Figure 4-3 Flowchart of the multi-objective optimization approach (adapted from (Jomaa, Levesque, Bocher, Divialle, & Gakwaya, 2017)).

Other complicated interrelationships among multiple performance characteristics using grey system theory based on Taguchi orthogonal array experimental data were previously

developed by Deng (Deng, 1989; Ju-Long, 1982). This method is widely applied in the performance of complex projects with little or incomplete information. The individual steps taken in this study for the multi-optimization approach are shown in Figure 4-4.

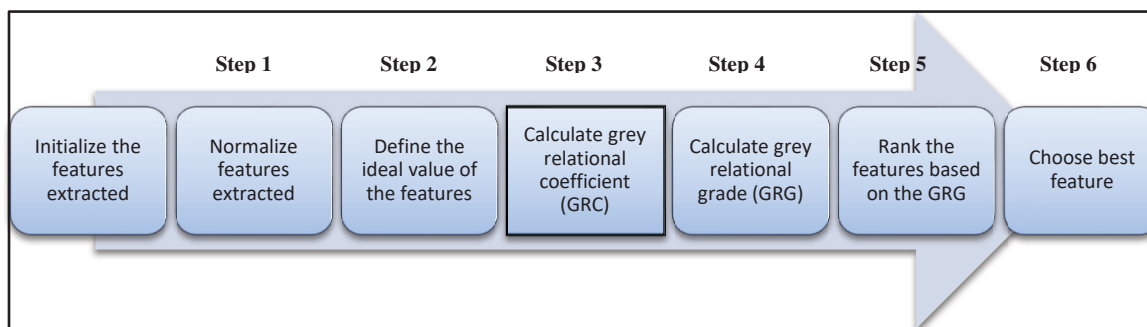


Figure 4-4 Grey relational analysis procedures.

**Step – 1:** Firstly, the experimental results are normalized to avoid a scaling problem with the results. The measured performance characteristics are then transformed to dimensionless parameters from 0 to 1 (Gopalsamy, Mondal, & Ghosh, 2009). Table 4-7 shows the results from the normalization of the responses. In this case, for the target value of the surface roughness, “*smaller is better*”; the surface roughness is then normalized using Eq. 4-4:

$$x_i^* (k) = \frac{\max x_i^0 (k) - x_i^0 (k)}{\max x_i^0 (k) - \min x_i^0 (k)}, \quad (4-4)$$

where,  $k = 1$  to  $n$  ( $n$  is the performance characteristic); and  $i = 1$  to  $m$  ( $m$  is the number of experimental data points):

$x_i^* (k)$  denotes the sequence after the data preprocessing

$x_i^0 (k)$  denotes the original sequence

$\min x_i^0 (k)$  denotes the smallest value of  $x_i^0 (k)$

$\max x_i^0 (k)$  denotes the largest value of  $x_i^0 (k)$

**Step - 2:** Definition of the ideal values by identifying the deviation of normalized results from ideal value i.e. lowest surface roughness (See Eq. 4-5):

$$\Delta_{0i}(k) = \|x_0^*(k) - x_i^*(k)\|, \quad (4-5)$$

where,  $\Delta_{0i}(k)$ , the deviation sequence is the absolute difference value between the reference sequence  $x_0^*(k)$  and the comparability sequence after normalization  $x_i^*(k)$ . In this case the  $x_0^*(k)$ , corresponds to the lowest surface roughness parameters value.

**Step - 3:** The calculation of the grey relational coefficient  $\xi_i(k)$  is performed by using Eq. 4- 6:

$$\xi_i(k) = \frac{\Delta_{min} + \zeta \Delta_{max}}{\Delta_{0i}(k) + \zeta \Delta_{max}}, \quad (4-6)$$

where,  $\Delta_{min}$  and  $\Delta_{max}$  are the minimum and maximum values of the absolute differences ( $\Delta_{0i}$ ) of all comparing sequences.  $\zeta$  is distinguishing or identification coefficient:  $\zeta \in [0, 1]$ .  $\zeta = 0.5$  is generally used (Gopalsamy et al., 2009; Lu, Chang, Hwang, & Chung, 2009; Tzeng, Lin, Yang, & Jeng, 2009).

**Step – 4:** The grey relation grade is calculated from the coefficients. It is the weighted sum of the grey relational coefficients and represents the level of correlation between the reference and compatibility sequences. It can be calculated using Eq. 4-7:

$$\gamma_i = \frac{1}{n} \sum_{k=1}^n \xi_i(k), \quad (4-7)$$

where,  $\gamma_i$  is grey relation grade and  $n$  is the number of response characteristics. A higher grey relational grade value represents a stronger relational degree between the reference sequence and compatibility sequence. The highest grey relational grade values represent the optimal parametric combination for multi-responses.

**Step – 5:** The ranking and determination of the optimal combination of process parameters from the experimental sets is then calculated. The GRG sequence denotes the measure of correlation between the most favourable conditions obtained and a comparison output sequence of its individual responses for a multi-performance evaluation. The grade values obtained range from 0 to 1. Therefore, the closer the values are to unity, the better the multi-performance characteristic, and product quality.

**Step – 6:** After optimal combination of process parameters is determined, the proposed approach is verified by running confirmation experiments. The prediction of the grey relational grade under optimum level parameters can be obtained as follows:

$$\hat{\gamma} = \gamma_m + \sum_{i=1}^o (\bar{\gamma}_i - \gamma_m), \quad (4-8)$$

where,  $\gamma_m$  is the total mean grey relational grade,  $\bar{\gamma}_i$  is the mean grey relational grade at the optimal level of each parameter, and  $o$  is number of the machining parameters that significantly affects the multiple performance characteristics (Kumar Sahoo & Sahoo, 2013; Nalbant, Gökkaya, & Sur, 2007; Panda, Sahoo, & Rout, 2016).

#### 4.2.5 Desirability Function Analysis (DFA)

Desirability function analysis is widely used in industry for multi-response processes. It follows the principle that the “quality” of a product or process that has multiple quality characteristics with one of them outside some “desired” limits is deemed “unacceptable”. The process finds the operating conditions  $\mathbf{x}$  which provide the “most desired” response values.

**Step – 1:** Calculation of the desirability index from three forms of desirability functions for the corresponding responses. It is based on the formula proposed by Derringer and Suich (1980), and the known functions are:

- i. Smaller is better: In this situation a smaller value of  $y_j$  indicates a more favourable result. Below a threshold, a desirability of 1 is given and the desirability of 0 if above.

$$d_i = \left\{ \begin{array}{l} 1, y_j \leq y_{min} \\ \left( \frac{y_j - y_{max}}{y_{min} - y_{max}} \right), 1, y_{min} \leq y_j \leq y_{max}, r \geq 0 \\ 0, y_j \geq y_{min} \end{array} \right\} \quad (4-9)$$

- ii. Nominal is better: The value of  $y_j$  is expected to reach a particular target value “T” to be desirable. Any deviation from this target value gives a desirability of 0.

$$d_i = \left\{ \begin{array}{l} \left( \frac{y_j - y_{min}}{T - y_{min}} \right)^s, y_{min} \leq y_j \leq T, s \geq 0 \\ \left( \frac{y_j - y_{min}}{T - y_{min}} \right)^s, T \leq y_j \leq y_{max}, s \geq 0 \\ 0 \end{array} \right\} \quad (4-10)$$

- iii. Larger is better: A larger value of  $y_j$  indicates a more favorable result. Above a threshold, a desirability of 1 is given and 0 if below (Bara, Sahoo, Naik, Sahu, & Mahapatra, 2018).

$$d_i = \left\{ \begin{array}{l} 0, y_j \leq y_{min} \\ \left( \frac{y_j - y_{max}}{y_{min} - y_{max}} \right), 1, y_{min} \leq y_j \leq y_{max}, r \geq 0 \\ 1, y_j \geq y_{min} \end{array} \right\} \quad (4-11)$$

**Step – 2:** An estimation the overall desirability of the responses is computed from the equation:

$$d_o = \sqrt[w]{(d_1^{w1} \times d_2^{w2} \dots d_i^{wi})}, \quad (4-12)$$

where,  $w$  and  $w_i$  are the weights for each partial desirability.

**Step – 3:** Determination of the optimal parameter and its level combination. Essentially, the greater the composite desirability, the better the multiple performance characteristics.

**Step – 4:** After optimal conditions have been determined, a verification of the calculated optimal conditions values with experimental tests is performed.

## 4.3 Results and Discussion

### 4.3.1 Measurement of Response Factors

The wear formation of cutting tools influences the quality of machined products. Part surface deterioration due to tool wear also has an effect on functionality. To mitigate wear formation, measurements are collected to establish its influence on the surface. The different grades of ceramic tools used in this study are listed in Table 4-4. In the literature, the presence of  $Al_2O_3$  improves the dissolution resistance of the material, but leaves it prone to local plastic

deformation at high temperatures (Skogsmo, Halvarsson, & Vuorinen, 1992). This is believed to be primarily as a result of the of  $\text{Al}_2\text{O}_3$  composition in the ceramic material, which improves its dissolution resistance during cutting. Two main types of wear mechanisms are observed in the study, namely, abrasion and micro-chipping, depending on tool edge preparation. Wear observed on tool grade KY4300 is mostly due to micro-scale abrasion, but micro-chipping is found with some cutting conditions. Some examples of tool wear observed on cutting tools are shown in Figure 4-5.

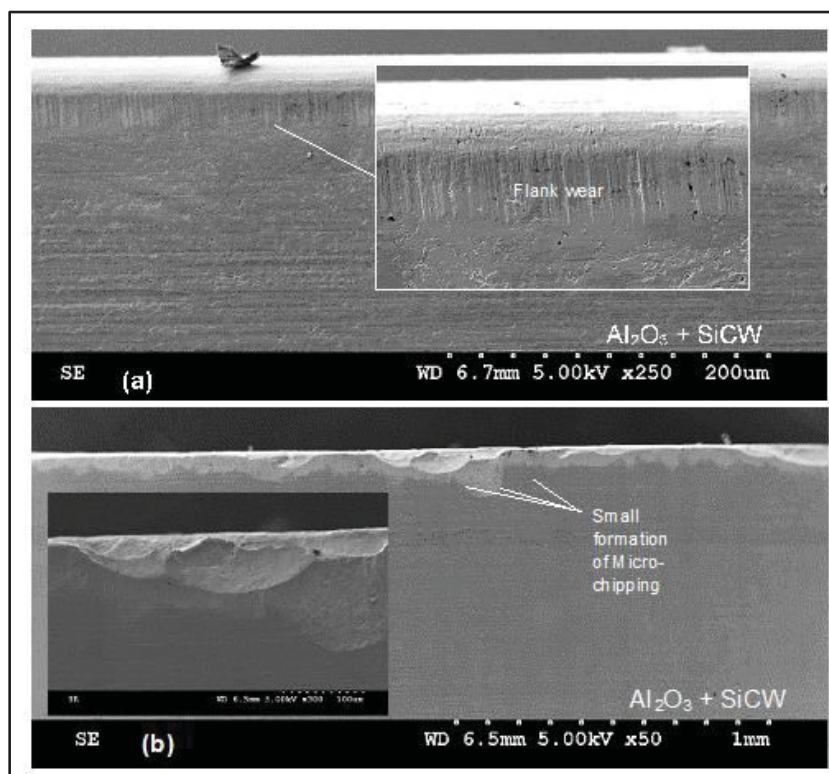


Figure 4-5 Example of SEM of tool wear in face milling experiments.  
 (a) Experiment: Honed – (300m/min, 0.17mm/th, 53HRC)  
 (b) Experiment: Chamfered – (200m/min, 0.17mm/th, 53HRC).

As indicated earlier, surface roughness defects on finished products influence the products' functionality and value, and consequently, for most products, the roughness values must be measured and estimated. Among the different known surface parameters, the Arithmetic and Root-mean-square are the most used in industry to establish the surface integrity of a product. These main parameters, as well as peak surface values, provide essential details on

the average roughness, the depth of the machined ridges, and the effects on cutting conditions, such as surface lubrication during cutting.

An assessment of the cutting conditions and quality of the product can also be established from the cutting forces. They provide information on changes in tool conditions and can be related to achievable surface quality. An example of a measured cutting force value is shown in Figure 4-6. The next sections show the multi-objective analyses performed by GRA and DFA in the estimation of the optimal parametric combinations for both roughing and finishing operations.

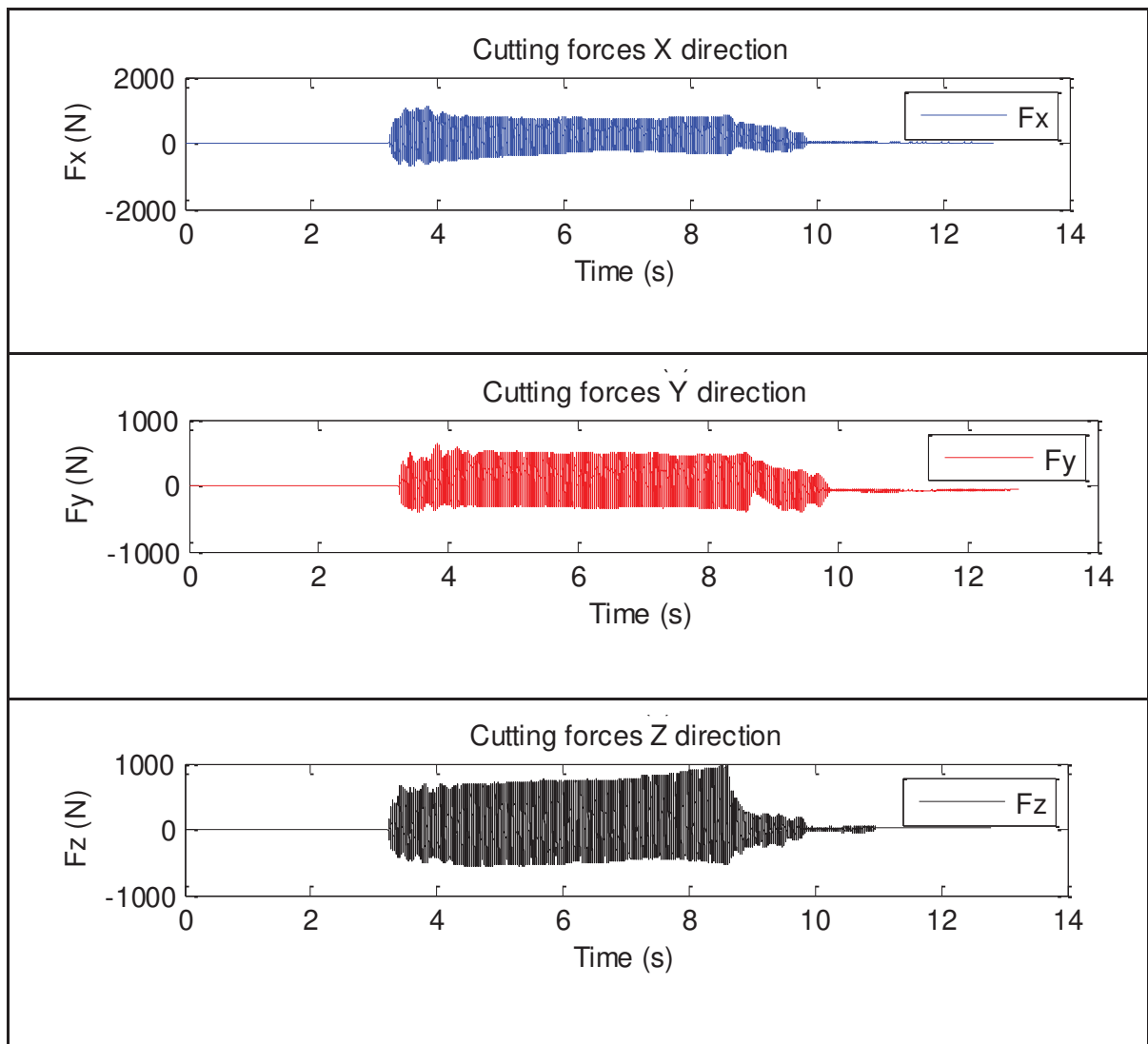


Figure 4-6 Sample force time acquisition (experiment 12).

### 4.3.2 Comparison for Roughing Parameters

The estimations derived in this section only consider response factors related to roughing operations which provide a reduced demand in power from the machine tool. As increased tool wear yields an increase in cutting forces, this multi-objective analysis comprises of the cutting forces ( $F_x$ ,  $F_y$ ) and the wear generated on the tools ( $V_B$ ).

### 4.3.3 GRA Analysis for Roughing Operation

The results of the GRA analysis for the roughing operations is shown in Table 4-7. This indicates the calculated grey normalized values, relational coefficients and grey relational grade values. The optimal grey relational grade value in this experiment was obtained on the 1<sup>st</sup> cutting test.

The determination of optimal conditions using the ANOVA and main effect plot allows a detailed review of the influence of each parameter on the GRG. The ANOVA results were used to assess the significance of the parameters influencing the multi-response results at a 95 percent confidence level (Table 4-8). This identified the hardness and feed rate as significant factors for a model solution for the data. However, the milling type, cutting speed and tool type were seen as insignificant.

Table 4-7 Grey relational normalized values, coefficient and grey relational grade values.

Run	Normalized values of		Grey relational coefficient		GRG	Rank
	Fxy	VB	Fxy	VB		
1	0.997	0.779	0.994	0.693	<b>0.844</b>	<b>1</b>
2	0.693	0.758	0.620	0.674	<b>0.647</b>	<b>20</b>
3	0.455	0.942	0.479	0.896	<b>0.687</b>	<b>16</b>
4	0.377	1.000	0.445	1.000	<b>0.723</b>	<b>11</b>
5	1.000	0.749	1.000	0.666	<b>0.833</b>	<b>3</b>
6	0.375	0.792	0.444	0.706	<b>0.575</b>	<b>27</b>
7	0.571	0.979	0.538	0.959	<b>0.749</b>	<b>8</b>
8	0.216	0.965	0.389	0.935	<b>0.662</b>	<b>18</b>
9	0.798	0.868	0.712	0.791	<b>0.752</b>	<b>7</b>
10	0.616	0.917	0.565	0.857	<b>0.711</b>	<b>13</b>
11	0.628	0.843	0.573	0.761	<b>0.667</b>	<b>17</b>
12	0.253	0.849	0.401	0.768	<b>0.585</b>	<b>26</b>
13	0.960	0.750	0.926	0.667	<b>0.796</b>	<b>4</b>
14	0.705	0.880	0.629	0.807	<b>0.718</b>	<b>12</b>
15	0.540	0.862	0.521	0.783	<b>0.652</b>	<b>19</b>
16	0.133	0.780	0.366	0.695	<b>0.530</b>	<b>30</b>
17	0.810	0.139	0.725	0.367	<b>0.546</b>	<b>29</b>
18	0.699	0.914	0.624	0.853	<b>0.739</b>	<b>10</b>
19	0.401	0.866	0.455	0.789	<b>0.622</b>	<b>21</b>
20	0.147	0.905	0.369	0.841	<b>0.605</b>	<b>23</b>
21	0.764	0.932	0.679	0.881	<b>0.780</b>	<b>5</b>
22	0.940	0.498	0.893	0.499	<b>0.696</b>	<b>15</b>
23	0.356	0.124	0.437	0.363	<b>0.400</b>	<b>32</b>
24	0.264	0.862	0.404	0.783	<b>0.594</b>	<b>24</b>
25	0.744	0.913	0.661	0.852	<b>0.757</b>	<b>6</b>
26	0.494	0.958	0.497	0.923	<b>0.710</b>	<b>14</b>
27	0.912	0.000	0.850	0.333	<b>0.592</b>	<b>25</b>
28	0.000	0.862	0.333	0.783	<b>0.558</b>	<b>28</b>
29	0.886	0.914	0.814	0.853	<b>0.833</b>	<b>2</b>
30	0.667	0.931	0.600	0.878	<b>0.739</b>	<b>9</b>
31	0.526	0.802	0.513	0.717	<b>0.615</b>	<b>22</b>
32	0.389	0.482	0.450	0.491	<b>0.471</b>	<b>31</b>

Table 4-8. ANOVA for Grey Relational Grade in roughing conditions.

SOURCE	DF	SEQ SS	ADJ SS	ADJ MS	F	P
A: Milling Type	1	0.0238	0.0238	0.0238	1.60	0.217
B: Speed V	1	12.9476	0.0264	0.0264	1.77	0.195
C: Feed $f_z$	1	0.1537	0.0678	0.0678	4.55	<b>0.043</b>
D: Hardness H	1	1.1135	1.1135	1.1135	74.76	<b>0.000</b>
E: Tool T	3	0.0315	0.0315	0.0104	0.70	0.558
Residual Error	25	0.3723	0.3723	0.0149		
Total	32	14.6424				

The main effects between parameters and GRG response are shown in Figure 4-7 and Table 4-9. Here, the correlation and trends between GRG to individual parameters are shown. The feed rate is the most influential parameter for the responses, followed by the hardness, cutting tool, milling type and cutting speed. Based on the above, the optimal cutting parameter combination is: milling type at  $A_1$  (up milling), cutting speed at  $B_1$  (200 m/min), feed rate at  $C_1$  (0.05 mm/tooth), hardness at  $D_3$  (48 HRC), and cutting tool at  $E_3$  (Honed KY4300), ( $A_1B_1C_1D_3E_3$ ).

The importance of selecting the right tool grade in roughing operations is highlighted in these results. The whisker ceramic reinforced with  $Al_2O_3 + SiCW$  matrix tools (tool 3, honed KY4300 and tool 4, T-land KY4300) produced improved GRG values. Roughing conditions mostly characterized to possess an increased material removal rate was identified as improving at low feeds using the up milling cutting mode. Due to the brittle nature of the tool, a reduced feed, in this condition is thus advantageous.

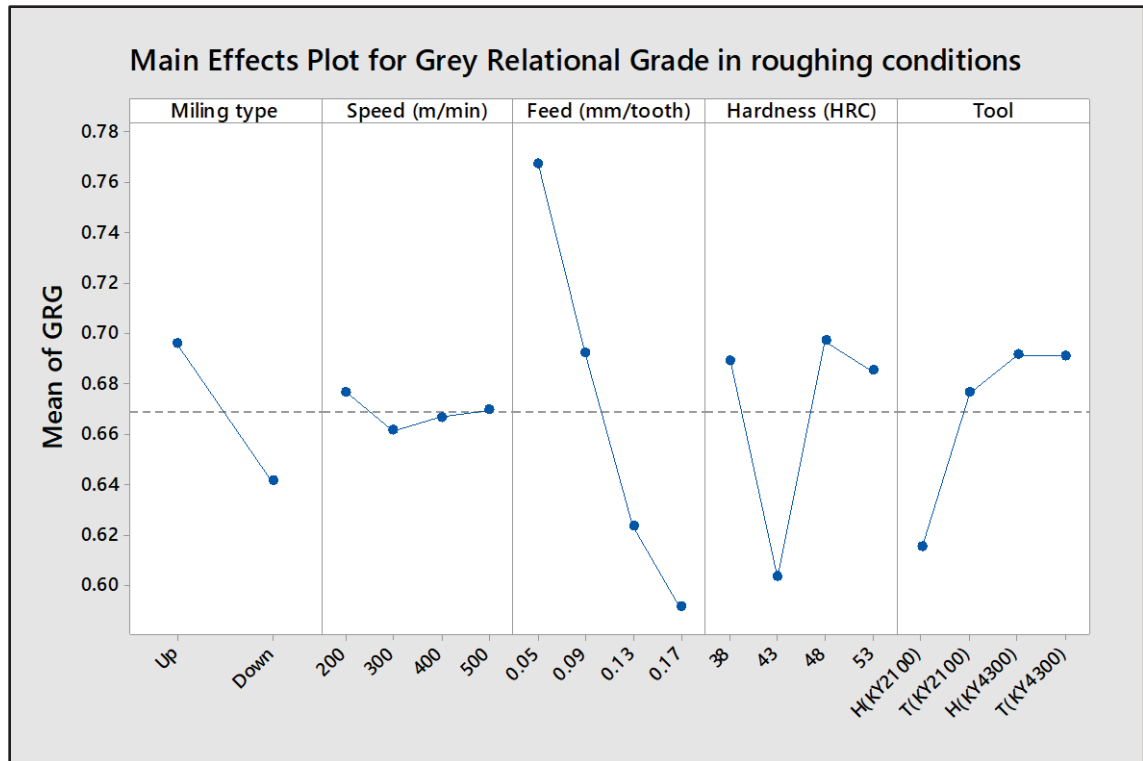


Figure 4-7 Main effects plot for GRA.

Table 4-9 Main effects on mean Grey Relational Grade in roughing conditions.

Level	Mean Grey Relational Grade				Delta	Rank
	1	2	3	4		
A: Milling type	0.6956	0.6410			0.0546	4
B: Speed (m/min)	0.6765	0.6611	0.6664	0.6693	0.0154	5
C: Feed (mm/tooth)	<b>0.7675</b>	0.6918	0.6230	0.5909	0.1766	1
D: Hardness (HRC)	0.6890	0.6026	<b>0.6969</b>	0.6848	0.0943	2
E: Tool	0.6151	0.6760	<b>0.6913</b>	0.6909	0.0763	3
<b>Total mean grey relational grade = 0.668</b>						

#### 4.3.4 DFA Analysis for Roughing Operation

The mean response and the total mean of the composite desirability at optimal conditions are shown in Figure 4-8. From the plot, optimal cutting parameters are found at 370 m/min, 0.05 mm/th, 38 Hardness, up milling and T-land (KY2100) tool grade. These results deviate from GRA at the selected cutting speed, material hardness and cutting tool. However, there is no significant difference in the performance of tool 2 and tool 3 (Figures. 4-8 and 4-9).

Therefore, the main differences between the optimal parameters given by the DFA and that given by the GRA analysis are in the cutting speed and in the workpiece material hardness.

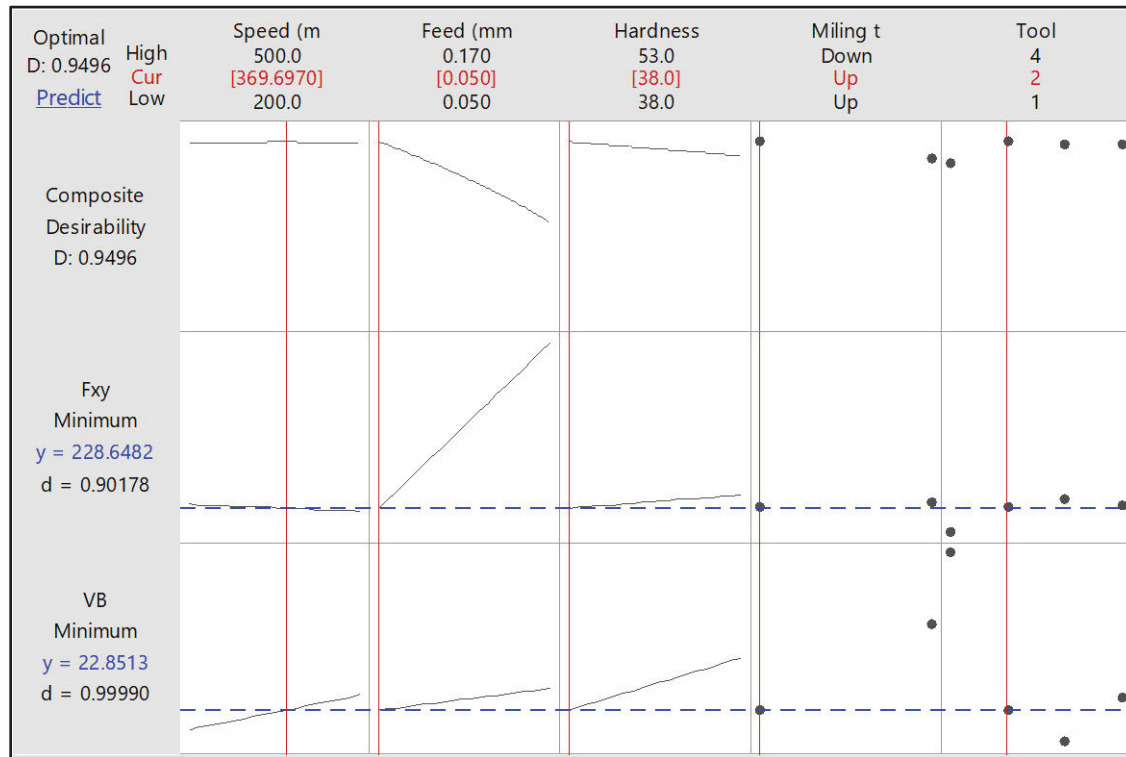


Figure 4-8 Desirability response optimization plot for roughing operation.

The ANOVA analysis also identifies a significant model solution at a 95 percent confidence level, with the feed rate and the hardness as significant factors. The milling type, cutting speed and tool type are also seen to be insignificant for model prediction (Table 4-10).

Figure 4-9 shows the main effect plot of the factors on the composite desirability values for the levels of the cutting parameters. The main effect plot in DFA analysis was only used to show the inclination of factors to the response, as DFA plots obtained already provide optimal conditions. Figure 4-9 shows an improvement in desirability at with a decrease in feed rate and hardness but an average cutting speed.

Table 4-10 ANOVA for Desirability Function Analysis in roughing conditions.

SOURCE		DF	SEQ SS	ADJ SS	ADJ MS	F	P
A: Milling Type		1	0.0525	0.0525	0.0525	2.16	0.155
B: Speed	V	1	12.3007	0.0987	0.0987	4.05	0.055
C: Feed	$f_z$	1	0.0001	0.4103	0.41034	16.85	<b>0.000</b>
D: Hardness	H	1	1.3013	1.3013	1.30132	53.45	<b>0.000</b>
E: TOOL	T	3	0.0399	0.0399	0.01329	0.55	0.655
Residual Error		25	0.6087	0.6087	0.02435		
Total		32	14.3032				

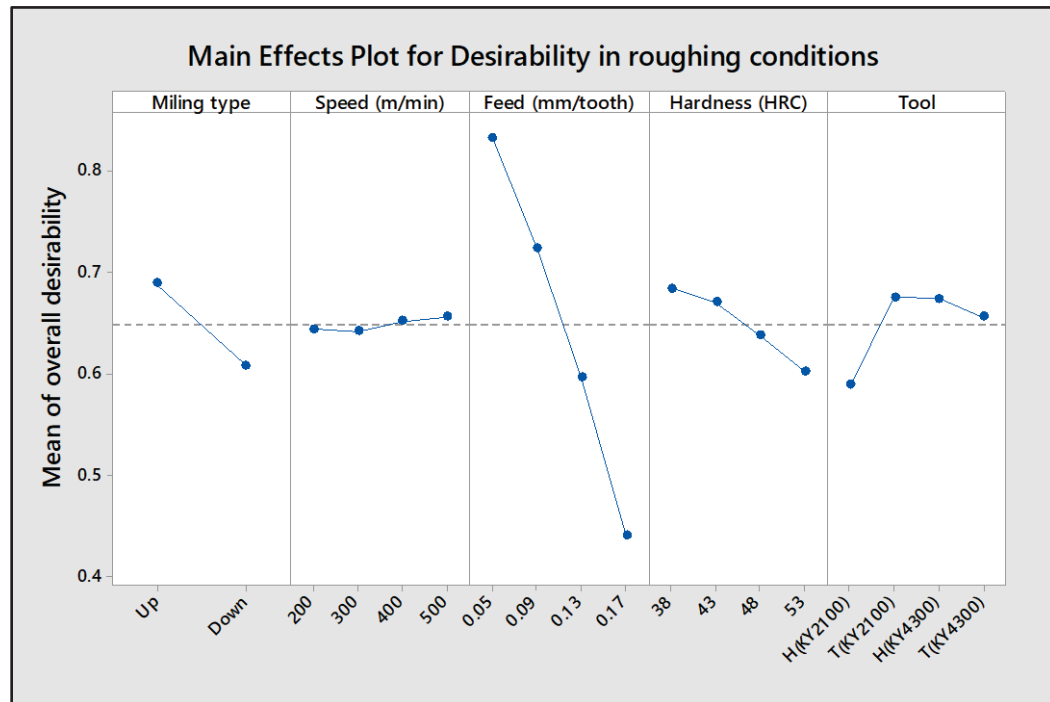


Figure 4-9 Main effects plot for DFA.

A review of the response table for DFA (Table 4-11) indicate that the feed rate type is the most significant cutting parameter affecting the multiple performance characteristics, followed by the cutting tool, the hardness of the material, the milling type and lastly the cutting speed. Therefore, in roughing operations, this technique also gives preference to up milling which possess a higher tool impact on entry but at a lower feed rate. Therefore,

selection of the right tool edge preparation is crucial tool life with improved results observed using chamfered edge.

Table 4-11 Response table for Desirability Function Analysis in roughing conditions.

Level	Means for Desirability Function Analysis				Delta	Rank
	1	2	3	4		
A: Milling type	<b>0.6897</b>	0.6087			0.0810	<b>4</b>
B: Speed (m/min)	0.6446	0.6428	0.6524	<b>0.6570</b>	0.0142	<b>5</b>
C: Feed (mm/tooth)	<b>0.8340</b>	0.7241	0.5976	0.4411	0.3928	<b>1</b>
D: Hardness (HRC)	<b>0.6848</b>	0.6712	0.6380	0.6028	0.0820	<b>3</b>
E: Tool	0.5895	<b>0.6759</b>	0.6748	0.6565	0.0864	<b>2</b>
<b>Total Means for Desirability Function Analysis = 0.649</b>						

The optimal cutting parameters combination from the desirability plot (Figure 4-8) gives: milling type at A<sub>1</sub>, cutting speed at B<sub>3</sub>, feed rate at C<sub>1</sub>, hardness at D<sub>1</sub>, and cutting tool at E<sub>2</sub> (A<sub>1</sub>B<sub>3</sub>C<sub>1</sub>D<sub>1</sub>E<sub>2</sub>).

#### 4.4 Confirmation Test for Roughing

To verify the performance characteristics of roughing parameters predicted, additional confirmation experiments of the optimized combination of both multi-optimization techniques was performed. From these confirmation tests, the percentage improvement from each technique is determined (Table 4-12 and 4-13).

Table 4-12 Confirmation test GRA grade optimization parameters in roughing conditions.

Grey Relational Grade for roughing operation			
Performance characteristics	Initial process parameters	Optimal process parameters	
		Prediction	Experiment
Level	A <sub>1</sub> B <sub>1</sub> C <sub>4</sub> D <sub>4</sub> E <sub>4</sub>	A <sub>1</sub> B <sub>1</sub> C <sub>1</sub> D <sub>3</sub> E <sub>3</sub>	A <sub>1</sub> B <sub>1</sub> C <sub>1</sub> D <sub>3</sub> E <sub>3</sub>
F <sub>xy</sub>	569		245
VB	22.84		26.69
GRG	0.723	0.844	0.869
<b>Improvement = 20.20 %</b>			

Table 4-13 Confirmation test DFA optimization parameters in roughing conditions.

<b>Desirability Function Analysis for roughing operation</b>			
Performance characteristics	Initial process parameters	Optimal processes parameter	
		Prediction	Experiment
Level	A <sub>1</sub> B <sub>1</sub> C <sub>4</sub> D <sub>4</sub> E <sub>4</sub>	A <sub>1</sub> B <sub>3</sub> C <sub>1</sub> D <sub>1</sub> E <sub>2</sub>	A <sub>1</sub> B <sub>3</sub> C <sub>1</sub> D <sub>1</sub> E <sub>2</sub>
F <sub>xy</sub>	569		224
VB	22.84		48.90
Desirability	0.436	0.949	0.909
<b>Improvement= 108.5 %</b>			

Tables 4-12 and 4-13, respectively show the results of the confirmation experiment using the optimal process parameters suggested by each technique (GRA- Table 4-12 and DFA- Table 4-13) and the initial process parameters (A<sub>1</sub>B<sub>1</sub>C<sub>4</sub>D<sub>4</sub>E<sub>4</sub>) provided by the tool manufacturer. From the confirmation test, it is seen that the GRA and DFA values are improved by 20.20 % and 108.50 % by using the optimal parametric combination. It is seen that the DFA multiple performance technique provided a higher percentage improvement (5 times than GRA) in the face milling of hardened steel AISI 1045.

#### **4.5 Finishing Optimization Parameters**

The estimations in this section considers response factors related to finishing conditions for a high quality surface of machined parts. Therefore, the parameters used in the multi-objective analysis are the surface response variables (Ra, Rq, Rt) and the wear generated on tools (V<sub>B</sub>).

##### **4.5.1 GRA Analysis for Finishing Operation**

The results of the GRA analysis for the finishing operations are shown in this section. Table 4-14 shows the calculated grey normalized values, relational coefficients and grey relational grade values. From the table, optimal cutting conditions are obtained at the 6<sup>th</sup> experimental test.

Table 4-14 Grey relational normalized values, coefficients and grey relational grades.

Run	Evaluation of				Grey relational coefficient				GRG	Rank
	Ra	Rq	Rt	VB	Ra	Rq	Rt	VB		
1	0.973	0.964	0.933	0.779	0.949	0.932	0.881	0.693	<b>0.864</b>	<b>2</b>
2	0.575	0.575	0.506	0.758	0.541	0.541	0.503	0.674	<b>0.565</b>	<b>24</b>
3	0.898	0.898	0.874	0.942	0.831	0.830	0.798	0.896	<b>0.839</b>	<b>4</b>
4	0.311	0.356	0.525	1.000	0.420	0.437	0.513	1.000	<b>0.593</b>	<b>22</b>
5	0.841	0.851	0.895	0.749	0.758	0.771	0.826	0.666	<b>0.755</b>	<b>12</b>
6	1.000	1.000	0.977	0.792	1.000	1.000	0.956	0.706	<b>0.916</b>	<b>1</b>
7	0.908	0.902	0.769	0.979	0.845	0.836	0.684	0.959	<b>0.831</b>	<b>5</b>
8	0.263	0.303	0.506	0.965	0.404	0.418	0.503	0.935	<b>0.565</b>	<b>23</b>
9	0.613	0.635	0.724	0.868	0.564	0.578	0.644	0.791	<b>0.644</b>	<b>17</b>
10	0.118	0.146	0.319	0.917	0.362	0.369	0.423	0.857	<b>0.503</b>	<b>27</b>
11	0.940	0.939	0.931	0.843	0.893	0.891	0.878	0.761	<b>0.856</b>	<b>3</b>
12	0.134	0.577	0.891	0.849	0.366	0.542	0.821	0.768	<b>0.624</b>	<b>18</b>
13	0.929	0.929	0.928	0.750	0.876	0.876	0.874	0.667	<b>0.823</b>	<b>6</b>
14	0.562	0.575	0.633	0.880	0.533	0.540	0.577	0.807	<b>0.614</b>	<b>19</b>
15	0.301	0.360	1.000	0.862	0.417	0.439	1.000	0.783	<b>0.660</b>	<b>15</b>
16	0.866	0.843	0.789	0.780	0.789	0.761	0.703	0.695	<b>0.737</b>	<b>13</b>
17	0.430	0.463	0.669	0.139	0.467	0.482	0.602	0.367	<b>0.480</b>	<b>29</b>
18	0.632	0.639	0.673	0.914	0.576	0.581	0.605	0.853	<b>0.654</b>	<b>16</b>
19	0.557	0.559	0.608	0.866	0.530	0.531	0.560	0.789	<b>0.603</b>	<b>20</b>
20	0.191	0.208	0.389	0.905	0.382	0.387	0.450	0.841	<b>0.515</b>	<b>26</b>
21	0.827	0.841	0.850	0.932	0.742	0.759	0.769	0.881	<b>0.788</b>	<b>9</b>
22	0.963	0.960	0.957	0.498	0.931	0.926	0.922	0.499	<b>0.819</b>	<b>7</b>
23	0.250	0.275	0.502	0.124	0.400	0.408	0.501	0.363	<b>0.418</b>	<b>31</b>
24	0.281	0.321	0.485	0.862	0.410	0.424	0.493	0.783	<b>0.528</b>	<b>25</b>
25	0.797	0.810	0.824	0.913	0.711	0.725	0.740	0.852	<b>0.757</b>	<b>11</b>
26	0.817	0.822	0.820	0.958	0.732	0.738	0.735	0.923	<b>0.782</b>	<b>10</b>
27	0.880	0.867	0.842	0.000	0.807	0.789	0.760	0.333	<b>0.672</b>	<b>14</b>
28	0.176	0.197	0.422	0.862	0.378	0.384	0.464	0.783	<b>0.502</b>	<b>28</b>
29	0.871	0.876	0.847	0.914	0.795	0.802	0.766	0.853	<b>0.804</b>	<b>8</b>
30	0.506	0.510	0.502	0.931	0.503	0.505	0.501	0.878	<b>0.597</b>	<b>21</b>
31	0.093	0.127	0.000	0.802	0.355	0.364	0.333	0.717	<b>0.442</b>	<b>30</b>
32	0.000	0.000	0.238	0.482	0.333	0.333	0.396	0.491	<b>0.389</b>	<b>32</b>

The multi-optimization of finishing operations places a high importance on the workpiece material hardness and on the feed rate as the most significant parameters (Table 4-15). Cutting tool edge preparation also plays a key role in increasing the surface finish. The main effect plot shows improved conditions at reduced feeds and higher material hardness (Figure 4-10). Preference is also given to the conventional milling mode, which cuts along the direction of feed.

Honed cutting tools with SiAlON tools outperformed the other tools with reinforced whisker ceramic matrices by a large margin. However, the ANOVA results shown in Table 4-15

identify only the hardness and milling type as significant factors in developing a prediction model.

Table 4-15 ANOVA for Grey Relational Grade in finishing conditions.

Source	DF	Seq SS	Adj SS	Adj MS	F	P
A: Milling type	1	0.0840	0.0840	0.08397	4.23	0.050
B: Speed	V	12.5974	0.0081	0.0081	0.41	0.528
C: Feed	$f_z$	0.1715	0.0756	0.07557	3.80	0.062
D: Hardness	H	1.2421	1.2421	1.2421	62.54	0.000
E: Tool	T	0.0383	0.0383	0.01278	0.64	0.594
Residual Error	25	0.4965	0.4965	0.01986		
Total	32	14.6299				

The main effects of the mean GRA shown in Table 4-16 show the feed rate as the most influential parameter for the responses, followed by the hardness, the milling type, the tool grade and the cutting speed. Based on the above, the optimal cutting parameter combination is: milling type at A<sub>1</sub>, cutting speed at B<sub>2</sub>, feed rate at C<sub>1</sub>, hardness at D<sub>3</sub>, and cutting tool at E<sub>1</sub> (A<sub>1</sub>B<sub>2</sub>C<sub>1</sub>D<sub>3</sub>E<sub>1</sub>).

Table 4-16 Main effects on mean Grey Relational Grade for finishing conditions.

Level	Mean Grey Relational Grade				Delta	Rank
	1	2	3	4		
A: Milling type	<b>0.7117</b>	0.6093			0.1025	3
B: Speed (m/min)	0.6389	<b>0.7025</b>	0.6676	0.6332	0.0693	5
C: Feed (mm/tooth)	<b>0.7394</b>	0.6811	0.6651	0.5565	0.1829	1
D: Hardness (HRC)	0.6117	0.6074	<b>0.7581</b>	0.6649	0.1507	2
E: Tool	<b>0.7165</b>	0.6237	0.6433	0.6585	0.0928	4
<b>Total mean grey relational grade = 0.661</b>						

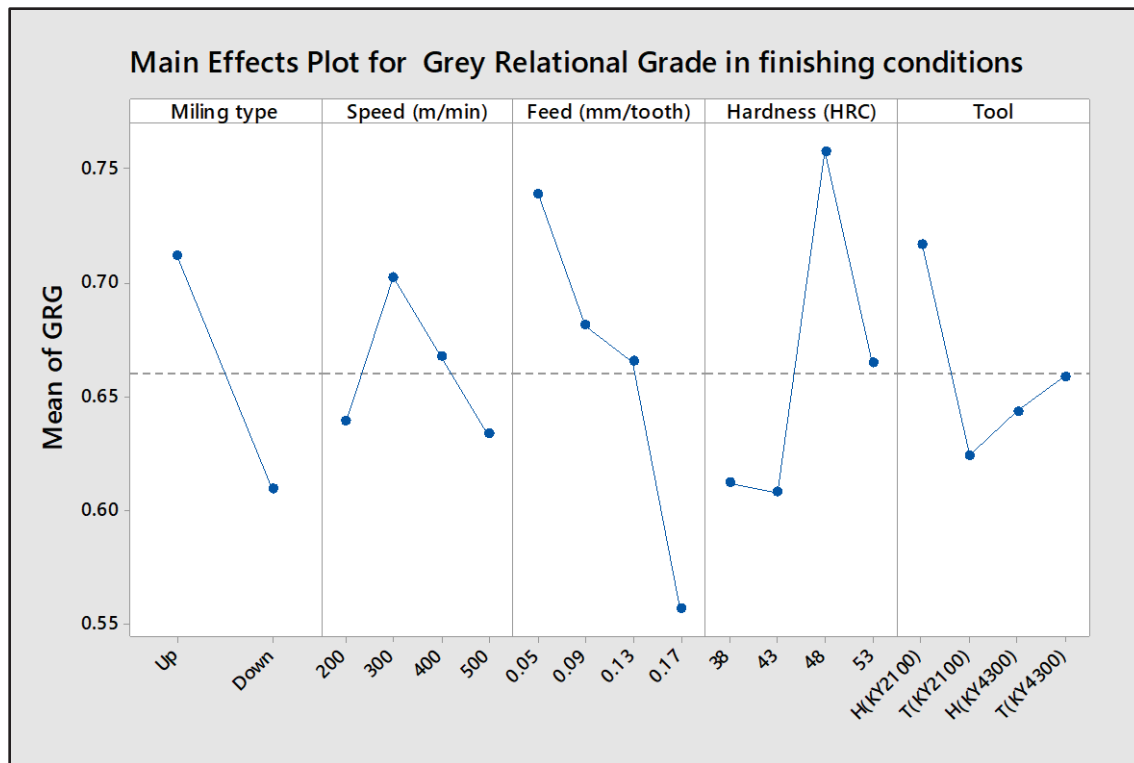


Figure 4-10 Main effects plot of GRA for finishing operation.

#### 4.5.2 DFA Analysis for Finishing Operation

The desirability response optimization plot for finishing operation shows optimal response at 200 m/min, 0.05 mm/th, 53 HRC, up milling and honed (KY4300) tool grade. These results however deviate considerably from GRA optimization shown above.

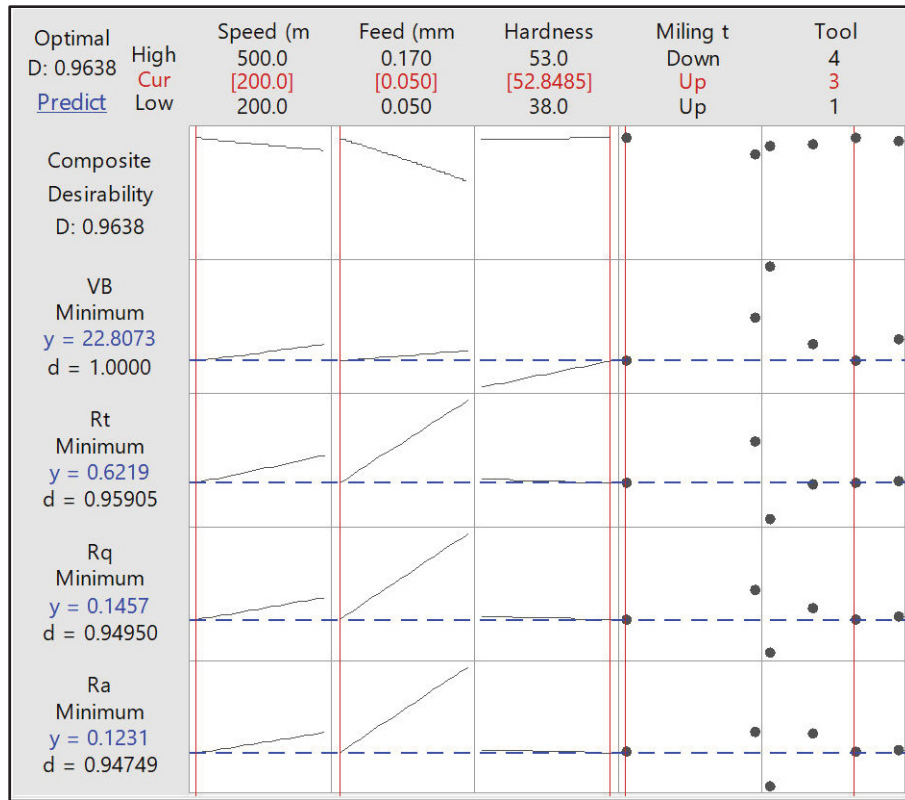


Figure 4-11 Desirability response optimization plot for finishing operation

In this analysis for finishing operations, the ANOVA results show a considerable influence of the material hardness and feed rate and milling type on the output response (Table 4-17). From Figure 4-12, decreasing feed rate is characterized by an improved desirability index.

Table 4-17 ANOVA for Desirability Function Analysis in finishing conditions.

SOURCE	DF	SEQ SS	ADJ SS	ADJ MS	F	P
A: Milling Type	1	0.1784	0.1784	0.17839	10.13	<b>0.004</b>
B: Speed	V	11.7750	0.0018	0.00183	0.10	0.750
C: Feed	$f_z$	0.0349	0.3329	0.33287	18.90	<b>0.000</b>
D: Hardness	H	1.7369	1.7369	1.73687	98.60	<b>0.000</b>
E: Tool	T	0.0437	0.0437	0.01457	0.83	0.492
Residual Error	25	0.4404	0.4404	0.01761		
Total	32	14.2092				

Table 4-18 shows the feed rate as the most significant cutting parameter, followed milling type, the tool, cutting speed, and lastly the hardness of material. DFA results vary in the ranking between the feed and hardness, lending more significance to the feed rate as primary factor influencing desirability.

Table 4-18 Response table for Desirability Function Analysis in finishing conditions.

Level	Means for Desirability Function Analysis				Delta	Rank
	1	2	3	4		
A: Milling type	<b>0.7219</b>	0.5726			0.0415	2
B: Speed (m/min)	<b>0.6888</b>	0.6664	0.6303	0.6035	0.0853	4
C: Feed	<b>0.8138</b>	0.7130	0.5949	0.4673	0.3466	1
D: Hardness	0.6405	0.6516	<b>0.6518</b>	0.6450	0.0113	5
E: Tool	<b>0.6969</b>	0.5949	0.6597	0.6375	0.1021	3
<b>Total Means for Desirability Function Analysis = 0.647</b>						

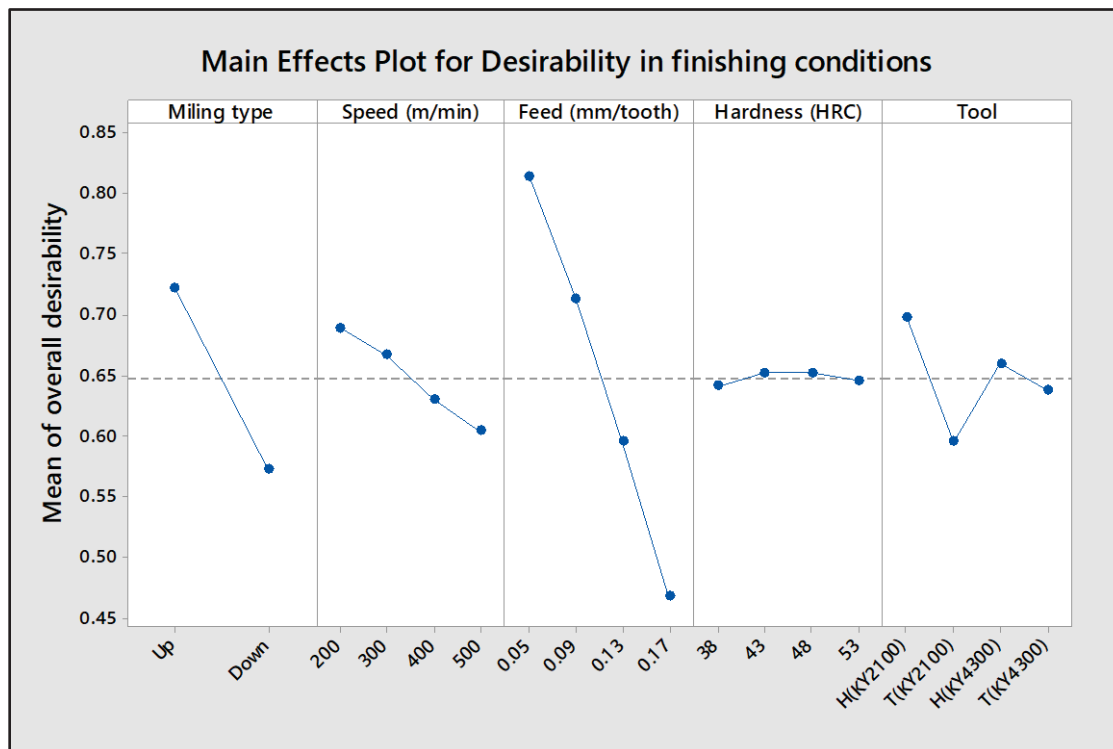


Figure 4-12 Main effects plot for DFA of finishing operation.

The trends from the main effects in DFA differs moderately from the optimal desirability solution shown in Figure 4-11 with an increase in hardness and change in tool grade. However, these show differences with the GRA solution. In the present study, the optimal parametric solution from the desirability plot calculations (Figure 4-11) is used. This solution presents: the milling type at A<sub>1</sub>, cutting speed at B<sub>1</sub>, feed rate at C<sub>1</sub>, hardness at D<sub>4</sub>, and tool at E<sub>3</sub> (A<sub>1</sub>B<sub>1</sub>C<sub>1</sub>D<sub>4</sub>E<sub>3</sub>).

#### 4.6 Confirmation Test for Finishing Conditions

Additional confirmation experiments of an optimized combination of parameters for finishing conditions was also performed. The optimal combinations (A<sub>1</sub>B<sub>2</sub>C<sub>1</sub>D<sub>3</sub>E<sub>1</sub>) and (A<sub>1</sub>B<sub>1</sub>C<sub>1</sub>D<sub>4</sub>E<sub>3</sub>) for the GRA and DFA analysis were experimentally validated and a percentage improvement result obtained from the respective techniques estimated.

Table 4-19 Confirmation tests for GRA grade optimization parameters in finishing conditions.

<b>Grey Relational Grade for finishing operation</b>			
Performance characteristics	Initial process parameters	Optimal process parameters	
		Prediction	Experiment
Level	A <sub>1</sub> B <sub>1</sub> C <sub>4</sub> D <sub>4</sub> E <sub>4</sub>	A <sub>1</sub> B <sub>2</sub> C <sub>1</sub> D <sub>3</sub> E <sub>1</sub>	A <sub>1</sub> B <sub>2</sub> C <sub>1</sub> D <sub>3</sub> E <sub>1</sub>
R <sub>a</sub>	0.602		0.328
R <sub>q</sub>	0.707		0.401
R <sub>t</sub>	3.036		2.643
V <sub>B</sub>	22.84		47.27
GRG	0.593	0.916	0.615
<b>Improvement = 3.78 %</b>			

Table 4-20 Confirmation tests for DFA optimization parameters in finishing conditions.

<b>Desirability Function Analysis for finishing operation</b>			
Performance characteristics	Initial process parameters	Optimal processes parameter	
		Prediction	Experiment
Level	A <sub>1</sub> B <sub>1</sub> C <sub>4</sub> D <sub>4</sub> E <sub>4</sub>	A <sub>1</sub> B <sub>1</sub> C <sub>1</sub> D <sub>4</sub> E <sub>3</sub>	A <sub>1</sub> B <sub>1</sub> C <sub>1</sub> D <sub>4</sub> E <sub>3</sub>
R <sub>a</sub>	0.602		0.200
R <sub>q</sub>	0.707		0.252
R <sub>t</sub>	3.036		1.694
V <sub>B</sub>	22.84		24.48
Desirability	0.584	0.926	0.792
<b>Improvement = 35.76 %</b>			

Tables 4-19 and 4-20 respectively show the results of the confirmation experiment using the optimal process parameters suggested by each technique (GRA and DFA) and the initial process parameters (A<sub>1</sub>B<sub>1</sub>C<sub>4</sub>D<sub>4</sub>E<sub>4</sub>) provided by the tool manufacturer. The confirmation test indicates that the GRA and DFA values are improved by 3.78% and 35.76% by setting the optimal parametric combination. A greater percentage performance improvement in desirability grade is obtained from the DFA multiple performance technique as compared to the improvement percentage from the GRA technique.

#### **4.7 Comparison of Optimization Techniques on Roughing and Finishing Results**

A comparison of the optimization results of both GRA and DFA for each cutting operation is shown in Figures 4-13 and 4-14. The plots show a similar flow of the trend for each experimental test. However, in both Figures, DFA has a greater deviation and disparity in the recognized optimal test conditions.

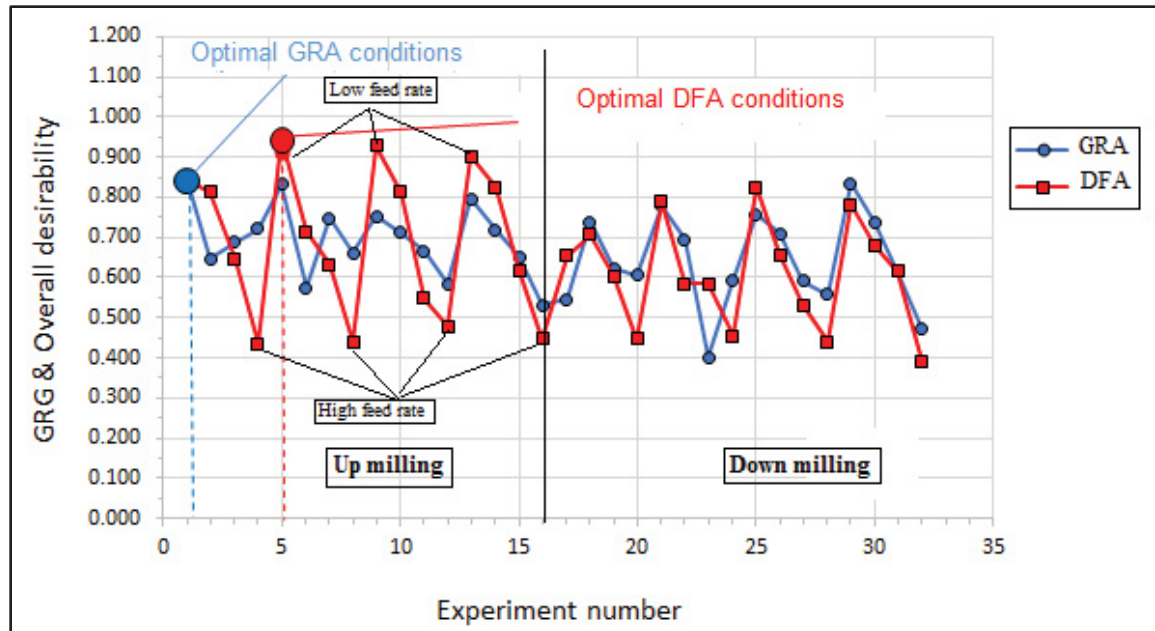


Figure 4-13 Comparison of optimal parameters between GRA and DFA for roughing operation.

In roughing operations, the results identify different optimal conditions from the two techniques. The plots in Figure 4-13 identify that optimal GRG was generated during experimental test 1 while overall improved desirability was obtained in experimental test 5. Generally, improved results values were found on the left portion of the figure which represents the up milling cutting methodology and has a negligible effect from cutting speed. The DFA analysis also shows an increased sensitivity depicted by higher variations and is directly related to the influence from cutting factors. Factors such as high cutting feed rates were responsible for all low desirability index. A more complex interplay from the effect of feed rate, hardness and cutting tool is observed using the GRA analysis. Therefore, due to these high variations in the DFA analysis in the roughness operation, a percentage improvement 5 times better than GRA using optimized conditions was achieved.

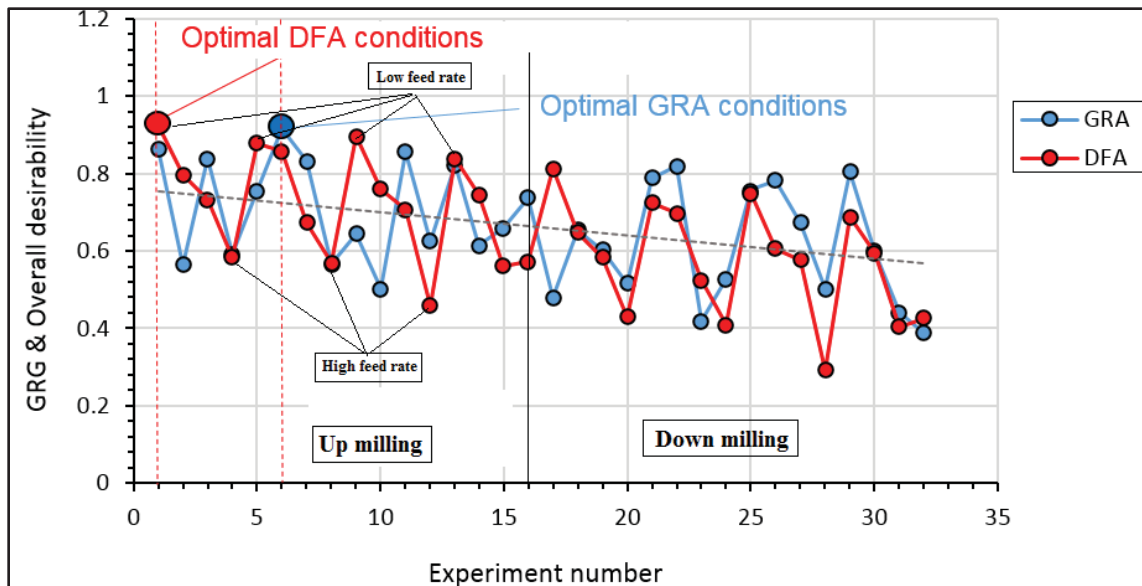


Figure 4-14 Comparison of optimal parameters between GRA and DFA for finishing operation.

Due to the sensitivity of finishing operations, the identification of significant factor plays a crucial role in optimal parameter determination by each technique. In finishing conditions, there is a lower variation in the DFA index as compared to GRA grade values for each experiment. A negative trend line is observed in Figure 4-14, indicating a drop-in performance with the down milling method. DFA desirability predictions were heavily influenced by the feed rate, with negative peaks associated with high feed rates of 0.17mm/th and positive peaks at low values of 0.05mm/th. Based on the differences in significant factors identified in sections 4.5.1 and 4.5.2, during finishing passes, a honed edge preparation is seen to outperform the chamfered tool edges. However, each multi-objective optimization technique identifies different tool grades for optimal performance. The DFA technique endorses whisker ceramic reinforced with  $Al_2O_3 + SiCW$  matrix, which have enhanced chemical stability to resist wear from the increased cutting temperature in its optimal solution. However, the honed SiAlON cutting tool is recommended by the GRA analysis. However, both analyses find that a reduced feed rate, cutting speed and increased hardness produces desired conditions for improved surface finish. The percentage improvement of the finishing surface roughness in DFA analysis was 10 times higher than with the GRA technique.

## 4.8 Conclusions

This paper investigates the machinability of AISI 1045 steel during milling with ceramic cutting inserts with different grades and edge preparations. It demonstrates that at optimal cutting conditions, improved surface integrity and reduced cutting force can be achieved in up milling operations. These conditions were found and confirmed using two Taguchi-based, multi-objective optimization techniques, namely, grey relational analysis and desirability function analysis. The following conclusions were drawn from the study:

- 1- The cutting feed rate was determined to be the most significant factor on forces, surface finish and tool wear during both roughing and finishing operations. At lower feed rates, improved responses were observed.
- 2- Optimal machining conditions in the face milling of AISI 1045 using ceramic inserts was obtained at low feed rates of 0.05mm/th, using conventional milling techniques, and at relatively low speeds (200 m/min). In finishing operations, increased material hardness in the 48 – 53 HRC range produced the best results in terms of surface roughness and tool wear.
- 3- Honed cutting tool edges generally presented better results (tool wear and part surface finish) than chamfered cutting edges. Honed edge preparation was further improved with whisker ceramic reinforced with an  $Al_2O_3 + SiC$  matrix grade composition as compared to sialon.
- 4- The optimized machining parameters obtained by the multi-objective optimizations showed significant improvements in percentage performance versus tool manufacturers' recommended parameters, using the DFA analysis; there was respectively a 108.5% and 35.75% improvement in both roughing and finishing operations as compared to the GRA analysis, which provided a 20.20% and 3.78% improvement in roughing and finishing operations, respectively.

- 5- Both multi-optimization methods (DFA and GRA) provided improved validation results during machining. However, the DFA technique performed at least 5 times better than GRA in both cutting operations. It appears that DFA was more sensitive to the variation of the main factors at extreme levels than was the GRA. Factors such as high cutting feed rates were responsible for all low desirability indexes. A more complex interplay from the effect of feed rate, hardness and the cutting tool was observed using the GRA analysis.

**CHAPTER 5**

**ON FINE PARTICLES EMISSION DURING FACE MILLING OF HARDENED AISI 1045 STEEL**

M. Shnfir<sup>1</sup>, J. Kouam<sup>1</sup> and V. Songmene<sup>1</sup>

<sup>1</sup>Department of Mechanical Engineering, École de Technologie Supérieure (ÉTS),  
1100 Notre-Dame St. West, Montréal, QC H3C 1K3, Canada.

Paper submitted for Journal Aerosol and Air Quality Research of, February, 21<sup>th</sup>, 2020

**Abstract**

With the development of cutting machines and cutting materials, the health of the workers and the environment surrounding them have become an important through minimizing the metallic particles emission during cutting operations. In this paper, the Taguchi method and regression analysis have been applied to assess the metallic particles emission when machining AISI 1045 steel with  $Al_2O_3 + SiCW$  ceramic insert (honed edge, T-land edge) under dry milling. Analysis of variance (ANOVA) was used to determine the effects of cutting parameters (cutting speed, feed rate and hardness of workpiece) on the fine metallic particles emission. The results show that the hardness of workpiece was the main factor affecting on generation fine metallic particles emission on both tools. Furthermore, the cutting speed has no significantly effect on the fine metallic particles emission during the face milling process. The relationship between factors and performance measure were determined using regression model.

**Keywords:** AISI 1045 steel; Face milling; Ceramic insert; Fine particles emission.

**5.1 Introduction**

Recently, the machining of hard materials in industry has become possible due to the technological advancements on machine-tools and on cutting tools development. High

cutting speed machine-tools are used for machining hardened steels and super alloy materials. High speed machining is widely used in industries due to its benefits on increasing productivity, reducing dust generation and reducing machining costs (Arumugam et al., 2006; Becze, Clayton, Chen, El-Wardany, & Elbestawi, 2000; X. Cui et al., 2013; Debnath, Reddy, & Yi, 2014; Diniz & de Oliveira, 2004; A Djebara, Songmene, Khettabi, & Kouam, 2012; Schultheiss, Zhou, Gröntoft, & Ståhl, 2013; Victor Songmene et al., 2012). Dry machining processes are not only economical but also produce clean chips that are easier to recycle (Durham, 2002; Enke, 1999; Jiang, Zhang, & Sutherland, 2012; Victor Songmene et al., 2012; P. Young, Byrne, & Cotterell, 1997). However, during dry cutting process metallic particles emitted deteriorate machine shop floor air quality and can have negative effect on the machine-tools operator's health.

Extensively experimental investigations have made to study the metallic particles generation mechanisms during dry machining (Balout et al., 2007; Khettabi et al., 2007; Khettabi, Songmene, & Masounave, 2010; Khettabi, Songmene, Masounave, & Zaghbani, 2008; Khettabi, Songmene, Zaghbani, et al., 2010; V Songmene et al., 2008a, 2008b; Sutherland et al., 2000). The metallic particles emission during metal cutting processes is influenced by workpiece material and its conditions, the cutting parameters (speed of cut, feed rate, and depth of cut), and the used cutting tools (material, coating, and geometry) (Balout et al., 2007; Khettabi et al., 2007; Khettabi, Songmene, & Masounave, 2010; V Songmene et al., 2008a, 2008b).

Cubic Boron Nitride (CBN), alumina-based composite ceramic (alumina ( $\text{Al}_2\text{O}_3$ ), and silicon nitride ( $\text{Si}_3\text{N}_4$ ) tool materials are the favorite when machining hardened steels due to their high temperature strength, good wear resistance, chemical stability and their performance: increased productivity, reduced energy consumption and environmental friendly (Boim & Sokolov, 1984; X. Cui et al., 2013; W. Liu et al., 2017; Y. Matsumoto, Magda, Hoepfner, & Kim, 1991; Panov, 1989; Trent & Wright, 2000). Alumina ( $\text{Al}_2\text{O}_3$ ) based ceramic is brittle and this usually influence on tool life (Aslan et al., 2007), and it is commonly reinforced with Ti(C,N) and  $\text{ZrO}_2$  additions to improve its toughness. However, the toughness of cemented carbides is still much higher than alumina  $\text{Al}_2\text{O}_3$  based ceramic cutting tools (Aslan et al., 2007; A. S. Kumar et al., 2003; X. S. Li & Low, 1994; Lo Casto et al., 1996). In high cutting

speed, ceramic cutting tools performance is higher (2-10 times) than that of cemented carbides. In order to improve the cutting tools' edge resistance to fracture and chipping, micro-preparation of the cutting edges is performed (Aslan et al., 2007; Chang & Tsai, 2003; Kennametal, 2013; Movahhedy, Altintas, & Gadala, 2002).

The manufacturers of cutting tools supply different types of edge preparation of tool, for example, Kennametal Inc. (Kennametal, 2013) provide generally three types of tool edge preparation including T-land, hone, and T-land plus hone. The chamfered (T-land) tool edges are used in hard machining, heavy rough, and interrupted cutting process to increase the strength of cutting edges (Chang & Tsai, 2003; Chou & Evans, 1999; Hirao, Tlustý, Sowerby, & Chandra, 1982; Movahhedy et al., 2002). For finishing and semi-finish cutting, honed tool edges are used (Schimmel, Endres, & Stevenson, 2002; Wertheim, Satran, & Ber, 1994). The cutting edge micro-preparation improves the tool's strength and the tool life but also change the chip formation (Hirao et al., 1982) and is expected to influence the metallic particles emission.

The particles emission during machining and cutting processes has effect on working area air quality and on occupational safety (Atmadi, Stephenson, & Liang, 2001; Zhong Chen et al., 2000; Elder et al., 2004; Rautio et al., 2007; Sutherland et al., 2000). Dust emission presents a serious danger to machine-tool operators' health because these particles go to the deepest parts of the lung (P. F. Holt, 1987; WHO, 1999; Zaghbani, Songmene, & Khettabi, 2009). Khettabi *et al.* (Khettabi et al., 2007; Khettabi, Songmene, & Masounave, 2010; Khettabi, Songmene, Zaghbani, et al., 2010) have identified in their research works that the cutting tool geometry (lead angle and rake angle) and the cutting speed have important effects on the generated metallic particles emission. They further identified that a tool with 90° lead angle, null or negative rake angle, combined to a high cutting speed generate less metallic particles. Furthermore, Cheng *et al.* (Cheng et al., 2014) found that the dust concentration decreases with a decreasing on insert rake angle and increasing cutting speed. Kamguem *et al.* (Kamguem et al., 2013) show that the TiCN-coated tool produces low metallic particles emission in comparison with the multi-layers (TiCN + Al<sub>2</sub>O<sub>3</sub>) during milling machining of aluminum alloys.

Balout *et al.* (Balout et al., 2007) and Songmene *et al.* (V Songmene et al., 2008a, 2008b) found that brittle materials generate dust emission less than ductile materials during dry drilling. Similarly, Khettabi *et al.* (Khettabi, Songmene, Zaghbani, et al., 2010) and Kouam *et al.* (Kouam et al., 2012) ) have shown that the brittle materials also produce less emission dust than ductile materials during dry turning and friction testing respectively.

Based on the above described research works, it comes that the dry milling process can be applied as an environmentally friendly technique to the machining hardened steel such as AISI 1045. To the author knowledge, no dedicated study has been conducted yet on the effects of workpiece material hardness, tool edge preparation and their interactions with machining parameters on metallic particles emission during dry face milling process. The aim of this study is to evaluate the effects of machining conditions (cutting speed, feed rate and hardness of workpiece) on fine particles emission during dry milling of AISI 1045 steel using ceramic inserts with two edge preparations: honed and T-land.

## 5.2 Experimental procedure

### 5.2.1 Workpiece Material

In this study, the material workpiece is AISI 1045 steel is used. Three hardness of workpiece material (as received 17 HRC, 38 HRC and 48 HRC) are used. The workpiece dimensions are 70 mm (length), 45 mm (width), and 25 mm (thickness). The chemical composition of the workpiece material used is illustrated in Table 5-1.

Table 5-1 Chemical composition AISI 1045 steel workpiece material (% weight).

C	Mn	P	S	Si	Fe
0.459	0.721	0.0086	0.0027	0.259	balance

The Olympus LEXT OLS4100 laser scanning digital microscope was used to analyze the microstructure of the tempered material. The samples were etched in a nital solution (3%) after coarse, medium grinding and final polishing with 1 micron diamond as shown in Figure 5-1.

### 5.2.2 Machining Tests

The milling experiments are carried on the MAZAK NEXUS 410A vertical CNC milling machine (12000 rev/min, power at 5000 rpm 25HP) in dry condition. The cutting parameters with their levels for the experiments are summarized on Table 5-2. The tool holder was shell mills type KDNR250RN40C3 with 63.5 mm diameter with four inserts as shown in Figure 5-2. Round ceramic inserts (grade KY4300) with two distinct edge preparations (honed and T-land), Figure 5-2, were used in the machining tests.

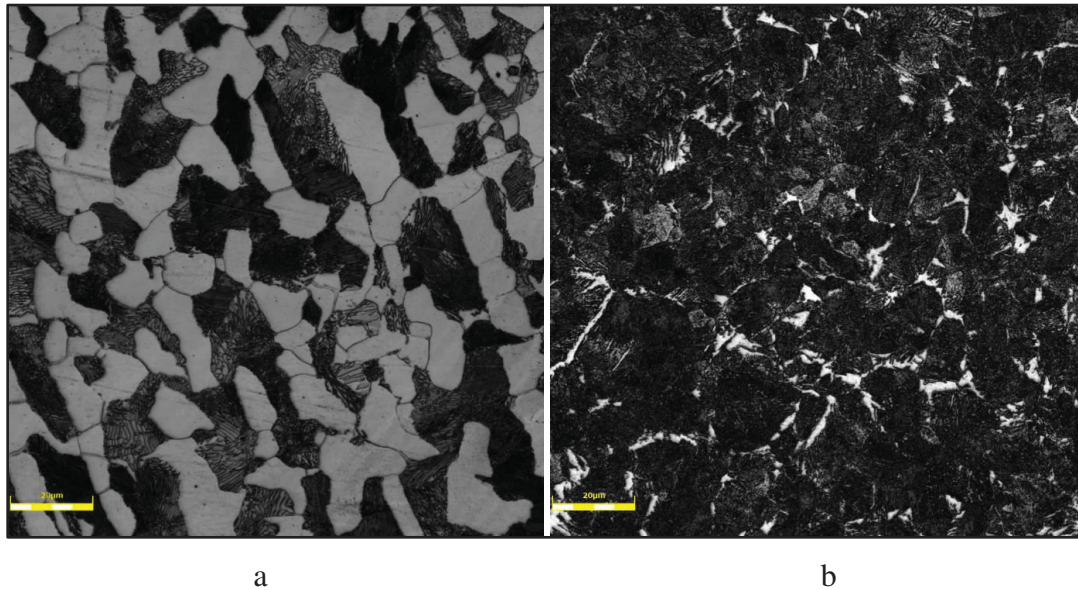


Figure 5-1 Microstructures of AISI 1045 steel: (a) before heat treatment consists of ferrite and pearlite structures, (b) after heat treatment consists of martensitic structures in retained austenite.

Table 5-2 Cutting parameters and their levels.

Factors	Level 1	Level 2	Level 3
Cutting speed: $V_c$	250	350	450
Feed rate: $f$	0.10	0.15	0.20
Hardness: $H$ (HRC)	17 (as received)	38	48
Lubrication	Dry		
Tool: Ceramic tool	Honed	T-land	
Axial depth of cut (mm)	1.0		
Radial depth of cut (mm)	22.50		

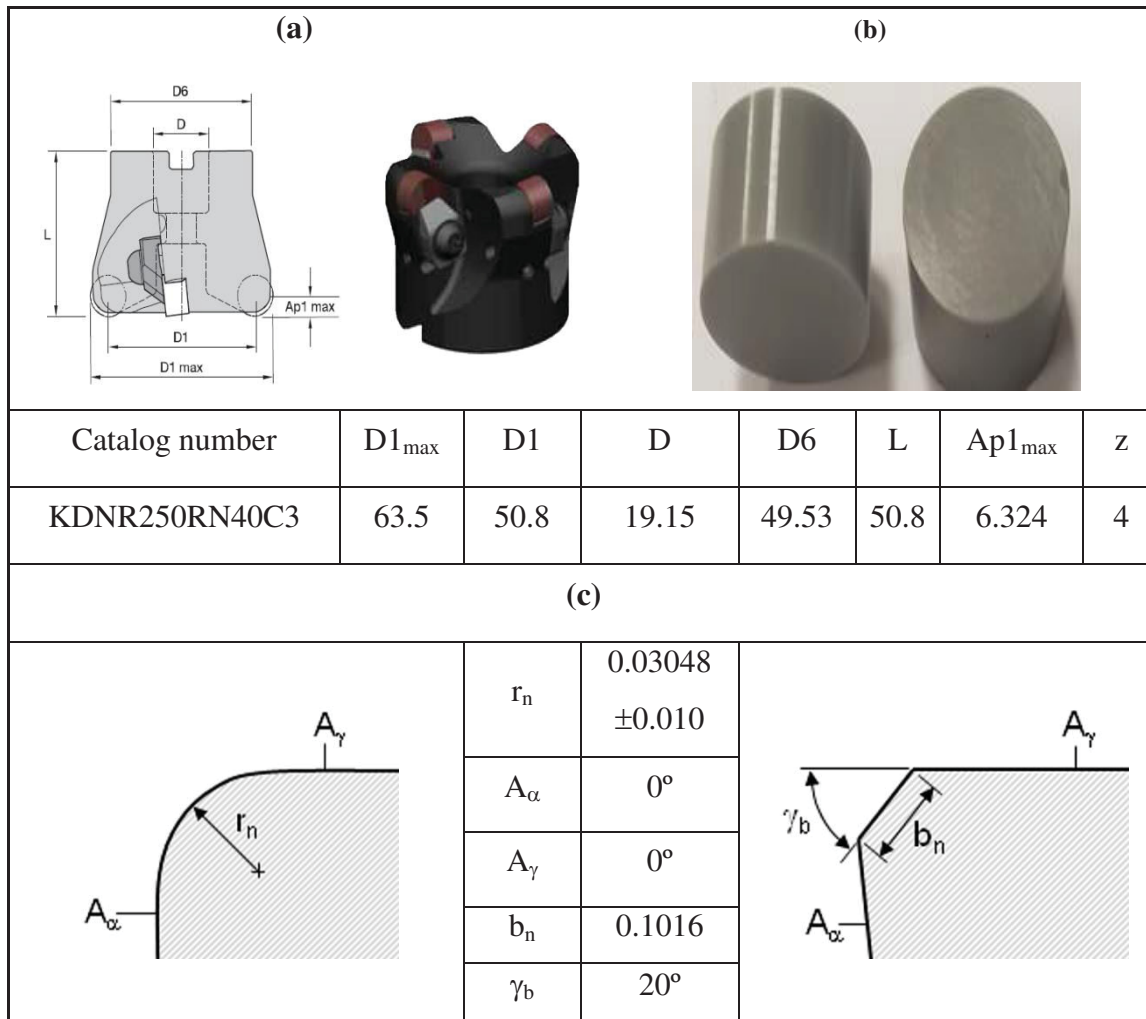


Figure 5-2 Cutting tools used: (a) tool holder, (b) ceramic insert, (c) specification cutting edge for honed and chamfered (T-land) in mm.

Particles emission was measured with an Aerosol Particles Sizer (APS), model 3321, TSI Inc., and Scanning Mobility Particles Sizer (SMPS) model 3080, TSI Inc. with Condensed Particles Counter (CPC) as shown in Figure 5-3. These devices are used to measure particles number concentration as a function of aerodynamic diameter ( $\mu\text{m}$ ) for APS, and mobility diameter (nm) for SMPS. In the current article, data from Aerosol Particles Sizer (Fine particles) only is presented and analyzed.

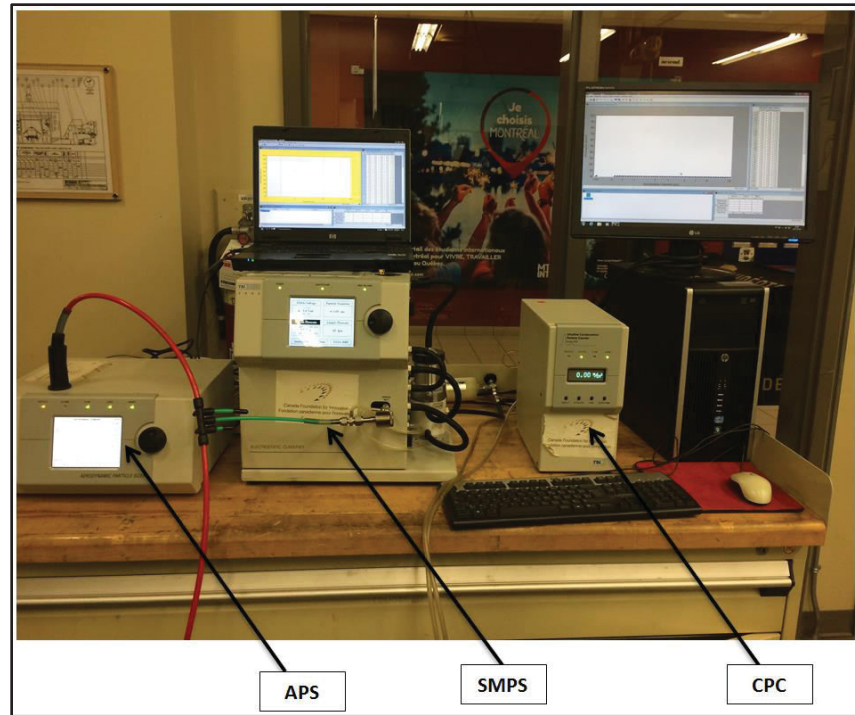


Figure 5-3 Metallic particles sampling instruments: APS (Aerosol Particles Sizer), SMPS (Scanning Mobility Particles Sizer) and CPC (Condensation Particles Counter).

### 5.2.3 Experimental Design

The Taguchi method has been commonly used in engineering design of experiments as a powerful investigative tool. Taguchi's DOE is a powerful optimization tool, which uses orthogonal arrays to examine the quality of factors while using a reduced amount of experiments. Its main advantage lies in the limited amount of experiments, its needs of orthogonal arrays design and the decrease effect of uncontrollable factors (also known as noise factors) thus providing stronger understanding of machining variables have and their consequences for improved engineering quality in the industries (Montgomery, 2017; Phadke, 1989). The cutting parameter and levels (Table 5-2) were selected according to  $L_{27}$  Taguchi orthogonal array which is shown in Table 5-3.

Table 5-3 Taguchi L<sub>27</sub> orthogonal design of experiment.

No	Cutting speed: $v_c$ (m/min)	Feed rate: $f$ (mm/tooth)	Hardness: $H$ (HRC)
1	250	0.10	17
2	250	0.10	38
3	250	0.10	48
4	250	0.15	17
5	250	0.15	38
6	250	0.15	48
7	250	0.20	17
8	250	0.20	38
9	250	0.20	48
10	350	0.10	17
11	350	0.10	38
12	350	0.10	48
13	350	0.15	17
14	350	0.15	38
15	350	0.15	48
16	350	0.20	17
17	350	0.20	38
18	350	0.20	48
19	450	0.10	17
20	450	0.10	38
21	450	0.10	48
22	450	0.15	17
23	450	0.15	38
24	450	0.15	48
25	450	0.20	17
26	450	0.20	38
27	450	0.20	48

### 5.3 Results and Discussion

The design of experiments was developed for estimating the influence of cutting speed, feed rate and workpiece hardness on the fine particles number concentration. Table 5-4 shows the analysis of variance (ANOVA) of the fine particles (FP) number concentration for honed

tool. It can be seen that the hardness of workpiece material (F-value = 7.13) was the most significant factor followed by the interaction between the speed and the hardness (speed  $\times$  hardness; F-value = 2.26), the interaction speed  $\times$  feed rate (F-value = 1.72), and the feed rate (F-value = 1.12). The cutting speed, and the interaction feed  $\times$  hardness had no significant effect on the fine particles number concentration. The contribution (%) provides an additional depiction of significance for the interpretation of the results. The results show that the contribution of the workpiece material hardness was 33.71%, whereas the interaction speed  $\times$  hardness contributed 21.35%, the interaction speed  $\times$  feed contributed 16.30%, the feed contributed 5.32%. That of the interaction feed  $\times$  hardness was 2.38% and the cutting speed contributed 2.02%.

Table 5-4 Analysis of Variance for FP (Honed tool)

Source	DF	Seq SS	Adj SS	Adj MS	F	P	C (%)
Cutting speed: $V_c$ (m/min)	2	3563992	3563992	1781996	0.43	0.667	2.02
Feed rate: $f$ (mm/th)	2	9388060	9388060	4694030	1.12	0.371	5.32
Hardness: $H$ (HRC)	2	59497831	59497831	29748915	7.13	0.017	33.71
Speed*Feed	4	28774327	28774327	7193582	1.72	0.237	16.30
Speed*Hardness	4	37693854	37693854	9423464	2.26	0.152	21.35
Feed*Hardness	4	4199079	4199079	1049770	0.25	0.901	2.38
Residual Error	8	33395278	33395278	4174410			18.92
Total	26	176512421					100

An analysis of the mean response of the fine particles number concentration for honed tool is shown in Figure 5-4. This Figure shows the optimal levels of the control factors for the fine particles number concentration values performed by the Taguchi method: high speed, high feed rate and hardest workpiece material. These optimal values are also appearing in Figure 5-5 main effects plots. Low particles number concentrations values were obtained at 350 m/min cutting speed, 0.20 mm/tooth feed rate, 48 HRC material hardness. From Figure 5-5, the reduce emitted fine particles by using high hardness of material and high feed rate, as already observed by Khettabi *et al* (Khettabi, Songmene, Zaghbani, et al., 2010).

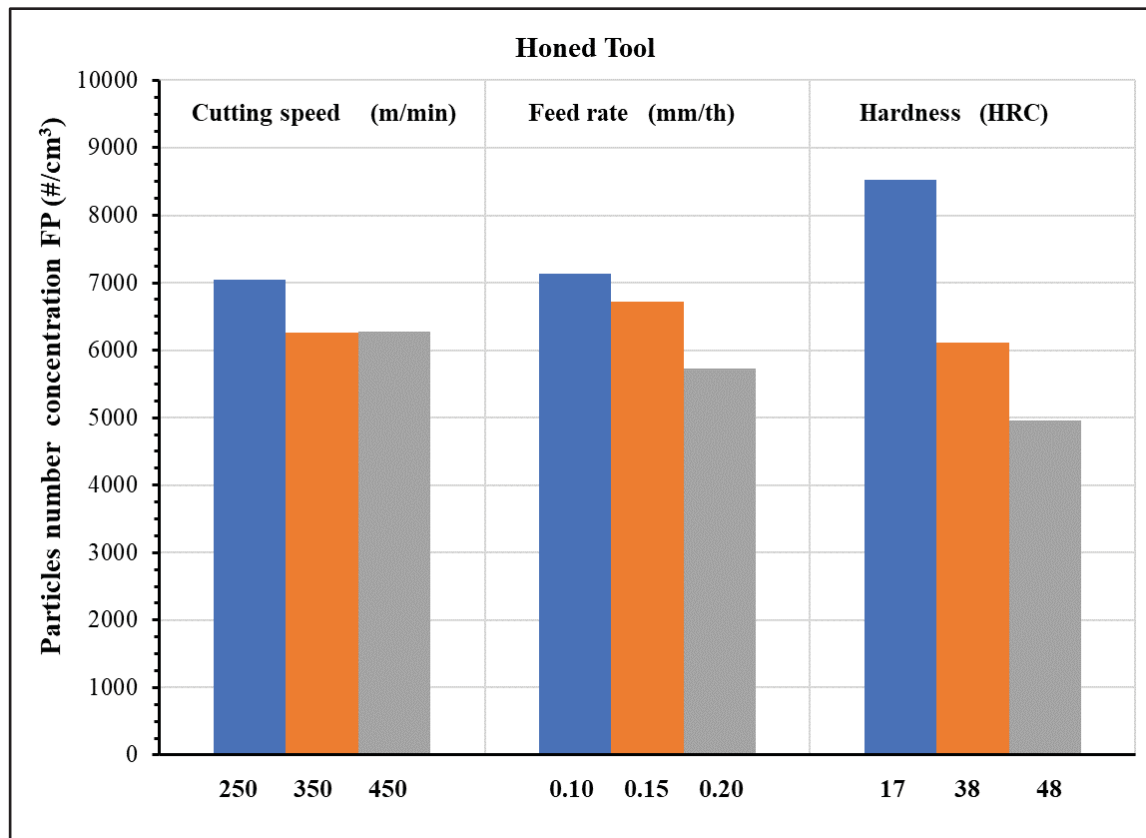


Figure 5-4 Means response for Fine Particles (Honed tool).

Machining workpiece material with increased hardness produces less fine metallic particles emission compared to workpiece material with low hardness. These results are in conformity with the study done by Malshe *et al.* (Malshe *et al.*, 1998), Songmene *et al.* (V. Songmene & Balazinski, 1999; V Songmene *et al.*, 2008a, 2008b), Djebara *et al.* (A Djebara, Zedan, Kouam, & Songmene, 2013), Songmene *et al.* (Victor Songmene & Njoya Doko, 2015), and Marani *et al.* (Marani, Songmene, Kouam, & Zedan, 2018). The generation of fine particles during machining could be related to the plastic deformation, friction and chip formation mode. In fact, the low hardness increases the production of particles as a result of plastic deformation that decreases the propagation of cracks and prevents the brittle rupture of chip. Conversely, in high hardness (brittle material) chip crack occurs by its brittleness (Balout, Songmene, & Masounave, 2003; Balout *et al.*, 2007).

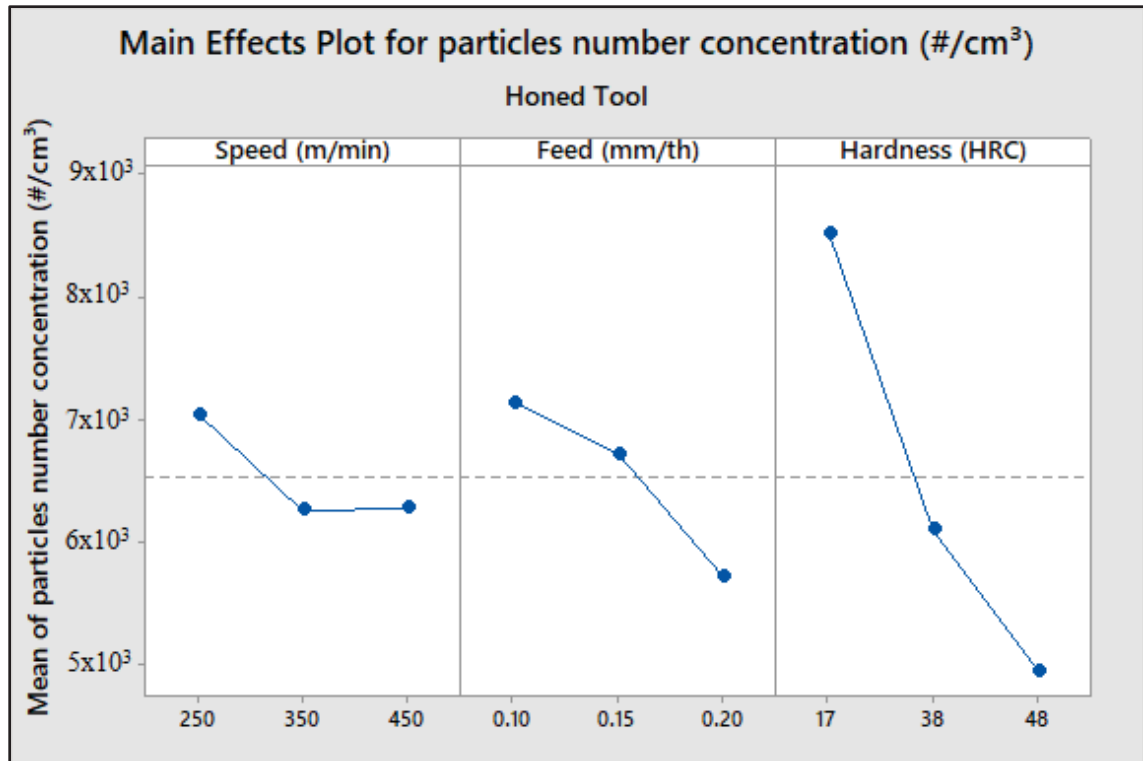
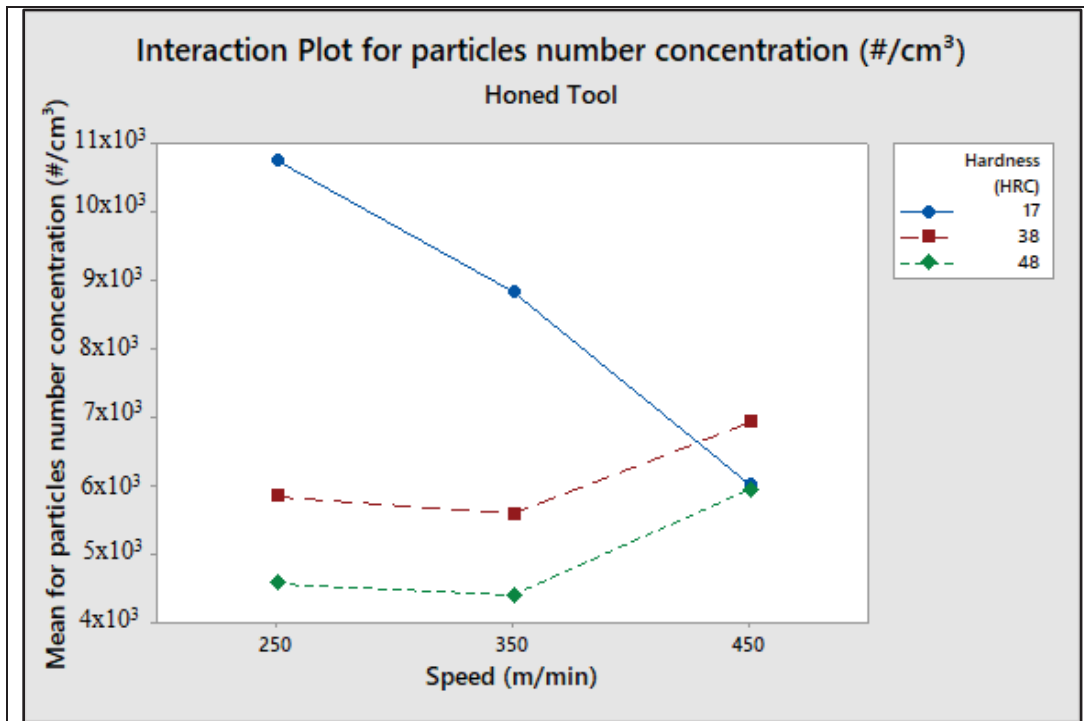
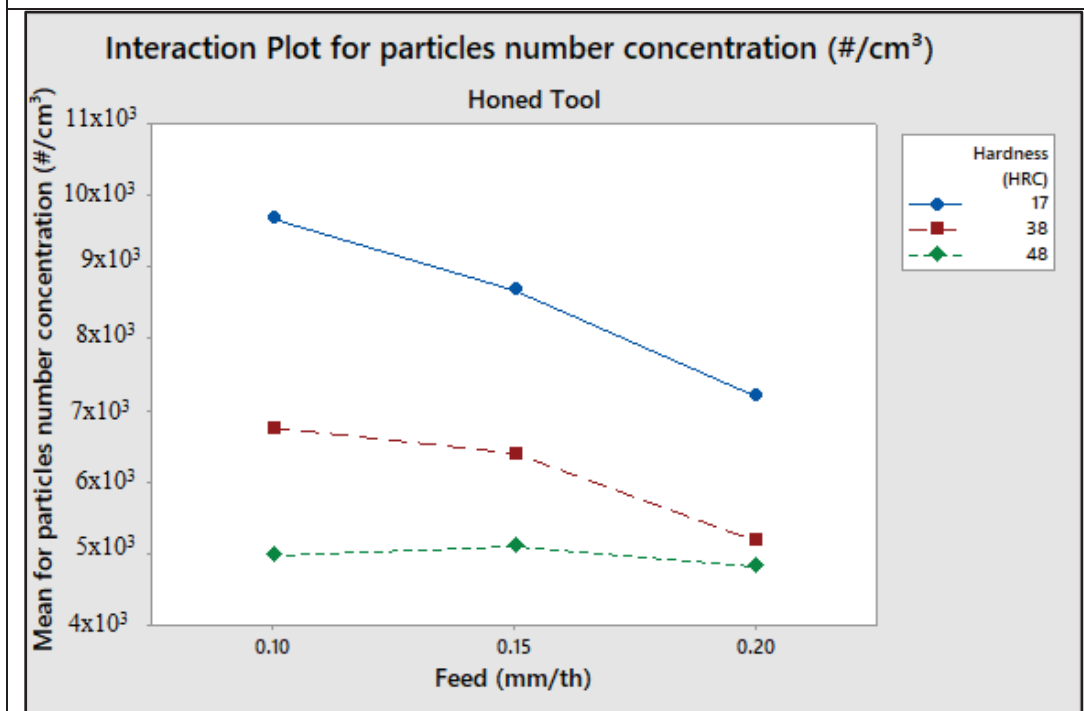


Figure 5-5 Main effects plot for Fine Particles (Honed tool).

The interaction plots for the fine particles number concentration are displayed in Figure 5-6 (a-b). These results show that the effect of hardness of workpiece material on the fine particles number concentration depends on the cutting speed and the feed rate used. In both graphs, less fine particles are generated when machining workpiece with high hardness. Reverse trend is observed at low hardness. In general, the particles number concentration decreases with increases in feed rate and cutting speed. This is conformity with previous research work, Khettabi, *et al* (Khettabi, Songmene, Zaghbani, et al., 2010).



(a)



(b)

Figure 5-6 Interaction plots for particles number concentration (Honed tool).

The analysis of variance (ANOVA) of the particles number concentration for T-land tool is shown in Table 5-5. This analysis shows that the hardness of workpiece material (F-value = 4.22) has the greatest influence terms on the particles number concentration and is followed by the interaction speed  $\times$  feed (F-value = 1.65). The cutting speed, the feed rate, and the other interactions have no significant effect on the particles number concentrations. The most important factors affecting the particles number concentrations were the hardness of workpiece material, the interaction speed  $\times$  feed, the interaction speed  $\times$  hardness, the feed rate, the interaction feed  $\times$  hardness and the cutting speed with respective percentages contribution values of 29.36%, 22.94%, 7.42%, 5.01%, 4.07% and 3.36%.

Table 5-5 Analysis of Variance for FP (T-land tool)

Source	DF	Seq SS	Adj SS	Adj MS	F	P	C (%)
Cutting speed: $V_c$ (m/min)	2	8009168	8009168	4004584	0.48	0.634	3.36
Feed rate: $f$ (mm/th)	2	11926195	11926195	5963098	0.72	0.516	5.01
Hardness: H (HRC)	2	69912944	69912944	34956472	4.22	0.056	29.36
Speed*Feed	4	54631118	54631118	13657779	1.65	0.254	22.94
Speed*Hardness	4	17681897	17681897	4420474	0.53	0.716	7.42
Feed*Hardness	4	9704374	9704374	2426093	0.29	0.875	4.07
Residual Error	8	66305047	66305047	8288131			27.84
Total	26	238170743					100

An analysis of the means response of the particles number concentration for T-land tool is shown in Figure 5-7 and the main factors effects plots are presented in Figure 5-8. These figures, which is made by using the Taguchi method, shows the optimal levels of the control factors for the particles number concentration values. Cutting parameters settings for minimizing the particles number concentration can be clearly seen from this Figure 5-8. The levels and mean ratios for factors giving the less of particles number concentrations were specified as medium hardness (Level 2, mean particles concentration = 4911 pcc), low feed rate (Level 1, mean particles concentration = 6154 pcc) and low cutting speed (Level 1, mean particles concentration = 6375 pcc). In other words, an optimum of particles number concentration value was obtained with cutting speed 250 m/min, feed rate 0.10 mm/tooth, and for a workpiece with hardness of 38 HRC.

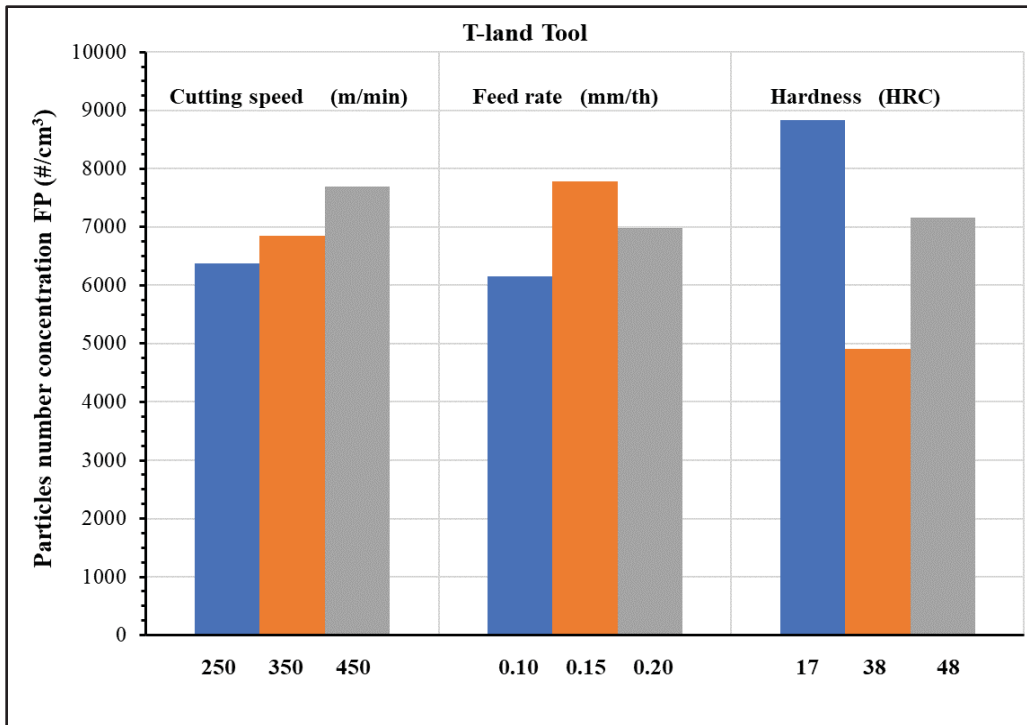


Figure 5-7 Means response for Fine Particles when using a T-land tool.

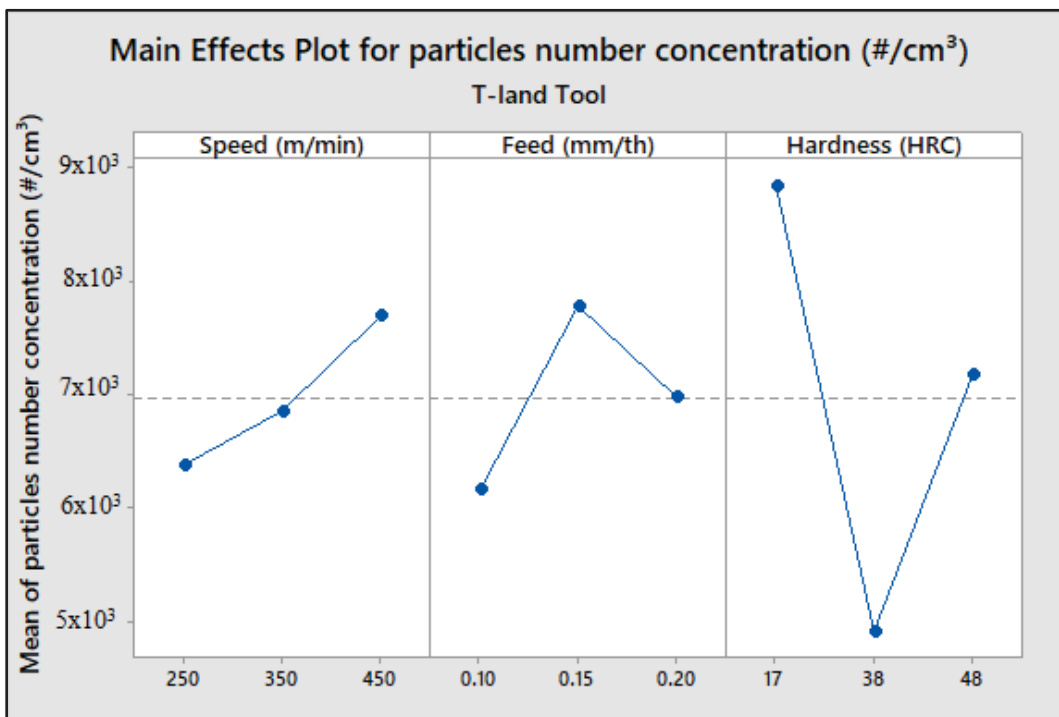
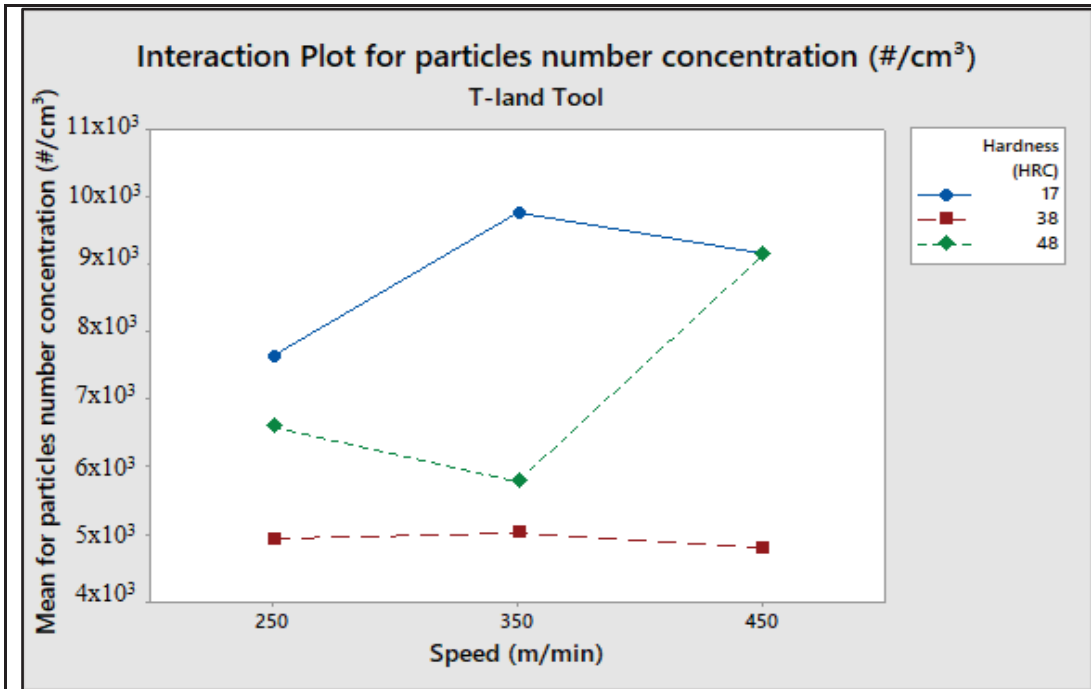
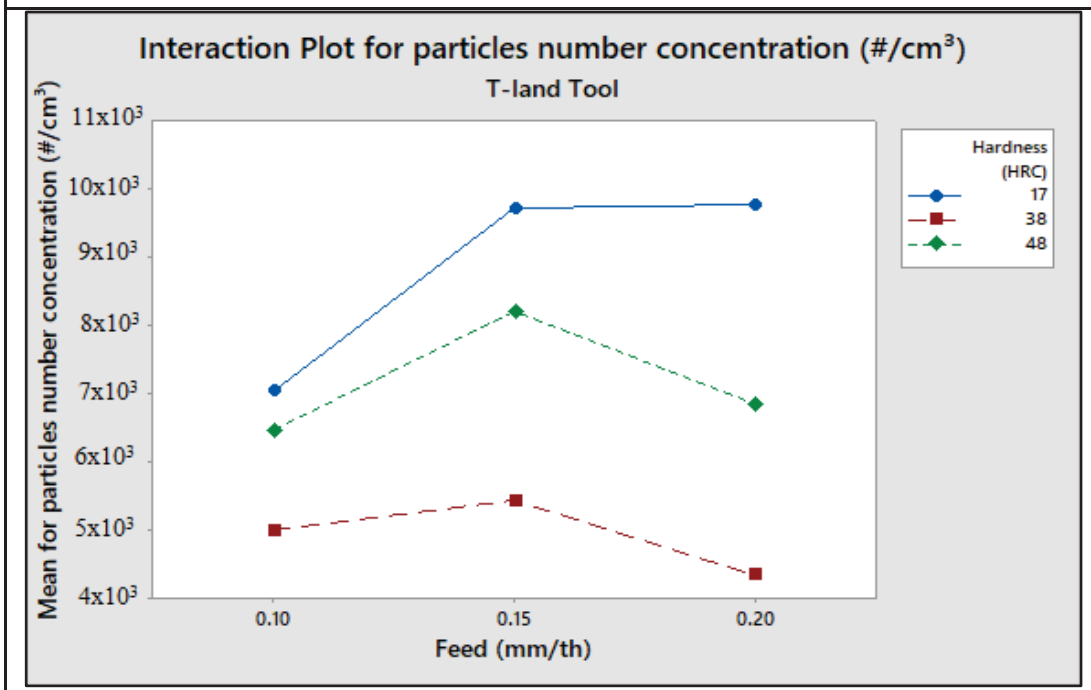


Figure 5-8 Main effects plot for Fine Particles when using a T-land tool.

Interaction plots for fine particles number concentration are presented in Figure 5-9 (a,b).



(a)



(b)

Figure 5-9 Interaction plots for particles number concentration when using T-land tool.

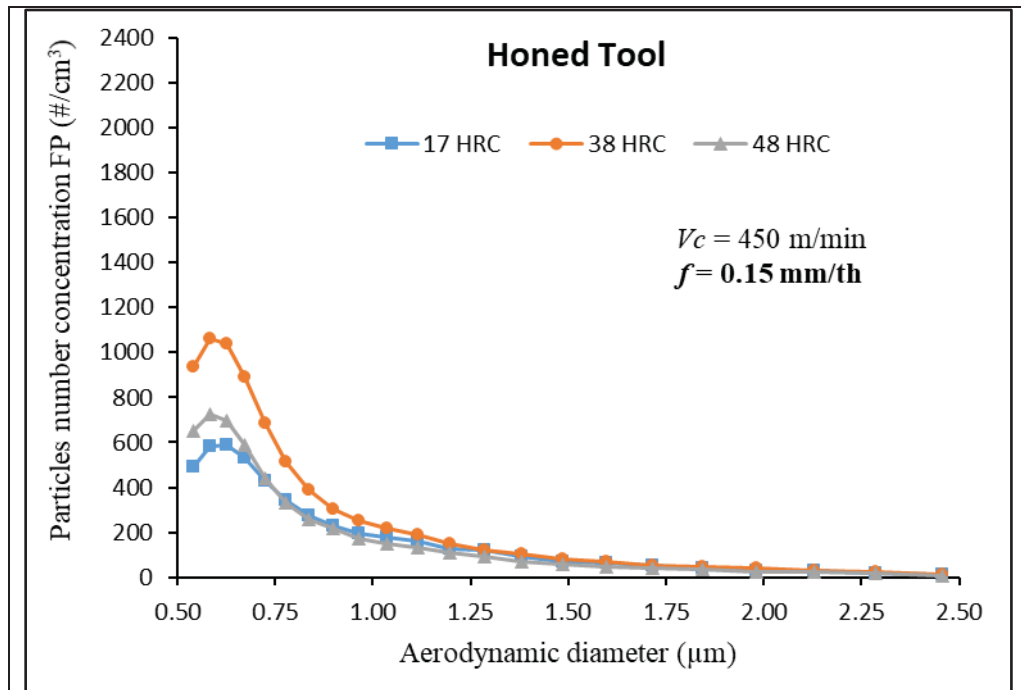
Low FP concentrations were obtained on workpiece material with medium hardness (38 HRC) for all the feed rates and the cutting speeds tested. Similarly, higher FP concentrations were obtained on softer workpiece (17 HRC). This can be explained by the larger deformations taking place during the machining of the soft material (Figure 5-12) and by the larger chip-tool contact length. For example, T-land tool led to more deformed chip. Consequently, the T-land tool generated fine particles as compared to the honed tool.

Figure 5-10 and Figure 5-11 illustrate the results of particles emission for number concentration of fine particles as function of aerodynamic diameters obtained from APS with particles diameter ranging from 0.5 to 2.5  $\mu\text{m}$  for honed tool and T-land, respectively.

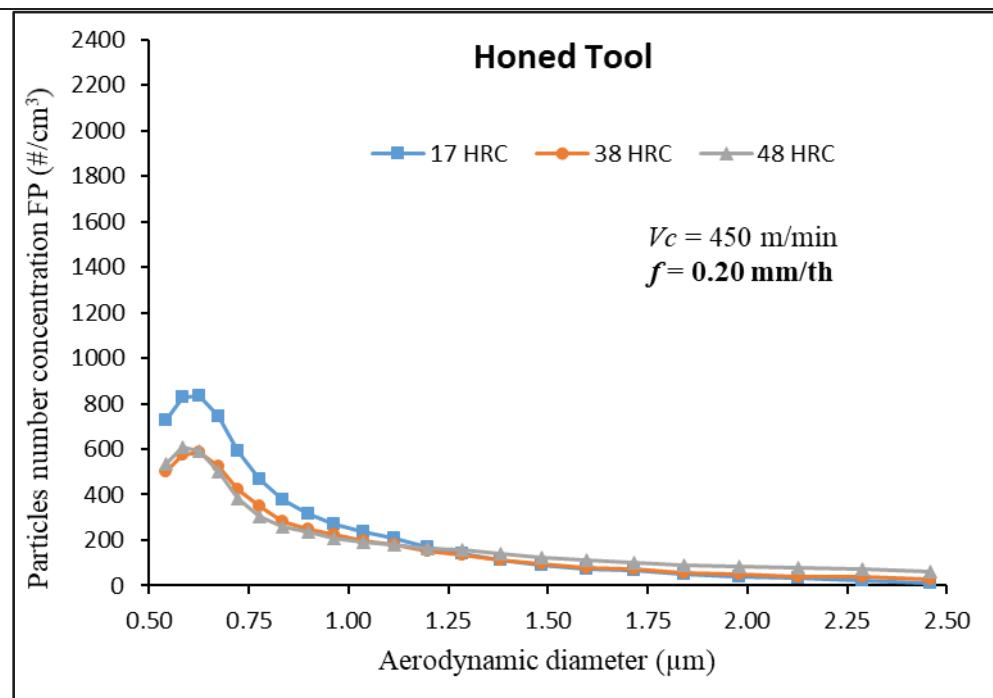
Changing the feed rate has more impact on FP emission when using a T-land tools that it is the case for honed tool. For example, for T-land tool, lowering the feed rate from 0.20 mm/th to 0.15 mm/th (which should improve the machined part surface finish) results in an increase of the particles emission by a factor of three when milling soft workpiece (17HRC) and by a factor of two for the case of a hard workpiece (48 HRC), Figures 5-11a and 5-11b. Make the same change when milling with a honed tool results only to a slight decrease of FP emission for soft steel material and for a harder material the FP concentration is increased by a factor of almost two, Figures 5-10a and 5-10b.

In general, using the honed edge preparation leads to the reduction of the generation of fine particles emission compared to T-land edge preparation 1.37 to 2 times depending on feed rate and workpiece material hardness used

In both Figures 5-10, 5-11, the change of cutting speed, feed rate and tool geometry didn't affect the sizes (aerodynamic diameters) of the fine particles generated (pic concentrations at 0.626  $\mu\text{m}$ ), but they did change the concentration of fine particles. It is also observed that most the fine particles generated between 0.50  $\mu\text{m}$  to 1.25  $\mu\text{m}$ .



(a)



(b)

Figure 5-10 Particles number concentration as function of aerodynamic diameter for different workpiece hardness and feed rates:  
(a) Feed rate  $f = 0.15 \text{ mm/th}$ ; (b) Feed rate  $f = 0.20 \text{ mm/th}$ .

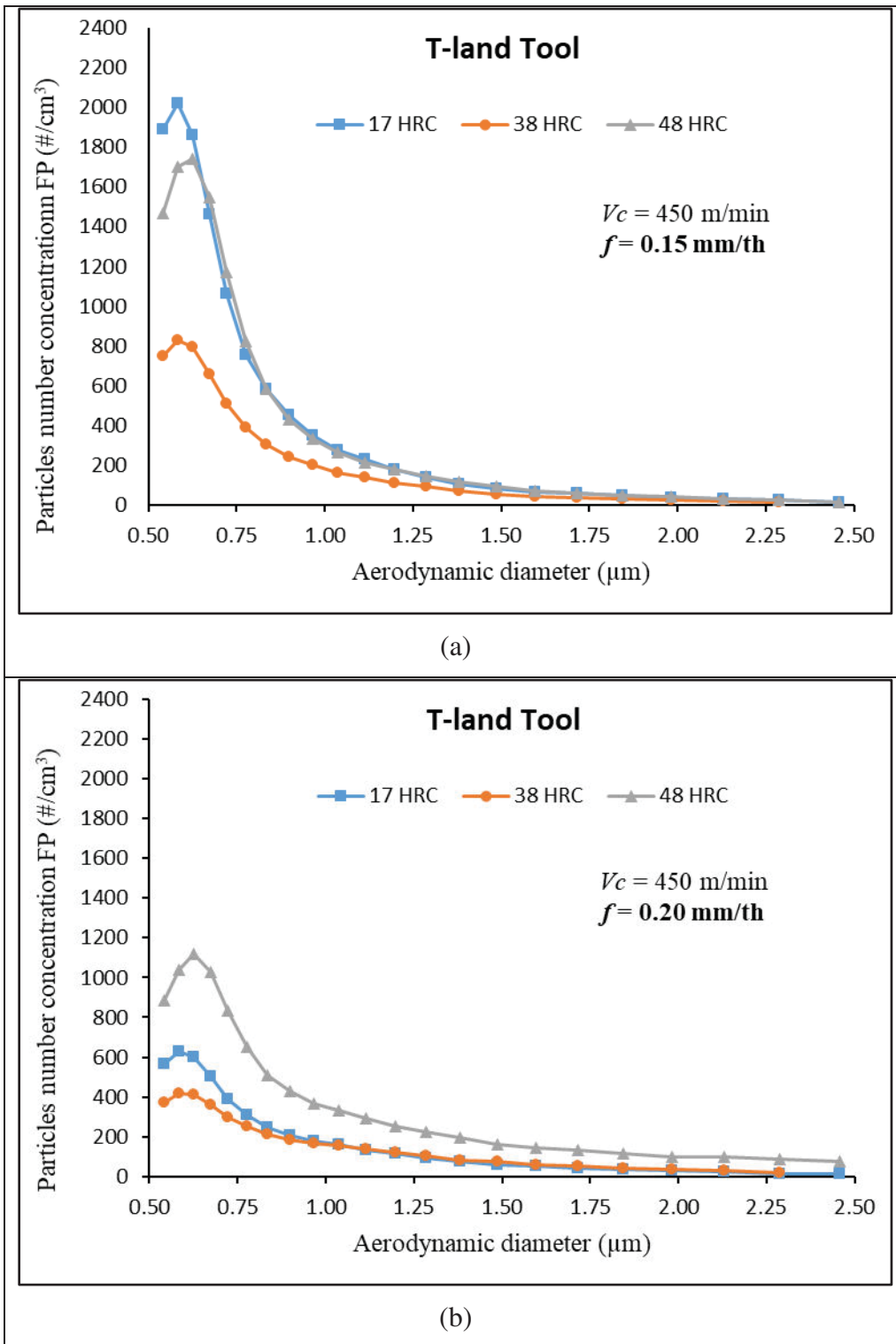


Figure 5-11 Particles number concentration for T-land tool as function of aerodynamic diameter for different workpiece hardness and feed rates:  
 (a) Feed rate  $f = 0.15$  mm/th; (b) Feed rate  $f = 0.20$  mm/th.

Figure 5-12 also presents the effect of tool on the morphology of the free surface of the chip for 38 HRC workpiece under the same cutting condition. An examination of the chip morphology reveals a larger segmentation in terms of width and depth on the free surface of the chip formed with the honed tool as compared to T-Land tool during the machining of the 38 HRC workpiece. This observation is also confirmed by what happened in Figures 5-10 and 5-11 when using honed tool and T-land tool about number particles concentration. This change in the chip morphology explains the increase of the number of particles concentration when using honed tool as compared to T-land tool at this cutting condition.

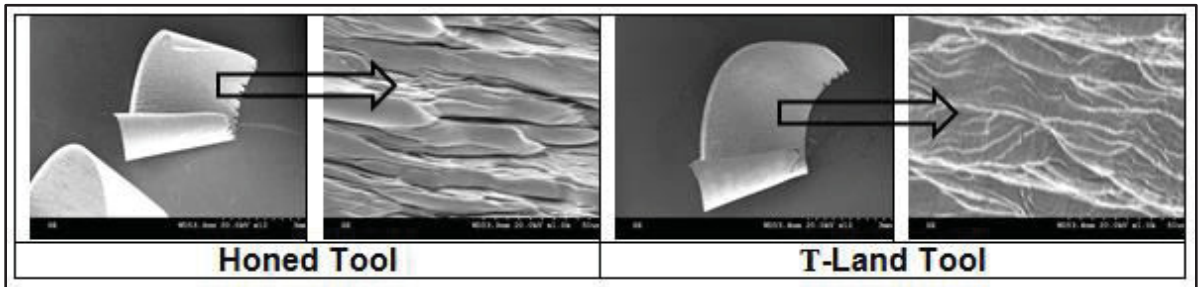


Figure 5-12 SEM image of chip showing the effect of tool on the morphology of the free surface of the chip (workpiece hardness = 38 HRC) under the same cutting parameters settings.

The empirical regression equation developed using Minitab 17 software for honed tool and T-land tool are as follow.

For honed tool (coefficient of determination  $R^2 = 93.23\%$ ; Adjusted  $R^2 = 89.84\%$  )

$$FP \left( \# / cm^3 \right) = 36.7 Vc + 133690 f - 227 H - 0.0899 Vc^2 - 489824 f^2 \quad (5-1)$$

$$- 2.21 H^2 - 20 (f * Vc) + 0.776 (H * Vc) + 241 (f * H)$$

For T-land tool (coefficient of determination  $R^2 = 90.79\%$ ; Adjusted  $R^2 = 86.18\%$ )

$$FP \left( \# / cm^3 \right) = 8.5 Vc + 207834 f - 760 H - 0.0033 Vc^2 - 549688 f^2 \quad (5-2)$$

$$+ 12.93 H^2 - 3 (f * Vc) + 0.033 (H * Vc) - 969 (f * H)$$

where, FP is the particles number concentration of fine particles produced when milling with honed tool or T-land tool, respectively;  $V_c$  is the cutting speed (m/min),  $f$  is feed rate (mm/th) and  $H$  (HRC) is the hardness of the workpiece material.

#### 5.4 Conclusions

In this study, detailed experimental investigations are presented for the effects of workpiece hardness and cutting edge preparation on generation of metallic particles emission in the face milling of AISI 1045 steel. From the findings of the investigation, the following conclusions have been made

- 1- The hardness of material was found to be the most significant parameter on fine metallic particles emission on both tools (honed and T-land). The ductile material produces more metallic particles emission as compared to brittle material. It is recommended that using high hardness of material to minimize the metallic particles emission.
- 2- Using the honed edge preparation leads to the reduction of the generation of fine particles emission compared to T-land edge preparation 1.37 to 2 times depending on feed rate used.
- 3- The statistical analysis of fine metallic particles emission indicates that the hardness of material is the greatest influence factor on the fine metallic particles emission (FP) with a percentage contribution of 33.71%, 29.36% for honed and T-land tools, respectively and following by the interaction speed  $\times$  hardness (21.35%), for honed, the interaction speed  $\times$  feed (22.94%) for T-land. The cutting speed had no significant effect on the fine metallic particles emission on both tools.
- 4- The optimum levels of the control factors for minimizing the on fine metallic particles emission using ANOVA approaches were determined. The optimal conditions for the FP were observed at cutting speed= 350 m/min, feed rate= 0.20 mm/tooth, and hardness= 48 HRC for honed tool. The optimal conditions for the FP were observed at cutting speed= 250 m/min, feed rate= 0.10 mm/tooth and hardness= 38 HRC for T-land tool.

- 5- A general regression model was developed based on the selected cutting parameters. The models for FP are satisfactory with good relationship ( $R^2 = 93.23\%$ ; Adj.  $R^2 = 89.84\%$ ) for honed and for T-land ( $R^2 = 90.79\%$ ; Adj. $R^2 = 86.18\%$ ).



## CHAPTER 6

### ULTRAFINE PARTICLES EMISSION DURING HIGH-SPEED MILLING OF HARDENED AISI 1045 STEEL

M. Shnfir<sup>1</sup>, J. Kouam<sup>1</sup> and V. Songmene<sup>1</sup>

<sup>1</sup>Department of Mechanical Engineering, École de Technologie Supérieure (ÉTS),  
1100 Notre-Dame St. West, Montréal, QC H3C 1K3, Canada.

Paper submitted For Journal of Advanced Manufacturing Technology, February, 20<sup>th</sup>, 2020

#### **Abstract**

In this study, the effects of cutting speed, feed rate and hardness of workpiece material on the particles number concentration ultrafine of particles in the face milling were experimentally investigated. AISI 1045 steel was hardened to 17, 38, 48 HRC, machining using ceramic insert (honed, T-land edge preparation). Three factors (cutting speed, feed rate, and workpiece hardness) and three levels fractional experiment designs completed ( $L_{27}$ ) with statistical analysis of variance (ANOVA) were performed. The analysis of the results show that workpiece hardness has the greatest influence on ultrafine of particles in both tools. Other significant effects such as the interaction between cutting milling parameters are also investigated. Overall, it is shown that the use of honed edge reduces the metallic particles emission.

*Keywords:* AISI 1045 steel; Face milling; Tool edge preparation; Ultrafine particles.

#### **6.1 Introduction**

Ceramic cutting tools is the one of most cutting tools used for machining super alloys and hard materials during the high speed due to their distinctive mechanical properties. Ceramics have high melting point, excellent hardness and good wear resistance and chemical stability inactivity (Aruna, Dhanalakshmi, & Mohan, 2010; Obikawa, Matsumura, Shirakashi, & Usui, 1997). Several researcher (Altin, Nalbant, & Taskesen, 2007; Amini, Fatemi, & Atefi,

2014; Aslan, 2005; Aslan et al., 2007; Camuşcu, 2006; X. B. Cui, Zhao, Zhou, & Pei, 2012; Das, Kumar, & Dhupal, 2015; J. Paulo Davim & Figueira, 2007; Karpuschewski et al., 2013; A. S. Kumar et al., 2003; Long, Zeng, & Shanghua, 2014; MA Shalaby et al., 2014; Soković et al., 2005; B. Wang & Liu, 2016) have conducted researches on the performance of ceramic tools in the machining of various hard materials, they have shown that the surface roughness, cutting forces, and tool wear are dependent on cutting condition and tool geometry.

In manufacturing industries dry cutting have been widely applied due to its assistance on increasing productivity, decrease air pollution, and decreasing machining costs (Arumugam et al., 2006; Debnath et al., 2014; Diniz & de Oliveira, 2004; A Djebara et al., 2012; Victor Songmene et al., 2012). In the dry machining, cutting tool life is short that is main problem when machining hardened materials. Ceramic tool inserts and carbide (coated by TiN, TiC) are recommended used on industrial for dry machining (Dudzinski et al., 2004; Kalss, Reiter, Derflinger, Gey, & Endrino, 2006; Sreejith & Ngoi, 2000). During cutting processes hardened steels on dry condition, the Alumina ( $Al_2O_3$ ) based ceramic is one recommended tool due to the suitable cutting tool materials because it has high hot hardness, good resistance to wear and chemical stability inactivity. For improve performance, they are commonly reinforced with Ti(C, N),  $ZrO_2$  additions (Aslan et al., 2007; A. S. Kumar et al., 2003; X. S. Li & Low, 1994; Lo Casto et al., 1996).

By dry cutting process can produce clean chips without pollution, because the cooling fluid is not used, and the recycling is minimized (Durham, 2002; Jiang et al., 2012; P. Young et al., 1997). However, the metallic particles emission obtained by that method its effect on environments and health of operation (Atmadi et al., 2001; Zhong Chen et al., 2000; Sutherland et al., 2000). The operator is exposed to dust particles through inhalation which expose him to several serious diseases (P. F. Holt, 1987; Ratnasingam, Scholz, & Natthondan, 2009; Rautio et al., 2007). The dry metallic particles emission produced during metal cutting process be influenced by workpiece material and its conditions also the cutting parameters (cutting speed, feed rate, and depth of cut) and cutting tool (material, coating, geometry) used (Balout et al., 2007; Khettabi et al., 2007; Khettabi, Songmene, & Masounave, 2010; V Songmene et al., 2008a, 2008b).

Several researchers have conducted extensive researches on the mechanism of the generation of dust emission during the dry turning machining (Enke, 1999; Khettabi et al., 2007; Khettabi, Songmene, & Masounave, 2010; Khettabi et al., 2008; Khettabi, Songmene, Zaghbani, et al., 2010; Sutherland et al., 2000).

Khettabi *et al.* (Khettabi et al., 2007; Khettabi, Songmene, & Masounave, 2010; Khettabi, Songmene, Zaghbani, et al., 2010) identified in their research that cutting tool geometry (lead angle, rake angle) and cutting speed have a significant effect on the dust emission generated depended on the type of material. They further identified that the lead angle of  $90^\circ$ , null or negative rake angle and high cutting generated the less dust emission during experimentation. Furthermore, Cheng *et al.* (Cheng et al., 2014) found that decreased dust concentration with insert rake angle decrease and increased with cutting speed. Kamguem *et al.* (Kamguem et al., 2013) found that TiCN-coated tool generated low metallic particles emission compared to multi-layers (TiCN +  $\text{Al}_2\text{O}_3$ ) and reduced dust generation during milling machining of aluminium alloys (6061-T6, 2024-T351 and 7075-T6).

With the rapid development in the technology of manufacturing Computer Numerical Control machine (CNC) and the material tools, the manufacture of ceramic tools has been improved gradually. The present paper the results of an experimental investigation on the effect of ceramic tool and workpiece hardness on the performance of ultrafine particles emission when machining AISI 1045 steel.

## **6.2 Experimental Procedure**

### **6.2.1 Design of Experiment**

In this study, Taguchi design is used. It is an optimization method that includes planning conducting and analyzing the outcomes of experiments in order to obtain the best control factor levels and help with data analysis and optimum results prediction. The control factors selected are cutting speed (m/min), feed rate (mm/th) and hardness of workpiece material (HRC). With three control factors at three levels each, the orthogonal array  $L_{27} (3^3)$  was selected.

### 6.2.2 Workpiece Material

The workpiece is AISI 1045 steel is used in this study. Three varying hardness of workpiece material (17 (as received) 38 and 48 HRC) were employed in the tests with same rectangular dimensions 70 mm (length), 45 mm (width), and 25 mm (thickness). The hardening process consists of austenitization temperature at 1550°F (844° C) for 1.5 hours and followed by quenching in water and tempering in the range between 500 - 875°F (260 - 470° C) for 2 hours depending on our selected hardness value (38, 48 HRC) respectively. The chemical composition of workpiece material is summarized in Table 6-1.

Table 6-1 Chemical composition of material AISI 1045 steel (% weight).

C	Mn	P	S	Si	Fe
0.459	0.721	0.0086	0.0027	0.259	balance

### 6.2.3 Machining Tests

The experimental trials were carried out on a MAZAK NEXUS 410A vertical CNC milling machine for machining (12000 rev/min, power at 5000 rpm 25HP) in dry machining conditions. The cutting parameters with their levels for the experiments are listed on Table 6-2. The tool holder was shell mills type KDNR250RN40C3 with 63.5 mm diameter with four inserts recommended by Kennametal Inc. The ceramic inserts had two different edges preparation (T-land and honed cutting edge) with negative rake angle, and grade type (KY4300: Whisker ceramic with a matrix of  $Al_2O_3 + SiCW$ ) as indicated in Figure 6-1.

Table 6-2 Cutting parameters and their levels.

Factors	Level 1	Level 2	Level 3
Cutting speed $V_c$ (m/min)	250	350	450
Feed rate $f$ (mm/tooth)	0.10	0.15	0.20
Hardness $H$ (HRC)	17 (as received)	38	48
Lubrication	Dry		
Tool	Ceramic (honed and T-land) negative rake angle		
Axial depth of cut (mm)	1.0		
Radial depth of cut (mm)	22.50		

Particles emission was measured with an Aerosol Particles Sizer (APS), model 3321, TSI Inc., and Scanning Mobility Particles Sizer (SMPS) model 3080, TSI Inc. with Condensed Particles Counter (CPC) as shown in Figure 6-2. These devices used to measure particles number concentration, mass concentration, and specific area concentration as a function of aerodynamic diameter ( $\mu\text{m}$ ) for APS, and mobility diameter (nm) for SMPS.

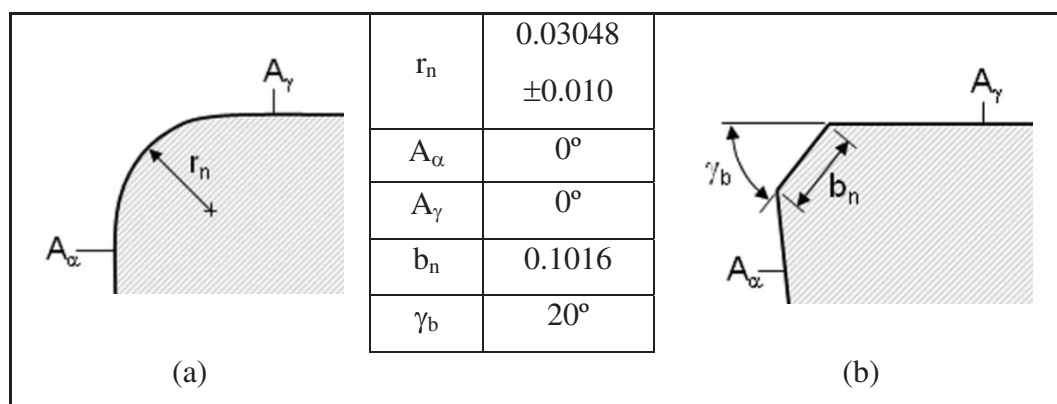


Figure 6-1 Specification cutting edge (a) honed, (b) T-land (chamfered) in mm.

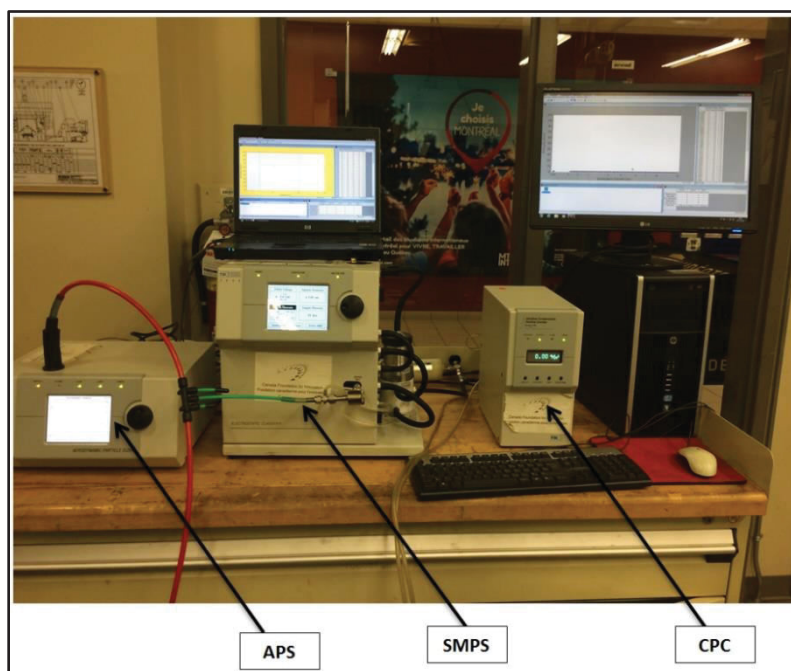


Figure 6-2 APS (Aerosol Particles Sizer), SMPS (Scanning Mobility Particles Sizer) and CPC (Condensation Particles Counter).

### 6.3 Experimental Results and Discussions

The mean response data are calculated using Minitab17 software (3.1 version). The smallest mean response would reflect the best response which results in the lowest for particles number concentration of ultrafine particles (UPF) by using honed tool. These are the criteria employed in this study to determine the optimal cutting parameters (cutting speed, feed rate and hardness of workpiece material). The main effects plot of mean ratio for selecting the best combination levels for minimum UFP is shown in Figure 6-3. The middle hardness of workpiece ( $H_2$ , 38 HRC), middle feed rate ( $f_2$ , 0.15 mm/th), and middle cutting speed ( $V_{C2}$ , 350 m/min) are determined to be the best optimal for obtaining the lowest UFP value with machining by honed tool. Therefore, the optimal parameters are set as  $V_{C2} f_2 H_2$ .

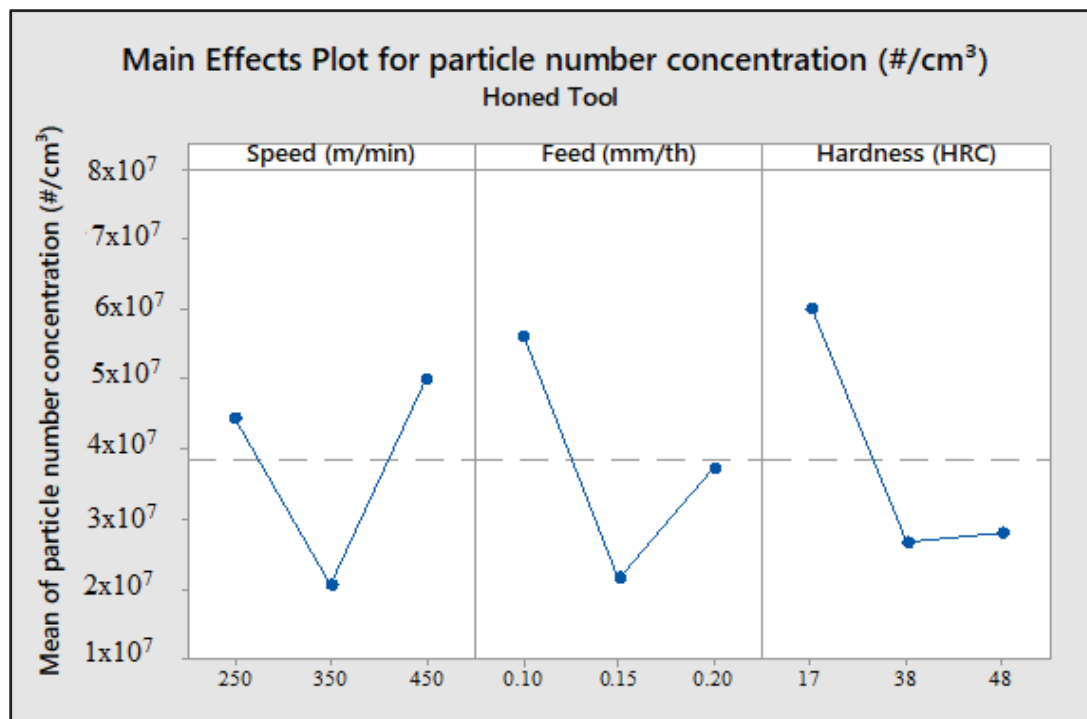
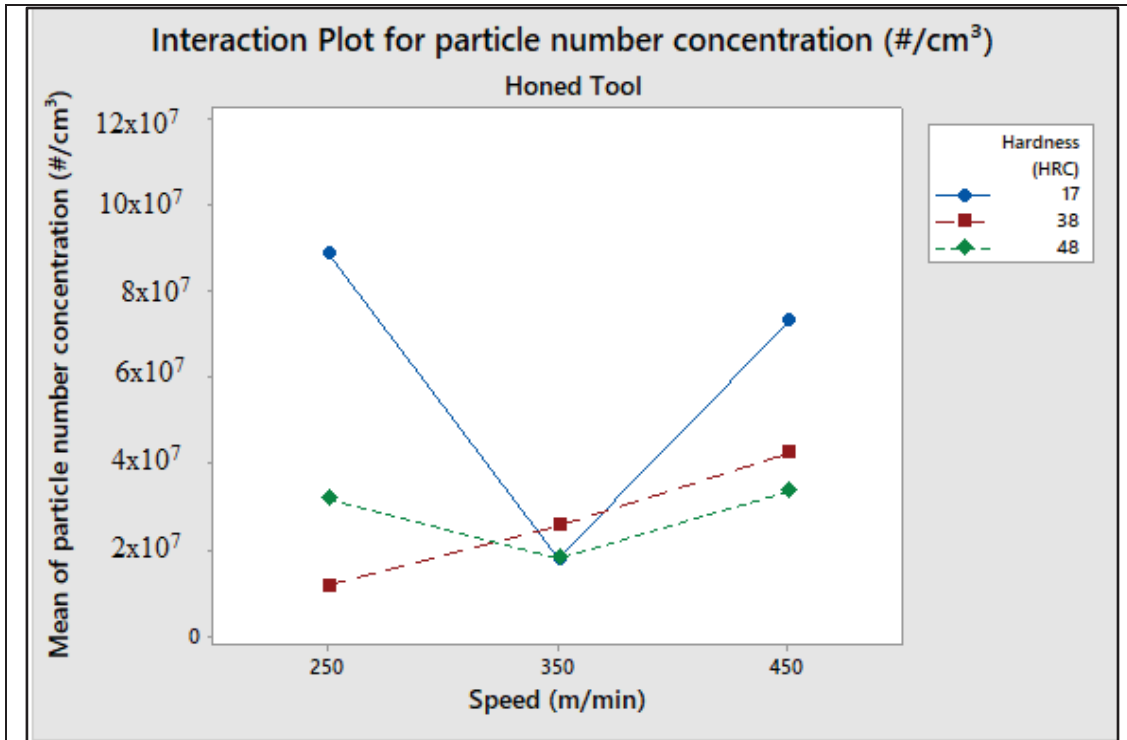
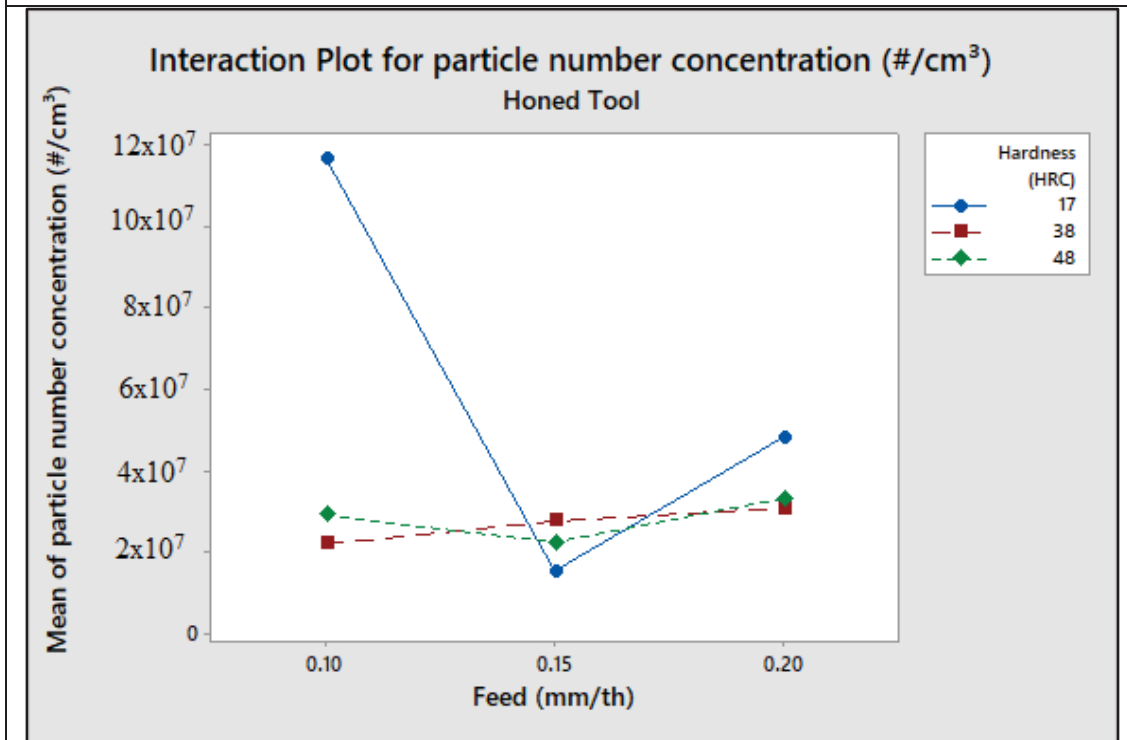


Figure 6-3 Main effects plot for UFP (Honed tool).

The interaction plots for the particles number concentration are displayed in Figure 6-4 (a and b). Figures show that interaction between the factors cutting speed, feed rate, and hardness of workpiece material. The interaction analysis shows that the particles number concentration at high hardness of workpiece material is less than at low hardness of workpiece material, the same trend found at high cutting speed (Figure 6-4 a).



(a)



(b)

Figure 6-4 Interaction plots for number concentration ultrafine particles (Honed tool).

On the other side, if the cutting speed is increased from 250 to 450 (m/min), there is an increase in the particles number concentration generated. In general, the ultrafine particles decrease with an increase in hardness of workpiece.

Table 6-3 shows analysis of variance (ANOVA) of particles number concentration for honed tool. It can be observed that the hardness of workpiece material (F-value =3.01) was the greatest significant to the response of the particles number concentration, followed by the interaction feed × hardness (F-value = 2.62), the feed rate (F-value = 2.51), the cutting speed (F-value = 2.03), the interaction speed × feed rate (F-value = 2.01), and the interaction speed × hardness (F-value = 1.38). The contribution (%) provided an additional characterization of significance for the interpretation of the results. The results show that the contribution due to the hardness of workpiece material was 12.78%, whereas the interaction feed × hardness contributed 22.19%, the interaction speed × feed contributed 17.10%, the interaction speed × hardness 11.72%, the feed contributed 10.65%, and the cutting speed contributed 8.60%.

Table 6-3 Analysis of Variance for UFP (Honed tool).

Source	DF	Seq SS	Adj SS	Adj MS	F	P	C (%)
Cutting speed (m/min)	2	4.31x10 <sup>15</sup>	4.31x10 <sup>15</sup>	2.15x10 <sup>15</sup>	2.03	0.194	8.60
Feed rate (mm/th)	2	5.33x10 <sup>15</sup>	5.33x10 <sup>15</sup>	2.66x10 <sup>15</sup>	2.51	0.142	10.65
Hardness (HRC)	2	6.40x10 <sup>15</sup>	6.40x10 <sup>15</sup>	3.20x10 <sup>15</sup>	3.01	0.106	12.78
Speed*Feed	4	8.55x10 <sup>15</sup>	8.55x10 <sup>15</sup>	2.13x10 <sup>15</sup>	2.01	0.186	17.10
Speed*Hardness	4	5.87x10 <sup>15</sup>	5.87x10 <sup>15</sup>	1.46x10 <sup>15</sup>	1.38	0.322	11.72
Feed*Hardness	4	1.11x10 <sup>16</sup>	1.11x10 <sup>16</sup>	2.78x10 <sup>15</sup>	2.62	0.115	22.19
Residual Error	8	8.49x10 <sup>15</sup>	8.49x10 <sup>15</sup>	1.06x10 <sup>15</sup>			16.96
Total	26	5.01x10 <sup>16</sup>					100

Table 6-4 shows analysis of variance (ANOVA) of particles number concentration for T-land tool. It can be seen that the interaction speed × feed rate (F-value = 3.77) was the most significant to the output response of the particles number concentration, followed by the hardness of workpiece material (F-value =2.70), the interaction speed × hardness of

workpiece (F-value = 1.53), the interaction feed rate  $\times$  hardness of workpiece (F-value = 1.39) and the cutting speed (F-value = 1.13).

The feed rate had no significant effect on the particles number concentration. The results show that the contribution due to the cutting speed was 5.25%, whereas the feed contributed 1.47%, the hardness of workpiece material contributed 12.52%, the interaction speed  $\times$  feed contributed 35.04%, the interaction speed  $\times$  hardness contributed 14.20%, and the interaction feed  $\times$  hardness contributed 12.95%. The best combination of milling parameters regarding the UFP (less generated UFP) is as follows cutting speed  $V_{C2}$  (350 m/min), feed rate  $f_2$  (0.15 mm/th), and hardness of workpiece  $H_3$  (48 HRC) as shown in Figure 6-5.

Table 6-4 Analysis of Variance for UFP (T-land tool).

Source	DF	Seq SS	Adj SS	Adj MS	F	P	C (%)
Cutting speed (m/min)	2	2.34x10 <sup>15</sup>	2.34x10 <sup>15</sup>	1.17x10 <sup>15</sup>	1.13	0.370	5.25
Feed rate (mm/th)	2	6.59x10 <sup>14</sup>	6.59x10 <sup>14</sup>	3.29x10 <sup>14</sup>	0.32	0.737	1.47
Hardness (HRC)	2	5.60x10 <sup>15</sup>	5.60x10 <sup>15</sup>	2.80x10 <sup>15</sup>	2.70	0.127	12.52
Speed*Feed	4	1.56x10 <sup>16</sup>	1.56x10 <sup>16</sup>	3.92x10 <sup>15</sup>	3.77	0.052	35.04
Speed*Hardness	4	6.35x10 <sup>15</sup>	6.35x10 <sup>15</sup>	1.58x10 <sup>15</sup>	1.53	0.282	14.20
Feed*Hardness	4	5.79x10 <sup>15</sup>	5.79x10 <sup>15</sup>	1.44x10 <sup>15</sup>	1.39	0.319	12.95
Residual Error	8	8.31x10 <sup>15</sup>	8.31x10 <sup>15</sup>	1.03x10 <sup>15</sup>			18.57
Total	26	4.47x10 <sup>16</sup>					100

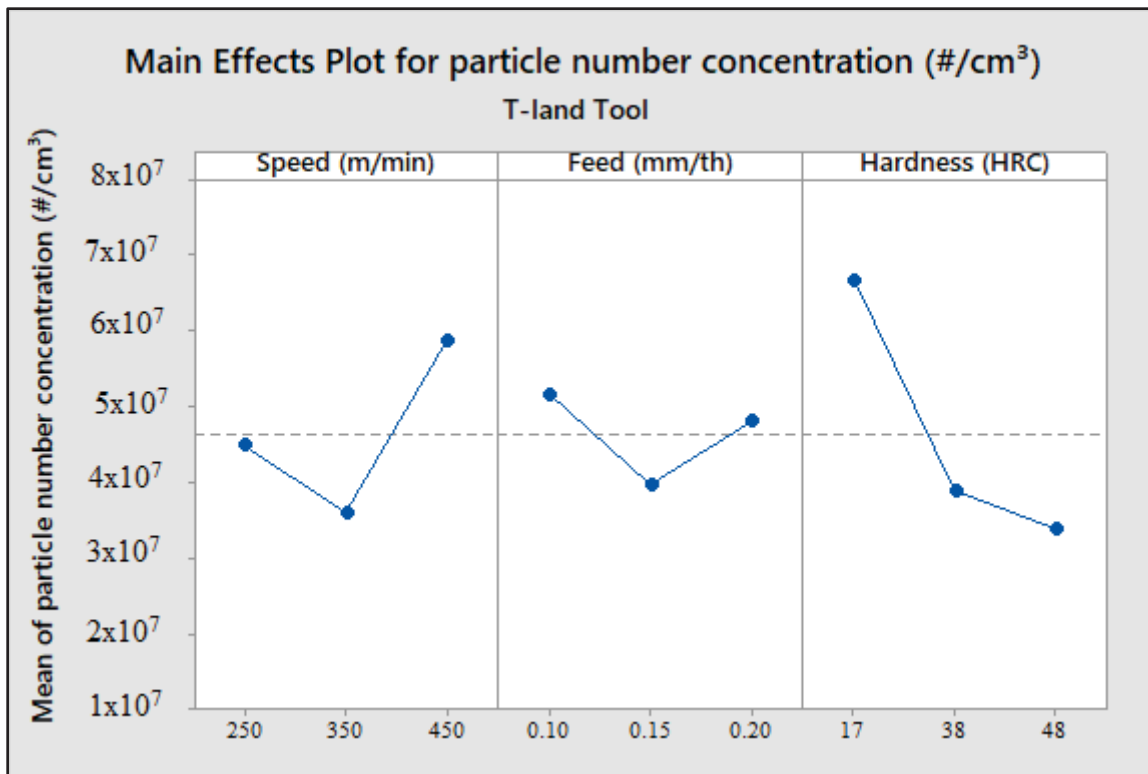
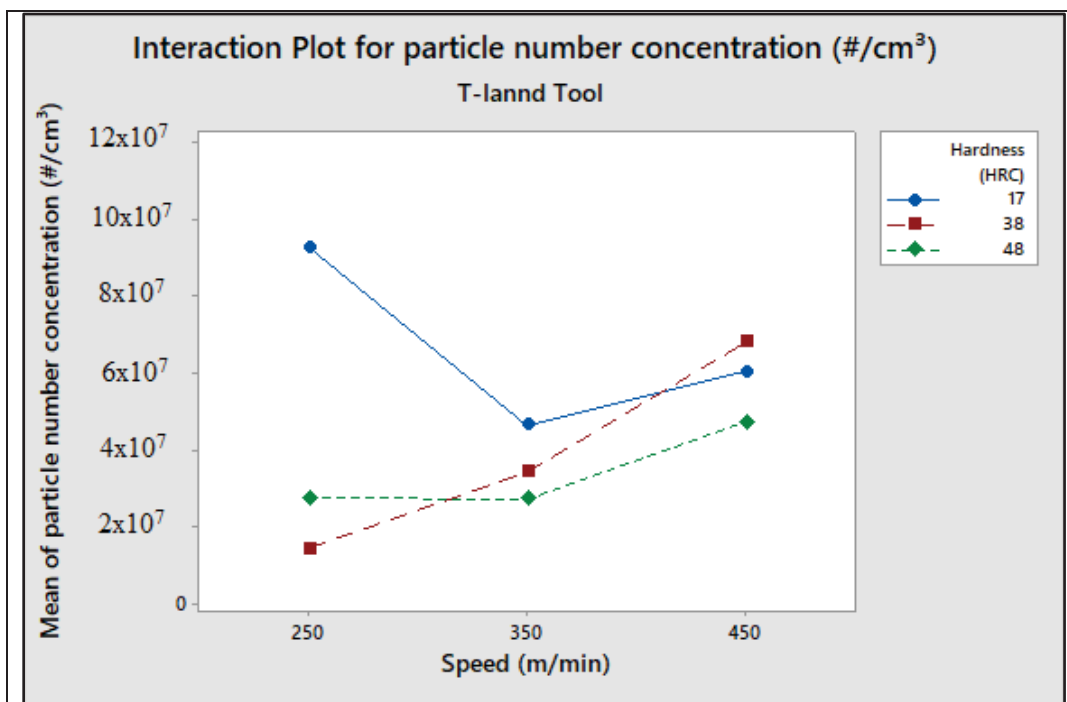
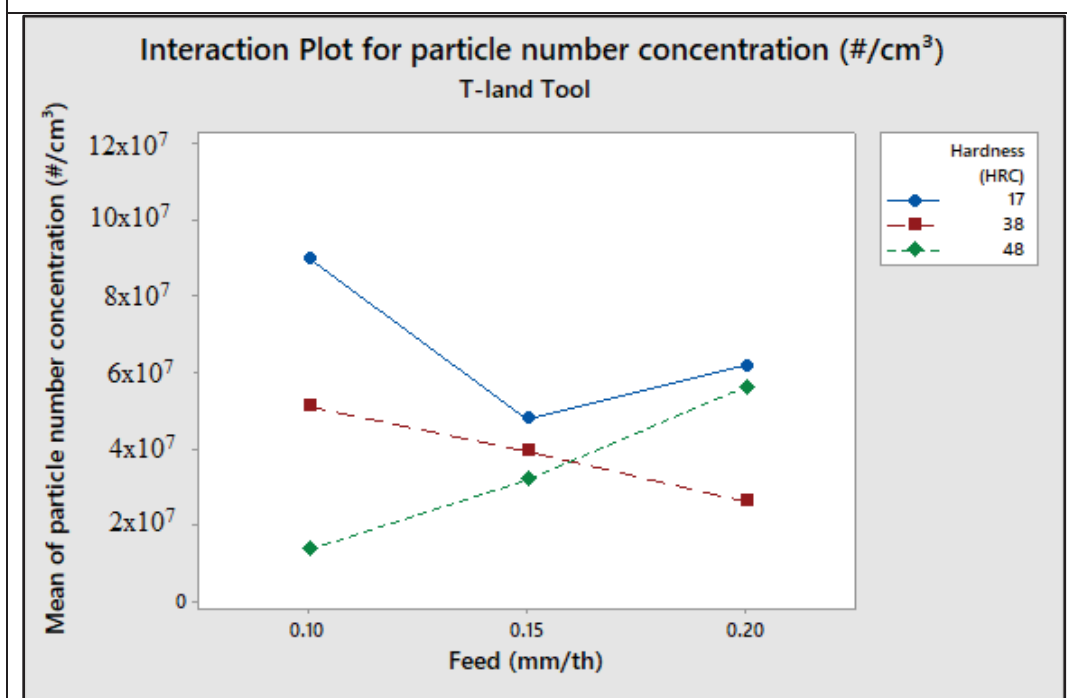


Figure 6-5 Main effects plot for UFP (T-land tool).

The interaction plots for the particles number concentration are indicated in Figure 6-6 (a and b). Outcomes demonstrate that the effect of cutting speed and feed rate on UFP is dependent on hardness of workpiece material. From Figure 6-6 (a) that the low hardness of workpiece produces high UFP at low cutting speed. On the other hand, the UFP increases with the hardness of workpiece increases at high cutting speed. From Figure 6-6 (b) shows that the high hardness of workpiece (48 HRC) generates more UFP with increase feed rate (0.20 mm/th) contrary, at low hardness of workpiece, the UFP decrease with increases feed rate.



(a)



(b)

Figure 6-6 Interaction plots for particles number concentration ultrafine (T-land tool).

Figures 6-7 and 6-8, present the particles number concentration of ultrafine particles as a function of the diameter during machining by using honed tool and T-land tool, respectively at different hardness of workpiece using a scanning mobility particles sizer (SMPS) particles size ranging from 10 to 100 nm. It is observed that the particles number concentration of ultrafine decreases with increase of feed rate and the hardness of workpiece on both tools. Also, it is noticed the particles number concentration of ultrafine generates by using T-land tool more than the honed tool at same cutting condition. It is clear noticed in Figure 6-9 that shown the average of total number concentration of ultrafine particles. The change of tool geometry from honed to T-land increased the dust during dry milling operation. Used honed tool reduced the particles emission significantly. In general, the temperatures generated and plastic strain are higher for T-land edge compared with honed edge (L. Chen, El-Wardany, Nasr, & Elbestawi, 2006).

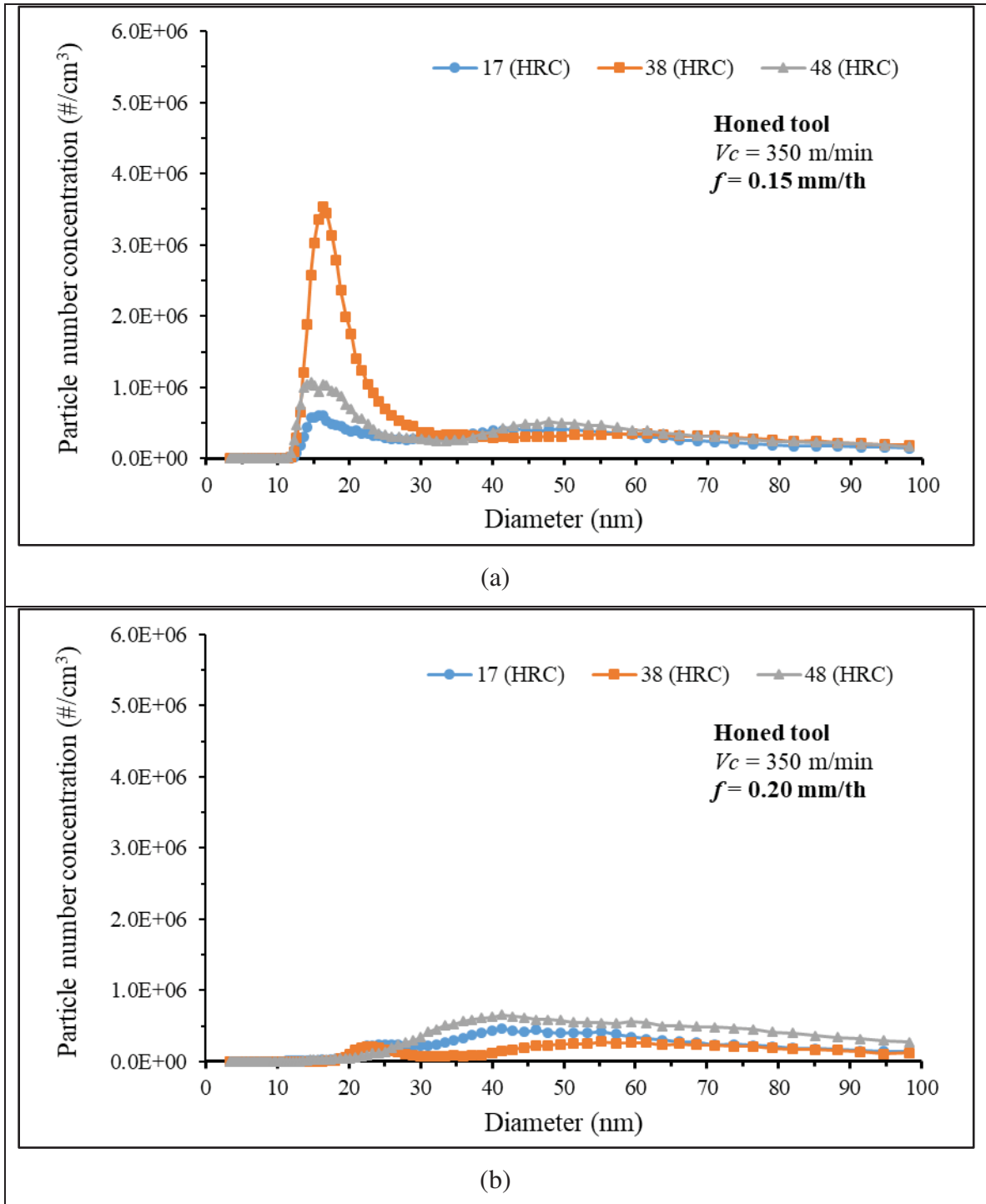


Figure 6-7 Particles number concentration of ultrafine particles as a function of diameter with various hardness of workpiece materials used honed tool.

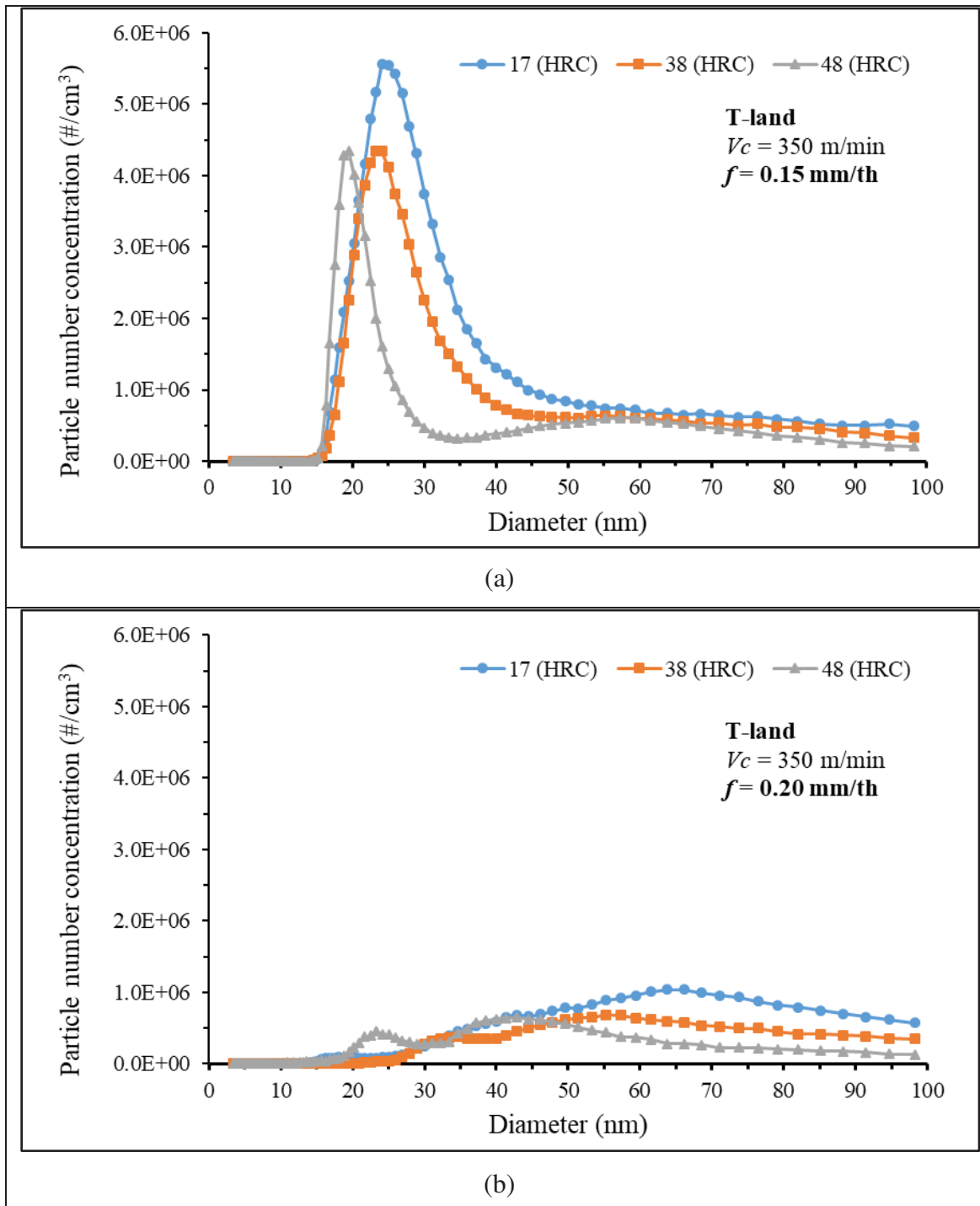


Figure 6-8 Particles number concentration of ultrafine particles as a function of diameter with various hardness of workpiece materials.

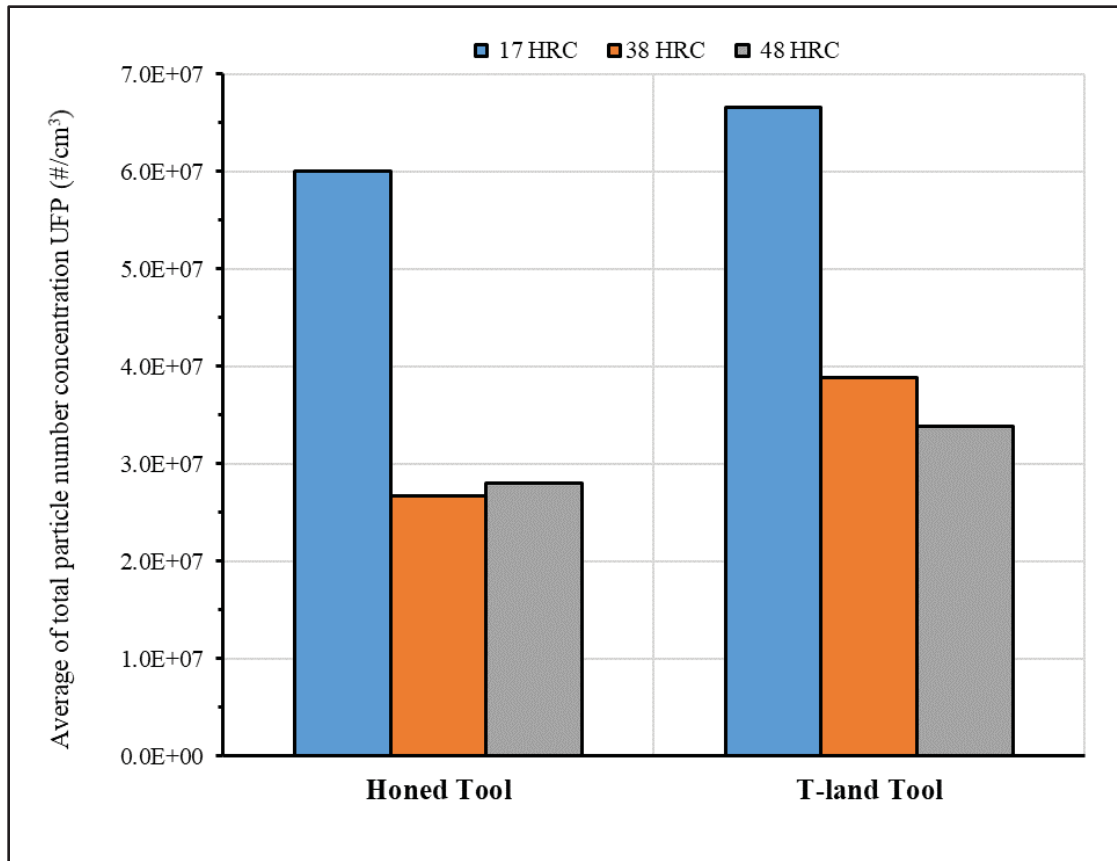


Figure 6-9 Average of total particles number concentration UFP during honed and T-land tools.

#### 6.4 Conclusions

In study the influence of machining parameters and the ceramic tools (Honed and T-land) on the particles number concentration of ultrafine particles during machining hardened AISI 1045 steel was studied. It is found that:

- From analysis of variance (ANOVA), the hardness of workpiece material was found to be most significant parameter on the particles number concentration of ultrafine particles with a percent contribution of 12.78% and 12.52% for honed tool and T-land tool, respectively.
- Based on the mean ratio using smaller is the better approach, it can determine that the best optimal cutting condition is  $V_{C2} f_2 H_2$  i.e. cutting speed is 350 m/min, feed rate is 0.15 mm/th, and workpiece hardness is 38 HRC for honed tool, while, the best

optimal cutting condition is  $V_{C2} f_2 H_3$  i.e. cutting speed is 350 m/min, feed rate is 0.15 mm/th, and workpiece hardness is 48 HRC for T-land tool.

- The feed rate has no significant influence on the particles number concentration of ultrafine particles by using T-land edge tool; nevertheless, the feed rate significantly influences the particles number concentration of ultrafine particles for honed edge tool.
- At same cutting conditions, using the honed edge cutting produces less ultrafine particles emission compared to T-land edge cutting. It is recommended honed edge to minimize the emission of dust on the work area which can have reduced the risk of injury to the operator.

## CONCLUSIONS

This research is thoroughly performed to understand the machinability of AISI 1045 hardened steel. The machinability indicators studied are cutting forces, power, surface finish, tool wear and metallic particle emissions. A Taguchi experimental design was used to explore the performance of ceramic tools in hard milling of AISI 1045 steel. The cutting edge preparation, the workpiece material hardness, the milling type and the machining parameters (cutting speed and feed rate) are the input factors investigated. Through all results obtained, the main conclusions are as follows:

- The feed rate was identified as the most significant factor in both roughing operations (for cutting forces and tool wear) and for finishing operations (tool wear and surface finish). The tool wear response was mostly influenced by tool grade and edge preparation. The range of workpiece hardness tested (38-54 HRC) did not affect significantly the cutting forces or the power but did have some effect on tool wear.
- The results obtained demonstrated that cutting conditions have direct effect on the fine and ultrafine metallic particles emission during the face milling process. Using honed edge cutting produces less fine and ultrafine particles emission compared to T-land edge cutting as a consequence of more deformation and segmentation taking place within the chip during machining with a honed tool.
- The Feed rate and the hardness of workpiece material were the main factors affecting fine and ultrafine metallic particles emissions when using honed tool and T-land edge tool. Choosing the feed rate is a very critical factor to minimizing ultrafine metallic particle emission on both tools. Low particle emissions were recorded when milling workpiece with high hardness, as a consequence of change in chip formation.
- The optimized machining parameters obtained by the multi-objective optimizations showed fundamental improvement in tool performance on manufacturers' recommended data on both roughing and finishing operations. The improvements were about 50% to 80% on resultant force, cutting power and tool wear.



## MAIN CONTRIBUTIONS

This thesis has generated machining data that can help to determine the heat treatment conditions and machining parameters settings which AISI 1045 steel should be machined to enhance tool performance, limit machine-tool power usage, and improve machined part surface quality while minimizing emissions of fine and ultrafine metallic particles dangerous to occupational health and safety of machine-tool operators.

The specific contributions of this research study are summarized as follows:

- Studied the machining of hardened AISI 1045 steel and established the machining parameters that lower the cutting forces, lower the power, and increase tool life (reduced tool wear).
- Determined the optimum cutting conditions for both roughing and finishing processes by using two Taguchi-based, multi-objective optimization techniques (grey relational analysis and desirability function analysis).
- Investigated the combined effect of material hardness and cutting tool (edge preparation, tool material) on metallic particles emission when machining AISI 1045 steel.



## **RECOMMENDATIONS**

Future research work related to this study will concentrate on the following aspects:

- Perform a deep analysis of the effect of temperatures during machining on the microstructure of the machined workpiece.
- Perform study on the martensite and remain austenite fraction and their effects on the machinability.
- Investigated the effect of repeated tempering process on the microstructure and machinability.



**APPENDIX I**  
**EXPERIENCE PLANS FOR ORTHOGONAL ARRAY**  
 **$L_{32} (2^1 4^4)$  OF TAGUCHI DESIGN**

**Table I-1 Cutting forces**

No	Milling type	Speed (m/min)	Feed (mm/tooth)	Hardness (HRC)	Tool	F <sub>x</sub> (N)	F <sub>y</sub> (N)	F <sub>z</sub> (N)
1	Up	200	0.05	38	1	133	101	47
2	Up	200	0.09	43	2	281	289	234
3	Up	200	0.13	48	3	474	329	207
4	Up	200	0.17	53	4	487	434	464
5	Up	300	0.05	38	2	184	179	162
6	Up	300	0.09	43	1	460	330	112
7	Up	300	0.13	48	4	322	309	292
8	Up	300	0.17	53	3	592	341	231
9	Up	400	0.05	43	3	255	190	82
10	Up	400	0.09	38	4	340	292	215
11	Up	400	0.13	53	1	311	272	218
12	Up	400	0.17	48	2	598	400	269
13	Up	500	0.05	43	4	108	266	169
14	Up	500	0.09	38	3	318	197	355
15	Up	500	0.13	53	2	429	210	325
16	Up	500	0.17	48	1	471	562	243
17	Down	200	0.05	53	1	126	286	92
18	Down	200	0.09	48	2	156	342	147
19	Down	200	0.13	43	3	237	546	163
20	Down	200	0.17	38	4	301	710	242
21	Down	300	0.05	53	2	100	300	119
22	Down	300	0.09	48	1	113	169	215
23	Down	300	0.13	43	4	170	574	221
24	Down	300	0.17	38	3	236	633	180
25	Down	400	0.05	48	3	115	313	87
26	Down	400	0.09	53	4	176	469	174
27	Down	400	0.13	38	1	108	221	289
28	Down	400	0.17	43	2	253	780	247
29	Down	500	0.05	48	4	82	236	118
30	Down	500	0.09	53	3	151	362	140
31	Down	500	0.13	38	2	186	499	256
32	Down	500	0.17	43	1	234	519	216

**Table I-2 Resultant force, tangential force, power and tool wear**

No	Milling type	Speed (m/min)	Feed (mm/tooth)	Hardness (HRC)	Tool	F (N)	Ft (N)	P (W)	VB ( $\mu\text{m}$ )
1	Up	200	0.05	38	1	167	127	422	47.27
2	Up	200	0.09	43	2	364	268	894	49.56
3	Up	200	0.13	48	3	518	424	1413	29.26
4	Up	200	0.17	53	4	569	496	1652	22.84
5	Up	300	0.05	38	2	165	205	1026	50.58
6	Up	300	0.09	43	1	570	433	2165	45.84
7	Up	300	0.13	48	4	443	387	1936	25.21
8	Up	300	0.17	53	3	673	415	2076	26.69
9	Up	400	0.05	43	3	296	241	1605	37.44
10	Up	400	0.09	38	4	414	354	2360	32.06
11	Up	400	0.13	53	1	406	262	1749	40.20
12	Up	400	0.17	48	2	649	468	3119	39.51
13	Up	500	0.05	43	4	191	154	1285	50.47
14	Up	500	0.09	38	3	356	329	2742	36.07
15	Up	500	0.13	53	2	463	411	3427	38.13
16	Up	500	0.17	48	1	727	792	6601	47.15
17	Down	200	0.05	53	1	288	319	1062	118.06
18	Down	200	0.09	48	2	360	236	786	32.36
19	Down	200	0.13	43	3	553	534	1779	37.65
20	Down	200	0.17	38	4	718	658	2194	33.29
21	Down	300	0.05	53	2	318	288	1442	30.34
22	Down	300	0.09	48	1	204	227	1134	78.31
23	Down	300	0.13	43	4	582	500	2499	119.62
24	Down	300	0.17	38	3	642	542	2710	38.13
25	Down	400	0.05	48	3	331	271	1807	32.41
26	Down	400	0.09	53	4	493	374	2496	27.48
27	Down	400	0.13	38	1	222	119	791	133.37
28	Down	400	0.17	43	2	813	751	5005	38.13
29	Down	500	0.05	48	4	239	220	1830	32.40
30	Down	500	0.09	53	3	381	305	2542	30.50
31	Down	500	0.13	38	2	472	487	4055	44.68
32	Down	500	0.17	43	1	561	506	4219	80.06

**Table I-3 Surface roughness**

No	Milling type	Speed (m/min)	Feed (mm/tooth)	Hardness (HRC)	Tool	Ra ( $\mu\text{m}$ )	Rq ( $\mu\text{m}$ )	Rt ( $\mu\text{m}$ )
1	Up	200	0.05	38	1	0.104	0.132	0.769
2	Up	200	0.09	43	2	0.403	0.500	3.147
3	Up	200	0.13	48	3	0.160	0.195	1.097
4	Up	200	0.17	53	4	0.602	0.707	3.036
5	Up	300	0.05	38	2	0.204	0.239	0.979
6	Up	300	0.09	43	1	0.084	0.098	0.521
7	Up	300	0.13	48	4	0.153	0.191	1.680
8	Up	300	0.17	53	3	0.638	0.757	3.143
9	Up	400	0.05	43	3	0.375	0.443	1.931
10	Up	400	0.09	38	4	0.746	0.905	4.185
11	Up	400	0.13	53	1	0.129	0.156	0.779
12	Up	400	0.17	48	2	0.735	0.498	1.001
13	Up	500	0.05	43	4	0.137	0.165	0.796
14	Up	500	0.09	38	3	0.413	0.500	2.438
15	Up	500	0.13	53	2	0.609	0.703	0.394
16	Up	500	0.17	48	1	0.184	0.246	1.570
17	Down	200	0.05	53	1	0.512	0.606	2.235
18	Down	200	0.09	48	2	0.361	0.439	2.213
19	Down	200	0.13	43	3	0.417	0.515	2.578
20	Down	200	0.17	38	4	0.692	0.846	3.796
21	Down	300	0.05	53	2	0.214	0.248	1.228
22	Down	300	0.09	48	1	0.111	0.136	0.631
23	Down	300	0.13	43	4	0.647	0.783	3.169
24	Down	300	0.17	38	3	0.624	0.740	3.261
25	Down	400	0.05	48	3	0.236	0.278	1.375
26	Down	400	0.09	53	4	0.222	0.266	1.397
27	Down	400	0.13	38	1	0.174	0.224	1.273
28	Down	400	0.17	43	2	0.703	0.857	3.609
29	Down	500	0.05	48	4	0.181	0.215	1.245
30	Down	500	0.09	53	3	0.455	0.561	3.169
31	Down	500	0.13	38	2	0.765	0.923	5.961
32	Down	500	0.17	43	1	0.835	1.043	4.636



**APPENDIX II**  
**EXPERIENCE PLANS FOR ORTHOGONAL ARRAY L<sub>27</sub> (3<sup>3</sup>) STUDY OF**  
**METALLIC PARTICLES EMISSION DURING MILLING PROCESS**

**Table II-1 Results of fine metallic particles emission for Honed edge.**

No	Speed (m/min)	Feed (mm/tooth)	Hardness (HRC)	Number (# /cm <sup>3</sup> )	Surface (μm <sup>2</sup> / cm <sup>3</sup> )	Mass (mg /m <sup>3</sup> )
1	250	0.10	17	1.18E+04	2.71E+03	1.27
2	250	0.10	38	5.76E+03	1.88E+03	1.04
3	250	0.10	48	4.01E+03	1.23E+03	0.66
4	250	0.15	17	1.49E+04	3.85E+03	1.84
5	250	0.15	38	6.41E+03	1.96E+03	1.05
6	250	0.15	48	5.70E+03	1.41E+03	0.68
7	250	0.20	17	5.43E+03	1.60E+03	0.85
8	250	0.20	38	5.33E+03	1.71E+03	0.94
9	250	0.20	48	3.97E+03	1.15E+03	0.60
10	350	0.10	17	1.14E+04	2.97E+03	1.47
11	350	0.10	38	7.34E+03	1.99E+03	1.02
12	350	0.10	48	4.48E+03	1.28E+03	0.68
13	350	0.15	17	5.93E+03	1.73E+03	0.92
14	350	0.15	38	4.66E+03	1.39E+03	0.74
15	350	0.15	48	4.02E+03	1.35E+03	0.79
16	350	0.20	17	9.09E+03	2.50E+03	1.30
17	350	0.20	38	4.73E+03	1.48E+03	0.81
18	350	0.20	48	4.67E+03	1.39E+03	0.75
19	450	0.10	17	5.76E+03	1.76E+03	0.95
20	450	0.10	38	7.17E+03	2.56E+03	1.58
21	450	0.10	48	6.41E+03	2.49E+03	1.59
22	450	0.15	17	5.17E+03	1.54E+03	0.83
23	450	0.15	38	8.11E+03	2.07E+03	1.04
24	450	0.15	48	5.56E+03	1.43E+03	0.72
25	450	0.20	17	7.08E+03	2.00E+03	1.05
26	450	0.20	38	5.47E+03	1.82E+03	1.06
27	450	0.20	48	5.80E+03	2.23E+03	1.47

**Table II-2 Results of fine metallic particles emission for T-land edge**

No	Speed (m/min)	Feed (mm/tooth)	Hardness (HRC)	Number (# /cm <sup>3</sup> )	Surface ( $\mu\text{m}^2/\text{cm}^3$ )	Mass (mg /m <sup>3</sup> )
1	250	0.10	17	5.640E+03	1.641E+03	0.868
2	250	0.10	38	4.773E+03	1.465E+03	0.792
3	250	0.10	48	7.241E+03	1.825E+03	0.882
4	250	0.15	17	8.805E+03	2.247E+03	1.126
5	250	0.15	38	5.843E+03	1.681E+03	0.893
6	250	0.15	48	7.241E+03	1.825E+03	0.882
7	250	0.20	17	8.415E+03	2.057E+03	0.987
8	250	0.20	38	4.139E+03	1.248E+03	0.667
9	250	0.20	48	5.283E+03	1.590E+03	0.848
10	350	0.10	17	6.752E+03	1.637E+03	0.790
11	350	0.10	38	5.967E+03	1.533E+03	0.766
12	350	0.10	48	7.255E+03	1.939E+03	0.974
13	350	0.15	17	6.643E+03	1.652E+03	0.812
14	350	0.15	38	4.197E+03	1.393E+03	0.779
15	350	0.15	48	4.805E+03	1.649E+03	0.978
16	350	0.20	17	1.586E+04	3.363E+03	1.454
17	350	0.20	38	4.884E+03	1.243E+03	0.612
18	350	0.20	48	5.265E+03	1.564E+03	0.842
19	450	0.10	17	8.698E+03	2.253E+03	1.101
20	450	0.10	38	4.199E+03	1.402E+03	0.796
21	450	0.10	48	4.863E+03	1.672E+03	0.970
22	450	0.15	17	1.370E+04	2.931E+03	1.320
23	450	0.15	38	6.240E+03	1.518E+03	0.730
24	450	0.15	48	1.256E+04	2.899E+03	1.351
25	450	0.20	17	5.038E+03	1.374E+03	0.714
26	450	0.20	38	3.961E+03	1.300E+03	0.743
27	450	0.20	48	9.967E+03	3.418E+03	2.078

**Table II-3 Results of ultrafine metallic particles emission for Honed edge.**

No	Speed (m/min)	Feed (mm/tooth)	Hardness (HRC)	Number (# /cm <sup>3</sup> )	Surface (nm <sup>2</sup> / cm <sup>3</sup> )	Mass (µg /m <sup>3</sup> )
1	250	0.10	17	2.163E+08	6.162E+11	4.632E+04
2	250	0.10	38	1.249E+07	6.786E+10	5.077E+03
3	250	0.10	48	3.612E+07	1.302E+11	7.709E+03
4	250	0.15	17	7.381E+06	1.137E+11	1.177E+04
5	250	0.15	38	1.289E+07	2.061E+11	2.119E+04
6	250	0.15	48	1.093E+07	1.220E+11	1.117E+04
7	250	0.20	17	4.332E+07	1.351E+11	9.831E+03
8	250	0.20	38	1.000E+07	8.433E+10	7.674E+03
9	250	0.20	48	4.902E+07	1.872E+11	1.361E+04
10	350	0.10	17	2.134E+07	2.220E+11	2.049E+04
11	350	0.10	38	1.834E+07	2.252E+11	2.093E+04
12	350	0.10	48	7.297E+06	1.389E+11	1.545E+04
13	350	0.15	17	1.953E+07	1.146E+11	9.292E+03
14	350	0.15	38	5.075E+07	1.588E+11	1.168E+04
15	350	0.15	48	2.851E+07	1.425E+11	1.149E+04
16	350	0.20	17	1.317E+07	1.124E+11	9.489E+03
17	350	0.20	38	8.015E+06	8.067E+10	7.320E+03
18	350	0.20	48	1.920E+07	1.900E+11	1.686E+04
19	450	0.10	17	1.129E+08	4.734E+11	3.575E+04
20	450	0.10	38	3.519E+07	1.658E+11	1.349E+04
21	450	0.10	48	4.383E+07	1.549E+11	1.095E+04
22	450	0.15	17	1.831E+07	1.700E+11	1.530E+04
23	450	0.15	38	1.912E+07	1.577E+11	1.323E+04
24	450	0.15	48	2.676E+07	1.195E+11	8.411E+03
25	450	0.20	17	8.807E+07	2.990E+11	2.103E+04
26	450	0.20	38	7.380E+07	4.197E+11	3.391E+04
27	450	0.20	48	3.061E+07	1.701E+11	1.228E+04

**Table II-4 Results of ultrafine metallic particles emission for T-land edge**

No	Speed (m/min)	Feed (mm/tooth)	Hardness (HRC)	Number (# /cm <sup>3</sup> )	Surface (nm <sup>2</sup> / cm <sup>3</sup> )	Mass (μg /m <sup>3</sup> )
1	250	0.10	17	1.62E+08	5.93E+11	3.32E+04
2	250	0.10	38	1.87E+07	1.08E+11	7.54E+03
3	250	0.10	48	7.24E+05	1.23E+10	1.36E+03
4	250	0.15	17	9.57E+06	1.55E+11	1.70E+04
5	250	0.15	38	5.01E+06	7.84E+10	8.32E+03
6	250	0.15	48	1.19E+07	1.72E+11	1.73E+04
7	250	0.20	17	1.07E+08	2.74E+11	1.73E+04
8	250	0.20	38	1.84E+07	1.42E+11	1.28E+04
9	250	0.20	48	6.92E+07	3.26E+11	2.45E+04
10	350	0.10	17	1.32E+07	1.61E+11	1.52E+04
11	350	0.10	38	1.24E+07	2.11E+11	2.31E+04
12	350	0.10	48	9.65E+06	1.03E+11	9.29E+03
13	350	0.15	17	9.94E+07	4.31E+11	3.05E+04
14	350	0.15	38	7.31E+07	3.19E+11	2.30E+04
15	350	0.15	48	5.37E+07	2.16E+11	1.60E+04
16	350	0.20	17	2.68E+07	3.28E+11	3.11E+04
17	350	0.20	38	1.73E+07	2.01E+11	1.87E+04
18	350	0.20	48	1.77E+07	1.29E+11	1.03E+04
19	450	0.10	17	9.51E+07	3.90E+11	2.98E+04
20	450	0.10	38	1.22E+08	3.66E+11	2.35E+04
21	450	0.10	48	2.98E+07	2.01E+11	1.63E+04
22	450	0.15	17	3.47E+07	2.78E+11	2.25E+04
23	450	0.15	38	4.00E+07	3.06E+11	2.52E+04
24	450	0.15	48	3.00E+07	2.40E+11	2.12E+04
25	450	0.20	17	5.13E+07	3.01E+11	2.47E+04
26	450	0.20	38	4.25E+07	3.17E+11	2.65E+04
27	450	0.20	48	8.16E+07	4.00E+11	2.90E+04

**Table II-5 Statistically influences factors and interactions on particles emission  
(by order of importance-1-most important)**

<b>Tool edge preparation</b>	<b>Fine particles (FP)</b>	<b>Ultrafine particles (UFP)</b>
<b>Honed Edge</b>	<b>1- Hardness</b>	<b>1- Hardness</b>
	2- Speed x Hardness	2- Feed rate
	3- Speed x Feed rate	3- Speed
	4- Feed rate	4- Feed x Hardness
		5- Feed x Speed
<b>T-land Edge</b>		
	<b>1- Hardness</b>	1- Speed x Feed rate
	2- Speed x Feed rate	<b>2- Hardness</b>
		3- Speed x Hardness

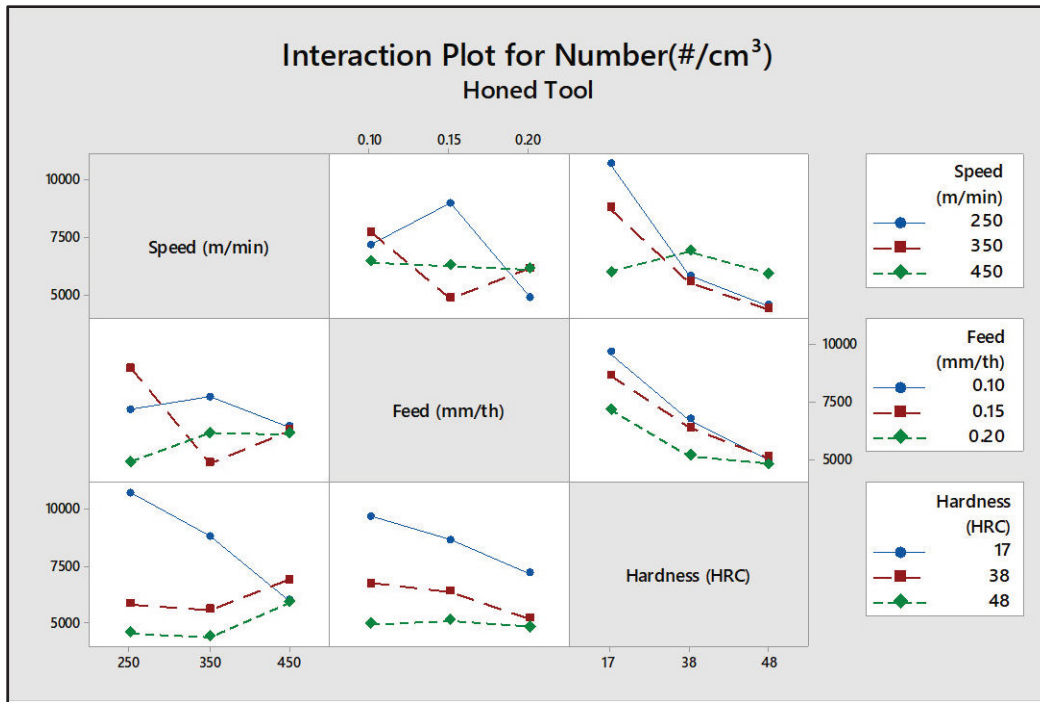


Figure II.1 Interaction plots for particles number concentration FP (Honed tool).

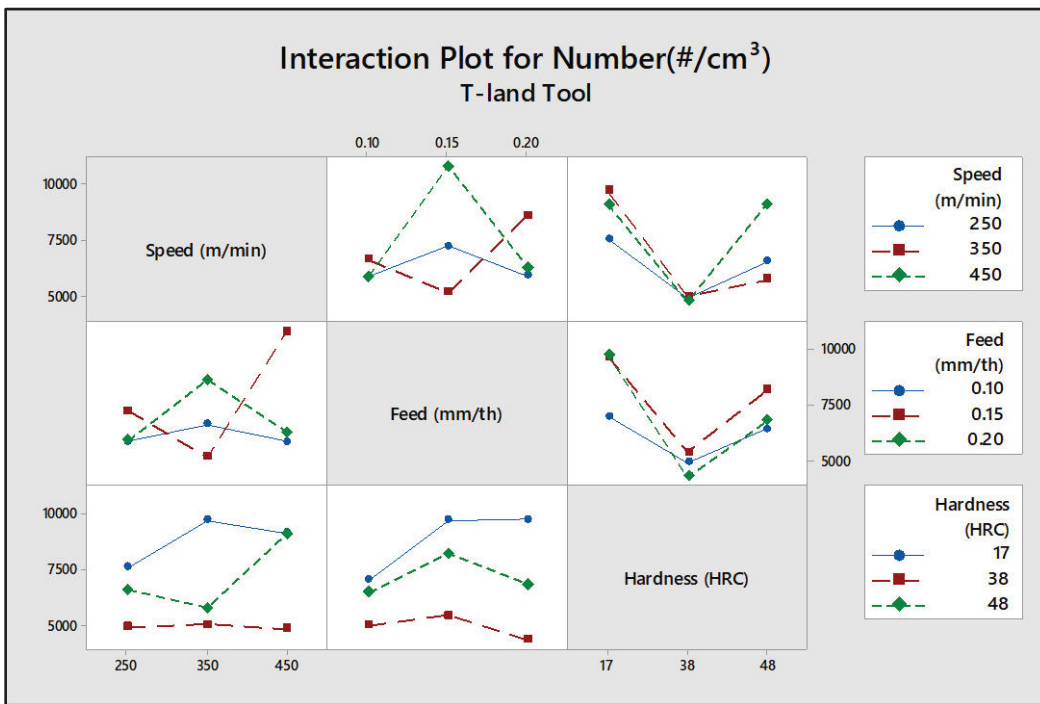


Figure II.2 Interaction plots for particles number concentration FP (T-land tool).

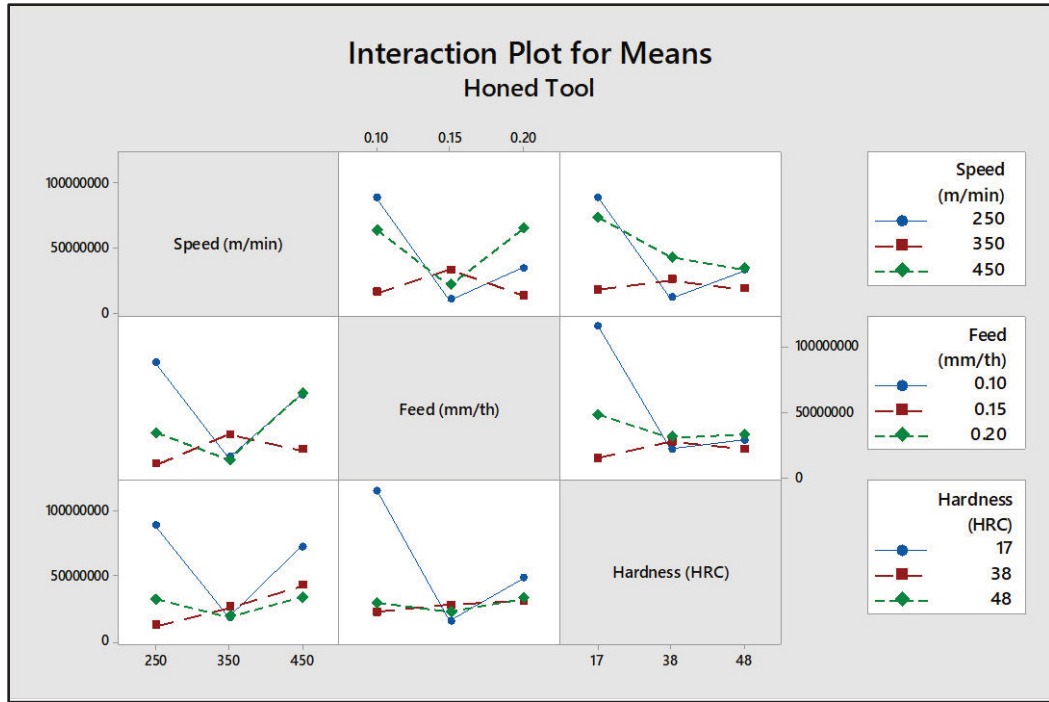


Figure II.3 Interaction plots for particles number concentration UFP (Honed tool).

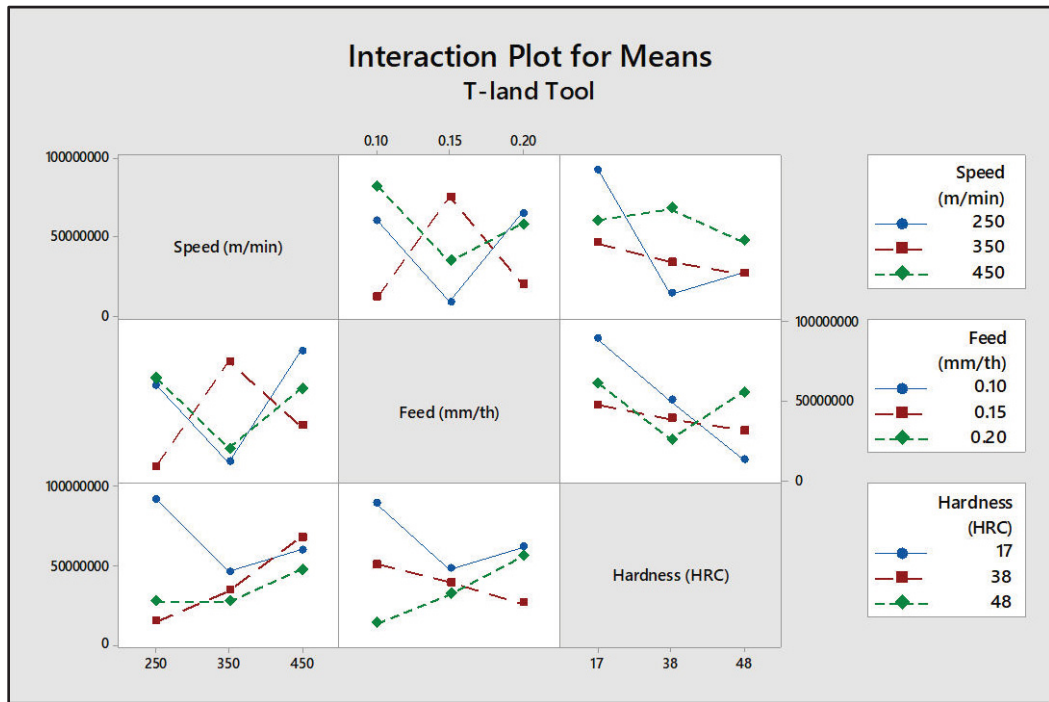


Figure II.4 Interaction plots for particles number concentration UFP (T-land tool).



## LIST OF REFERENCES

- Abdulkadir, L. N., Abou-El-Hossein, K., Jumare, A. I., Odedeyi, P. B., Liman, M. M., & Olaniyan, T. A. (2018). Ultra-precision diamond turning of optical silicon—a review. *The International Journal of Advanced Manufacturing Technology*, 96(1), 173-208. doi:10.1007/s00170-017-1529-x
- Aitken, R., Creely, K., & Tran, C. (2004). *Nanoparticles: an occupational hygiene review*: HSE Books.
- Aitken, R. J., Chaudhry, M., Boxall, A., & Hull, M. (2006). Manufacture and use of nanomaterials: current status in the UK and global trends. *Occupational medicine*, 56(5), 300-306.
- Ajaja, J., Jomaa, W., Bocher, P., Chromik, R. R., Songmene, V., & Brochu, M. (2019). Hard turning multi-performance optimization for improving the surface integrity of 300M ultra-high strength steel. *The International Journal of Advanced Manufacturing Technology*. doi:10.1007/s00170-019-03863-3
- Akhyar, I., & Sayuti, M. (2015). *Effect of heat treatment on hardness and microstructures of AISI 1045*. Paper presented at the Advanced Materials Research.
- Alok, A., & Das, M. (2019). Multi-objective optimization of cutting parameters during sustainable dry hard turning of AISI 52100 steel with newly develop HSN2-coated carbide insert. *Measurement*, 133, 288-302. doi:<https://doi.org/10.1016/j.measurement.2018.10.009>
- Altin, A., Nalbant, M., & Taskesen, A. (2007). The effects of cutting speed on tool wear and tool life when machining Inconel 718 with ceramic tools. *Materials & design*, 28(9), 2518-2522.
- Amini, S., Fatemi, M., & Atefi, R. (2014). High speed turning of Inconel 718 using ceramic and carbide cutting tools. *Arabian Journal for Science and Engineering*, 39(3), 2323-2330.
- Aouici, H., Bouchelaghem, H., Yallese, M., Elbah, M., & Fnides, B. (2014). Machinability investigation in hard turning of AISI D3 cold work steel with ceramic tool using response surface methodology. *The International Journal of Advanced Manufacturing Technology*, 73(9-12), 1775-1788.
- Aouici, H., Fnides, B., Elbah, M., Benlahmidi, S., Bensouilah, H., & Yallese, M. (2016). Surface roughness evaluation of various cutting materials in hard turning of AISI H11. *International Journal of Industrial Engineering Computations*, 7(2), 339-352.
- Aouici, H., Yallese, M. A., Belbah, A., Ameer, M. F., & Elbah, M. (2013). Experimental investigation of cutting parameters influence on surface roughness and cutting forces in hard turning of X38CrMoV5-1 with CBN tool. *Sadhana : Academy proceedings in engineering sciences*, 38(3), 429-445.
- Aouici, H., Yallese, M. A., Fnides, B., & Mabrouki, T. (2010). Machinability investigation in hard turning of AISI H11 hot work steel with CBN tool. *Mechanika*, 86(6), 71-77.
- Arumugam, P. U., Malshe, A. P., & Batzer, S. A. (2006). Dry machining of aluminum–silicon alloy using polished CVD diamond-coated cutting tools inserts. *Surface and Coatings Technology*, 200(11), 3399-3403.

- Arumugam, P. U., Malshe, A. P., Batzer, S. A., & Bhat, D. G. (2003). Study of airborne dust emission and process performance during dry machining of aluminum-silicon alloy with PCD and CVD diamond-coated tools. *Journal of manufacturing processes*, 5(2), 163-169.
- Aruna, M., Dhanalakshmi, V., & Mohan, S. (2010). Wear analysis of ceramic cutting tools in finish turning of Inconel 718. *International Journal of Engineering Science and Technology*, 2(9), 4253-4262.
- Ashley, S. (1995). High-speed machining goes mainstream. *Mechanical Engineering*, 117(5), 56.
- Aslan, E. (2005). Experimental investigation of cutting tool performance in high speed cutting of hardened X210 Cr12 cold-work tool steel (62 HRC). *Materials & design*, 26(1), 21-27. doi:<https://doi.org/10.1016/j.matdes.2004.04.004>
- Aslan, E., Camuscu, N., & Birgoren, B. (2007). Design optimization of cutting parameters when turning hardened AISI 4140 steel (63 HRC) with Al<sub>2</sub>O<sub>3</sub>+TiCN mixed ceramic tool. *Materials & design*, 28(5), 1618-1622. doi:10.1016/j.matdes.2006.02.006
- Aslantas, K., Uzun, I., & Cicek, A. (2012). Tool life and wear mechanism of coated and uncoated Al<sub>2</sub>O<sub>3</sub>/TiCN mixed ceramic tools in turning hardened alloy steel. *Wear*, 274, 442-451. doi:10.1016/j.wear.2011.11.010
- Atmadi, A., Stephenson, A., & Liang, S. Y. (2001). Cutting Fluid Aerosol from Splash in Turning: Analysis for Environmentally Conscious Machining. *The International Journal of Advanced Manufacturing Technology*, 17(4), 238-243. doi:10.1007/s001700170175
- Aurich, J. C., Zimmermann, M., & Leitz, L. (2011). The preparation of cutting edges using a marking laser. *Production Engineering*, 5(1), 17-24.
- Bagaber, S. A., & Yusoff, A. R. (2017). Multi-objective optimization of cutting parameters to minimize power consumption in dry turning of stainless steel 316. *Journal of Cleaner Production*, 157, 30-46. doi:<https://doi.org/10.1016/j.jclepro.2017.03.231>
- Balout, B., Songmene, V., & Masounave, J. (2003). *Dust formation during the high-speed machining of light alloys and brass*. Paper presented at the Light Metals(Metals Legers) 2003: International Symposium on Light Metals as held at the 42 nd Annual Conference of Metallurgists of CIM(COM 2003).
- Balout, B., Songmene, V., & Masounave, J. (2007). An experimental study of dust generation during dry drilling of pre-cooled and pre-heated workpiece materials. *Journal of manufacturing processes*, 9(1), 23-34.
- Bara, A., Sahoo, S. K., Naik, S. S., Sahu, A. K., & Mahapatra, S. S. (2018). Multi Response Optimization of Nd:YAG Laser Micro Drilling Characteristics of 304 Stainless Steel using Desirability Function Approach. *Materials Today-Proceedings*, 5(9), 18975-18982. doi:DOI 10.1016/j.matpr.2018.06.248
- Bartarya, G., & Choudhury, S. (2012). State of the art in hard turning. *International Journal of Machine Tools and Manufacture*, 53(1), 1-14.
- Bassett, E., Köhler, J., & Denkena, B. (2012). On the honed cutting edge and its side effects during orthogonal turning operations of AISI1045 with coated WC-Co inserts. *CIRP Journal of Manufacturing Science and Technology*, 5(2), 108-126.

- Becze, C., Clayton, P., Chen, L., El-Wardany, T., & Elbestawi, M. (2000). High-speed five-axis milling of hardened tool steel. *International Journal of Machine Tools and Manufacture*, 40(6), 869-885.
- Benga, G. C., & Abrao, A. M. (2003). Turning of hardened 100Cr6 bearing steel with ceramic and PCBN cutting tools. *Journal of Materials Processing Technology*, 143, 237-241.
- Benlahmidi, S., Aouici, H., Boutaghane, F., Khellaf, A., Fnides, B., & Yallese, M. (2017). Design optimization of cutting parameters when turning hardened AISI H11 steel (50 HRC) with CBN7020 tools. *The International Journal of Advanced Manufacturing Technology*, 89(1-4), 803-820.
- Bhattacharya, A., Das, S., Majumder, P., & Batish, A. (2009). Estimating the effect of cutting parameters on surface finish and power consumption during high speed machining of AISI 1045 steel using Taguchi design and ANOVA. *Production Engineering*, 3(1), 31-40. doi:10.1007/s11740-008-0132-2
- Bian, R., He, N., Ding, W., & Liu, S. (2017). A study on the tool wear of PCD micro end mills in ductile milling of ZrO<sub>2</sub> ceramics. *The International Journal of Advanced Manufacturing Technology*, 92(5-8), 2197-2206.
- Björkeborn, K., Klement, U., & Oskarson, H.-B. (2010). Study of microstructural influences on machinability of case hardening steel. *The International Journal of Advanced Manufacturing Technology*, 49(5-8), 441-446.
- Boim, N. G., & Sokolov, I. N. (1984). USE OF SUPER-HARD MATERIAL AND CERAMIC CUTTING TOOLS IN MACHINE TOOL CONSTRUCTION. *Soviet engineering research*, 4(7), 55-56.
- Boothroyd, G., & Knight, W. A. (2006). *Fundamentals of machining and machine tools* (3rd ed. ed.). Boca Raton, Flor.: CRC/Taylor and Francis.
- Bouacha, K., Yallese, M. A., Mabrouki, T., & Rigal, J.-F. (2010). Statistical analysis of surface roughness and cutting forces using response surface methodology in hard turning of AISI 52100 bearing steel with CBN tool. *International Journal of Refractory Metals and Hard Materials*, 28(3), 349-361. doi:<https://doi.org/10.1016/j.jirmhm.2009.11.011>
- Bouzakis, K.-D., Michailidis, N., Skordaris, G., Bouzakis, E., Biermann, D., & M'Saoubi, R. (2012). Cutting with coated tools: Coating technologies, characterization methods and performance optimization. *CIRP annals*, 61(2), 703-723.
- Bouzakis, K.-D., Michailidis, N., Skordaris, G., Kombogiannis, S., Hadjiyiannis, S., Efstathiou, K., . . . Wirth, I. (2003). Optimisation of the cutting edge roundness and its manufacturing procedures of cemented carbide inserts, to improve their milling performance after a PVD coating deposition. *Surface and Coatings Technology*, 163, 625-630.
- Bouzakis, K. D., Gerardis, S., Katirtzoglou, G., Makrimallakis, S., Michailidis, N., & Lili, E. (2008). Increasing tool life by adjusting the milling cutting conditions according to PVD films' properties. *CIRP annals*, 57(1), 105-108. doi:<https://doi.org/10.1016/j.cirp.2008.03.070>
- Boy, M., Yaşar, N., & Çiftçi, İ. (2016). *Experimental investigation and modelling of surface roughness and resultant cutting force in hard turning of AISI H13 steel*. Paper presented at the IOP Conference Series: Materials Science and Engineering.

- Brito, T., Paiva, A., Paula, T., Dalosto, D., Ferreira, J., & Balestrassi, P. (2016). Optimization of AISI 1045 end milling using robust parameter design. *The International Journal of Advanced Manufacturing Technology*, 84(5-8), 1185-1199.
- Camuşcu, N. (2006). Effect of cutting speed on the performance of Al<sub>2</sub>O<sub>3</sub> based ceramic tools in turning nodular cast iron. *Materials & design*, 27(10), 997-1006. doi:<https://doi.org/10.1016/j.matdes.2005.02.011>
- Chandrasekaran, H., & M'Saoubi, R. (2006). Improved machinability in hard milling and strategies for steel development. *CIRP Annals-Manufacturing Technology*, 55(1), 93-96.
- Chang, C. S., & Tsai, G. C. (2003). A force model of turning stainless steel with worn tools having nose radius. *Journal of Materials Processing Technology*, 142(1), 112-130. doi:10.1016/S0924-0136(03)00591-0
- Chao, B., & Trigger, K. (1951). Cutting temperatures and metal cutting phenomena. *Trans. ASME*, 73(6), 771.
- Chen, L., El-Wardany, T., Nasr, M., & Elbestawi, M. (2006). Effects of edge preparation and feed when hard turning a hot work die steel with polycrystalline cubic boron nitride tools. *CIRP Annals-Manufacturing Technology*, 55(1), 89-92.
- Chen, Z., Atmadi, A., Stephenson, D. A., Liang, S. Y., & Patri, K. V. (2000). Analysis of cutting fluid aerosol generation for environmentally responsible machining. *CIRP Annals-Manufacturing Technology*, 49(1), 53-56.
- Chen, Z., Liang, S., & Yamaguchi, H. (2002). Predictive Modeling of Cutting Fluid Aerosol Generation in Cylindrical Grinding, NAMRC, May 21-24 2002 (West Lafayette, ID). *Society of Manufacturing Engineers*, 1-8.
- Chen, Z., Wong, K., Li, W., Liang, S. Y., & Stephenson, D. A. (2001). Cutting fluid aerosol generation due to spin-off in turning operation: analysis for environmentally conscious machining. *Journal of manufacturing science and engineering*, 123(3), 506-512.
- Cheng, Y., Liu, L., Wang, H., Wu, M., & Liu, Y. (2014). Investigations on the dust distribution characteristics of dry milling using inserts with various groove profiles. *The International Journal of Advanced Manufacturing Technology*, 74(1-4), 551-562.
- Chinchanikar, S., & Choudhury, S. (2015). Machining of hardened steel—experimental investigations, performance modeling and cooling techniques: a review. *International Journal of Machine Tools and Manufacture*, 89, 95-109.
- Chinchanikar, S., & Choudhury, S. (2016). Cutting force modeling considering tool wear effect during turning of hardened AISI 4340 alloy steel using multi-layer TiCN/Al<sub>2</sub>O<sub>3</sub>/TiN-coated carbide tools. *The International Journal of Advanced Manufacturing Technology*, 83(9-12), 1749-1762.
- Chou, Y. K., & Evans, C. J. (1999). White layers and thermal modeling of hard turned surfaces. *International Journal of Machine Tools and Manufacture*, 39(12), 1863-1881.
- Collin, M., & Rowcliffe, D. (2000). Analysis and prediction of thermal shock in brittle materials. *Acta materialia*, 48(8), 1655-1665.
- Coromant, S. (1994). *Modern metal cutting: a practical handbook*: Sandvik Coromant.
- Costa, D. M. D., Brito, T. G., de Paiva, A. P., Leme, R. C., & Balestrassi, P. P. (2016). A normal boundary intersection with multivariate mean square error approach for dry

- end milling process optimization of the AISI 1045 steel. *Journal of Cleaner Production*, 135, 1658-1672.
- Cui, X., Jiao, F., Zhao, B., & Guo, J. (2017). A review of high-speed intermittent cutting of hardened steel. *The International Journal of Advanced Manufacturing Technology*, 93(9-12), 3837-3846.
- Cui, X., Zhao, J., & Tian, X. (2013). Cutting forces, chip formation, and tool wear in high-speed face milling of AISI H13 steel with CBN tools. *The International Journal of Advanced Manufacturing Technology*, 64(9), 1737-1749. doi:10.1007/s00170-012-4137-9
- Cui, X. B., Zhao, J., Zhou, Y. H., & Pei, Z. (2012). *Cutting forces and tool wear in intermittent turning processes with Al<sub>2</sub>O<sub>3</sub>-based ceramic tools*. Paper presented at the Key Engineering Materials.
- Das, S. R., Kumar, A., & Dhupal, D. (2015). Surface roughness analysis of hardened steel using TiN coated ceramic inserts. *International Journal of Machining and Machinability of Materials*, 17(1), 22-38.
- Davim, J. P. (2010). *Surface integrity in machining* (Vol. 1848828742): Springer.
- Davim, J. P. (2014). *Machinability of advanced materials*: John Wiley & Sons.
- Davim, J. P., & Figueira, L. (2007). Machinability evaluation in hard turning of cold work tool steel (D2) with ceramic tools using statistical techniques. *Materials & design*, 28(4), 1186-1191. doi:<https://doi.org/10.1016/j.matdes.2006.01.011>
- Davoudinejad, A., & Noordin, M. Y. (2014). Effect of cutting edge preparation on tool performance in hard-turning of DF-3 tool steel with ceramic tools. *Journal of Mechanical Science and Technology*, 28(11), 4727-4736. doi:10.1007/s12206-014-1039-9
- de Faoite, D., Browne, D. J., & Stanton, K. T. (2013). Regression analysis of temperature-dependent mechanical and thermal properties of dielectric technical ceramics. *Journal of Materials Science*, 48(1), 451-461.
- De Godoy, V. A. A., & Diniz, A. E. (2011). Turning of interrupted and continuous hardened steel surfaces using ceramic and CBN cutting tools. *Journal of Materials Processing Technology*, 211(6), 1014-1025.
- Debnath, S., Reddy, M. M., & Yi, Q. S. (2014). Environmental friendly cutting fluids and cooling techniques in machining: a review. *Journal of Cleaner Production*, 83, 33-47. doi:<https://doi.org/10.1016/j.jclepro.2014.07.071>
- Demir, H. (2008). The effects of microalloyed steel pre-heat treatment on microstructure and machinability. *The International Journal of Advanced Manufacturing Technology*, 35(9-10), 1041-1046.
- Demir, H., Gündüz, S., & Erden, M. A. (2018). Influence of the heat treatment on the microstructure and machinability of AISI H13 hot work tool steel. *The International Journal of Advanced Manufacturing Technology*, 95(5-8), 2951-2958.
- Deng, J. L. (1989). Introduction to Grey system theory. *J. Grey Syst.*, 1(1), 1-24.
- Denkena, B., & Biermann, D. (2014). Cutting edge geometries. *CIRP annals*, 63(2), 631-653.
- Denkena, B., & Breidenstein, B. (2011). *Cohesive damage of PVD-coated cutting tools—a result of the residual stress distribution*. Paper presented at the Proc. 9th Intern. Conf. THE-“A” Coatings in Manufacturing Engineering.

- Denkena, B., Koehler, J., & Rehe, M. (2012). Influence of the honed cutting edge on tool wear and surface integrity in slot milling of 42CrMo4 steel. *Procedia CIRP*, *1*, 190-195.
- Denkena, B., Köhler, J., & Mengesha, M. S. (2012). Influence of the cutting edge rounding on the chip formation process: Part 1. Investigation of material flow, process forces, and cutting temperature. *Production Engineering*, *6*(4-5), 329-338.
- Denkena, B., Lucas, A., & Bassett, E. (2011). Effects of the cutting edge microgeometry on tool wear and its thermo-mechanical load. *CIRP annals*, *60*(1), 73-76.
- Denkena, B., Reichstein, M., Brodehl, J., & de León García, L. (2005). *Surface preparation, coating and wear performance of geometrically defined cutting edges*. Paper presented at the Proceedings of the 5th international conference the coatings in manufacturing engineering.
- Derringer, G., & Suich, R. (1980). Simultaneous Optimization of Several Response Variables. *Journal of Quality Technology*, *12*(4), 214-219. doi:10.1080/00224065.1980.11980968
- Dewes, R., & Aspinwall, D. (1997). A review of ultra high speed milling of hardened steels. *Journal of Materials Processing Technology*, *69*(1-3), 1-17.
- Dhar, N., Islam, M., Islam, S., & Mithu, M. (2006). The influence of minimum quantity of lubrication (MQL) on cutting temperature, chip and dimensional accuracy in turning AISI-1040 steel. *Journal of Materials Processing Technology*, *171*(1), 93-99.
- Diniz, A. E., & de Oliveira, A. J. (2004). Optimizing the use of dry cutting in rough turning steel operations. *International Journal of Machine Tools and Manufacture*, *44*(10), 1061-1067.
- Djebara, A. (2012). *Méetrologie des particules ultrafines d'usinage: optimisation de la caractérisation et de la mesure*. École de technologie supérieure,
- Djebara, A., Songmene, V., Khettabi, R., & Kouam, J. (2012). An experimental investigation on ultrafine particles emission during milling process using statistical analysis. *International Journal of Advances in Machining and Forming Operations*, *4*(1), 15-37.
- Djebara, A., Zedan, Y., Kouam, J., & Songmene, V. (2013). The Effect of the Heat Treatment on the Dust Emission During Machining of an Al-7Si-Mg Cast Alloys. *Journal of materials engineering and performance*, *22*(12), 3840-3853.
- Dossett, J. L., & Boyer, H. E. (2006). *Practical heat treating*: ASM International.
- Dudzinski, D., Devillez, A., Moufki, A., Larrouquere, D., Zerrouki, V., & Vigneau, J. (2004). A review of developments towards dry and high speed machining of Inconel 718 alloy. *International Journal of Machine Tools and Manufacture*, *44*(4), 439-456.
- Durham, D. R. (2002). Environmentally benign manufacturing: Current practice and future trends. *Journal of Minerals, Metals and Materials Society*, *54*(5), 34-37.
- Elbestawi, M. A., Chen, L., Becze, C. E., & El-Wardany, T. I. (1997). High-speed milling of dies and molds in their hardened state. *CIRP Annals-Manufacturing Technology*, *46*(1), 57-62.
- Elder, A. C., Gelein, R., Azadniv, M., Frampton, M., Finkelstein, J., & Oberdörster, G. (2004). Systemic effects of inhaled ultrafine particles in two compromised, aged rat strains. *Inhalation toxicology*, *16*(6-7), 461-471.

- Enke, K. (1999). Dry machining and increase of endurance of machine parts with improved doped DLC coatings on steel, ceramics and aluminium. *Surface and Coatings Technology*, 116, 488-491.
- Fang, N. (2005). Tool-chip friction in machining with a large negative rake angle tool. *Wear*, 258(5), 890-897.
- Fang, N., & Wu, Q. (2005). The effects of chamfered and honed tool edge geometry in machining of three aluminum alloys. *International Journal of Machine Tools and Manufacture*, 45(10), 1178-1187.
- Fnides, M., Yallese, M., Khattabi, R., Mabrouki, T., & Girardin, F. (2017). Modeling and optimization of surface roughness and productivity thru RSM in face milling of AISI 1040 steel using coated carbide inserts. *International Journal of Industrial Engineering Computations*, 8(4), 493-512.
- Fratila, D., & Caizar, C. (2011). Application of Taguchi method to selection of optimal lubrication and cutting conditions in face milling of AlMg3. *Journal of Cleaner Production*, 19(6-7), 640-645.
- Fulemova, J., & Janda, Z. (2014). Influence of the cutting edge radius and the cutting edge preparation on tool life and cutting forces at inserts with wiper geometry. *Procedia Engineering*, 69, 565-573.
- Gadelmawla, E., Koura, M., Maksoud, T., Elewa, I., & Soliman, H. (2002). Roughness parameters. *Journal of Materials Processing Technology*, 123(1), 133-145.
- Gaitonde, V., Karnik, S., Figueira, L., & Davim, J. P. (2009). Machinability investigations in hard turning of AISI D2 cold work tool steel with conventional and wiper ceramic inserts. *International Journal of Refractory Metals and Hard Materials*, 27(4), 754-763.
- Ghali, E., Sastri, V. S., & Elboudjaini, M. (2007). *Corrosion prevention and protection: practical solutions*: John Wiley & Sons.
- Ghani, J. A., Choudhury, I., & Hassan, H. (2004). Application of Taguchi method in the optimization of end milling parameters. *Journal of Materials Processing Technology*, 145(1), 84-92.
- Gopalsamy, B. M., Mondal, B., & Ghosh, S. (2009). Optimisation of machining parameters for hard machining: grey relational theory approach and ANOVA. *The International Journal of Advanced Manufacturing Technology*, 45(11-12), 1068.
- Groover, M. P. (2010). *Fundamentals of modern manufacturing: materials processes, and systems*: John Wiley & Sons.
- Guo, Y., Li, W., & Jawahir, I. (2009). Surface integrity characterization and prediction in machining of hardened and difficult-to-machine alloys: a state-of-art research review and analysis. *Machining Science and Technology*, 13(4), 437-470.
- Hadi, M. A., Ghani, J. A., Haron, C. H. C., & Kasim, M. S. (2013). Comparison between Up-milling and Down-milling Operations on Tool Wear in Milling Inconel 718. *Procedia Engineering*, 68, 647-653. doi:<https://doi.org/10.1016/j.proeng.2013.12.234>
- Hirao, M., Tlustý, J., Sowerby, R., & Chandra, G. (1982). Chip formation with chamfered tools. *Journal of Engineering for Industry*, 104(4), 339-342.
- Holt, P. E. (1988). *Inhaled dust and disease*.
- Holt, P. F. (1987). *Inhaled dust and disease*. Chichester, Angleterre: J. Wiley and Sons.

- Hornig, J.-T., Liu, N.-M., & Chiang, K.-T. (2008). Investigating the machinability evaluation of Hadfield steel in the hard turning with Al<sub>2</sub>O<sub>3</sub>/TiC mixed ceramic tool based on the response surface methodology. *Journal of Materials Processing Technology*, 208(1-3), 532-541.
- Hoseiny, H., Caballero, F., Högman, B., San Martín, D., Capdevila, C., Nordh, L.-G., & Andrén, H.-O. (2012). The effect of the martensitic packet size on the machinability of modified AISI P20 prehardened mold steel. *Journal of Materials Science*, 47(8), 3613-3620.
- Hoseiny, H., Högman, B., Andrén, H.-O., Klement, U., Ståhl, J.-E., & Thuvander, A. (2013). The influence of microstructure and mechanical properties on the machinability of martensitic and bainitic prehardened mould steels. *International Journal of Materials Research*, 104(8), 748-761. doi:10.3139/146.110926
- Hosseini, A., Hussein, H., & Kishawy, H. (2015). On the machinability of die/mold D2 steel material. *The International Journal of Advanced Manufacturing Technology*, 1-6.
- Hua, J., Shivpuri, R., Cheng, X., Bedekar, V., Matsumoto, Y., Hashimoto, F., & Watkins, T. R. (2005). Effect of feed rate, workpiece hardness and cutting edge on subsurface residual stress in the hard turning of bearing steel using chamfer+ hone cutting edge geometry. *Materials Science and Engineering: A*, 394(1), 238-248.
- Iqbal, S., Mativenga, P., & Sheikh, M. (2007). Characterization of machining of AISI 1045 steel over a wide range of cutting speeds. Part 2: evaluation of flow stress models and interface friction distribution schemes. *Proceedings of the Institution of Mechanical Engineers, Part B: Journal of Engineering Manufacture*, 221(5), 917-926.
- Janmanee, P., Wonthaisong, S., & Araganont, D. (2014). *Effect of Machining Parameters and Wear Mechanism in Milling Mold Steel AISI-P20 and AISI-1050*. Paper presented at the Applied Mechanics and Materials.
- Janmanee, P., Wonthaisong, S., Saodaen, R., & Ithisoponakul, S. (2014). *Surface Roughness of Mold Steel AISI-P20 and AISI-1050 During Milling Machining*. Paper presented at the Advanced Materials Research.
- Jiang, Z. G., Zhang, H., & Sutherland, J. W. (2012). Development of an environmental performance assessment method for manufacturing process plans. *International Journal of Advanced Manufacturing Technology*, 58(5-8), 783-790. doi:10.1007/s00170-011-3410-7
- Jomaa, W., Levesque, J., Bocher, P., Divialle, A., & Gakwaya, A. (2017). Optimization study of dry peripheral milling process for improving aeronautical part integrity using Grey relational analysis. *International Journal of Advanced Manufacturing Technology*, 91(1-4), 931-942. doi:10.1007/s00170-016-9777-8
- Jomaa, W., Songmene, V., & Bocher, P. (2016). An Investigation of Machining-Induced Residual Stresses and Microstructure of Induction-Hardened AISI 4340 Steel. *Materials and Manufacturing Processes*, 31(7), 838-844. doi:10.1080/10426914.2015.1070431
- Jovane, F., Yoshikawa, H., Alting, L., Boer, C. R., Westkamper, E., Williams, D., . . . Paci, A. (2008). The incoming global technological and industrial revolution towards competitive sustainable manufacturing. *CIRP annals*, 57(2), 641-659.
- Ju-Long, D. (1982). Control problems of grey systems. *Systems & Control Letters*, 1(5), 288-294. doi:[https://doi.org/10.1016/S0167-6911\(82\)80025-X](https://doi.org/10.1016/S0167-6911(82)80025-X)

- Jun, Z., Jianxin, D., Jianhua, Z., & Xing, A. (1997). Failure mechanisms of a whisker-reinforced ceramic tool when machining nickel-based alloys. *Wear*, 208(1-2), 220-225.
- Junior, A. S. A., Sales, W. F., da Silva, R. B., Costa, E. S., & Machado, Á. R. (2017). Lubri-cooling and tribological behavior of vegetable oils during milling of AISI 1045 steel focusing on sustainable manufacturing. *Journal of Cleaner Production*, 156, 635-647.
- Kalss, W., Reiter, A., Derflinger, V., Gey, C., & Endrino, J. (2006). Modern coatings in high performance cutting applications. *International Journal of Refractory Metals and Hard Materials*, 24(5), 399-404.
- Kamguem, R., Djebara, A., & Songmene, V. (2013). Investigation on surface finish and metallic particle emission during machining of aluminum alloys using response surface methodology and desirability functions. *The International Journal of Advanced Manufacturing Technology*, 69(5-8), 1283-1298.
- Kandráč, L., Maňková, I., & Vrabel, M. (2013). Cutting edge preparation in machining processes. *tom XXX*, 149.
- Karpuschewski, B., Schmidt, K., Prilukova, J., Beňo, J., Maňková, I., & Hieu, N. T. (2013). Influence of tool edge preparation on performance of ceramic tool inserts when hard turning. *Journal of Materials Processing Technology*, 213(11), 1978-1988.
- Katz, L., Burkhalter, A., & Dreyer, W. (1984). Fluorescent latex microspheres as a retrograde neuronal marker for in vivo and in vitro studies of visual cortex.
- Kennametal. (2013). *Kennametal, Inc.*, . Retrieved from Latrobe, PA 15650 USA:
- Khettabi, R., Songmene, V., & Masounave, J. (2007). Effect of tool lead angle and chip formation mode on dust emission in dry cutting. *Journal of Materials Processing Technology*, 194(1), 100-109.
- Khettabi, R., Songmene, V., & Masounave, J. (2010). Effects of speeds, materials, and tool rake angles on metallic particle emission during orthogonal cutting. *Journal of materials engineering and performance*, 19(6), 767-775.
- Khettabi, R., Songmene, V., Masounave, J., & Zaghbani, I. (2008). Understanding the formation of nano and micro particles during metal cutting. *International Journal of Signal System Control and Engineering*, 1(3), 203-210.
- Khettabi, R., Songmene, V., Zaghbani, I., & Masounave, J. (2010). Modeling of particle emission during dry orthogonal cutting. *Journal of materials engineering and performance*, 19(6), 776-789.
- Kim, K. W., Lee, W. Y., & Sin, H. C. (1999). A finite-element analysis of machining with the tool edge considered. *Journal of Materials Processing Technology*, 86(1), 45-55.
- Kıvık, T. (2014). Optimization of surface roughness and flank wear using the Taguchi method in milling of Hadfield steel with PVD and CVD coated inserts. *Measurement*, 50, 19-28. doi:<https://doi.org/10.1016/j.measurement.2013.12.017>
- Kıvık, T., Samtaş, G., & Çiçek, A. (2012). Taguchi method based optimisation of drilling parameters in drilling of AISI 316 steel with PVD monolayer and multilayer coated HSS drills. *Measurement*, 45(6), 1547-1557.
- Klocke, F., Brinksmeier, E., & Weinert, K. (2005). Capability profile of hard cutting and grinding processes. *CIRP annals*, 54(2), 22-45.
- Koshy, P., Dewes, R., & Aspinwall, D. (2002). High speed end milling of hardened AISI D2 tool steel (~ 58 HRC). *Journal of Materials Processing Technology*, 127(2), 266-273.

- Kouam, J., Songmene, V., Djebara, A., & Khettabi, R. (2012). Effect of friction testing of metals on particle emission. *Journal of materials engineering and performance*, 21(6), 965-972.
- Kreyling, W., Semmler, M., Erbe, F., Mayer, P., Takenaka, S., Schulz, H., . . . Ziesenis, A. (2002). Translocation of ultrafine insoluble iridium particles from lung epithelium to extrapulmonary organs is size dependent but very low. *Journal of Toxicology and Environmental Health Part A*, 65(20), 1513-1530.
- Krolczyk, G. M., Maruda, R. W., Krolczyk, J. B., Wojciechowski, S., Mia, M., Nieslony, P., & Budzik, G. (2019). Ecological trends in machining as a key factor in sustainable production – A review. *Journal of Cleaner Production*, 218, 601-615. doi:<https://doi.org/10.1016/j.jclepro.2019.02.017>
- Kumar, A. S., Durai, A. R., & Sornakumar, T. (2003). Machinability of hardened steel using alumina based ceramic cutting tools. *International Journal of Refractory Metals and Hard Materials*, 21(3-4), 109-117.
- Kumar, A. S., Durai, A. R., & Sornakumar, T. (2006). Wear behaviour of alumina based ceramic cutting tools on machining steels. *Tribology International*, 39(3), 191-197.
- Kumar, C. S., & Patel, S. K. (2017). Experimental and numerical investigations on the effect of varying AlTiN coating thickness on hard machining performance of Al<sub>2</sub>O<sub>3</sub>-TiCN mixed ceramic inserts. *Surface and Coatings Technology*, 309, 266-281.
- Kumar, R., Sahoo, A. K., Mishra, P. C., & Das, R. K. (2018). Comparative investigation towards machinability improvement in hard turning using coated and uncoated carbide inserts: part I experimental investigation. *Advances in Manufacturing*, 6(1), 52-70. doi:10.1007/s40436-018-0215-z
- Kumar Sahoo, A., & Sahoo, B. (2013). Performance studies of multilayer hard surface coatings (TiN/TiCN/Al<sub>2</sub>O<sub>3</sub>/TiN) of indexable carbide inserts in hard machining: Part-II (RSM, grey relational and techno economical approach). *Measurement*, 46(8), 2868-2884. doi:<https://doi.org/10.1016/j.measurement.2012.09.023>
- Kumari, S., Kumar, A., Kumar Yadav, R., & Vivekananda, K. (2018). Optimisation of Machining Parameters using Grey Relation Analysis integrated with Harmony Search for Turning of AISI D2 Steel. *Materials Today: Proceedings*, 5(5, Part 2), 12750-12756. doi:<https://doi.org/10.1016/j.matpr.2018.02.259>
- Lalwani, D., Mehta, N., & Jain, P. (2008). Experimental investigations of cutting parameters influence on cutting forces and surface roughness in finish hard turning of MDN250 steel. *Journal of Materials Processing Technology*, 206(1-3), 167-179.
- Li, B., Zhang, S., Yan, Z., & Jiang, D. (2018). Influence of edge hone radius on cutting forces, surface integrity, and surface oxidation in hard milling of AISI H13 steel. *The International Journal of Advanced Manufacturing Technology*, 95(1-4), 1153-1164.
- Li, B., Zhang, S., Yan, Z., & Zhang, J. (2018). Effect of edge hone radius on chip formation and its microstructural characterization in hard milling of AISI H13 steel. *The International Journal of Advanced Manufacturing Technology*, 97(1-4), 305-318.
- Li, W., Guo, Y., & Guo, C. (2013). Superior surface integrity by sustainable dry hard milling and impact on fatigue. *CIRP annals*, 62(1), 567-570.
- Li, X. S., & Low, I. M. (1994). *Ceramic cutting tools-an introduction*. Paper presented at the Key Engineering Materials.

- Liu, W., Chu, Q., Zeng, J., He, R., Wu, H., Wu, Z., & Wu, S. (2017). PVD-CrAlN and TiAlN coated Si<sub>3</sub>N<sub>4</sub> ceramic cutting inserts-2. High speed face milling performance and wear mechanism study. *Ceramics International*, 43(12), 9488-9492.
- Liu, Z., Ai, X., Zhang, H., Wang, Z., & Wan, Y. (2002). Wear patterns and mechanisms of cutting tools in high-speed face milling. *Journal of Materials Processing Technology*, 129(1-3), 222-226.
- Lo Casto, S., Lo Valvo, E., Lucchini, E., Maschio, S., Piacentini, M., & Ruisi, V. (1996). *Machining of steel with advanced ceramic cutting-tools*. Paper presented at the Key Engineering Materials.
- Lobato, F. S., Sousa, M. N., Silva, M. A., & Machado, A. R. (2014). Multi-objective optimization and bio-inspired methods applied to machinability of stainless steel. *Applied Soft Computing*, 22, 261-271. doi:<https://doi.org/10.1016/j.asoc.2014.05.004>
- Long, Y., Zeng, J., & Shanghua, W. (2014). Cutting performance and wear mechanism of Ti-Al-N/Al-Cr-O coated silicon nitride ceramic cutting inserts. *Ceramics International*, 40(7, Part A), 9615-9620. doi:<https://doi.org/10.1016/j.ceramint.2014.02.038>
- Lu, H. S., Chang, C. K., Hwang, N. C., & Chung, C. T. (2009). Grey relational analysis coupled with principal component analysis for optimization design of the cutting parameters in high-speed end milling. *Journal of Materials Processing Technology*, 209(8), 3808-3817. doi:<https://doi.org/10.1016/j.jmatprotec.2008.08.030>
- M'Saoubi, R., Outeiro, J., Chandrasekaran, H., Dillon Jr, O., & Jawahir, I. (2008). A review of surface integrity in machining and its impact on functional performance and life of machined products. *International Journal of Sustainable Manufacturing*, 1(1-2), 203-236.
- Malshe, A. P., Taher, M. A., Muyschondt, A., Schmidt, W. F., Mohammed, H., & Mohammed, H. (1998). *A comparative study of dry machining of A390 alloy using PCD and CVD diamond tools* (Vol. XXVI): Society of Manufacturing Engineers.
- Manav, O., & Chinchankar, S. (2018). Multi-Objective Optimization Of Hard Turning: A Genetic Algorithm Approach. *Materials Today-Proceedings*, 5(5), 12240-12248. doi:DOI 10.1016/j.matpr.2018.02.201
- Marani, M., Songmene, V., Kouam, J., & Zedan, Y. (2018). Experimental investigation on microstructure, mechanical properties and dust emission when milling Al-20Mg 2 Si-2Cu metal matrix composite with modifier elements. *The International Journal of Advanced Manufacturing Technology*, 99(1-4), 789-802.
- Matsumoto, Y., Barash, M., & Liu, C. (1987). Cutting mechanism during machining of hardened steel. *Materials Science and Technology*, 3(4), 299-305.
- Matsumoto, Y., Magda, D., Hoepfner, D. W., & Kim, T. Y. (1991). Effect of Machining Processes on the Fatigue-Strength of Hardened Aisi-4340 Steel. *Journal of Engineering for Industry-Transactions of the Asme*, 113(2), 154-159. doi:Doi 10.1115/1.2899672
- McClellan, R., & Miller, F. (1997). An overview of EPA's proposed revision of the particulate matter standard. *CIIT Activities*, 17(4), 1-22.
- Meyer, R., Köhler, J., & Denkena, B. (2012). Influence of the tool corner radius on the tool wear and process forces during hard turning. *The International Journal of Advanced Manufacturing Technology*, 58(9-12), 933-940.

- Mia, M., Rifat, A., Tanvir, M. F., Gupta, M. K., Hossain, M. J., & Goswami, A. (2018). Multi-objective optimization of chip-tool interaction parameters using Grey-Taguchi method in MQL-assisted turning. *Measurement*, 129, 156-166. doi:<https://doi.org/10.1016/j.measurement.2018.07.014>
- Mills, & Mills, B. (1983). *Machinability of Engineering Materials*.
- Misal, N. D., & Sadaiah, M. (2018). Multi-Objective Optimization of Photochemical machining of Inconel 601 using Grey Relational Analysis. *Materials Today-Proceedings*, 5(2), 5591-5600.
- Montgomery, D. C. (2017). *Design and analysis of experiments*: John wiley & sons.
- More, A. S., Jiang, W., Brown, W. D., & Malshe, A. P. (2006). Tool wear and machining performance of cBN-TiN coated carbide inserts and PCBN compact inserts in turning AISI 4340 hardened steel. *Journal of Materials Processing Technology*, 180(1), 253-262. doi:<https://doi.org/10.1016/j.jmatprotec.2006.06.013>
- Movahhedy, M., Altintas, Y., & Gadala, M. (2002). Numerical analysis of metal cutting with chamfered and blunt tools. *Journal of manufacturing science and engineering*, 124(2), 178-188.
- Muñoz-Escalona, P., Díaz, N., & Cassier, Z. (2012). Prediction of tool wear mechanisms in face milling AISI 1045 steel. *Journal of materials engineering and performance*, 21(6), 797-808.
- Mustafic, A., Lovric, S., Nasic, E., Halilovic, J., Osmic, M., & Becirovic, D. (2018). TAGUCHI-BASED GREY RELATIONAL ANALYSIS OF PERFORMANCE CHARACTERISTICS IN THE MQL TURNING PROCESS OF X5CrNi18-10 STEEL.
- Nalbant, M., Gökkaya, H., & Sur, G. (2007). Application of Taguchi method in the optimization of cutting parameters for surface roughness in turning. *Materials & design*, 28(4), 1379-1385.
- Narayanan, N. S., Baskar, N., & Ganesan, M. (2018). Multi Objective Optimization of machining parameters for Hard Turning OHNS/AISI H13 material Using Genetic Algorithm. *Materials Today-Proceedings*, 5(2), 6897-6905.
- Ng, E.-G., & Aspinwall, D. K. (2002). The effect of workpiece hardness and cutting speed on the machinability of AISI H13 hot work die steel when using PCBN tooling. *Journal of manufacturing science and engineering*, 124(3), 588-594.
- O. Witschger ; F. Fabrie's. (2005). Particules ultra-fines et sante' au travail 1-caractéristiques et effets potentiels sur la sante. *INRS*, 199, p 21–35.
- Oberdörster, G., Oberdörster, E., & Oberdörster, J. (2005). Nanotoxicology: an emerging discipline evolving from studies of ultrafine particles. *Environmental health perspectives*, 823-839.
- Obikawa, T., Matsumura, T., Shirakashi, T., & Usui, E. (1997). Wear characteristic of alumina coated and alumina ceramic tools. *Journal of Materials Processing Technology*, 63(1-3), 211-216.
- Okada, M., Hosokawa, A., Tanaka, R., & Ueda, T. (2011). Cutting performance of PVD-coated carbide and CBN tools in hardmilling. *International Journal of Machine Tools & Manufacture*, 51(2), 127-132. doi:10.1016/j.ijmactools.2010.10.007

- Okushima, K., Iwata, K., & Kurimoto, T. (1964). A Study of Machinability of Metals: Effect of Microstructure of Metals on Tool Life and Surface Finish. *Bulletin of JSME*, 7(25), 183-191.
- Ozcatalbas, Y., & Ercan, F. (2003). The effects of heat treatment on the machinability of mild steels. *Journal of Materials Processing Technology*, 136(1), 227-238.
- Ozcelik, B., & Bayramoglu, M. (2006). The statistical modeling of surface roughness in high-speed flat end milling. *International Journal of Machine Tools and Manufacture*, 46(12-13), 1395-1402.
- Özel, T., Karpat, Y., Figueira, L., & Davim, J. P. (2007). Modelling of surface finish and tool flank wear in turning of AISI D2 steel with ceramic wiper inserts. *Journal of Materials Processing Technology*, 189(1-3), 192-198.
- Pa, N. M. N., Sarhan, A. A. D., Shukor, M. H. A., & Mohamed, M. A. H. (2013). *Investigate the lubrication effects on cutting force and power consumption in up and down end milling*. Paper presented at the Advanced Materials Research.
- Panda, A., Sahoo, A., & Rout, R. (2016). Multi-attribute decision making parametric optimization and modeling in hard turning using ceramic insert through grey relational analysis: A case study. *Decision Science Letters*, 5(4), 581-592.
- Panda, A., Sahoo, A. K., Rout, A. K., Kumar, R., & Das, R. K. (2018). Investigation of flank wear in hard turning of AISI 52100 grade steel using multilayer coated carbide and mixed ceramic inserts. *Procedia Manufacturing*, 20, 365-371.
- Panov, A. A. (1989). Intensifying component machining by means of tools provided with synthetic superhard materials and ceramics. *Soviet engineering research*, 9(11), 45-49.
- Patel, D. A., Mistry, J. M., Kapatel, V. P., & Joshi, D. R. (2015). *Optimization and Prediction of Cutting Force and Surface Roughness in End Milling Process of AISI 304 Stainless Steel*. Paper presented at the Applied Mechanics and Materials.
- Phadke, M. (1989). *Quality Engineering Using Robust Design* (Englewood Cliffs, NJ, Prentice Hall).
- Poulachon, G., Bandyopadhyay, B. P., Jawahir, I. S., Pheulpin, S., & Seguin, E. (2004). Wear behavior of CBN tools while turning various hardened steels. *Wear*, 256(3), 302-310. doi:[https://doi.org/10.1016/S0043-1648\(03\)00414-9](https://doi.org/10.1016/S0043-1648(03)00414-9)
- Poulachon, G., Moisan, A., & Jawahir, I. (2001). Tool-wear mechanisms in hard turning with polycrystalline cubic boron nitride tools. *Wear*, 250(1), 576-586.
- Pu, Z., & Singh, A. (2013). High speed ball nose end milling of hardened AISI A2 tool steel with PCBN and coated carbide tools. *Journal of manufacturing processes*, 15(4), 467-473.
- Qasim, A., Nisar, S., Shah, A., Khalid, M. S., & Sheikh, M. A. (2015). Optimization of process parameters for machining of AISI-1045 steel using Taguchi design and ANOVA. *Simulation Modelling Practice and Theory*, 59, 36-51.
- Ramu, I., Srinivas, P., & Vekatesh, K. (2018). *Taguchi based grey relational analysis for optimization of machining parameters of CNC turning steel 316*. Paper presented at the IOP Conference Series: Materials Science and Engineering.
- Ratnasingam, J., Scholz, F., & Natthondan, V. (2009). Minimizing dust emission during routing operation of rubberwood. *European Journal of Wood and Wood Products*, 67(3), 363-364.

- Rautio, S., Hynynen, P., Welling, I., Hernmila, P., Usenius, A., & Narhi, P. (2007). Modelling of airborne dust emissions in CNC MDF milling. *Holz als Roh-und Werkstoff*, 65(5), 335-341. doi:10.1007/s00107-007-0179-3
- Reddy, N. S. K., & Rao, P. V. (2006). Experimental investigation to study the effect of solid lubricants on cutting forces and surface quality in end milling. *International Journal of Machine Tools and Manufacture*, 46(2), 189-198.
- Richetti, A., Machado, A., Da Silva, M., Ezugwu, E., & Bonney, J. (2004). Influence of the number of inserts for tool life evaluation in face milling of steels. *International Journal of Machine Tools and Manufacture*, 44(7-8), 695-700.
- Rodríguez, C. J. C. (2009). *Cutting edge preparation of precision cutting tools by applying micro-abrasive jet machining and brushing*: Kassel university press GmbH.
- Ruano, O. A., & Sherby, O. D. (1995). High-Temperature Deformation Mechanisms in Ceramic Materials. In R. C. Bradt, C. A. Brookes, & J. L. Routbort (Eds.), *Plastic Deformation of Ceramics* (pp. 369-380). Boston, MA: Springer US.
- Sarhan, A. A., Sayuti, M., & Hamdi, M. (2012). Reduction of power and lubricant oil consumption in milling process using a new SiO<sub>2</sub> nanolubrication system. *The International Journal of Advanced Manufacturing Technology*, 63(5-8), 505-512.
- Schimmel, R. J., Endres, W. J., & Stevenson, R. (2002). Application of an internally consistent material model to determine the effect of tool edge geometry in orthogonal machining. *Journal of manufacturing science and engineering*, 124(3), 536-543.
- Schultheiss, F., Zhou, J., Gröntoft, E., & Ståhl, J.-E. (2013). Sustainable machining through increasing the cutting tool utilization. *Journal of Cleaner Production*, 59, 298-307.
- Shalaby, M., El Hakim, M., Abdelhameed, M. M., Krzanowski, J., Veldhuis, S., & Dosbaeva, G. (2014). Wear mechanisms of several cutting tool materials in hard turning of high carbon–chromium tool steel. *Tribology International*, 70, 148-154.
- Shalaby, M., & Veldhuis, S. (2018). New observations on high-speed machining of hardened AISI 4340 steel using alumina-based ceramic tools. *Journal of Manufacturing and Materials Processing*, 2(2), 27.
- Shaw, M. C. (2005). *Metal Cutting Principles*, Oxford Series on Advanced Manufacturing. Publ. Oxford University Press, New York (USA).
- Singh, D., & Rao, P. V. (2007). A surface roughness prediction model for hard turning process. *The International Journal of Advanced Manufacturing Technology*, 32(11-12), 1115-1124.
- Skogsmo, J., Halvarsson, M., & Vuorinen, S. (1992). Microstructural study of the  $\kappa$ -Al<sub>2</sub>O<sub>3</sub> →  $\alpha$ -Al<sub>2</sub>O<sub>3</sub> transformation in CVD  $\kappa$ -Al<sub>2</sub>O<sub>3</sub>. *Surface and Coatings Technology*, 54-55, 186-192. doi:[https://doi.org/10.1016/S0257-8972\(09\)90048-2](https://doi.org/10.1016/S0257-8972(09)90048-2)
- Smith, G. T. (2008). *Cutting tool technology: industrial handbook*: Springer.
- Soković, M., Mikula, J., Dobrzański, L., Kopač, J., Koseč, L., Panjan, P., . . . Piech, A. (2005). Cutting properties of the Al<sub>2</sub>O<sub>3</sub>+ SiC (w) based tool ceramic reinforced with the PVD and CVD wear resistant coatings. *Journal of Materials Processing Technology*, 164, 924-929.
- Songmene, V., & Balazinski, M. (1999). Machinability of Graphitic Metal Matrix Composites as a Function of Reinforcing Particles. *CIRP Annals - Manufacturing Technology*, 48(1), 77-80. doi:[https://doi.org/10.1016/S0007-8506\(07\)63135-7](https://doi.org/10.1016/S0007-8506(07)63135-7)

- Songmene, V., Balout, B., & Masounave, J. (2008a). Clean machining: Experimental investigation on particle formation, Part I: Influence of machining Parameters and Chip Formation. *Int. J. Environ. Conscious. Des. Manuf.(ECDM)*, 14(1), 1-16.
- Songmene, V., Balout, B., & Masounave, J. (2008b). Clean machining: Experimental investigation on particle formation, Part II: Influence of machining strategies and drill condition. *Int. J. Environ. Conscious. Des. Manuf.(ECDM)*, 14(1), 17-33.
- Songmene, V., Khettabi, R., & Kouam, J. (2012). Dry high-speed machining: a cost effective and green process. *International Journal of Manufacturing Research*, 7(3), 229-256.
- Songmene, V., & Njoya Doko, R. (2015). *Fine metallic particle emission when milling aluminium alloys and aluminium metal matrix composites*. Paper presented at the Materials Science Forum.
- Sreejith, P., & Ngoi, B. (2000). Dry machining: machining of the future. *Journal of Materials Processing Technology*, 101(1-3), 287-291.
- Suresh Kumar Reddy, N., & Venkateswara Rao, P. (2005). Performance improvement of end milling using graphite as a solid lubricant. *Materials and Manufacturing Processes*, 20(4), 673-686.
- Suresh, R., Basavarajappa, S., & Samuel, G. (2012). Some studies on hard turning of AISI 4340 steel using multilayer coated carbide tool. *Measurement*, 45(7), 1872-1884.
- Sutherland, J., Kulur, V., King, N., & Von Turkovich, B. (2000). An experimental investigation of air quality in wet and dry turning. *CIRP Annals-Manufacturing Technology*, 49(1), 61-64.
- Syahmi Shahrom, M., Mat Yahya, N., & Razlan Yusoff, A. (2013). *Taguchi Method Approach on Effect of Lubrication Condition on Surface Roughness in Milling Operation* (Vol. 53).
- Tamizharasan, T., Selvaraj, T., & Haq, A. N. (2006). Analysis of tool wear and surface finish in hard turning. *The International Journal of Advanced Manufacturing Technology*, 28(7-8), 671-679.
- Tan, E., Ovali, I., Mavi, A., Kaplan, M., & Okay, Ş. (2015). Influence of repeated tempering on the machinability and microstructure of an AISI 52100 steel. *Materials Testing*, 57(11-12), 947-953.
- Thiele, J. D., & Melkote, S. N. (1999). Effect of cutting edge geometry and workpiece hardness on surface generation in the finish hard turning of AISI 52100 steel. *Journal of Materials Processing Technology*, 94(2), 216-226.
- Toenshoff, H. K., & Denkena, B. (2013). Basics of cutting and abrasive processes.
- Tönshoff, H., Karpuschewski, B., & Glatzel, T. (1997). Particle emission and immission in dry grinding. *CIRP Annals-Manufacturing Technology*, 46(2), 693-695.
- Trent, E. M., & Wright, P. K. (2000). *Metal cutting*: Butterworth-Heinemann.
- Tzeng, C.-J., Lin, Y.-H., Yang, Y.-K., & Jeng, M.-C. (2009). Optimization of turning operations with multiple performance characteristics using the Taguchi method and Grey relational analysis. *Journal of Materials Processing Technology*, 209(6), 2753-2759.
- Umamaheswarrao, P., Raju, D. R., Suman, K. N. S., & Sankar, B. R. (2018). Multi objective optimization of process parameters for hard turning of AISI 52100 steel using Hybrid GRA-PCA. *Procedia Computer Science*, 133, 703-710. doi:<https://doi.org/10.1016/j.procs.2018.07.129>

- Ventura, C., Köhler, J., & Denkena, B. (2015). Influence of cutting edge geometry on tool wear performance in interrupted hard turning. *Journal of manufacturing processes*, 19, 129-134.
- Ventura, C. E., Chaves, H. S., Rubio, J. C. C., Abrão, A. M., Denkena, B., & Breidenstein, B. (2017). The influence of the cutting tool microgeometry on the machinability of hardened AISI 4140 steel. *The International Journal of Advanced Manufacturing Technology*, 90(9-12), 2557-2565.
- Verdeja, L. F., Verdeja, J. I., & González, R. (2009). Machinability improvement through heat treatment in 8620 low-carbon alloyed steel. *Machining Science and Technology*, 13(4), 529-542.
- Vipindas, K., Anand, K. N., & Mathew, J. (2018). Effect of cutting edge radius on micro end milling: force analysis, surface roughness, and chip formation. *The International Journal of Advanced Manufacturing Technology*, 97(1), 711-722. doi:10.1007/s00170-018-1877-1
- Vivancos, J., Luis, C., Costa, L., & Ortiz, J. (2004). Optimal machining parameters selection in high speed milling of hardened steels for injection moulds. *Journal of Materials Processing Technology*, 155, 1505-1512.
- Vivancos, J., Luis, C., Ortiz, J., & González, H. (2005). Analysis of factors affecting the high-speed side milling of hardened die steels. *Journal of Materials Processing Technology*, 162, 696-701.
- Vojcak, E. (1992). The interaction of metallurgical conditions of low carbon steel on tool wear of a high speed steel. *Materials Issues in Machining*, 27-38.
- Wang, B., & Liu, Z. (2016). Cutting performance of solid ceramic end milling tools in machining hardened AISI H13 steel. *International Journal of Refractory Metals and Hard Materials*, 55, 24-32.
- Wang, J. J., & Zheng, M. (2003). On the machining characteristics of H13 tool steel in different hardness states in ball end milling. *The International Journal of Advanced Manufacturing Technology*, 22(11-12), 855-863.
- Wertheim, R., Satran, A., & Ber, A. (1994). Modifications of the cutting edge geometry and chip formation in milling. *CIRP Annals-Manufacturing Technology*, 43(1), 63-68.
- WHO, W. H. O. (1999). Hazard prevention and control in the work environment:: airborne dust, Prevention and Control Exchange (PACE), World Health Organization, WHO/SDE/OEH/99.14. pp.1-219.
- Wojciechowski, S. (2015). The estimation of cutting forces and specific force coefficients during finishing ball end milling of inclined surfaces. *International Journal of Machine Tools and Manufacture*, 89, 110-123. doi:<https://doi.org/10.1016/j.ijmachtools.2014.10.006>
- Wojciechowski, S., Wiackiewicz, M., & Krolczyk, G. M. (2018). Study on metrological relations between instant tool displacements and surface roughness during precise ball end milling. *Measurement*, 129, 686-694. doi:<https://doi.org/10.1016/j.measurement.2018.07.058>
- Wulandhari, L. A., Wibowo, A., & Desa, M. I. (2014). Improvement of adaptive GAs and back propagation ANNs performance in condition diagnosis of multiple bearing system using grey relational analysis. *Comput Intell Neurosci*, 2014, 419743. doi:10.1155/2014/419743

- Wyen, C.-F., Knapp, W., & Wegener, K. (2012). A new method for the characterisation of rounded cutting edges. *The International Journal of Advanced Manufacturing Technology*, 59(9-12), 899-914.
- Wyen, C.-F., & Wegener, K. (2010). Influence of cutting edge radius on cutting forces in machining titanium. *CIRP annals*, 59(1), 93-96.
- Xavior, M. A., & Jeyapandiarajan, P. (2018). Multi-Objective Optimization during Hard Turning of AISI D2 Steel Using Grey Relational Analysis. *Materials Today-Proceedings*, 5(5), 13620-13627.
- Yallese, M. A., Chaoui, K., Zeghib, N., Boulanouar, L., & Rigal, J.-F. (2009). Hard machining of hardened bearing steel using cubic boron nitride tool. *Journal of Materials Processing Technology*, 209(2), 1092-1104. doi:<https://doi.org/10.1016/j.jmatprotec.2008.03.014>
- Yang, Y.-K., Chuang, M.-T., & Lin, S.-S. (2009). Optimization of dry machining parameters for high-purity graphite in end milling process via design of experiments methods. *Journal of Materials Processing Technology*, 209(9), 4395-4400.
- Yen, Y.-C., Jain, A., & Altan, T. (2004). A finite element analysis of orthogonal machining using different tool edge geometries. *Journal of Materials Processing Technology*, 146(1), 72-81.
- Young, H.-T., Mathew, P., & Oxley, P. (1994). Predicting cutting forces in face milling. *International Journal of Machine Tools and Manufacture*, 34(6), 771-783.
- Young, P., Byrne, G., & Cotterell, M. (1997). Manufacturing and the environment. *The International Journal of Advanced Manufacturing Technology*, 13(7), 488-493.
- Yue, Y., Sun, J., Gunter, K., Michalek, D., & Sutherland, J. (2004). Character and behavior of mist generated by application of cutting fluid to a rotating cylindrical workpiece, Part 1: Model development. *Journal of manufacturing science and engineering*, 126(3), 417-425.
- Zaghbani, I., Songmene, V., & Khettabi, R. (2009). Fine and ultrafine particle characterization and modeling in high-speed milling of 6061-T6 aluminum alloy. *Journal of materials engineering and performance*, 18(1), 38-48.
- Zeilmann, R. P., Ost, C. A., & Fontanive, F. (2018). Characterization of edge preparation processes and the impact on surface integrity after milling of AISI P20 steel. *Journal of the Brazilian Society of Mechanical Sciences and Engineering*, 40(9), 421.
- Zhang, Q., Kusaka, Y., & Donaldson, K. (2000). Comparative pulmonary responses caused by exposure to standard cobalt and ultrafine cobalt. *Journal of Occupational Health*, 42(4), 179-184.
- Zhao, X. F., He, L., Liu, W., & Zheng, W. J. (2016). *Influence of cutting tool edge preparation on cutting force and surface integrity*. Paper presented at the Materials Science Forum.
- Zhao, Z. Y., Xiao, Y. S., Zhu, Y. Q., & Liu, B. (2010). *Influence of Cutting Speed on Cutting Force in High-Speed Milling*. Paper presented at the Advanced Materials Research.